Proceedings of

THE 5th INTERNATIONAL CONFERENCE OF HYOJEONG ACADEMY

Date: : February 20~21, 2025.
Venue: Online Conference (Peace TV studio, Korea)

www.ichja.org

Table of Contents

Session 3: Physical Science for Co-Prosperity

Session 4: Bio Science for Co-Prosperity

Session 5: Medical & Health Studies for Co-Prosperity

Session 6: Social & Religious Studies for Co-Righteousness

Keynote Speech

This symposium is intended to testify to the revolutionary thought known as Unification Thought, Godism. This ground-breaking thought of Godism has content can overcome materialism and humanism within the scope of broad category of science, such as physics, biology- philosophy, et cetra. Through this endeavor, unification scholars aim to revolutionalize the materialistic and humanistic viewpoint of today's scientific scholarly researches to one centered upon God to systemize every academic field of study.

Unification thoughts is presented as a system. They can offer a solution to the confusion affecting the human and social science and natural sciences and the arts. The unity and harmony which it brings to the various theories competing in these fields must based on the fundamental principle of the universe. By applying unification thought to each area of academic study a turning point for forming the reconstructing a new science will be achieved. When this movement influences the scholarly world, peace in this era of global village will come even more quickly. I also hope that through this economic endeavor, unification thought- ...Will become the basis for the movement for the unity of sciences. In this sense, as central future point, the unification thought-based movement will build momentum for the new science.

The unity of science approach as an ideal to strive for with an immense rapidity in the 17th Century, Newton united- The description of two phenomena, the motion of the object falling to the ground Newton's mechanism reached the point where it began to de-exclude the notion of spirits and God under the name of Laplace reductionism. Laplace attempted to bring about physical normative unity. That excluded any outside metaphysical reality.

In the 1930's, there was a second attempt of unity of science movement centering on the Vienna Circle. The Institute for the Unity of Science was set up under positivistic auspice maintaining inductive logic. Its members' original thesis of the unity of science was based on the belief. That all scientific concepts are definable in the strictest sense of language, of sense data, namely the physical language. Today, the claims of Vienna Circle looks rather nigh. The Institute for the Unity of Science has recently dissolved and the original positivistic manifesto has been abandoned.

The fight between empiricism and rationalism has been at the center of epistemological disputes throughout the entire history of philosophy, without any possibility of reconciliation. First of all, we will discuss this topic in connection with the epistemological basis of universal science. The foundation of universal science cannot be obtained only through the evidence of deductivist logic, nor can it depends on inductive logic.

Unification thought however, acknowledges the special characteristics both method-methodology It seeks a way to synthesize the unity, both methodologies from a practical standpoint. Unification thought is not a science of particular fields like physics and philosophy, but it is the basic science of all sciences with its academic methodology and system-system. In fact, the purpose of first ever university in human history.

The Academy of Plato was construct a science with God namely- The idea of goodness at its zenith. This ideal of academia will finally return to its original status through the academic model of unification thought.

Thank you very much

Dr. Jin Sung-Bae,
Chair of Hyojeong Academic Foundation

Congratulatory Message

Honorable guests, distinguished participants, ladies and gentlemen,

It is a great honor to extend my heartfelt congratulations on the occasion of the 5th Hyojeong International Academic Conference.

I sincerely thank Dr. Pyun Youngsik and all those who have worked tirelessly to organize this significant event. A special appreciation goes to the scholars presenting their research today; your contributions have the potential to play a vital role in advancing global peace.

As we navigate the 21st century, shaped by the Fourth Industrial Revolution, humanity faces unprecedented challenges and rapid transformations.

The rise of generative artificial intelligence has brought remarkable advancements and convenience to our daily lives, yet it has also raised fundamental questions about human identity and the essence of our existence.

Meanwhile, global conflicts continue to escalate.The war between Russia and Ukraine, which began in February 2022, remains unresolved, impacting nations and lives worldwide. The conflict triggered by Hamas's attack on Israel in October 2023 has resulted in devastating loss.

Increasing tensions between countries and individuals continue to fuel violence, while the division between North and South Korea remains a pressing challenge to regional and global peace. At the same time, climate change and global warming pose existential threats to the future of humanity.

In light of these complex and urgent global issues, the importance of the 5th Hyojeong International Academic Conference cannot be over stated.

I encourage all of you to use this gathering as an opportunity to explore new values, strategies, and solutions for sustaining human prosperity and ensuring lasting peace.

I sincerely wish for the success of this conference and hope that all participants are blessed in their endeavors.

Thank you.

Dr. Moon Seong-Jae,
President of Sun Moon University

Proceedings of
THE 5th INTERNATIONAL CONFERENCE OF
HYOJEONG ACADEMY 2025

Session 1

Environmental Studies for Co-Existence

www.ichja.org

5th International Conference of Hyojeong Academy
International Joint Conference 2025

Impact of Land Use/Land Cover Changes on Ecosystem Service Values: A Case Study of the Suluh River Basin, Northern Ethiopia

Hailay Hagos Entahabu[1, 2, *], Amare Sewnet Minale[2, 3] and Emiru Birhane[4, 5]

[1]Department of Geography and Environmental Studies, Raya University, May'Chew, Ethiopia
[2]Department of Geography and Environmental Studies, Bahir Dar University, Bahir Dar, Ethiopia
[3]Bahir Dar University, Spearheads Climate Resilient Green Economy Research in North Western Ethiopia (BDU-IUC Programme), Bahir Dar University, Bahir Dar, Ethiopia
[4]Institute of Climate and Society, Mekelle University, Mekelle, Ethiopia
[5]Faculty of Environmental Sciences and Natural Resource Management Norwegian, University of Life Sciences, Åas, Norway
*Correspondence: tjoh3782@hailayhagos@rayu.edu.et

Abstract: The total value of ecosystem services in the Suluh River Basin is significantly impacted by land use and land cover change. Alterations in near-natural habitats lead to substantial changes in specific ecosystem services. This study examines land cover and use changes over the last three decades using Geographic Information Systems (GIS) and Remote Sensing (RS) technology. Land use and cover values were assessed alongside global datasets created for biomes to evaluate total and specific changes in ecosystem service values (ESV) for the designated study area and timeframe. A sensitivity analysis was conducted to test the reliability of our estimations using proxies. The findings show that plantation areas increased by 43.7%, built-up lands expanded by 135.5%, cultivated land rose by 7.98%, and barren land grew by 9.8%. Conversely, several land categories experienced notable declines: grazing land decreased by 48.6%, shrub-bushland fell by 61.7%, water bodies declined by 79.6%, and forest land was drastically reduced by 576.7%. As a result of these changes, total ESVs diminished from $32,993,373.58 in 1990 to $26,595,778.37 in 2018, reflecting a net decline of 19.4%. Alarmingly, essential services such as Gas Regulation, Erosion Control, Waste Treatment, Food Production and Habitat/Refuge services have fallen to zero, jeopardizing ecosystem functionality and exacerbating climate change impacts. Overall, both the river basin and individual ESV have declined during this period, highlighting the urgent need for improved land management techniques to enhance the sustainability of ecosystem service delivery in the area.

Keywords: Change analysis, ecosystem service valuation, sustainability, impact

1. Introduction

Land use and land cover changes (LULCC) have profound implications for ecosystem services, which are critical for maintaining ecological balance and supporting human livelihoods [1]. The Suluh River Basin, like many regions worldwide, has experienced significant alterations in land use due to urbanization, agricultural expansion, and deforestation [2, 3]. These changes not only affect the quantity and quality of ecosystem services but also pose challenges for sustainable development and biodiversity conservation [4]. The degradation of these ecosystem services can lead to increased vulnerability to climate change, loss of biodiversity, and diminished quality of life for local communities [5].

Ecosystem services, defined as the benefits humans derive from functioning ecosystems, can be categorized into provisioning, regulating, cultural, and supporting services [6]. Understanding the changes in these services due to LULCC is essential for developing effective management strategies. This study aims to provide an in-depth analysis of the changes in land use and cover in the Suluh River Basin, evaluating their impacts on ecosystem service values over 30 years.

The Suluh River Basin is characterized by diverse ecosystems that provide vital services to local communities. These ecosystems support agriculture, regulate climate, and maintain water quality. However, increasing human pressures have led to significant land conversion, impacting these crucial services. Studies have shown that urban expansion and agricultural intensification are primary drivers of LULCC, which can disrupt ecological balance and lead to service decline [7]. For instance, the conversion of forests to agricultural land can negatively affect carbon sequestration and biodiversity [1, 8]. Similarly, urbanization often leads to habitat fragmentation, further

threatening ecosystem integrity [9]. In the context of the Suluh River Basin, understanding these dynamics is necessary for informing policy and land management decisions.

Numerous studies have documented the impacts of LULCC on ecosystem services. For instance, Costanza et al. [10] highlighted the economic value of ecosystem services, while De Groot et al. [11] provided a framework for classifying and valuing these services. Recent research has also focused on the spatial and temporal dynamics of ecosystem services in relation to land cover changes [3]. An essential aspect of understanding LULCC is the use of remote sensing and GIS technologies, which allow for the accurate monitoring and analysis of land cover changes over time [12]. These technologies enable researchers to quantify changes in land use and correlate them with ecosystem service values, providing a robust basis for policy and management decisions.

2. Methodology

This study employs a combination of GIS and Remote Sensing (RS) technologies to analyze land cover changes over the past three decades. The methodology consists of several key steps:

1. Data Collection: Satellite imagery from various sources, including Landsat 5, 7 and 8, was obtained to assess land cover types. Historical data was gathered from government and international databases.
2. Land Cover Classification: Using object-based fuzzy classification techniques in eCognition developer, different land cover types were identified, including forests, agricultural lands, built-up areas, and water bodies.
3. Change Detection Analysis: A change detection analysis was performed to quantify the extent of land cover changes between 1990 and 2018. This involved comparing classified images to identify areas of gain and loss.
4. Ecosystem Service Valuation: Ecosystem services were valued using established economic models, integrating local data with global datasets to estimate total and specific changes in ESV [13].
5. Sensitivity Analysis: A sensitivity analysis was conducted to test the reliability of our estimations, ensuring that the findings are robust. This analysis involved varying key assumptions and evaluating the impact on estimated ESVs [11].

3. Results

The results indicate a significant transformation in land use within the Suluh River Basin. Plantation areas increased by 43.7%, reflecting a trend toward intensified agricultural practices. Built-up lands expanded by 135.5%, indicating rapid urbanization and infrastructure development. Conversely, grazing land decreased by 48.6%, and forest land saw a drastic reduction of 576.7%. These changes have led to a decline in total ESV from $32,993,373.58 in 1990 to $26,595,778.37 in 2018, representing a net decrease of 19.4%.

Critical ecosystem services were affected, with Gas Regulation, Erosion Control, and Waste Treatment services dropping to zero [5, 14]. The loss of these services not only threatens the ecological integrity of the basin but also undermines the livelihoods of communities that depend on these services for their well-being [1].

4. Discussion

The decline in ESV highlights the urgent need for sustainable land management practices. Effective strategies must be implemented to mitigate the adverse effects of LULCC and enhance ecosystem service delivery. Community engagement and policy advocacy for biodiversity conservation are essential components of this approach [15, 16].

Integrating ecosystem service valuation into land use planning can help decision-makers understand the trade-offs involved in land management and promote practices that sustain ecosystem services [17]. The findings of this study align with the broader literature, which emphasizes the importance of ecosystem services in guiding sustainable development [6].

Moreover, the study underscores the need for continuous monitoring of land use changes and their impacts on ecosystem services. Technologies such as remote sensing and GIS can provide valuable data for assessing trends and informing adaptive management strategies [18].

5. Conclusion

The findings of this study underscore the significant impacts of land use changes on ecosystem services in the Suluh River Basin. Immediate action is required to implement sustainable land management techniques that can restore and preserve ecosystem functionality, ensuring the continued provision of vital services for both the environment and local communities. Policymakers must prioritize the integration of ecosystem service considerations into development planning to safeguard the ecological health of the Suluh River Basin.

References

1. Fischer, J., Turner, J. R. and Lindenmayer, D. B. Landscape modification and habitat fragmentation: a synthesis of the ecological effects of land use change. *Ecology and Society 14*(1), 1-15 (2009).
2. Barbier, E. B. Valuing ecosystem services for sustainable development. *Environmental Economics and Policy Studies 3*(1), 1-20 (2000).
3. Liu, Y., Bi, J., Lv, J., Ma, Z. and Wang, C. Spatial multi-scale relationships of ecosystem services: A case study using a geostatistical methodology. *Scientific Reports* 7, 1-12 (2017).
4. Hassan, R., Scholes, R. and Ash, N. Ecosystems and human well-being: Current state and trends. *Millennium Ecosystem Assessment 1*, 1-137 (2005).
5. Ecosystems and human well-being: Synthesis. In *Millennium Ecosystem Assessment* (Island Press, 2005).
6. TEEB for Local and Regional Policy Makers. In *TEEB (The Economics of Ecosystems and Biodiversity)* (Earthscan, 2010).
7. Seto, K. C., Fragkias, M., Güneralp, B. and Reilly, M. K. A meta-analysis of global urban land expansion. *PLOS ONE 7*(7), e45740 (2012).
8. Lamb, D., Erskine, P. D. and Parrotta, J. A. Restoration of degraded tropical forest landscapes. *Global Ecology and Biogeography 25*(3), 289-298 (2016).
9. Grimm, N. B. et al. Global change and the ecology of cities. *Science 319*(5864), 756-760 (2008).
10. Costanza, R. et al. The value of the world's ecosystem services and natural capital. *Nature 387*(6630), 253-260 (1997).
11. De Groot, R. S., Wilson, M. A. and Boumans, R. M. J. A typology for the classification, description, and valuation of ecosystem services. *Ecological Economics* 69(3), 253-268 (2010).
12. Zhang, Y., Chen, L. and Wang, Y. Remote sensing and GIS for land use and land cover change analysis. *International Journal of Applied Earth Observation and Geoinformation 64*, 1-12 (2018).
13. Costanza, R., de Groot, R. S. and Farber, S. Valuing ecosystem services: Theory, practice, and the path ahead. *Ecosystem Services* 12, 81-92 (2014).
14. Daily, G. C. *Nature's services: Societal dependence on natural ecosystems* (Island Press, 1997).
15. Bennett, E. M., Peterson, G. D. and Gordon, L. J. Understanding relationships among multiple ecosystem services. *Ecology Letters 12*, 1394-1404 (2009).
16. Folke, C., Carpenter, S. R. and Walker, B. Regime shifts, resilience, and biodiversity in ecosystem management. *Annual Review of Ecology, Evolution, and Systematics 35*, 557-581 (2004).
17. Benessaiah, K. et al. The role of ecosystem services in land use planning: A case study of the Upper Mississippi River Basin. *Ecological Economics 86*, 1-10 (2013).
18. Pettorelli, N. et al. The need for applied ecological monitoring: A case study from the Serengeti. *Ecological Indicators 45*, 4-12 (2014).

5th International Conference of Hyojeong Academy
International Joint Conference 2025

Management of the Temporal Variations of Nutrient Flux in Topographical Closed Lake Hashenge, Tigray, North Ethiopia

Berhanu Menasbo[1,2,*], Emiru Birhane[2,3], Abraha Gebrekidan[1], Ståle Haaland[3], Fasil Ejigu[3] and Tesfamariam Tekilu[1]

[1]College of Natural and Computational Science, Mekelle University, Mekelle, Ethiopia
[2] College of Agriculture, Mekelle University
[3] Norwegian university of life science, Ås, Norway
*Correspondence: berhanu.menasbo@mu.edu.et

Abstract: This study evaluates the effectiveness of a double-layer capping system composed of biochar (BC) and zeolite (ZE) with Non-woven Fabric mats (NWFM) in controlling nutrient fluxes and improving water quality in Lake Hashenge, Ethiopia. Three configurations were tested: NWFM/ZE/BC (ZE above BC), NWFM/BC/ZE (BC above ZE), and an uncapped control. Laboratory experiments assessed nutrient release (NH_4-N, NO_3-N, T-N, PO_4-P, T-P) under two temperatures (16°C and 24°C) over 60 days. Capped setups NWFM/ZE/BC and NWFM/BC/ZE significantly reduced NH_4-N fluxes, achieving 2.27 ± 1.08 mg/m² day and 1.5 ± 0.39 mg/m² day at 16°C, and 1.82 ± 0.66 mg/m².day and 2.34 ± 1.64 mg/m².day at 24°C, respectively. T-N flux followed a similar trend, with NWFM/ZE/BC achieving the lowest value at 16°C (1.03 mg/m² day) and the highest flux observed in uncapped conditions at 24°C (5.02 ± 1.36 mg/m².day). The NWFM/ZE/BC configuration reduced NH_4-N flux by 95%, retained up to 98% of phosphorus, and mitigated temperature-dependent nutrient release while maintaining dissolved oxygen (DO) and reducing chemical oxygen demand (COD). These findings underscore the potential of such capping materials for restoring eutrophic ecosystems and highlight the need for integration with catchment management practices. Field trials are recommended to validate long-term performance.

Keywords: Double-layer Cap, Eutrophication problems, Cold and warm temperature (16°C and 24°C), Nitrogen and phosphorous removal.

1. Introduction

Eutrophication, driven by excessive nitrogen (N) and phosphorus (P) in aquatic systems, results in algal blooms, oxygen depletion, biodiversity loss, and destabilizing ecosystems [1, 2]. Human activities like agricultural runoff and wastewater discharge increase nutrient loading, further intensified by climate change and rising carbon emissions [3]. Lakes typically begin as oligotrophic (low nutrient levels) and progress through mesotrophic, eutrophic, and hypertrophic stages as nutrient levels rise (Fig. 1).

Biochar (BC), derived from biomass pyrolysis, and zeolite (ZE), a mineral with high cation exchange capacity, have emerged as cost-effective solutions for immobilizing N and P in sediments, reducing algal growth and eutrophication [4, 5]. Double-layer capping systems combining BC and ZE effectively decrease nutrient flux and stabilize sediments [6, 7].

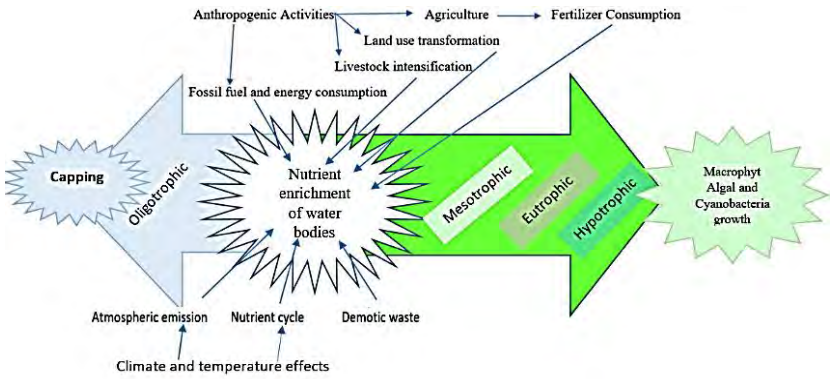

Figure 1. Simplified conceptual model for illustrations of Eutrophication driven by synergistic action of direct and indirect drivers (Climate, Temperature, and Anthropogenic activities).

Lake Hashenge in Ethiopia faces severe eutrophication due to nutrient-rich sediment deposition from unsustainable agricultural practices and deforestation, threatening its ecology and socio-economic importance. Annual sediment loads exceed 45,865 tons, worsening algal blooms and oxygen depletion [8]. This study examines the effectiveness of BC and ZE double-layer capping systems integrated with non-woven fabric mats (NWFM) under varying seasonal temperatures, in offering a sustainable solution to restore eutrophic ecosystems in Lake Hashenge (developing regions).

2. Materials and Methods

This study employed BC, ZE, and non-woven fabric mats (NWFM) as key materials. BC was produced by pyrolyzing *Prosopis Juliflora* wood at 500 °C, then sieved to an 80-mesh size [4, 9, 10]. ZE was ground to a 1.5–5 mm grain size at Ezana Mining Laboratory, Mekelle. Seasonal lake water nutrient concentrations varied, with warmer months (24 °C) showing lower levels (e.g., 5.2 mg/L NH_4-N) compared to colder months (16 °C) with higher levels (e.g., 9.3 mg/L NH_4-N).

Sediment incubation experiments tested the effectiveness of capping materials in reducing nutrient release at 16 °C and 24 °C, following protocols from previous studies [11, 12]. Experimental setups included uncapped sediment (UN), NWFM with ZE at top of BC (NWFM/ZE/BC), and NWFM with BC at top of ZE (NWFM/BC/ZE), alongside a control column with a sand layer. Columns were filled with 2.8 L of lake water using a peristaltic pump to prevent sediment disturbance and monitored for 60 days in sealed at light-tight conditions.

Data were analyzed using IBM SPSS Statistics 20 and OriginPro 2024. A two-way ANOVA evaluated mean differences among treatments, while Mann-Whitney U and Kruskal-Wallis tests assessed the significance of nutrient fluxes, pH, and temperature effects. Interaction effects were analyzed using Dunn-Bonferroni's multiple comparison test.

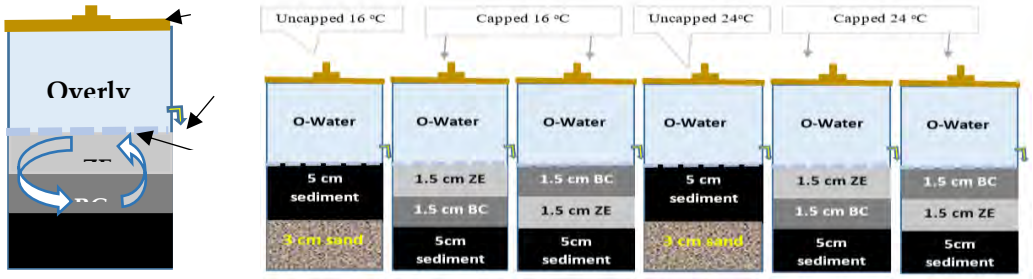

Figure 2. Simplified set-up of the sediment incubation experiments with ZE\BC double layer cap at 16^0 C and 24^0 C.

3. Result

3.1. Effect of temperature and capping on water environment

Electrical conductivity (EC) increased gradually, peaking at 24°C under uncapped conditions, likely due to enhanced ion release from sediments. Two-way ANOVA revealed significant effects of temperature ($p = 0.018$), capping type ($p < 0.001$), and their interaction ($p = 0.005$) on EC. pH ranged from 7.0 to 8.5, with the highest levels (8.4 ± 0.30) in the NWFM/ZE/BC setup at 24°C, attributed to alkaline compounds in biochar. Although biochar is most effective at pH 4–5, the higher pH may result from the reducing properties of its organic groups [13, 14]. ANOVA showed significant effects of temperature ($p < 0.001$) and capping ($p < 0.001$) on pH, with no interaction effect ($p = 0.855$). Dissolved oxygen (DO) levels declined across all setups, decreasing faster at 24°C than at 16°C.

3.2. Effect of temperature and capping on the release of C, N, and P from sediments

NH_4-N concentrations were highest in uncapped conditions, reaching 33.1 ± 12.1 mg/L at 16°C and 39 ± 11.5 mg/L at 24°C. In contrast, capped setups (NWFM/ZE/BC, NWFM/BC/ZE) substantially reduced NH_4-N fluxes, achieving values of 2.3 ± 1.08 mg/m²·day and 1.5 ± 0.39 mg/m²·day at 16°C, and 1.8 ± 0.66 mg/m²·day and 2.3 ± 1.64 mg/m²·day at 24°C. The NWFM/ZE/BC cap was the most effective in adsorbing or immobilizing NH_4-N, this is due to ZE complement the NH_4-N adsorption of BC. ANOVA indicated significant effects of temperature and capping on NH_4-N inactivation ($p < 0.001$) with no interaction effect ($p = 0.569$).

COD concentrations in the O-water increased quickly in uncapped conditions until day 15, then gradually leveled off by day 40, with a slight decline afterward. COD concentration was lower in capped conditions, with NWFM/ZE/BC at 23.5 ± 2.2 mg/L and NWFM/BC/ZE at 20.4 ± 2.45 mg/L, compared to 27.3 ± 2.85 mg/L in the uncapped setup at 16°C.

Many studies suggested that P compounds are insoluble in water but have high adsorption capacity to soil and sediment particles. In the uncapped setup, PO4-P averaged 0.6 ± 0.2 mg/L at 16°C and 0.4 ± 0.11 mg/L at 24°C, increasing steadily until day 45, then leveling off. No significant difference was found between these temperatures ($p = 0.33812$).

4. Discussion

The NWFM/ZE/BC cap (Fig. 3) exhibited superior performance in reducing NH_4-N flux compared to NWFM/BC/ZE and uncapped setups, as confirmed by significant differences in ammonium flux across treatments ($p < 0.03$). At 24°C, NH_4-N flux increased from 9.5% to 15.4% in the NWFM/ZE/BC setup and from 25.6% to 39.2% in uncapped conditions, indicating the critical role of temperature in modulating nutrient release. The lower adsorption capacity of biochar for NH_4-N when placed in the top layer underscores the importance of optimizing the arrangement of capping materials for enhanced performance.

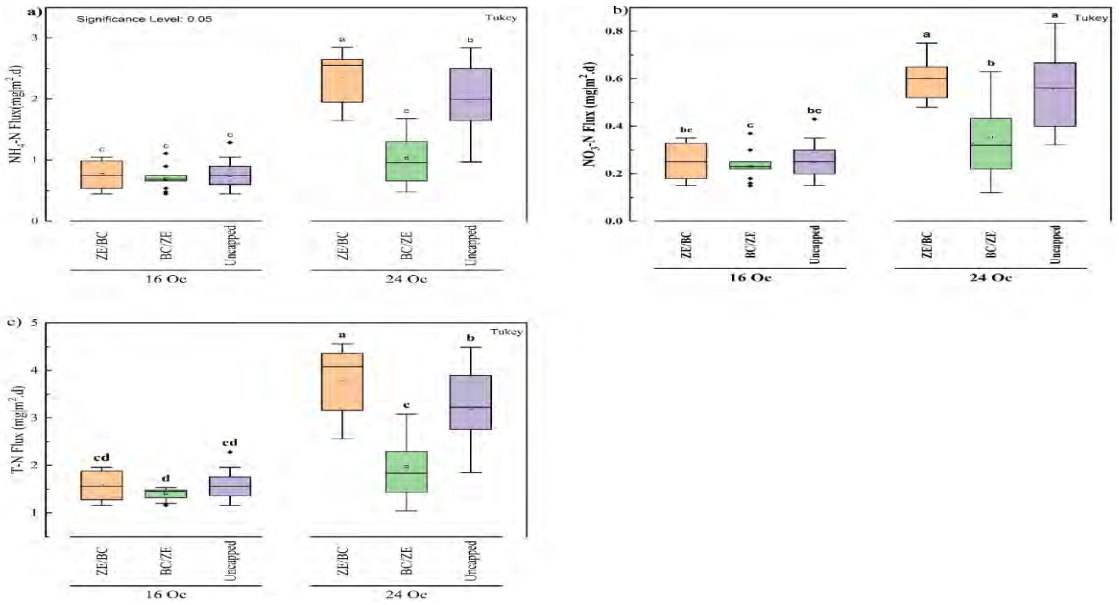

Figure 3. Comparison of fluxes of (a) NH_4^+-N; (b) NO_3^--N; (c) T-N in uncapped sediments and those capped with ZE or BC using NWFM at 16^0 C and 24^0 C. Significant differences (Tukey's test, $p < 0.05$) are indicated by letters above the box plots. Capping efficiency was calculated from 60-day incubation, with error bars showing the standard deviation from duplicate experiments.

In uncapped conditions (Fig. 4), T-N flux was higher at 24°C than at 16°C. Capping materials NWFM/ZE/BC and NWFM/BC/ZE did not affect T-N flux significantly. Still, the Mann-Whitney U-Test found that T-N flux was significantly different between temperatures ($p = 0.019$), while the Kruskal-Wallis and Dunn-Bonferroni tests revealed differences across capping types ($p < 0.001$). NWFM/ZE/BC capping reduced nitrogen release, while NWFM/BC/ZE minimized NH_4-N flux. Zeolite removes NH_4-N via cation exchange, and biochar adsorbs organic nitrogen due to its high surface area [12].

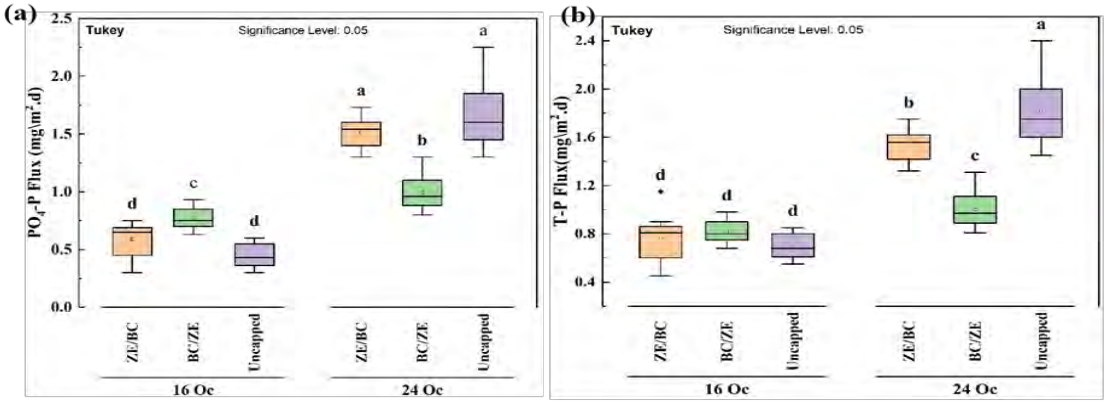

Figure 4. Comparison of (a) PO_4-P and (b) T-P fluxes in uncapped versus double-layer-capped sediments at 16°C and 24°C. Letters above box plots indicate significant diffences ($p < 0.05$) from Tukey's test.

Phosphorus fluxes (Fig. 4), including PO_4-P and T-P, also varied significantly across capping setups and temperatures. Uncapped sediments exhibited higher phosphorus flux at 24°C (97.41% for PO_4-P and 97.23% for T-P) compared to 16°C, indicating a transition from phosphorus retention at cooler temperatures to phosphorus release under warmer conditions. This aligns with seasonal patterns of phosphorus release, where warmer conditions enhance microbial activity and promote phosphorus desorption from sediments.

5. Conclusion

The findings provide critical insights into the role of capping materials in controlling NH_4-N, NO_3-N, T-N, PO_4-P, and T-P fluxes, as well as maintaining water quality by stabilizing DO, EC, pH, ORP and COD:

1. The NWFM/ZE/BC cap demonstrated the highest efficiency in reducing NH_4-N, PO_4-P, and T-P fluxes at both 16°C and 24°C, with nutrient retention rates exceeding 95% in most cases.
2. NH_4-N was the dominant nitrogen species released under low-oxygen conditions, accounting for over 97% of total nitrogen flux.
3. Phosphorus fluxes were higher at 24°C compared to 16°C, reflecting the temperature-dependent nature of nutrient release and adsorption. This aligns with the seasonal pattern of higher phosphorus desorption during warmer conditions**.**
4. COD, and maintained higher DO levels in the overlying water. These effects are critical for mitigating eutrophication and improving aquatic ecosystem health.

References

1. Sunaryani, A., Soewondo, P. and Santoso, A. B. Sediment capping technology for eutrophication control and its potential for application in Indonesian lakes: a review. *LIMNOTEK Perairan Darat Tropis Di Indonesia 29*(1), (2023). https://doi.org/10.55981/limnotek.2023.2366
2. Sinha, E., Michalak, A. M. and Balaji, V. Eutrophication will increase during the 21st century as a result of precipitation changes. *Science 357*(63499), 405-408 (2017).
3. Kessouri, F. et al. Coastal eutrophication drives acidification, oxygen loss, and ecosystem change in a major oceanic upwelling system. *Proceedings of the National Academy of Sciences of the United States of America 118*(21), 1–8 (2021). https://doi.org/10.1073/pnas.2018856118
4. Lehmann, J., Gaunt, J. and Rondon, M. (2006). BIO-CHAR SEQUESTRATION IN TERRESTRIAL ECOSYSTEMS – A REVIEW. *Mitigation and Adaptation Strategies for Global Change 2*, 403–427 (2006). https://doi.org/10.1007/s11027-005-9006-5
5. Zhou, J., Lin, J. and Zhan, Y. Control of phosphorus release from sediment by iron/aluminum co-modified zeolite: efficiency, mechanism, and response of microbial communities in sediment. *Environmental Science and Pollution Research 31*(23), 33708–33732 (2024). https://doi.org/10.1007/s11356-024-33482-9
6. Forsberg, S. C. et al. Thin-layer capping with granular activated carbon and calcium-silicate to remediate organic and metal polluted harbor sediment. *Science of the Total Environment 946*(10), 174263(2024). https://doi.org/10.1016/j.scitotenv.2024.174263
7. Dai, Y., Wang, W., Lu, L., Yan, L. and Yu, D. Utilization of biochar for the removal of nitrogen and phosphorus. 257. *Journal of Cleaner Production 257*, 120573 (2020). https://doi.org/10.1016/j.jclepro.2020.120573

8. Shimbahri, M.G. Assesment of Sediment Accomulation in a Topographically Closed Highland Lake: The Case of Lake Hashenge, Northeren Ethiopia. *International Journal of Current Research 7*(6), 16639-16643 (2015). http://www.journalcra.com
9. Bruun, E. W., Ambus, P. and Egsgaar Effects of slow and fast pyrolysis biochar on soil C and N turnover dynamics. *Soil Biology and Biochemistry 46*, 73-79 (2012). https://doi.org/10.1016/j.soilbio.2011.11.019
10. Joseph, S. and Lehmann, J. eds. *Biochar for environmental management* (Routledge, 2015).
11. Gu, B., Lee, C., Lee, T. and Park, S. Evaluation of sediment capping with activated carbon and nonwoven fabric mat to interrupt nutrient release from lake sediments. *Science of the Total Environment 599–600*, 413–421 (2017). https://doi.org/10.1016/j.scitotenv.2017.04.212
12. Zhu, Y., Shan, B., Huang, J., Teasdale, P. R. and Tang, W. In situ biochar capping is feasible to control ammonia nitrogen release from sediments evaluated by DGT. *Chemical Engineering Journal 374*, 811–821 (2019). https://doi.org/10.1016/j.cej.2019.06.007
13. Huang, C. P. and Blankenship, D. W. The removal of mercury(II) from dilute aqueous solution by activated carbon. *Water Research 18*(1), 37-46 (1984).
14. Kang, L., Mucci, M. and Lürling, M. Influence of temperature and pH on phosphate removal efficiency of different sorbents used in lake restoration. *Science of the Total Environment 812*, 151489 (2022). https://doi.org/10.1016/j.scitotenv.2021.151489

5th International Conference of Hyojeong Academy
International Joint Conference 2025

Stone bund effects on soil carbon stock and sequestration on rain-fed cropland in the highlands of Tigray, Northern Ethiopia

Tsegay Assefa[1]*, Mitiku Haile[2] and Melaku Berhe[3]

[1]Department of Agricultural and Resources Economics, Mekelle University, Mekelle, Ethiopia
[2]Department of Land Resources Management and Environmental Protection, Mekelle University
[3]Department of Agricultural and Resources Economics, Mekelle University
*Correspondence: tsegayassefa2100@gmail.com

Abstract: This study investigates the role of stone bunds, which are earth barriers implemented to prevent soil erosion, increasing soil organic carbon (SOC) sequestration within the rain-fed highlands of Northern Ethiopia. As climate change mitigation efforts become increasingly vital, understanding the influence of land management practices on carbon storage is essential. We investigate the impact of stone bunds at different ages on carbon sequestration rates and SOC stock levels through soil sampling and field measurements at cropland. Findings reveal a significant positive correlation between stone bund age and increased SOC stock, with the most notable carbon sequestration observed in croplands with 15-year-old stone bunds. Result shown that stone bunds have significantly enhanced the levels of SOC in topsoil layers (0-30 cm) when compared to unconserved croplands. The study highlights the significance of managing stone bunds in reducing soil erosion, increasing accomulation of organic matter, and fostering sustainable agricultural practices. These insights provide practical solutions to boost local productivity and play a notable role in mitigating global climate change. This study highlights the intersection between local farming practices and global environmental goals, offering insights for achieving carbon neutrality and enhancing climate resilience in similar agricultural ecosystems worldwide.

Keywords: Land degradation, Land management strategies, Stone bund, Soil carbon stock, Carbon sequestration, Agricultural productivity, Ethiopia

1. Introduction

Soil is a vital natural resource, playing a central role in the global carbon, nitrogen, and water cycles [1]. It holds the largest land-based carbon reservoir [2] and contributes significantly to carbon sequestration [3], with croplands alone storing substantial amounts of carbon [4]. However, land degradation, driven by poor policies, unsustainable farming practices, and deforestation, has led to soil erosion [5, 6], which threatens both soil quality and ecosystem services [7]. In Ethiopia, soil erosion especially on steep slopes has worsened due to poor land management and deforestation, negatively affecting crop yields and livelihoods [8–10].

Erosion depletes soil fertility [11], reduces carbon storage [12], and increases greenhouse gas emissions [3]. The loss of stable organic carbon further diminishes soil health and reduces agricultural productivity [13]. Effective soil and water conservation (SWC) practices, such as soil bunds [10] and watershed management [14], have proven to significantly reduce soil erosion, increase soil organic carbon, and improve agricultural output. SWC measures also contribute to climate change mitigation [15] by lowering greenhouse gas (GHG) emissions [16] and enhancing carbon sequestration [17, 18].

While the Ethiopian government has invested in SWC practices, much of the research has focused on their immediate impact [19, 20, 22, 24–31]. Limited attention has been given to the long-term effects of SWC practices, especially the age of interventions like stone bunds, on soil organic carbon (SOC) stocks [21, 23, 32–35]. This study aims to assess the impact of varying-aged stone bunds on SOC sequestration in southern Tigray, Ethiopia, and provide data for policy improvements to enhance sustainable land management.

2. Materials and Methods

2.1. Description of the study

The research was conducted in Emba Alajie and Endamehoni woredas in southern Tigray, northern Ethiopia, to study soil conditions in croplands with varying stone bund ages. Emba Alajie has 76,722 hectares of land,

including arable, grazing, and forest lands [36], while Endamehoni covers 17,992 hectares, mostly cultivated and forested [37]. The dominant soil types in the area are leptosols, cambisols, and vertisols, with variations based on slope and elevation [38, 39].

2.2. Treatment selection and soil sampling

Soil samples were collected from three watersheds: Adi Ginbot and Adi Awulie in Emba Alajie, and May Muk in Endamehoni, each with croplands having stone bunds of different ages (6, 15, 14, and 25 years) and adjacent un-conserved croplands. Soil was sampled from different slope positions (lower, middle, upper) for comparison. Disturbed samples were taken for organic carbon content, and undisturbed samples for bulk density. The samples were analyzed using standard methods at the University of Mekelle.

2.3. Statistical analysis

Statistical analysis was done using IBM-SPSS, with t-tests and ANOVA to compare soil properties across different bund ages and slope positions.

3. Results

3.1. Stone bund effects on soil bulk density, carbon stock and sequestration

The study assessed the impact of different stone bund ages on soil bulk density (BD), organic carbon (OC), organic matter (OM), and carbon stock. As indicated in Table 1, significant differences in these soil properties were observed between treated and un-conserved croplands. Stone bunds, particularly those aged 6, 14, and 25 years, reduced soil BD, with the lowest values found in conserved croplands. Stone bunds also improved soil OC, OM, and carbon stock, with the 15-year-old bunds showing the highest OC content and stock. These results are consistent with previous studies that highlight the benefits of stone bunds in improving soil quality by reducing erosion and enhancing organic matter retention [25, 27, 33, 40, 41].

As shown in Table 1 and Fig 1(a), soil OC was significantly higher in conserved croplands, with substantial increases in OC stock observed over time. For instance, after 15 years of bunding, OC stock reached 95.23 t/ha, a 43.61% increase compared to un-conserved croplands. Stone bunds also played a role in carbon sequestration, with the greatest sequestration occurring in 6-year-old bunds. Soil OC stock varied across slope positions, with the highest values found in lower slopes due to sediment and organic matter accumulation (Fig 1(b)).

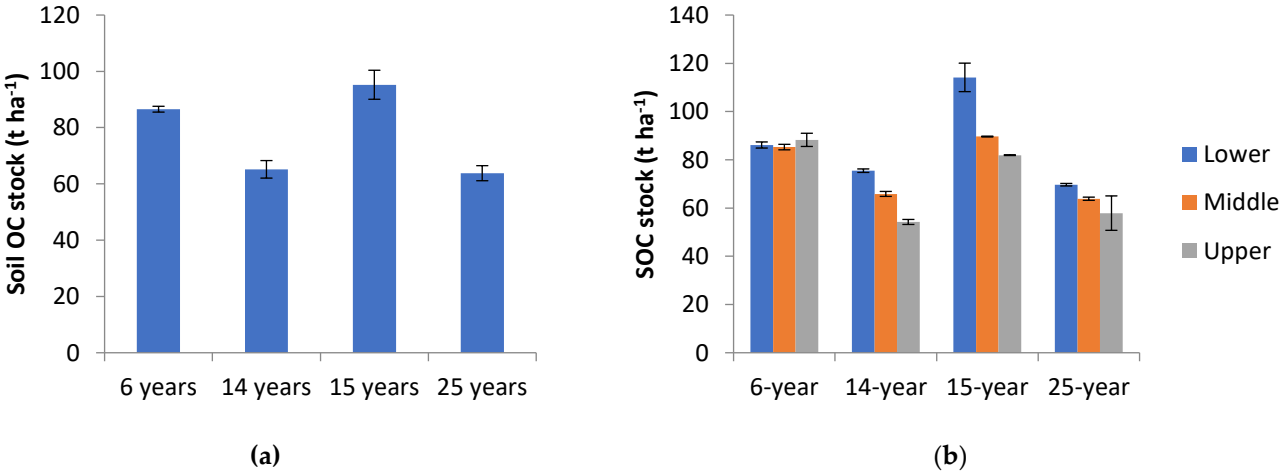

Figure 1. Graphical representation of soil OC stock: (**a**) Average soil OC stock variation under varying ages of stone bunds; (**b**) Average soil OC stock variations across different slope positions in croplands with stone bunds of various ages.

Table 1. Average values of selected soil parameters in the topsoil (0-30 cm) from croplands conserved with stone bunds for 6, 14, 15, and 25 years, compared to adjacent un-conserved croplands

Variables	BD (g/cm^{-3})	OC (%)	OM (%)	SOC stock (t ha^{-1})	Sequestration (t CO_2 y^{-1})
6-years	1.24	2.33	4.01	86.58	317.75
Un-conserved	1.36	1.49	2.56	60.29	221.27
p-value	0.000	0.000	0.000	0.000	0.000
14-years	1.18	1.86	3.21	65.18	239.21
Un-conserved	1.3	1.19	2.05	46.15	169.37
p-value	0.000	0.002	0.002	0.005	0.005
15-years	1.24	2.58	4.44	95.23	349.48
Un-conserved	1.3	1.52	2.63	59.36	217.84
p-value	0.078	0.000	0.000	0.000	0.000
25-years	1.15	1.87	3.22	63.8	234.13
Un-conserved	1.29	1.25	2.15	48.2	176.88
p-value	0.001	0.000	0.000	0.000	0.000

3.2. Estimation of soil OC stock and carbon sequestration

The following formula was used to calculate soil OC stock for each field:

$$\text{SOC stock} = \text{SOC con.} * \text{BD sample} * \text{depth} \quad (1)$$

The soil OC_{stock} represented the soil organic carbon stock (t/ha^{-1}) of the studied field, while the soil $OC\ con_{fine\ soil}$ denoted the soil organic carbon content of fine soil (%), BD sample is the value of bulk density (g/cm^{-3}) and, depth indicated the depth of the respective soil sample (cm), in this case 0-30 cm.

$$\text{Percent change in SOC stock} = \frac{\text{SOC stock in SB years} - \text{SOC stock in un} - \text{conserved}}{\text{SOC stock in un} - \text{conserved}} \text{x100} \quad (2)$$

$$\text{Rate of change in SOC stock (t } ha^{-1}y^{-1}) = \frac{\text{SOC stok in SB years} - \text{SOC stock in un} - \text{conserved}}{\text{years of stone bunds (SB)}} \quad (3)$$

Soil carbon sequestration, measured in tones of CO_2 per hectare, refers to the amount of soil carbon stored as carbon dioxide (CO_2). To calculate this, the soil OC stock is multiplied by 3.67, which is the result of dividing the molecular mass of carbon dioxide (CO_2) by the atomic mass of carbon (C) (44/12 ≈ 3.67).

$$\text{Soil C sequestration (t of CO2 } ha^{-1}) = \text{SOC stock (t } ha^{-1})\text{x } 3.67 \quad (4)$$

The soil carbon (C) sequestration rate can therefore be calculated using the following formula:

$$\text{Rate of soil C seqestration in t of CO2 } ha^{-1}y^{-1} = \frac{\text{Soil C sequestration of the SB(t of CO2 } ha^{-1}) - \text{ soil c sequestration of the un} - \text{conserved (t of CO2 } ha^{-1})}{\text{years of stone bunds (SB)}} \quad (5)$$

Croplands conserved with stone bunds showed a significant increase in soil OC stock. Soil OC stock increased by 43.61% after 6 years and 60.43% after 15 years. Stone bunds aged 14 and 25 years also showed increase in soil

OC stock by 41.24% and 32.37%, respectively (Table 2). These increases are likely due to reduced soil disturbances and enhance carbon accommulation. Similar results were found in a study by [21], which reported a 5.83% higher OC stock in conserved farmland for 6 years. Moreover, this result showed stone bunds boosted soil carbon sequestration compared to un-conserved croplands. Over 6, 14, 15, and 25 years, the treated croplands sequestared more carbon ranging from 234. 13 t CO_2 ha^{-1} to 349.48 t CO_2 ha^{-1} (Table 1). The 15 year old bunds showed the highest sequestration, with rates of 16.08 t $ha^{-1}y^{-1}$ for 6 years, 4.99 t $ha^{-1}y^{-1}$ for 14 years, 8.78 t $ha^{-1}y^{-1}$ for 15 years, and 2.29 t $ha^{-1}y^{-1}$ for 25 years, all higher than un-conserved croplands (Table 2).

Table 2. Summary of descriptive statistics comparing the age groups of stone bunds (SB) and the control groups on the mean percentage and rate of change in SOC stock, as well as the rate of change in carbon sequestration

Variables	Percent change in SOCs (t ha^{-1})	Rate of change in SOCs (t $ha^{-1}y^{-1}$)	Rate of change in soil carbon sequestration (t of CO_2 ha^{-1} y^{-1})
SB-6 years	43.61	4.38	16.08
SB-14 years	41.24	1.36	4.99
SB-15 years	60.43	2.39	8.78
SB-25 years	32.37	0.62	2.29

4. Discussion

Stone bunds significantly improve soil properties, particularly in terms of bulk density, organic carbon, and carbon stock. The results show that conserved croplands have lower BD and higher OC, OM, and carbon stock compared to un-conserved lands. This confirms that stone bunds are effective in reducing soil erosion, preventing loss of organic matter, and enhancing carbon sequestration. The impact of stone bunds on soil properties was most pronounced in younger bunds (6-15 years), with older bunds (14-25 years) showing diminishing returns, likely due to reduced sediment trapping efficiency over time. Soil OC stock increased faster in croplands with stone bunds than in control croplands. However, the rate of increase declined as the bunds aged, likely due to reduced sediment trapping efficiency and lack of maintainance. This reason is supprted by [42]. The variation in soil OC stock across age groups may be due to factors like the quality of stone bunds, grazing practices, and the presence of grasses in the bunds, which reduce erosion, retain plant residue, and enhance biomass, boosting soil OM.

The variations in soil properties between slope positions suggest that stone bunds capture sediment and organic matter more effectively in lower slopes, contributing to higher soil OC and OM values in these areas. These findings align with previous studies [25,27,33,40,41] indicating that conservation measures, especially stone bunds, enhance soil fertility by stabilizing slopes and reducing erosion and others such as [27,35,43–48]. Furthermore, the study supports the role of stone bunds in carbon sequestration, with the highest carbon stocks observed in 15 year old bunds, which are more efficient at trapping sediment and organic residues. As indicated by [17] cultivated lands that were manged with SWC practices over a 13 years period demonstrated a notable increments in soil OC stock and carbon sequestration rates, in contrast to lands that were left un-conserved. Other studies such as [49, 50] found higher soil OC stock as well as sequestration due to SWC interventions.

In summary, the study highlights the effectiveness of stone bunds in improving soil quality and sequestering carbon, with greater benefits observed in younger bunds and lower slope positions. However, the diminishing returns in older bunds underscore the need for maintenance and potential improvements in conservation practices.

5. Conclusions

In conclusion, stone bunds in the rain-fed croplands of Tigray, Ethiopia, significantly improve soil organic matter (OM), organic carbon (OC) stock, and carbon sequestration, enhancing soil fertility and crop yield. Soil OC stock increased by 32-60% in croplands with stone bunds compared to un-conserved lands. Stone bunds also help retain moisture and act as a nature-based solution to mitigate climate change. Carbon stock varies by slope position, with higher accumulation at lower slopes due to better soil movement. Older bunds show reduced carbon stock due to maintenance issues and sediment buildup. To maximize benefits, it's important to monitor older bunds,

assist farmers with conservation practices, and support policies that integrate stone bunds with other methods for optimal carbon sequestration and agricultural productivity.

Author Contributions: Tsegay Assefa: Conceptualization, methodology, software, validation, formal analysis, investigation, resources, data curation, writing—original draft preparation, visualization, project administration. **Mitiku Haile**: Conceptualization, methodology, validation, writing—review and editing, supervision. **Melaku Berhe**: Conceptualization, methodology, validation, writing—review and editing, supervision. All authors have read and agreed to the published version of the manuscript.

Funding: This research received no external funding.

Data Availability Statement: Data will be made available on request.

Acknowledgments: The authors acknowledge the farmers of Sesat, Atsela and Mekhan Tabias of Emba Alajie and Endamehoni woredas of the southern zone of Tigray who allowed their land for this study.

Conflicts of Interest: The authors declare that there are no known conflicts of interest that could have appeared to influence the work described in this manuscript.

References

1. Laban, P., Metternicht, G. and Davies, J. *Soil biodiversity and soil organic carbon: keeping drylands alive* (IUCN, 2018). https://doi.org/10.2305/iucn.ch.2018.03.en.
2. Scharlemann, J., Tanner, E., Hiederer, R. and Kapos, V. Global soil carbon: understanding and managing the largest terrestrial carbon pool. *Carbon Manag 5*(1), 81–91 (2014). https://doi.org/10.4155/cmt.13.77
3. Lal, R. Soil carbon management and climate change. *Carbon Manag 4*(4), 439–462 (2013). https://doi.org/10.4155/cmt.13.31
4. Padarian, J., Minasny, B., McBratney, A. and Smith, P. Soil carbon sequestration potential in global croplands. *PeerJ. 10*, 1–21 (2022). https://doi.org/10.7717/peerj.13740
5. FAO. Soil organic carbon : the hidden potential. *Nature Reviews Genetics 9*(4), (2017). https://doi.org/10.1038/nrg2350
6. *Status of the World's soil resources (SWSR)–technical summary* (FAO, 2015).
7. Eekhout, J. and de Vente, J. Global impact of climate change on soil erosion and potential for adaptation through soil conservation. *Earth-Science Rev. 226*:103921, (2022). https://doi.org/10.1016/j.earscirev.2022.103921
8. Asmamaw, L. B. and Mohammed, A. A. Identification of soil erosion hotspot areas for sustainable land management in the Gerado catchment, North-eastern Ethiopia. Remote Sensing applications. *Appl Soc Environ* 13, 306–317 (2019). https://www.sciencedirect.com/science/article/pii/S2352938518300405
9. Sisay, Taddese. The Impacts of land degradation on crop productivity in Ethiopia. A review. *J Environ Earth Sci. 8*, (2018).
10. Wolka, K., Biazin, B., Martinsen, V. and Mulder, J. Soil and water conservation management on hill slopes in southwest Ethiopia. Modeling effects of soil bunds on surface runoff and maize yield using AquaCrop. *J Environ Manage 296*:113187, (2021). https://www.sciencedirect.com/science/article/pii/S0301479721012494
11. Horamo, Y. and Chernet, M. Effects of soil and water conservation structures on crop yield, Lemo district, Southern Ethiopia. *Int J Food Sci Agric. 5*(4), 519–527 (2021). https://doi.org/10.26855/ijfsa.2020.12.021
12. Olson, K. R., Al-Kaisi, M., Lal, R. and Cihacek, L. Impact of soil erosion on soil organic carbon stocks. *J Soil Water Conserv. 71*(3), 61A-67A (2016). https://doi.org/10.2489/jswc.71.3.61A.
13. Gebresamuel, G. et al. Changes in soil organic carbon stock and nutrient status after conversion of pasture land to cultivated land in semi-arid areas of northern Ethiopia. *Arch Agron Soil Sci 68*(1), 44–60 (2022). https://doi.org/10.1080/03650340.2020.1823372
14. Alewoye, G. M., Legesse, S. A., Mekonnen, M. and Aschalew, A. Soil properties and crop productivity strategies as a potential climate variability adaptation options in Adefwuha watershed, Ethiopia. *Earth Syst Environ 4*(2), 359–68 (2020). https://doi.org/10.1007/s41748-020-00156-8
15. Anshori, A., Suswatiningsih, T. E. and Mujiyo, S. Traditions of soil and water conservation based on farmer knowledge as an adaptation to climate condition in dry land. *IOP Conf Ser Earth Environ Sci. 1165*(1), (2023). https://doi.org/10.1088/1755-1315/1165/1/012038
16. Jat, M. et al. Carbon sequestration potential, challenges, and strategies towards climate action in smallholder agricultural systems of South Asia. *Crop Environ 1*(1), 86–101 (2022). https://doi.org/10.1016/j.crope.2022.03.005
17. Mahajan, G. et al. Soil and water conservation measures improve soil carbon sequestration and soil quality under cashews. *Int J Sediment Res 36*(2), 190–206 (2021). https://www.sciencedirect.com/science/article/pii/S1001627920300810
18. Shelar, R., Nandgude, S., Tiwari, M., Gorantiwar, S. and Atre, A. Impact assessment of soil and water conservation measures on carbon sequestration: a case study for the tropical watershed using advanced geospatial techniques. *Sustain. 15*(1) (2023) https://doi.org/10.3390/su15010531.

19. Mohammed, M., Takele, G. and Kibret, K. Effects of physical soil and water conservation structures and slope gradients on soil physicochemical properties in West Oromia, Ethiopia. *Int J Soil Sci. 15*(1), 1–7 (2020).
20. Alemayehu, T. and Fisseha, G. Effects of soil and water conservation practices on selected soil physico-chemical properties in Debre-Yakob Micro-Watershed, Northwest Ethiopia. *Ethiop J Sci Technol. 11*(1), 29 (2018). https://doi.org/10.4314/ejst.v11i1.3
21. Hailu, L and Betemariyam, M. Comparison of soil organic carbon and total nitrogen stocks between farmland treated with three and six years level soil bund and adjacent farmland without conservation measure: in the case of southwestern Ethiopia. *PLoS One 16*(5), (2021). https://doi.org/10.1371/journal.pone.0252123
22. Hishe, S., Lyimo, J. and Bewket, W. Soil and water conservation effects on soil properties in the Middle Silluh Valley, northern Ethiopia. I*nt Soil Water Conserv Res. 5*(3), 231–40 (2017). https://www.sciencedirect.com/science/article/pii/S2095633917300679
23. Tanto, T. and Laekemariam, F. Impacts of soil and water conservation practices on soil property and wheat productivity in Southern Ethiopia. *Environ Syst Res. 8*(1), (2019). https://doi.org/10.1186/s40068-019-0142-4
24. Sinore, T. and Doboch, D. Effects of soil and water conservation at different landscape positions on soil properties and farmers' perception in hobicheka sub-watershed, southern Ethiopia. *Appl Environ Soil Sci. 2021*(1), 1-12 (2021). https://doi.org/10.1155/2021/9295650
25. Sinore, T., Kissi E. and Aticho, A. The effects of biological soil conservation practices and community perception toward these practices in the Lemo District of Southern Ethiopia. *Int Soil Water Conserv Res 6*(2), 123–130 (2018). http://dx.doi.org/10.1016/j.iswcr.2018.01.004
26. Belayneh, M., Yirgu, T. and Tsegaye, D. Effects of soil and water conservation practices on soil physicochemical properties in Gumara watershed, Upper Blue Nile Basin, Ethiopia. *Ecol Process. 8*(1), (2019). https://doi.org/10.1186/s13717-019-0188-2.
27. Belay, A. and Eyasu, E. Effect of soil and water conservation (SWC) measures on soil nutrient and moisture status, a case of two selected watersheds. *J Agric Ext Rural Dev. 11*(4), 85–93 (2019). https://doi.org/10.5897/jaerd2017.0862
28. Gadisa, S. and Hailu, L. Effect of level soil bund and Fayna Juu on soil physico-chemical properties, and farmers adoption towards the practice at Dale Wabera District, western Ethiopia. *Am J Environ Prot. 9*(5), 107 (2020). https://doi.org/10.11648/j.ajep.20200905.12
29. Hailu, W. Impact of physical soil and water conservation structure on selected soil physicochemical properties in Gondar Zuriya Woreda. *Resour Enviroment. 7*(2), 40-48 (2017).
30. Mesfin, S. et al. Short-term effects of bench terraces on selected soil physical and chemical properties: landscape improvement for hillside farming in semi-arid areas of northern Ethiopia. *Environ Earth Sci 77*(11), 399 (2018). https://doi.org/10.1007/s12665-018-7528-x
31. Amare, T. et al. Soil properties and crop yields along the terraces and toposequece of Anjeni Watershed, Central highlands of Ethiopia. *J Agric Sci. 5*(2), 134–144 (2013). https://doi.org/10.5539/jas.v5n2p134
32. Seid, H., Fekadu, E. and Yimam, F. Age of soil and water conservation practices on selected soil properties along the toposequence of Gerado Watershed , Habru District , Eastern Amhara , Ethiopia. *Appl Environ Soil Sci. 2024*(1), 1–10 (2024).
33. Wolka, K., Moges, A. and Yimer, F. Effects of level soil bunds and stone bunds on soil properties and its implications for crop production: the case of Bokole watershed, Dawuro zone, Southern Ethiopia. *Agric Sci. 02*(03), 357–363 (2011). https://doi.org/10.4236/as.2011.23047
34. Guadie, M., Molla, E., Mekonnen, M. and Cerdà, A. Effects of soil bund and stone-faced soil bund on soil physicochemical properties and crop yield under rain-fed conditions of Northwest Ethiopia. *Land. 9*(1), 1–15 (2020). https://doi.org/10.3390/land9010013
35. Alemayehu, A. A., Getu, L. A. and Addis, H. K. Impacts of stone bunds on selected soil properties and crop yield in Gumara-Maksegnit watershed Northern Ethiopia. *Cogent Food Agric. 6*(1), 1–16 (2020). https://doi.org/10.1080/23311932.2020.1785777
36. Tesfay G, et al. Participatory rural appraisal report: Raya-Alamata woreda, Tigray region. *CASCAPE working paper* 2.6.4. (ResearchGate, 2014).
37. Ayenew, A. and Memhur, A. *Baseline survey of Endamehoni woreda of Tigray Region* (CMP, 2014).
38. Gebremeskel, Y., Gebrehiwot, W. and Gebresamuel, G. *CASCAPE experiences in integrated soil fertility and nutrient management in Southern Tigray* (CASCAPE, 2020). https://doi.org/10.13140/RG.2.2.20430.59201
39. Zenebe, A., Gebresamuel, G. and Atkilt, G. Characterisation of agricultural soils in Cascape intervention woredas in southern Tigray , Ethiopia (Hawassa Univ., 2015).
40. Husen, D., Esimo, F. and Getechew, F. Effects of soil bund on soil physical and chemical properties in Arsi Negelle woreda, Central Ethiopia. *African J Environ Sci Technol. 11*(10), 509–516 (2017).
41. Mengistu, D., Bewket, W. and Lal, R. Conservation effects on soil quality and climate change adaptability of Ethiopian watersheds. *L Degrad Dev. 27*(6), 1603-1621 (2016). https://doi.org/10.1002/ldr.2376
42. Mekonnen, M. Impacts of soil and water conservation practices after half of a generation age, northwest highlands of Ethiopia. *Soil Tillage Res*. *205*:104755, (2021). https://doi.org/10.1016/j.still.2020.104755
43. Miheretu, B. A. and Yimer, A. A. Spatial variability of selected soil properties in relation to land use and slope position in Gelana sub-watershed, Northern highlands of Ethiopia. *Phys Geogr 39*(3), 230–245 (2018).

https://doi.org/10.1080/02723646.2017.1380972
44. Mekuria, W. et al. Restoration of degraded landscapes for ecosystem services in North-Western Ethiopia. *Heliyon 4*(8), e00764 (2018). https://www.sciencedirect.com/science/article/pii/S2405844018307321
45. Retta, M. A., Addis, H. K. and Beyene, T. F. Impact of soil and water conservation measures and slope position on selected soil attributes at a watershed scale. *Appl Environ Soil Sci. 2022*(1), 1–11 (2022). https://doi.org/10.1155/2022/9743511
46. Yaebiyo, G., Kifle, M. and Darcha, G. Effect of soil and water conservation on rehabilitation of degraded lands and crop productivity in Maego watershed, North Ethiopia. *J Degrad Min Lands Manag*. *5*, 1191–205 (2018). https://doi.org/10.15243/jdmlm.2018.053.1191
47. Bekele, W., Alemayehu, G. and Kebede, M. Soil bunds effect on soil properties under different topographies of Southwest Ethiopia. *J Environ Earth Sci. 04*(01), 54–63 (2022).
48. Muktar, M., Bobe, B., Kibebew, K. and Yared, M. Soil organic carbon stock under different land use types in Kersa sub watershed, Eastern Ethiopia. *African J Agric Res. 13*(24), 1248–1256 (2018). https://doi.org/10.5897/ajar2018.13190
49. Okolo, C. et al. Soil organic carbon, total nitrogen stocks and CO_2 emissions in top- and subsoils with contrasting management regimes in semi-arid environments. *Sci Rep. 13*:1117, (2023).
50. Gebeyehu, G. and Soromessa, T. Status of soil organic carbon and nitrogen stocks in Koga Watershed Area, Northwest Ethiopia. *Agric Food Secur. 7*(1):9, (2018). https://doi.org/10.1186/s40066-018-0162-8

5th International Conference of Hyojeong Academy
International Joint Conference 2025

Effect of Faidherbia albida trees on teff grain and soil micronutrients

Gebrekiros Gebremedhin[1,4*], Emiru Birhane[2, 3, 4], Amanuel Zenebe[2,4] and Philip J. Semethurst[5]

[1]Tigray Agricultural Research Institute, Abergele Agricultural Research Center, Ethiopia
[2]Department of Land Resource Management and Environmental Protection, Mekelle University, Tigray, Ethiopia
[3]Faculty of Bioscience and Aquaculture, Nord University, P.O. Box 2501, NO-7729 Steinkjer, Norway
[4]Institute of Climate and Society, Mekelle University
[5]CSIRO Forestry and Forest Products, Hobart TAS 7001, Australia
*Correspondence: kiroskey@gmail.com

Abstract: Agroforestry trees have the potential to positively influence the microclimate, and soil physicochemical properties thereby increase crop yield and grain nutrients underneath. A field experiment was executed to collect soil and grain samples from controlled plots under and outside canopy of the Faidherbia albida trees. The soil and teff grain samples were extracted using diethylene triamine penta acetic acid (DTPA) method and measured their nutrient concentration using atomic absorption spectrometry (AAS) and flame method. The collected data was analyzed using an independent sample t-test, correlation and regression analysis using SPSS and AMOS software's. The soil micronutrients were significantly higher beneath than outside canopy of the F. albida trees. This was attributed to the existing higher soil physicochemical properties beneath the canopy of F. albida trees. Similarly, the soil physicochemical properties had significant and positive associations with the availability of soil micronutrients. Apart from the soil micronutrients, significantly higher concentrations of teff grain iron, zinc, and manganese were obtained beneath the canopy of F. albida trees. In general, F. albida trees improved the soil and teff grain micronutrients through improving the physicochemical properties of the soil underneath. Hence, agroforestry species that improve soil physicochemical properties could enhance soil and grain micronutrients.

Keywords: AAS, agroforestry, canopy, DTPA, micronutrients, teff

1. Introduction

Micronutrients are essential for crop growth and development even if their requirement is small. Several edaphic, environmental, genetic, and management factors affect the availability of nutrients in soil and crop grains. One of the environmental factors that might influence the microclimate and the physicochemical characteristics of the soil is agroforestry [1]. The mechanisms through which agroforestry contributes to higher soil physicochemical properties below the canopy include lowering soil erosion, retaining moisture, improving soil structure and nutrients by adding litter fall, and lowering temperature, root exudates, and decompositions. Additionally, trees take up nutrients from the soil's deeper layer and move them to the top layer [2]. These agroforestry attributes improve soil organic matter, cation exchange capacity, total nitrogen, available phosphorus, and soil moisture content under different agroforestry systems compared with their respective open areas [3]. These variations in soil factors beneath and outside the canopy of agroforestry tree species could concurrently affect the availability of soil and crop grain micronutrients. However, research attempts on investigating grain micronutrient contents of teff grown in association with *F. albida* trees is scarce. Hence, the objectives of this study were (1) to assess the effect of *F. albida* trees on soil micronutrients, (2) to explore the effect of *F. albida* trees on teff grain micronutrient concentrations, and (3) to develop relationships between the soil physicochemical properties and the micronutrients.

2. Materials and Methods

The study was conducted in North Ethiopia, at a specific site called Zongi. It is located between 13°59' - 14°02' N and 38°59'-39°02' E. The area is well known in teff (Quncho) cultivation integrated with *F. albida*-based traditional agroforestry system. Twelve *F. albida* trees with uniform growth parameters (height, diameter, crown size and shape) were selected. Soil samples (0-30 cm depth) were collected from beneath and outside (15 meters

from canopy edge) of these trees to analyze selected physical and chemical soil properties. Soil moisture content was estimated at the sowing and grain-filling stages of the crop. The soil moisture content was computed by subtracting weight of oven dry soil from the weight of wet soil and dividing to the weight of oven dry soil multiplied by hundred. Besides, teff grain samples were collected from twenty-four plots (1 x1 meter) beneath and outside canopy of the *F. albida* trees. The samples were hand-threshed inside cloth bags to avoid soil contamination. The soil and grain samples were extracted by diethylene triamine penta acetic acid (DTPA) method [4]. The ashing method [5] was used to prepare the teff grain samples to extract available micronutrients using the DTPA method. Besides, tri ethanolamine (TEA) was used as a chelating agent during the soil and grain micronutrient extractions. After the DTPA extraction, the concentrations of iron, zinc, copper, and manganese were measured by atomic absorption spectrometry (AAS), and the flame photometer method for boron concentration.

2.1. Statistical data analysis

The collected data was checked against the assumptions of parametric tests. Shapiro Wilk and Levens tests were used to assess normality and homogeneity of variance respectively. The soil micronutrients manganese, copper, and boron were Ln transformed. An independent sample t-test was used to assess the mean difference in soil and grain nutrient concentrations under and outside the canopy of F. albida trees. Moreover, the Mann-Whitney U test was used to analyze grain iron and copper. Pearson correlation coefficient was employed to evaluate the relationship between the soil micronutrients and soil factors. Besides, the IBM SPSS - AMOS was used to develop a structural regression model between soil moisture content and the soil micronutrients. Model fitness was assessed by the comparative fitness index (CFI), Tucker-Lewis's coefficient (TLI), root mean square error of approximation (RMSEA) and minimum discrepancy divided by its degrees of freedom (CMIN/DF).

3. Results

3.1. Soil and teff grain micronutrients beneath F. albida trees

Available soil micronutrients significantly varied between outside and beneath the canopy of the *F. albida* trees ($p < 0.05$). The higher nutrient concentrations beneath the canopy of *F. albida* trees could be attributed to the different nutrient retention and addition nature of the trees. Manganese and iron had relatively the highest concentration values compared to the other micronutrients (Figure 1(a)). *F. albida* trees significantly ($p < 0.05$) improved the availability of teff grain iron, zinc, and manganese concentrations compared to the control. However, there was no significant difference in extractable boron and copper between the outside and under the canopy of the *F. albida* trees ($p > 0.05$). The amount of DTPA extractable nutrients in teff grain was low compared with its availability in the soil (Figure 1(b)). The different soil factors, such as pH, soil organic matter, temperature, and moisture affect the availability of micronutrients to crops [6]. Teff grown under the canopy of *F. albida* trees takes a long time to mature, which gives time to capture more nutrients from the soil. On the contrary, plots outside the canopy of the trees face moisture shortages and mature earlier than crops grown beneath the canopy of the trees.

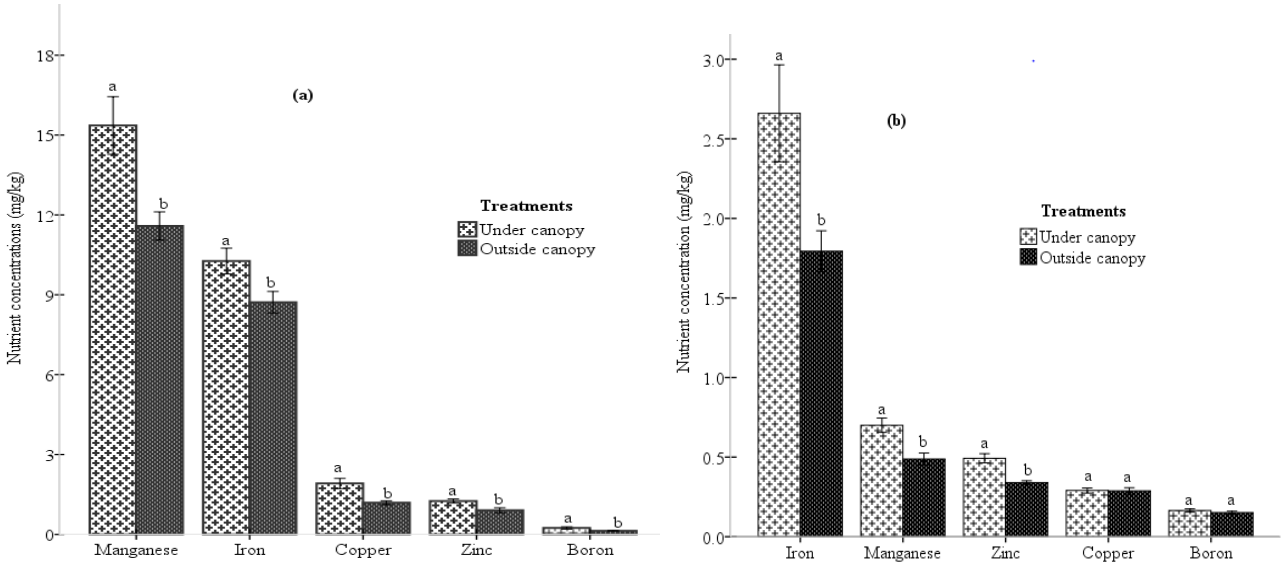

Figure 1. Soil (a) and teff grain (b) micronutrients beneath and outside the canopy of *F. albida* trees.

3.2. Soil moisture and micronutrients

The canopy of the *F. albida* trees had a significant effect ($p < 0.01$) on the soil moisture content. The soil moisture beneath the canopy was 57% higher than its respective outside canopy. This is associated with the availability of higher soil organic carbon beneath the canopy which improves water-holding capacity of the soil while the shade also reduces evapotranspiration. This was further supported by the positive and strong correlation ($r = 0.61$) between the soil moisture content and the soil physicochemical properties (Figure 2). The structural regression model disclosed that soil physicochemical properties and the moisture content explain 95% of the soil micronutrient variability. The soil micronutrients copper and boron revealed a higher coefficient of determination (r^2) than iron, zinc and manganese. This indicates that the availability of copper and boron micronutrients is mostly explained by soil moisture compared to the others. The model constructs produced in Figure 2 have achieved better CFI, TLI, GFI, RMSEA, and CMIN/DF fitness indexes. In Figure 2, SM represents soil moisture and the e stand for other exogenous variables which are not included in the model (error term). The rectangles represent observed (endogenous) variables and the ellipse represents the latent (unobserved) variables. Moreover, the single-headed and double-headed arrows represent for regression and covariance respectively.

Figure 2. The standardized regression path coefficients between the structural model constructs.

4. Discussion

There is sufficient evidence that agroforestry species can alter soil physicochemical properties and the microclimate underneath [7]. Agroforestry maintains and increases available plant nutrients by reducing nutrient losses [8], nitrogen fixation, litter, and biomass addition and decomposition [9] and creating favorable microclimate [10]. Moreover, trees absorb nutrients from deeper soil layers and return to the topsoil [7, 11]. These factors under the canopy of the trees concurrently affect the availability of soil micronutrients. The current study similarly discloses significantly higher soil micronutrients beneath than outside the canopy of *F. albida* trees. The availability of higher soil micronutrients beneath than outside canopy was attributed to the higher organic matter, low soil pH, and low available phosphorus [12]. Consistent with these studies, the soil physicochemical properties beneath the canopy of *F. albida* trees significantly improved available soil micronutrients compared with the outside canopy of the *F. albida* trees. Differently, Abewa et al. [13] reported lower soil micronutrients under agroforestry systems than sole crops. Significantly higher teff grain micronutrients were obtained beneath the canopy of *F. albida* trees. Literatures consistently depicted higher iron and zinc contents of wheat grain near forests than in open areas [14]. On the contrary, lower grain micronutrients of barley [2] and wheat [15] were reported under poplar plantations and near eucalyptus trees respectively. Similarly, Dahiya et al. [16] reported lower wheat and barley grain nutrients under different agroforestry systems than the sole crops. This could be attributed to the difference in tree crop interactions. In general, teff grain nutrient concentration values of this study were comparable with Arredondo et al. [17] and lower than the results of Gashu et al. [14].

The soil pH, CEC, soil moisture content, and available phosphorus significantly ($p < 0.01$) predicted the availability of soil boron. The soil pH had the highest model importance value, followed by available phosphorus, soil moisture, and cation exchange capacity. According to Arredondo et al. [17] soil pH is the primary factor in determining the bioavailability of soil boron. The soil organic carbon and CEC significantly predicted soil copper. The CEC retains cations from leaching and provides essential nutrients from the roots of plants via the exchange of H^+ ions [6]. Similarly, available phosphorus and soil moisture content significantly ($p < 0.05$) predicted the availability of soil zinc with uniform importance values. The soil moisture had a positive influence on the

availability of zinc. This was consistent with Alloway et al. [18] who reported soil moisture content and phosphorus as predictor variables of soil available zinc. Soil phosphorus can stimulate either root growth and zinc uptake or precipitate to form insoluble zinc phosphate and trigger deficiency. In contrast, Botoman et al. [19] identified soil pH and organic matter as predictor variables of soil zinc. Soil micronutrients are most available under acid conditions (pH < 5.5) but at a higher pH, the ionic forms of the cations precipitate into oxide or hydroxide forms and reduce their bioavailability [6, 12]. The soil pH in our study site was greater than 5.5, and it had a negative impact on the availability of the micronutrients (Table 2). Apart from soil pH, most soil factors had significant and positive correlations with soil micronutrients. Soil moisture content and organic carbon were significantly correlated with iron, zinc, manganese, copper, and boron micronutrients and this is consistent with the reports of Botoman et al. [19]. The soil micronutrients were also significantly correlated with the total nitrogen [20]. The higher available soil phosphorus reduces the availability of micronutrients and cations [6,17], which is consistent with some micronutrients of this study (Table 4). As a concluding remark, the growing environment (beneath the canopy of *F. albida* trees) has significantly affected the soil and teff grain micronutrient concentrations under similar management and with the same crop variety. Significantly, higher teff grain and soil micronutrient concentrations were obtained under the canopy of *F. albida* trees. This was mainly attributed to the availability of higher organic carbon, total nitrogen, soil moisture and CEC values beneath the canopy of the trees. This finding suggests that micronutrient deficiencies can be decreased by preserving and incorporating *F. albida* trees into croplands.

Author Contributions: Gebrekiros Gebremedhin and Emiru Birhane, conceptualize the methodology, analyze, investigate, write, review and edit the manuscript. Amanuel Zenebe and Philip J. Semethurst review, edit, supervise the work. All authors have read and agreed on the prepared manuscript.

Funding: This research was funded by the Institute of International Education-Scholars Rescue Fund (IIE-SRF), and Nord University, Faculty of Bioscience and Aquaculture (FBA) for supporting the research stay of Emiru Birhane at Nord University. Moreover, it was also funded by Tigray Agricultural Research Institute (TARI), FSRP project, and Mekelle University (MU).

Acknowledgments: The authors would like to acknowledge, Abergelle agricultural research center, Mekelle soil research center particularly Dr. Bereket Haileselassie and Lijalem Gebregzabiher, district farmers and development agents.

Conflicts of Interest: The authors declare no conflict of interest

References

1. Sirohi, C., Bangarwa, K.S., Dhillon, R.S., Chavan, S.B. and Handa, A.K. Productivity of wheat (Triticum aestivum L.) and soil fertility with poplar (populus deltoids) agroforestry system in the semi-arid ecosystem of Haryana, India. *Current Science* 122(*9*), 1072-1080 (2022). doi: 10.18520/cs/v122/i9/1072-1080.
2. Kumar, et al. Status of soil and plant micronutrients and their uptake by barley varieties intercropped with Populus deltoides plantation. *ECJ*. 23(*3*),14-22 (2022). doi: 10.36953/ECJ.11422296.
3. Hailie, S.W., Lemma, B. and Mengistu, T. Effects of Ziziphus Spina-Christi (L.) on selected soil properties and Sorghum yield in Habru District, North Wollo, Ethiopia. *MJMBR* 6(*2*), 85-92 (2019). doi: 10.18034/mjmbr.v6i2.477.
4. Lindsay, W.L. and Norvella, W.A. Development of a DTPA soil test for zinc, iron, manganese, and copper. *Soil Sci. Soc. Am. J.* 42(*3*), 421-428 (1978). doi: 10.2136/sssaj1978.03615995004200030009x.
5. Chibarabada, T.P., Modi, A.T. and Mabhaudhi, T. Nutrient Content and Nutritional Water Productivity of Selected Grain Legumes in Response to Production Environment. *Int.J.Environ.Res.Public Health. 14*(11), 1300 (2017). doi: 10.3390/ijerph14111300.
6. Fageria, N.K, Baligar, V.C. and Clark, R.B. Micronutrients in crop production. *Advances in Agronomy 77*, 185-268 (2002). doi: 10.1016/S0065-2113(02)77015-6.
7. Felton, M., Jones, P. and Tranter, R. Farmers' attitudes towards, and intentions to adopt, agroforestry on farms in lowland South-East and East England. *j.landusepol. 131* (2023). doi: 10.1016/j.landusepol.2023.106668.
8. Smethurst, et al. Accurate crop yield predictions from modeling tree-crop interactions in gliricidia-maize agroforestry. *j.agsy. 155*, 70–77 (2017). doi: 10.1016/j.agsy.2017.04.008.
9. Sida, T.S, Baudron, F., Ndoli, A., Tirfessa, D. and Giller, K.E. Should fertilizer recommendations be adapted to parkland agroforestry systems? Case studies from Ethiopia and Rwanda. *Plant and Soil 453*(1-2), 173-188 (2020). doi: 10.1007/s11104-019-04271-y.
10. Nesper, M., Kueffer, C., Krishnan, S., Kushalappa, C. and Ghazoul, J. Simplification of shade tree diversity reduces nutrient cycling resilience in coffee agroforestry. *J Appl Ecol. 56*, 119–131 (2018). doi: 10.1111/1365-2664.13176
11. Kaur, et al. The Role of Agroforestry in Soil Conservation and Sustainable Crop Production: A Comprehensive Review. *IJECC 13*(11), 3089-3095 (2023). doi: 10.9734/IJECC/2023/v13i113478

12. Zhuo, Z., Xing. A., Li, Y., Huang, Y. and Nie, C. Spatio-Temporal Variability and the Factors Influencing Soil-Available Heavy Metal Micronutrients in Different Agricultural Sub-Catchments. *Sustainability 11*(21), 5912 (2019). doi:10.3390/su11215912.
13. Abewa, A. et al. Teff grain physical and chemical quality responses to soil physicochemical properties and the environment, *Agronomy 9*(6), 283 (2019). doi: 10.3390/agronomy9060283
14. Gashu, D. et al. The nutritional quality of cereals varies geospatially in Ethiopia and Malawi. *Nature 594*, 71-76 (2021). doi: 10.1038/s41586-021-03559-3.
15. Gill, R., Singh, B. and Kaur, N. Productivity and nutrient uptake of newly released wheat varieties at different sowing times under poplar plantation in Northwestern India. *Agroforest Syst 76*(3), 579–590 (2009). doi: 10.1007/s10457-009-9223-0.
16. Dahiya, G. et al. Influence of different agroforestry systems on crop yield and nutrient uptake in semi-arid region of Haryana. *Eco. Env. & Cons. 28*(2), 984-988 (2022). doi: 10.53550/EEC.2022.v28i02.062
17. Arredondo, G. and Bonomelli, C. Effect of three boron concentrations on growth and physiology in sweet cherry trees. *Plants 12*(6), 1240 (2023). doi: 10.3390/plants12061240
18. Alloway, B.J. Soil factors associated with zinc deficiency in crops and humans. *Environ. Geochem, Health 31*, 537-548 (2009). doi: 10.1007/s10653-009-9255-4
19. Botoman, L. et al. Agronomic biofortification increases grain zinc concentration of maize grown under contrasting soil types in Malawi. *Plant Direct 6*(11): e458 (2022). doi: 10.1002/pld3.458.
20. Wei, L. et al. Comparing carbon and nitrogen stocks in paddy and upland soils: accumulation, stabilization mechanisms, and environmental drivers. *Geoderma 398*, 115121 (2021). doi: 10.1016/j.geoderma.2021.115121

5th International Conference of Hyojeong Academy
International Joint Conference 2025

Arbuscular mycorrhizal fungi reduce lodging of tef [Eragrostis tef (Zucc.) Trotter] under N fertilizer applications

Kidu Gebremeskel[1,*], Emiru Birhane[1, 2, 3], Zerihun Tadele[4], Solomon Habtu[1], Mitiku Haile[1], Solomon Chanyalew[5] and Kbebew Assefa[5]

[1]Department of Land Resource Management and Environmental Protection, Mekelle University, Mekelle, Ethiopia,
[2]Institute of Climate and Society, Mekelle University
[3]Faculty of Bioscience and Aquaculture, Nord University, Steinkjer, Norway
[4] University of Bern, Institute of Plant Sciences, Altenbergrain 21, CH-3013 Bern, Switzerland
[5]Ethiopian Institute of Agricultural Research, Addis Ababa, Ethiopia
[*]Correspondence: kidu1136@gmail.com

Abstract: Lodging in tef reduces yield, and N application worsens its impact. This study assesses the combined effects of arbuscular mycorrhizal fungi (AMF) and N fertilizer on lodging and yield in tef. Two groups of AMF (Inoculated and non-inoculated) and five levels of N (0, 46, 92, 138, and 184 kg/ha) were arranged in two consecutive years. The analysis of variance revealed that plant height (PH), panicle length (PL), total number of tillers (TNT), lodging index (LI), shoot biomass yield (SBY), grain yield (GY), and harvest index (HI) were significantly influenced by AMF, N levels, and their interactions ($P< 0.05$). AMF inoculated groups increased PH by 59.87%, PL by 18.20%, TNT by 87.13%, SBY by 30.14%, GY by 37.60%, HI by 10.71, and reduced LI by 229.63%, as compared to the non-inoculated. AMF-inoculated groups did not show a change in LI with increasing N levels, indicating AMF inoculations minimize the impact of excessive N application from causing lodging. In contrast, non-inoculation showed a trend of increasing LI with higher N levels, reducing yield. AMF-inoculated tef crops do not experience lodging, even with higher N levels which can help prevent yield loss caused by lodging from N application.

Keywords: Tef lodging, Excessive N, Symbiosis, Inoculation, Arbuscular mycorrhizal fungi

1. Introduction

Eragrostis tef, commonly known as tef, is an important ancient cereal crop in Ethiopia, cultivated on about 2.9 million hectares and serving over 85 million people [1]. Its gluten-free grain is gaining global attention, especially among those with celiac disease [2]. However, tef's average yield of only 1.9 tons per hectare is significantly lower than that of wheat and maize in the region [3]. Factors contributing to this low productivity include limited use of advanced agricultural technologies [4], susceptibility to lodging [5], poor soil fertility [6], blanket fertilizer recommendations and unpredictable rainfall due to climate change [7]. The small size of tef seeds requires shallow planting, which can hinder root development and increase the risk of lodging [8, 9]. Notably, lodging can result in up to 51% grain yield loss [10] and affects marketability [11]. To combat lodging, it's essential to examine traits such as internode diameter and culm length, as thicker internodes and shorter culms can enhance lodging resistance [12, 13]. Although nitrogen is vital for crop growth, its excessive use can lead to adverse outcomes such as lodging and increased costs [14]. Therefore, optimizing nitrogen application is crucial for maximizing yield while minimizing lodging risks. Soil microbes, particularly AMF, promote root growth and improve nutrient uptake, which can strengthen root morphological growths [15-17]. AMF enhances phosphorus availability and aids in nitrogen uptake, leading to improved growth and balanced root-to-shoot ratios [18-21]. Increased N fertilizer is vital for tef growth, but excessive N also heightens the risk of lodging [14, 22]. Consequently, it is essential to develop strategies that balance N application to maximize grain yield while minimizing the likelihood of lodging. Understanding the relationship between N levels and lodging risk is crucial for optimizing yield without leading to lodging issues. Previous research has indicated that tef is a mycorrhizal plant. However, the combined effects of AMF and N fertilizer levels on reducing the risk of lodging and maximizing yield through optimal N fertilizer application are unknown. This study addressed the following objectives: 1) Establish the interaction effects of AMF and N levels on yield and yield traits, 2) Determine the interaction effects of AMF and N levels on

the level of lodging, 3) Analyze the relationship among N, lodging, and yield under AMF conditions, and 4) Identifying the optimum level of N fertilizer for both AMF conditions.

2. Materials and Methods

2.1. Description of Study Sites

The research was conducted in the Dura district at the Axum Agricultural Research Center, located at 14°06'22"N, 38°39'57"E and an altitude of 2042 meters, and in the Kara Adishaho district at the Mokhoni Agricultural Research Center, positioned at 12°44'13"N, 39°43'25"E, at 1750 meters above sea level. The study covered two consecutive irrigation cropping seasons from October 2021 to April 2022. The soil types in Dura and Kara Adishaho were identified as Haplic vertisols and Haplic leptosols, respectively. Both agroecological zones range from tepid sub-moist lowland to mid-highland, influenced by growing period, temperature, and altitude. Mixed crop and livestock farming dominate these areas, with tef as the primary rain-fed cereal crop. Notably, there is an increasing trend in irrigated tef cultivation, reflecting advances in agricultural practices in the region.

2.2. Experimental Materials and Treatments

The "*Kora*"tef variety seed was obtained from the Debre Zeit Agricultural Research Center, known to yield between 2 and 2.8 tons per hectare under rain-fed conditions [23]. The AMF inoculum was prepared following Birhane, Sterck [24]. In this study, seedlings were classified as "Inoculated" when they received approximately 400 AMF spores, while those without inoculum were "non-inoculated." The seedlings were exposed to five nitrogen fertilizer levels (0, 46, 92, 138, and 184 kg/ha), resulting in ten treatment combinations using urea (46% N). The design was a factorial randomized complete block, with each treatment replicated three times per location and season. Each plot measured 4 m x 2 m (8 m²) with ten rows, and spacing between blocks, plots, and rows was 1.5 m, 1.2 m, and 0.15 m, respectively. Data collection focused on the eight central rows, resulting in a net plot size of 6.4 m².

2.3. Sampling procedure and data collection

Fertilization followed soil test recommendations [25], with nitrogen applied in two phases for non-control treatments: during the first two weeks post-transplanting and at tiller initiation [26]. While all treatments received identical nutrients, nitrogen application varied according to the Ethiopian Soil Information System guidelines. CROPWAT software version 8.1 was used to calculate and schedule crop water requirements (ETc) based on FAO procedures [27]. The growing period for tef was 120 days, with an average rooting depth of 40 cm, and water stress factors referenced from FAO sources. Soil nutrient demands and climate data were obtained from regional meteorological stations, aligning irrigation with ETc estimates. Soil samples, taken at a 0-20 cm depth, were analyzed for physical and chemical properties, with AMF spores extracted from half [24]. Vegetative growth and yield data were collected from experimental plots, measuring plant height (PH) and panicle length (PL) from ten randomly selected plants per plot. Total number of tillers (TNT) was recorded from tagged plants. Shoot Biomass Yield (SBY) was determined by weighing the entire plant mass, while Grain Yield (GY) was harvested from a central plot to minimize border effects. The Harvest Index (HI) was calculated as the ratio of grain yield to shoot biomass yield. The lodging index (LI) was assessed based on severity prior to harvest [28], using a scale from 0 (no lodging) to 4 (complete lodging), with averages calculated for each plot.

2.4. Statistical Analysis

We examined growth and yield response variables, including PH, PL, TNT, SBY, GY, HI, and LI. Data analysis was performed using R-statistical software version 4.2.3 [29], ensuring ANOVA assumptions were met through the Global Variability of Linear Model Assumptions (GVLMA) procedure. The LI was square root transformed for normality. Mean comparisons were conducted using the least significance difference test at the 5% significance level, following Gomez and Gomez [30]. This approach strengthens our findings and conclusions.

3. Results

3.1. Effects on response variables (PH, PL, TNT)

The AMF-inoculated group exhibited significant increases in PH by 59.87%, PL by 18.20%, and TNT by 87.13% compared to non-inoculated groups. A clear upward trend was observed as N application increased from 0 to 184 kg/ha, resulting in enhancements of 75.28% in PH, 47.31% in PL, and 191.68% in TNT. The highest values for PH, PL, and TNT were noted in the inoculated group at 184 kg/ha, while the lowest were in non-inoculated groups receiving 0 kg/ha.

In both groups, increasing N consistently boosted growth metrics, though no significant change in PH was seen in the inoculated group between 138 and 184 kg/ha. The overall changes in PH ranged from 1.29% to 175.66%, PL from 3.20% to 69.99%, and TNT from 7.41% to 566.67%.

3.2. Effect of AMF and N level on Lodging Index

The interaction analysis of AMF and N levels indicated that non-inoculated groups receiving 184 kg/ha of N had the highest LI at 28.25% (5.27), followed by 138 kg/ha of N at 17.86% (4.17). Inoculated groups receiving 0 kg/ha of N showed a lower LI of 1% (0.71), highlighting the effectiveness of AMF in reducing LI, particularly at higher N levels (Table 1). Non-inoculated groups showed a significant increase in LI as N levels rose from 0 to 184 kg/ha, while inoculated groups maintained lower LIs despite increasing N. This suggests that AMF can help mitigate lodging effects associated with higher N fertilization, supporting the optimization of N levels in tef cultivation with AMF (Table 1).

Table 1. The main and interaction effects of AMF and N fertilizer levels on plant height (PH cm), panicle length (PL cm), total number of tillers (TNT), lodging index (LI), shoot biomass yield (SBY kg/ha), grain yield (GY kg/ha), and harvest index (HI) of tef grown in two districts (*Dura* and *Kara Adishaho*) in Tigray, Ethiopia during the 2021-2022 irrigation cropping season

Source of variations	PH	PL	TNT	LI	SBY	GY	HI	
AMF	Inoculated	114.95 a	52.40a	15.12	1.67 (1.08 b)	9078.43 a	2788.36 a	0.31 a
	non-inoculated	71.90 b	44.33b	8.08	13.17 (3.56 a)	6975.83 b	2026.37 b	0.28 b
LSD (5%)		0.86	0.64	0.56	0.29	104.95	88.42	0.01
N	0	65.54 e	38.13 e	5.77 e	1.21 (0.84 e)	6274.58 e	1683.21 d	0.26 b
	46	75.75 d	44.75 d	8.67 d	2.25 (1.32 d)	7120.42 d	2112.65 c	0.30 a
	92	96.04 c	48.42 c	11.71 c	3.74 (1.8 c)	8190.44 c	2494.49 b	0.30 a
	138	113.91 b	54.33 b	15.11 b	7.12 (2.57 b)	9187.53 b	2886.96 a	0.31 a
	184	115.88 a	56.17 a	16.83 a	12.06 (3.4 a)	9362.75 a	2860.64 a	0.30 a
LSD (5%)		1.35	0.98	0.88	0.47	166.96	155.62	0.02
AMF X N	Inoculated X 0	78.58 e	41.44 f	8.58 f	1 (0.71 f)	7122.51 e	2078.94 e	0.29 ab
	Inoculated X 46	88.41 c	50.51 d	12.17 de	1(0.71 f)	8120.83 d	2413.90 c	0.30 ab
	Inoculated X 92	120.08 b	53.75 c	15.75 c	1(0.71 f)	9212.51 c	2795.67 b	0.30 ab
	Inoculated X 138	142.91 a	57.16 b	18.75 b	1.46 (0.98 ef)	10340.11 b	3283.72 a	0.32 a
	Inoculated X 184	144.75 a	59.21 a	20.33 a	2.83 (1.53 de)	10596.33 a	3369.60 a	0.32 a
	non-inoculated X 0	52.51 h	34.83 h	3.0 h	1.46(0.98 ef)	5426.67 g	1287.62 g	0.24 c
	non-inoculated X 46	63.06 g	39.03 g	5.17 g	4.25 (1.94 d)	6120.10 f	1811.41 f	0.29 ab
	non-inoculated X 92	72.01 f	43.09 e	7.67 f	8.86 (2.89 c)	7168.33 e	2193.16 de	0.31 ab
	non-inoculated X 138	84.93 d	51.53 d	11.33 e	17.86 (4.17 b)	8035.43 d	2490.07 c	0.31ab
	non-inoculated X 184	87.21 c	53.18 c	13.33 d	28.25 (5.27 a)	8129.16 d	2352.68 cd	0.28 b
LSD (5%)		1.92	1.34	1.24	0.67	234.69	220.1	0.02
CV		2.57	3.46	13.14	18.91	3.65	11.37	11.21

AMF=Arbuscular Mycorrhizal Fungi: Inoculated groups received AMF inoculum, while non-inoculated groups did not; N=Nitrogen levels: 0, 46, 92, 138, and 184 kg/ha; Means sharing a common lowercase letter within

a column is not significantly different at p <0.05; Mean comparison was done using LSD (least significant difference) at 5%.

3.3. Effect of AMF and N Level on Shoot Biomass yield, Grain Yield, and Harvest Index

The analysis of AMF and N levels indicated that the highest SBY and GY were in the AMF-inoculated group receiving 184 kg/ha of N, while the lowest were in non-inoculated groups with 0 kg/ha N. SBY increased significantly in the inoculated group as N levels rose from 0 to 184 kg/ha, but this trend plateaued in non-inoculated groups beyond 138 kg/ha. GY also increased with N application up to 138 kg/ha, showing similar trends for both groups. Notably, the non-inoculated groups at 138 and 184 kg/ha N had no significant difference in SBY and GY compared to inoculated groups at 46 kg/ha, indicating that AMF inoculated groups could reduce N application by three to four times while achieving similar yields. Even 92 kg/ha N in non-inoculated groups was statistically comparable to 0 kg/ha in the inoculated groups, showing a two-fold reduction in N application with maintained yields. Inoculated groups showed the highest HI regardless of N levels, while non-inoculated groups had the lowest HI at 0 kg/ha N. Non-inoculated HI changed little with N increases, but decreased at higher N levels. Inoculated groups maintained a consistent HI, indicating AMF may optimize N for grain and biomass yields (Table1).

3.4. Relationships among Tef growth traits

The relationships among tef growth traits reveal significant positive correlations. HI correlates with SBY, TNT, PL, and PH, with coefficients of 0.41, 0.42, 0.41, and 0.39, respectively (Figure 1). GY shows strong correlations with HI, SBY, TNT, PL, and PH, with coefficients of 0.74, 0.91, 0.88, 0.85, and 0.88. SBY is also positively correlated with TNT, PL, and PH (coefficients of 0.95, 0.93, and 0.96). TNT shows strong positive correlations with PL and PH (0.92 and 0.93), while PL has a coefficient of 0.88. Overall, all traits exhibit positive correlations, ranging from 0.39 to 0.96, although LI showed no significant correlations with the other traits (Figure 1). The regression analysis showed a strong correlation between LI and N levels in the non-inoculated groups (p=0.001), with 98% of the variations in LI attributed to changes in N application (R^2=0.98). Increasing N fertilizer consistently raised the LI. However, no significant changes were observed in the LI with increasing N fertilizer application in the inoculated groups (R^2=0.06) as depicted in Figures 2(a) and 2(b). In the non-inoculated groups, an increase in LI led to a significant drop in SBY and GY, as shown in Figures 2(c) and 2(e). Conversely, the inoculated groups did not display a substantial impact on SBY and GY with changes in LI (p=0.05), as illustrated in Figures 2(d) and 2(f), which results suggested that the inoculation may have a mitigating effect on the relationship between LI and SBY/GY.

4. Discussion

4.1. Shoot traits

In groups inoculated with AMF and provided higher N levels, there was a significant increase in PH, PL, and TNT compared to non-inoculated groups with lower N applications. This improvement is likely due to AMF's ability to extend mycorrhizal networks, enhancing the uptake of nutrients including N [31, 32]. AMF might also tend to improve root architecture and biomass, enhancing overall nutrient and water uptake [32-34]. Additionally, AMF's strong affinity for P and the synergistic uptake of P and N during the vegetative stage [35] may lead to higher TNT. This supports the findings by Mulyadi and Jiang [36], which indicated that AMF-inoculated groups receiving higher N rates showed significant improvements in PH, PL, and TNT. The inoculated group showed no significant changes in the LI as N levels increased from 0 to 138 kg/ha, indicating a strong symbiotic relationship essential for cereal crops like tef, which are prone to lodging [5]. This relationship is crucial since minimizing lodging through moderate N application could potentially limit yield [37]. Factors such as enhanced root development, improved nutrient uptake, and regulated plant height due to AMF might have contributed to this stability. When N application rose from 138 to 184 kg/ha, LI in the inoculated group remained largely unchanged, with no significant yield impact. The potential acidification of the rhizosphere may affect the symbiotic relationship [38], suggesting that a 138 kg/ha N application could optimize growth traits alongside AMF interactions. In contrast, the non-inoculated group exhibited a significant increase in LI as N levels increased, attributed to heightened PH, PL, and lower TNT [39]. Notably, at maximum N application, the non-inoculated LI reached 28.25%,

lower than the 71.9% reported by Mengie, Assefa [40], possibly due to different irrigation and transplanting methods used in this study.

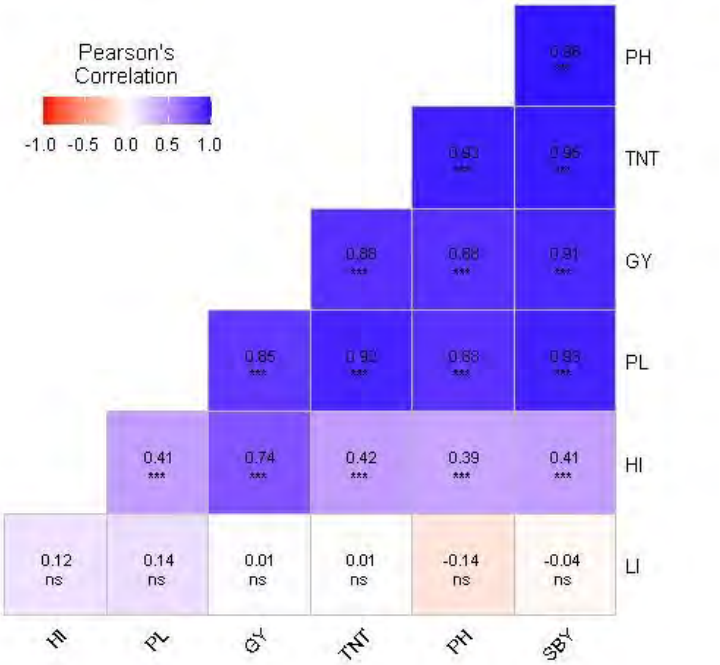

Figure 1. Pearson's correlation coefficient; "ns" = not significant, while *, **, and *** signify significance at the 0.05, 0.01, and 0.001 probability levels respectively. HI = harvest index, PL = panicle length (cm), GY = grain yield (kg/ha), TNT = total tillers per plant, PH = plant height (cm), SBY = shoot biomass yield (kg/ha), and LI = lodging index.

4.2. Yield

The observed increase in SBY and GY in the inoculated groups, as compared to the non-inoculated groups, may be influenced by a variety of factors. AMF may facilitate enhanced nutrient uptake, which could boost photosynthesis efficiency and, consequently, elevate both SBY and GY [41]. AMF might improve nutrient availability in the soil, further contributing to these yield increases [42]. The presence of AMF could also enhance root stability and encourage morphological adaptations, minimizing the risk of lodging (Panda et al., 2021). The increasing trend in SBY and GY among the inoculated groups with higher N fertilizer applications suggests that AMF may effectively convert applied N into plant biomass [43]. The higher N levels in the inoculated groups do not appear to negatively impact SBY and GY despite any potential for lodging; rather, it seems that the reduction in lodging attributed to AMF may mitigate its detrimental effects on yield. Interestingly, while the non-inoculated group reached peak SBY and GY at an N application of 184 kg/ha, the inoculated groups achieved comparable yields with only 46 kg/ha of N (Table 1). This indicates that AMF inoculation allows for similar yield outcomes with a significantly lower N input, presenting notable environmental and economic benefits, particularly for small-scale farmers [44, 45].

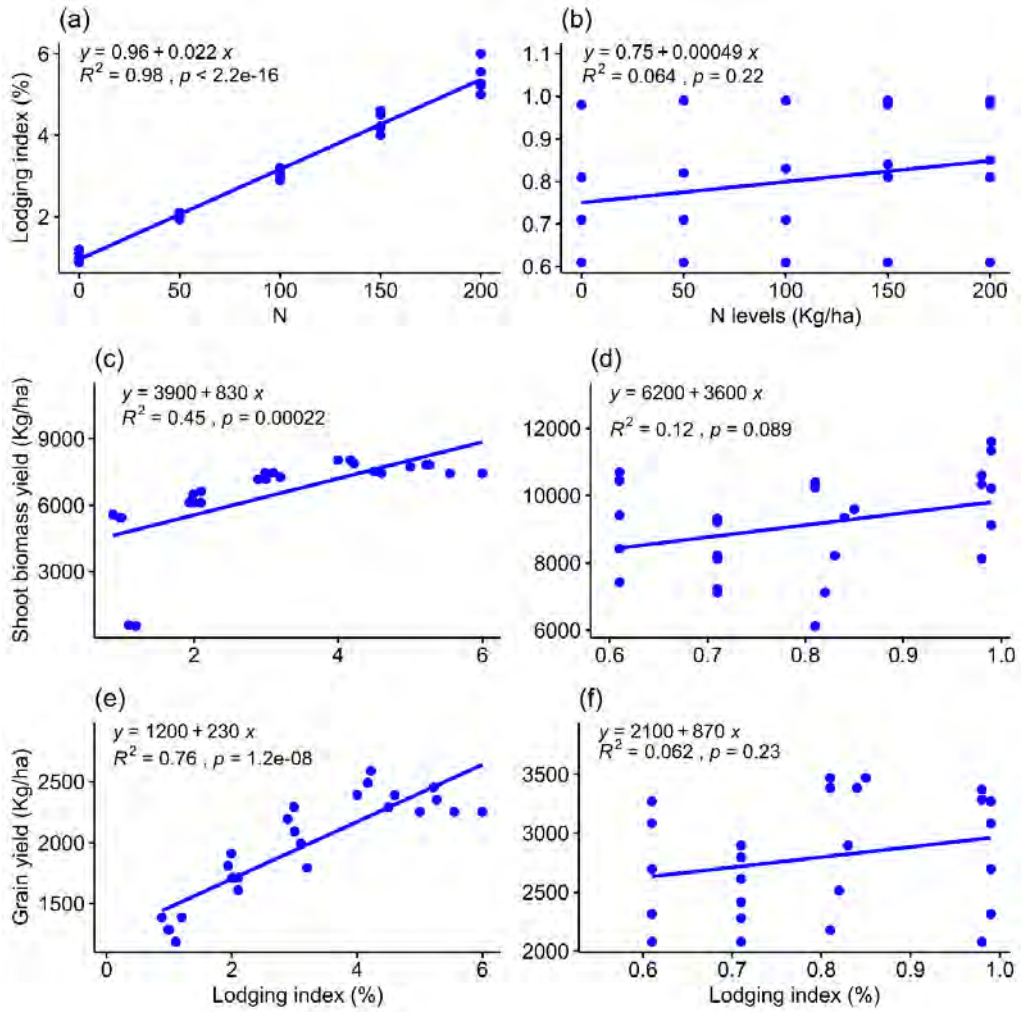

Figure 2. The predicted lodging index (LI) values for different N levels under non-inoculated (a) and inoculated (b); the predicted shoot biomass yield (SBY) at various LI levels under non-inoculated (c) and inoculated (d); and the predicted grain yield (GY) at various LI levels under non-inoculated (e) and inoculated (f). R^2 is the coefficient of determination, and p is the probability level at 5%, 1%, and 0.1%. The LI values were square root transformed.

4.3 N, Lodging, and Yield Relationships under AMF groups

Understanding the relationship between N, LI, and crop yield is essential for optimizing yields while mitigating the risk of lodging caused by N application. This study revealed that in AMF-inoculated groups, higher N applications did not lead to reductions in SBY and GY, as demonstrated in Figures 2(d) and 2(f). The findings suggest that, for AMF-inoculated tef plants, N application did not induce changes in LI that would compromise yield, as illustrated in Figure 2(b). These results highlight the vital role of AMF as beneficial soil microorganisms that not only enhance nutrient uptake and utilization but also help minimize nitrogen losses, thus reducing the environmental impacts associated with nitrogen use. Moreover, our results indicated that the morphological traits contributing to lodging were only non-significantly correlated with LI, suggesting that the impacts of N on LI might be understated. This observation underscores the potential of AMF to strengthen root anchorage, thereby reducing lodging risk even under substantial panicle weights. By improving nutrient uptake, AMF promotes balanced growth and enhanced shoot-to-root ratios, which may lead to increased lodging tolerance, as evidenced by improvements in root length, root volume, weight, and total tiller numbers. These findings align with the work of Mulyadi and Jiang [36], who documented that AMF enhances traits and nutrient uptake that bolster lodging resistance. Contrasting earlier studies, such as Berhe, Girmay [46], which indicated that an application rate of 138 kg/ha of N could result in a 99% lodging index, our research found that an application of 184 kg/ha of N did not produce a significant LI that would lead to yield reductions. Additionally, our results stand in contrast to Wato [22], who reported that increasing N from 0 to 90 kg/ha heightened the LI due to excessive vegetative growth.

Instead, the presence of AMF in our study facilitated effective N uptake and improved morphological traits, mitigating lodging and ultimately enhancing yield. However, it is important to note that in non-inoculated groups, a LI exceeding 4 resulted in a significant decline in both SBY and GY, as indicated in Figure 3(b). It appears that an N application above 138 kg/ha is critically linked to a LI greater than 4%, as represented in Figure 3(a). This suggests that N levels exceeding this threshold could be deemed excessive and could adversely affect yield.

Consequently, to maximize yield without risking lodging, a N fertilizer level of 138 kg/ha is recommended. This indicates that tef cultivation under irrigation without AMF inoculation should ideally limit N applications to this amount to prevent potential yield reductions attributable to lodging.

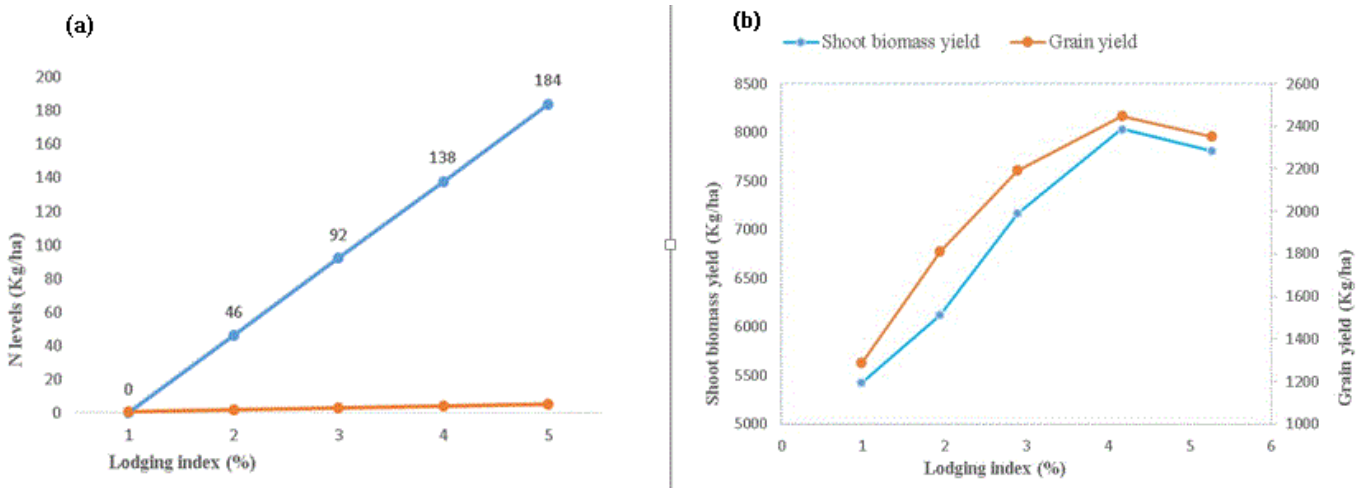

Figure 3. The relationship between lodging index (LI) and nitrogen (N) levels from 0 to 184 kg/ha plate (a), and relationship among shoot biomass yield (kg/ha), grain yield (kg/ha), and lodging index (%), plate (b), all under non-inoculated AMF groups. Lodging index values (1-5) were back square root transformed.

Author Contributions: Kidu Gebremeskel: Conceptualization, Investigation, Data collection, Formal analysis, Visualization, Writing - original draft, manuscript editing. Emiru Birhane: Investigation, Data collection, Formal analysis, manuscript editing, Supervision. Zerihun Tadele: Investigation, Data collection, Formal analysis, manuscript editing, and Supervision. Solomon Habtu Investigation, Formal analysis, manuscript editing. Mitiku Haile: Investigation, manuscript editing, Supervision. Solomon Chanyalew: Investigation, Formal analysis, manuscript editing. Kbebew Assefa: Investigation, Formal analysis, manuscript editing.

Funding: Not applicable

Data Availability Statement: Data will be made available upon request.

Acknowledgments: We acknowledge the Institute of International Education-Scholars Rescue Fund (IIE-SRF), Nord University, Faculty of Bioscience and Aquaculture (FBA) for supporting the research stay of Emiru Birhane at Nord University, and the University of Bern, Institute of Plant Sciences, Switzerland, for financial and technical support throughout the experimentation.

Conflicts of Interest: The authors declare that they have no conflict of interest.

References

1. Fikadu, A., Wedu, T. D. and Derseh, E. Review on economics of teff in Ethiopia. *Open Access Biostatistics & Bioinformatics 2*(3), 1-8 (2019).
2. Spaenij-Dekking, L., Kooy-Winkelaar, Y. and Koning, F. The Ethiopian cereal tef in celiac disease. *New England Journal of Medicine 353*(16), 1748-1749 (2005).
3. Muluye, M.Y. The Role of Agricultural Sector Economy for the development of Ethiopia. *MSc. thesis* 2021, Budapest Business School, Budapest, Hungary.
4. Belachew, K.Y. et al. Yield gaps of major cereal and grain legume crops in Ethiopia: A review. *Agronomy 12*(10), 2528 (2022).
5. Gebru, M., Alemayehu, G. and Bitew, Y. Yield and lodging response of tef [Eragrostis tef (Zucc) trotter] varieties to nitrogen and silicon application rates. *Heliyon 9*(12): e22576, (2023).

6. Ayalew, H., Chamberlin, J. and Newman, C. Site-specific agronomic information and technology adoption: A field experiment from Ethiopia. *Journal of Development Economics 156*, 102788 (2022).
7. Tofu, D.A. and Mengistu, M. Observed time series trend analysis of climate variability and smallholder adoption of new agricultural technologies in west Shewa, Ethiopia. *Scientific African 19*: e01448, (2023).
8. Tafes Desta, B., Mekuria, G. F. and Gezahegn, A. M. Exploiting the genetic potential of tef through improved agronomic practices: a review. *Cogent Food & Agriculture 8*(1), 2083539 (2022).
9. Bedada, W. Growth, Lodging and yield of TEF (Eragrostis tef) as influenced by seed size and depth of sowing. *MSc. thesis* 2009, Haramaya University, College of Agriculture, Alemaya, Ethiopia.
10. Chanyalew, S. et al. Significance and prospects of an orphan crop tef. *Planta 250*, 753-767 (2019).
11. Ijara, G.A. Biosciences and Plant Biology. *Int. J. Curr. Res. Biosci. Plant Biol. 9*(2), 8-13 (2022).
12. Blösch, R. et al. *Panicle angle is an important factor in tef lodging tolerance.* Frontiers in plant science, 2020. **11**: p. 61.
13. Assefa, K., et al. Genetic diversity in tef [Eragrostis tef (Zucc.) Trotter]. *Frontiers in plant science 6*, 177 (2015).
14. Gezahegn, A.M. et al. Timing and splitting of nitrogen application to increase tef (Eragrostic Tef (Zucc.) Trotter) yield and nitrogen use efficiency at central highlands of Ethiopia. *Communications in Soil Science and Plant Analysis 52*(10), 1100-1114 (2021).
15. Ebbisa, A. *Arbuscular mycorrhizal fungi (AMF) in optimizing nutrient bioavailability and reducing agrochemicals for maintaining sustainable agroecosystems*, in *Arbuscular mycorrhizal fungi in agriculture-new insights* (IntechOpen, 2022).
16. Wu, S. et al. Arbuscular mycorrhizal fungi increase crop yields by improving biomass under rainfed condition: a meta-analysis. *PeerJ 10*: e12861, (2022).
17. Ruiz-Lozano, J.M. et al. Contribution of arbuscular mycorrhizal symbiosis to plant drought tolerance: state of the art. In *Plant responses to drought stress* (Springer, 2012).
18. Parihar, M. *Arbuscular Mycorrhizal Fungi in Sustainable Agriculture: Nutrient and Crop Management*. (Springer Nature, 2024).
19. Jakobsen, I., Leggett, M. E. and Richardson, A. E. Rhizosphere microorganisms and plant phosphorus uptake. *Phosphorus: agriculture and the environment 46*, 437-494 (2005).
20. Griffiths, M. et al. Optimisation of root traits to provide enhanced ecosystem services in agricultural systems: A focus on cover crops. *Plant, Cell & Environment 45*(3), 751-770 (2022).
21. Gusain, S., Kumari, K. and Joshi, R. Physiological, hormonal and molecular dynamics of root system architectural response to drought stress signaling in crops. *Rhizosphere 31*: 100922, (2024).
22. Wato, T. Tef [Eragrostis tef (Zucc)] grain yield response to nitrogen fertilizer rates in East Badewacho district, Hadiya Zone, Southern Ethiopia. *Cogent Food & Agriculture 7*(1), 1909203 (2021).
23. Assefa, K. et al. Tef (Eragrostis tef) variety kora. *Ethiopian Journal of Agricultural Sciences 27*(2), 137-140 (2017).
24. Birhane, E. et al. Arbuscular mycorrhizal fungi enhance photosynthesis, water use efficiency, and growth of frankincense seedlings under pulsed water availability conditions. Oecologia *169*, 895-904 (2012).
25. Gebremeskel, K. et al. Evaluation of grain protein content in Eragrostis for different N fertilizer application under irrigated condition. *J. Innovative Agriculture 10*(3), 12-36 (2023).
26. Gebretsadik, H., Haile, M. and Yamoah, C. F. Tillage frequency, soil compaction and N-fertilizer rate effects on yield of teff (Eragrostis tef (Zucc) Trotter) in central zone of Tigray, Northern Ethiopia. *Momona Ethiopian journal of science 1*(1), 82-94 (2009).
27. Doorenbos, J. and Pruitt W. Crop water requirements. In *FAO irrigation and drainage paper 24* (FAO, Rome, 1977).
28. Caldicott, J. and Nuttall, A. A method for the assessment of lodging in cereal crops. *J. National Inst. Agricultural Botany 15*(1), 88-91 (1979).
29. Team, R.D.C. R: A language and environment for statistical computing. http://www.R-project.org
30. Gomez, K.A. and Gomez, A. A. *Statistical procedures for agricultural research* (John wiley & sons, 1984).
31. Jansa, J. et al. Arbuscular mycorrhiza and soil organic nitrogen: network of players and interactions. *Chemical and Biological Technologies in Agriculture 6*(1), 1-10 (2019).
32. de Oliveira, I.F. et al. Agronomic Practices for Optimizing the AMF Abundance and Diversity for Sustainable Food Production. In *Arbuscular Mycorrhizal Fungi in Sustainable Agriculture: Nutrient and Crop Management* (Springer, 2024).
33. Liu, C.-Y. et al. Arbuscular mycorrhizal fungi improve drought tolerance of tea plants via modulating root architecture and hormones. *Plant Growth Regulation 102*(1), 13-22 (2024).
34. Khaliq, A. et al. Arbuscular mycorrhizal fungi symbiosis to enhance plant–soil interaction. *Sustainability 14*(13), 7840 (2022).
35. Clayton, J. et al. Two-way NxP fertilisation experiment on barley (Hordeum vulgare) reveals shift from additive to synergistic NP interactions at critical phosphorus fertilisation level. *Frontiers in Plant Science 15*, 1346729 (2024).
36. Mulyadi and Jiang, L. Combined application of arbuscular mycorrhizal fungi (AMF) and nitrogen fertilizer alters the physicochemical soil properties, nitrogen uptake, and rice yield in a polybag experiment. *Agriculture 13*(7), 1364 (2023).
37. Liu, S. et al. Optimal N fertilizer management method for improving maize lodging resistance and yields by combining controlled-release urea and normal urea. *European Journal of Agronomy 156*, 127159 (2024).
38. Wang, R. et al. Research progress in crop root biology and nitrogen uptake and use, with emphasis on cereal crops. *Agronomy 13*(7), 1678 (2023).
39. Tekle, M.G., Alemayehu, G. and Bitew, Y. Yield, lodging, and water use efficiency of Tef [Eragrostis tef (zucc) Trotter] in response to carbonized rice husk application under variable moisture condition. *Plos one 19*(3): e0298416, (2024).

40. Mengie, Y., Assefa, A. and Jenber, A. J. Sowing methods and seeding rates effects on yield and yield components of Tef (Eragrostis tef [Zucc.] Trotter) at Adet, North West Ethiopia. *Heliyon 7*(3): e06519, (2021).
41. Masrahi, A.S. et al. Role of arbuscular mycorrhizal fungi and phosphate solubilizing bacteria in improving yield, yield components, and nutrients uptake of barley under salinity soil. *Agriculture 13*(3), 537 (2023).
42. Duan, H.-X. et al. AM fungus promotes wheat grain filling via improving rhizospheric water & nutrient availability under drought and low density. *Applied Soil Ecology 193*, 105159 (2024).
43. Zaman, F. et al. The pivotal role of arbuscular mycorrhizal fungi in enhancing plant biomass and nutrient availability under drought stress conditions: A global meta-analysis. *Science of The Total Environment 955*, 176960 (2024).
44. Demiss, M., et al., *Teff (Eragrostis tef) dry matter yield, nutrient uptake partitioning, and nitrogen use efficiency indices affected by nitrogen rate under balanced fertilization.* Sustainable Environment, 2024. **10**(1): p. 2367842.
45. Gashu, K., et al., *Tef (Eragrostis tef Trotter) responses to nitrogen fertigation under semi-arid Mediterranean climate.* Agronomy, 2020. **10**(12): p. 1870.
46. Berhe, T., G. Girmay, and A. Kidanemariam, *Validation of blended NPSB fertilizer rates on yield, yield components of Teff [Eragrostis tef (Zuccagni) Trotter] at vertisols of Hatsebo, Central Tigray, Ethiopia.* Journal of Soil Science and Environmental Management, 2020. **11**(2): p. 75-86.

5th International Conference of Hyojeong Academy
International Joint Conference 2025

Determinants of Participation by Farm Households in Local Agricultural Groups and the Adoption of Climate-Smart Agriculture Practices: Insights from Uganda

Tesfaalem Hagos Gebremedhn[1,*], Tewodros Tadesse[1], Melaku Berhe[1] and Bihon Kassa[2]

[1]Department of Agricultural and Resource Economics, Mekelle University, Mekelle, Tigray, Ethiopia.
[2]Department of Development Studies, Mekelle University
*Correspondence: tesfalemhagos2018@gmail.com

Abstract: The agriculture sector, heavily reliant on rainfall, faces significant challenges due to climate change, particularly in developing countries where it supports many communities. In response, climate-smart agricultural practices have been developed to address these adverse effects. Numerous factors influence the adoption of climate-smart practices, particularly membership in local agricultural groups. This study aims to examine the determinants that influence the decisions of farm households to participate in local agricultural groups and adopt climate-smart agricultural practices in the Rakai district of Uganda. The used data were collected through a cross-sectional survey involving 343 farm households, and the joint factors affecting their decisions were analyzed using a bivariate probit regression model. The econometric analysis indicates that several factors, including gender, land ownership, access to extension services, the ability to utilize climate information, the sharing of climate information with non-household members, experiences of drought-related climate shocks, and the use of autonomous climate change adaptation strategies, positively influence farm households' decisions to join local agricultural groups and adopt climate-smart agricultural practices. Consequently, development actors should facilitate the formation of local agricultural groups and encourage the active participation of farm households to promote the adoption of climate-smart agricultural practices systematically. The membership in local agricultural groups and adopting climatesmart agricultural practices are mutually reinforcing. Moreover, enhancing the awareness and knowledge of farm households through disseminating relevant climate information by local agricultural groups is essential for fostering informed decision-making in agricultural practices.

Keywords: Farm households; Local agricultural groups; Climate smart agriculture; bivariate probit model; adoption

1. Introduction

The agriculture sector, which heavily relies on rainfall, is facing significant challenges due to climate change. This is especially true in developing countries, where it supports many communities, as their livelihoods are directly affected by erratic rainfall, land degradation, the expansion of aridity and desertification, and shorter growing seasons [1, 2]. These impacts are particularly significant for poor smallholder farmers in sub-Saharan Africa (SSA) who rely heavily on rain-fed agriculture. To reduce climate change impacts on smallholder farm households, innovative solutions that enhance rural resilience are needed [3]. Climate-smart agriculture (CSA) practices can help, but their adoption is influenced by several factors that warrant further investigation.

Farm households' membership in local agricultural groups plays a crucial role in the adoption of climate smart agricultural (CSA) practices [4]. The dynamics driving farm households' decisions to join these groups such as access to resources, social networks, and shared knowledge also significantly impact their willingness and ability to implement climate-smart practices. The likelihood of adopting CSA practices increases as more farm households become members of local community groups. This highlights the importance of farm group membership in reducing the adverse effects of climate change through CSA adoption. Therefore, it is essential to investigate the factors influencing farm households' decisions to join local agricultural groups and adopt CSA practices. Such an investigation would provide valuable insights into the interrelationship between these two outcomes—membership in local agricultural groups and CSA adoption.

The main research question of this study is: What factors determine farm households' joint decision to join local agricultural groups and adopt climate-smart agricultural (CSA) practices? This issue has not been adequately addressed in existing literature. Accordingly, this study aims to fill this gap by examining the relationship between farm households' membership in local agricultural groups and their adoption of CSA practices. Investigating the determinants of both decisions is crucial for understanding the factors that contribute to these outcomes. Thus, the objective of this paper is to explore the key factors influencing farm households' simultaneous decision to join local agricultural groups and adopt CSA practices.

2. Methods and Materials Data

The data for this study comes from the IMPACT Lite survey conducted by CCAFS in Uganda, Rakai district. The district is already experiencing climate change impacts, prompting efforts to support farm households' adaptation strategies [5]. Using purposive sampling, districts were selected based on their vulnerability to climate change, followed by random sampling to select 343 households. The dataset captures household decision-making on CSA practices and local agricultural group membership. It includes information on farming decisions, climate change perceptions, and access to climate information, adaptation practices, institutional services, and agricultural group membership.

2.1. Data analysis The Bivariate Probit Model

Farm households make decisions based on multiple factors to improve productivity and income, and these decisions often influence one another. For example, the decision to join a local agricultural groups (LAG) may impact the subsequent decision to adopt climate-smart agricultural (CSA) practices. This study investigates the relationship between farm households' membership in local groups and their adoption of CSA practices, assuming that factors influencing membership in LAGs also positively affect CSA adoption. Given the interdependent nature of these decisions, the membership in local agricultural groups and the adoption of CSA practices are potentially jointly determined. To analyze this, the study employs the bivariate probit model, which is commonly used to estimate interrelated decisions. This model specifies two equations: one for the decision to join local agricultural groups and the other for the adoption of CSA practices. Following Alidu et al. [6], the bivariate probit model corrects for potential sample selection bias. They suggest that if the correlation value (rho) between the two decisions is statistically significant, then the bivariate probit model is appropriate for joint estimation. If the correlation is not significant, separate probit models would be more suitable for analysis.

According to Seyoum et al. [7], the bivariate probit model is a joint model for two binary dependent variables with assumed correlated disturbances. The two latent variables resulting from the bivariate probit model are unobserved. This model is used to estimate two binary choice decision equations [8]. The bivariate probit model yields two binary results expressed mathematically as two unobserved continuous latent variables. In this study, Y_1^* , represents the use of climate smart agriculture practices by farm households in the study area and Y_{2^*}, represents the farm households membership to local groupings. Equations (1) and (2) can represent the two unobserved latent variables.

$$Y_{1^*} = x_1\beta_1 + \mu_i \quad (1)$$

$$Y_{2^*} = x_1\beta_2 + \mu_2 \quad (2)$$

Both errors (μ_i, μ_2) are jointly distributed normally with a mean of 0 and a variance of 1. The variable x_1 is a vector of independent variables with estimators β that are common to both outcomes respectively. The two binary outcomes are expected to be observed as shown in equations (3) and (4).

$$Y_1 = \begin{cases} 1 \; if \; y^* > 0 \\ 0 \; otherwise \end{cases} \quad (3)$$

$$Y_2 = \begin{cases} 1 \; if \; y^* > 0 \\ 0 \; otherwise \end{cases} \quad (4)$$

3. Results and Discussion

3.1. Types of local agricultural groups available in the study area

In the study district, various local agricultural groups were available to farm households as indicated in Table 1. Of the total sample households, membership in these groups was generally low, with the exception of credit and microfinance groups, where 61.81% of households were members. Overall, only 39% of the sampled farm households were members of the listed local agricultural groups. Membership in these local social or agricultural groups is a key enabler of climate-smart agricultural practices adoption. Therefore, it is essential to systematically explore the factors that hinder farm households' membership in local agricultural groups.

Table 1. Percentage of farm households' membership to the local agricultural groups in the study area

Types of local agricultural groups	**Percentage of membership to local agricultural groups**
Agricultural producers group	171 (49.85%)
Livestock producers group	146 (42.57%)
Tree nursery group	109 (31.78%)
Credit, microfinance group	212 (61.81%)
Marketing and income group	136 (39.65%)
Civic group	117 (34.11%)
Religious group	112 (32.65)%
Water user group	69 (27.99%)

3.2. CSA practices and the percentage of adoption in the study area

Different climate-smart agricultural (CSA) practices have varying adoption rates. The major practices adopted in this study included agroforestry (61.31%), improved livestock feed management (51.24%), composting (49.07%), improved grain storage (47.52%), and rangeland management (42.40%) (Table 2). In contrast, a study in Ethiopia reported a higher compost adoption rate (66%) but a lower agroforestry adoption rate (21%) [9]. Similarly, moderate adoption of water management practices in Upper West Region of Ghana was reported by Djido et al. [10], which aligns with the irrigation practice adoption in this study. Agroforestry was the most widely adopted CSA practice in the study area. Despite low irrigation use in Rakai district due to recurrent drought [11], farm households are increasingly adopting irrigation to cope with drought. In West Africa, drought and rising temperatures pose significant risks to rain-fed crop production and smallholder livelihoods [12].

Table 2. Percentage of CSA practices adopted by farm households in the study area

CSA practices	**Percentage of adoption**
Agroforestry	61.31%
Use of irrigation	35.15%
Composting	49.07%
Efficient use of fertilizer	33.11%
Use stress tolerant varieties	28.67%
Improved grain storage	47.52%
Improved stoves	42.40%
Improved feed management	51.24%
Grazing, pasture, or rangeland management	44.74%

3.3. Determinants of membership to local agricultural groups and adoption of climate smart agriculture practices

The bivariate probit regression results for farm households' joint decision to join local agricultural groups and adopt CSA practices are presented in Table 3. For bivariate probit regression to be valid, the error terms of the two outcomes must be correlated. The results in Table 3 show that the error terms, indicated by the value of rho, are indeed correlated, suggesting that the two decisions are jointly determined. The statistical significance of the ancillary parameter rho (p) was tested and found to be significant at the 1% level, confirming that the two outcomes are strongly related and can be estimated using the bivariate probit model.

3.4. Determinants of membership to local agricultural groups

Farm households' membership in local agricultural groups (LAGs) and adoption of climate-smart agricultural (CSA) practices were both low, as shown in Table 1 and Table 2 of this study. These two variables are strongly interrelated, with previous studies, such as Birir [4], indicating that LAG membership positively influences the adoption of CSA practices. To promote CSA adoption, practitioners have developed strategies to increase farmers' participation in local community groups.

The bivariate probit regression results in Table 3 reveal that access to extension services, ability to use climate information, land ownership, climate information sharing with non-family members, gender, and age were positively associated with LAG membership at the 1% significance level. Older farm households were more likely to join LAGs, likely due to their extensive farming experience, which helps them appreciate the benefits of information sharing for improving agricultural productivity. Additionally, maleheaded households were more likely to join LAGs, as they often have greater exposure to socio-cultural settings that facilitate participation in local community affairs. This finding contrasts with Birir [4], who reported that female-headed households were more likely to join LAGs than their male counterparts. Households experiencing drought-related climate shocks are more likely to join LAGs. Those who have taken measures to protect themselves from climate change impacts also have a higher probability of joining. These factors are interconnected, as sharing climate information encourages adaptation measures, while climate shocks motivate farmers to take protective actions, requiring knowledge gained through information sharing. Thus, all these factors contribute to farm households joining local agricultural groups.

Access to extension services positively influences farm households' membership in local agricultural groups. Increasing membership in these groups supports the adoption of Climate-Smart Agriculture (CSA) practices [4]. Farm households with access to extension services are more likely to seek solutions to climate change impacts. The effective use of adaptation strategies also encourages involvement in local agricultural groups and is significant at the 5% level. Households that have previously adopted adaptation strategies are more likely to join these groups.

3.5. Determinants of the adoption of climate smart agriculture practices

Adoption of Climate-Smart Agricultural (CSA) practices among smallholder farmers in developing countries remains low due to various factors [14] which include drought shocks, climate information sharing, the ability to use climate information, and years of formal education, which significantly promote CSA adoption at the 1% level. Other factors like gender, land ownership, climate change perception, and prior protective measures also positively impact adoption. Educated households are more likely to engage in CSA practices, reinforcing the importance of climate information services. Similarly, the ability to use climate information is crucial for adopting CSA practices, consistent with findings by Owusu et al. [15], that climate information services are essential for adopting adaptation measures.

Gender plays a role in CSA adoption, with studies showing it positively affects uptake. Similar findings were reported by Negera et al. [14] and Oyawole et al. [16], where gender and age influenced CSA adoption. Additionally, extension services significantly increase the likelihood of adopting CSA. Households that perceive climate change are more motivated to adopt CSA and improve their adaptive capacity. This finding aligns with Owusu et al. [15] and Asrat & Simane [17], who noted that while the risk of climate impacts was high, households withvariability, they are more likely to adjust their farming practices to maintain productivity.

Table 3 presents the bivariate probit regression estimates for the factors influencing farm households' adoption of Climate-Smart Agricultural (CSA) practices and membership in local agricultural groups (LAGs).

Table 3. Bivariate Probit results of farm households' determinants of group membership and use of climate smart agriculture practices

Variables	Group membership to local community groups		Adoption of climate smart agricultural practices		Marginal effect	
	Coefficient	SE	Coefficient	SE	Coefficient	SE
Cons	-1.306	0.788				
Age	0.426***	0.132	0.138	0.089	0.115	0.119
Gender	0.236***	0.055	0.239**	0.117	0.054 *	0.031
Education years	0.113	0.124	0.352***	0.125	0.118	0.122
Disability/health status	0.019	0.015	0.012	0.016	0.007	0.011
Land ownership	0.456***	0.132	0.264**	0.131	0.234*	0.122
Access to irrigation	0.142	0.112	0.004	0.027	0.038	0.024
Able to use climate information	0.272***	0.090	0.232***	0.086	0.065**	0.028
Climate information sharing with household members	-0.20	0.064	-0.159	0.108	-0.039	0.047
Climate information sharing nonhousehold members	0.217***	0.056	0.251***	0.090	0.069*	0.039
Extension service	0.104***	0.038	0.112***	0.040	0.113***	0.035
Access to credit	-0.152	0.293	-0.118	0.286	-0.079	0.053
Episodes of drought shock	0.094**	0.041	0.216***	0.043	0.203***	0.049
Climate change perception	-0.018	0.035	0.118**	0.056	0.077	0.050
Have protected self from the impact of climate change	0.024 **	0.012	0.367**	0.185	0.035***	0.011
Plan to protect from the potential impact of climate change	-0.278	0.193	-0.205	-0.121	0.035	0.022
Rho	0.480***	0.104	0.564***	0.116	0.202***	0.026

(Note: *, ** and *** indicate statistical differences at the 10%, 5% and 1% levels respectively)

Greater climate change awareness was better able to adapt. When farm households strongly perceive climate-Key factors such as land ownership, ability to use climate information, climate information sharing with non-household members, access to extension services, experience with climate change adaptation measures, and drought shocks all positively and significantly influenced both membership in LAGs and adoption of CSA practices. The ability to use climate information, sharing with non-household members, and access to extension services were significant at the 1% level for both outcomes. Land ownership was a significant factor at the 1% level for LAG membership and at the 5% level for CSA adoption, highlighting the importance of land as a valuable asset in decision-making. This aligns with Alidu et al. [6], who found that owning assets positively impacts CSA adoption. However, the number of education years only significantly influenced CSA adoption.

Farm households' ability to use climate information was positively associated with their joint decision to adopt Climate-Smart Agricultural (CSA) practices and join local agricultural groups (LAGs), with statistical significance at the 1% level. Households that could use climate information were more likely to both adopt CSA practices and become members of local agricultural groups. The adoption of climate information was the most significant factor for joining local agricultural groups, which in turn facilitates CSA adoption. Similar findings were reported by

Owusu et al. [15], who noted that membership in farm household-based organizations positively influences the adoption of adaptation measures.

The variable access to extension service was positively influenced farm households uptake of CSA and membership to LAG at 1% significance level. Farm households who had contacts with extension agents and services tend to jointly adopt CSA practices and at the same time be member of LAG. Access to extension service is a prerequisite for all other measures to be taken to tackle climate change impact. Farm households' perception and awareness of climate change comes as a result of their contact with extension agents which encourage them to pursue methods of alleviating climate change risks and these are adaptation strategies which often provided to them through various mechanisms such as climate information. The use of climate information help farm households to participate in local agricultural groups that enhance their awareness of climate smart agricultural practices and eventually adopt climate smart agricultural practices to effectively minimize climate change vulnerabilities. The relationship of climate change perception and use of agricultural practices was also investigated by [10] and underscore that farm households' perception of climate change was relevant in the decision to use agricultural practices.

Access to extension services positively influenced farm households' adoption of Climate-Smart Agricultural (CSA) practices and membership in Local Agricultural Groups (LAGs) at the 1% significance level. Households in contact with extension agents were more likely to both adopt CSA practices and join LAGs. Extension services play a crucial role in raising awareness about climate change and providing adaptation strategies, such as climate information. This information helps farmers engage in local agricultural groups, boosting their understanding of CSA practices and reducing climate change vulnerabilities. Djido et al. [10] also found that farm households' perception of climate change influences their decision to adopt agricultural practices. All in all, membership in local agricultural groups helps farm households adopt climate-smart agricultural (CSA) practices by facilitating information sharing through regular group interactions [18]. Similar findings from Masaba South sub-county, Kisii, Kenya, showed that group membership increases awareness of CSA practices, motivating adoption to combat climate change and improve livelihoods [19]. Stefanovic et al. [18] further emphasized the importance of community groups in sharing CSA practices, innovations, and farming information to enhance resilience. Adeagbo et al. [20] also highlighted the role of social groups in sharing market, production, and credit access information. However, in this study, many local agricultural households were not members of available agricultural groups, limiting their awareness and adoption of CSA practices.

4. Conclusion

The findings of this study emphasize the importance of local agricultural groups (LAGs) and climate-smart agricultural (CSA) practices as essential tools for minimizing the adverse effects of climate change on farm households in developing countries. The research indicates that various factors, including gender, land ownership, access to extension services, climate information usage, and experiences with climate shocks, significantly influence the likelihood of farm households joining LAGs and adopting CSA practices. The correlation between LAG membership and CSA adoption highlights the value of collaborative efforts and information sharing in promoting sustainable agricultural practices.

To effectively address climate change challenges, it is crucial for local governments, development practitioners, and extension agents to support the formation and expansion of LAGs. These groups can serve as platforms for knowledge exchange, enabling farm households to learn from each other and adopt innovative practices. Moreover, ensuring that farm households have access to reliable climate information is vital, as it empowers them to make informed decisions about climate adaptation and agricultural strategies. By enhancing the availability and use of climate information, the adoption of CSA practices and participation in LAGs can be significantly increased, ultimately contributing to more resilient agricultural communities.

Acknowledgments: The authors are grateful to the IMPACT Lite survey authors: CCAFS, IFPRI, and ILRI

Authors' contributions: All authors were designed the study, contributed in reviewing, editing and revising; all authors read and approved the final manuscript.

Availability of data and materials: Please contact the corresponding author for data requests

References

1. Muthayya, S. et al. The Global Hidden Hunger Indices and Maps: An Advocacy Tool for Action. *PLoS One 8*(6):e67860, (2013). doi: 10.1371/JOURNAL.PONE.0067860.
2. IPCC, *Climate Change 2014: Mitigation of Climate Change* (Cambridge Univ. Press, 2014). doi:10.1017/cbo9781107415416.
3. Jost, C. et al. Understanding gender dimensions of agriculture and climate change in smallholder farming communities. *Clim. Dev*. 8(2), 133–144 (2016). doi: 10.1080/17565529.2015.1050978.
4. Birir, A. Influence of Social Capital on Adoption of Climate Smart Agriculture: Evidence From Nyando Basin, Southwestern Kenya. 2021. http://erepository.uonbi.ac.ke/handle/11295/160232 (accessed on 27 Oct. 2023).
5. UNDP, United Nations Development Programme crisis prevention and recovery climate risk management for sustainable crop production in Uganda: Rakai and Kapchorwa districts prepared by the International Institute for Sustainable Development (IISD), 2013. www.undp.org (accessed on 06 Feb. 2024).
6. Alidu, A. F., Man, N., Ramli, N. N., Mohd Haris, N. B. and Alhassan, A. Smallholder farmers access to climate information and climate smart adaptation practices in the northern region of Ghana. *Heliyon* 8(5): e09513, (2022). doi: 10.1016/J.HELIYON.2022.E09513.
7. Seyoum, S. and Senayit, S. Analysis of Prevalence of Malaria and Anemia Using Bivariate Probit Model *Ann. Data Sci. 5*(2), 301–312 (2018). doi: 10.1007/S40745-018-0138-3.
8. Chen, S. and Zhou, Y. Estimating a generalized correlation coefficient for a generalized bivariate probit model *J. Econom.141*(2), 1100–1114 (2007). doi: 10.1016/J.JECONOM.2007.01.012.
9. Teklu, A., Simane, B. and Bezabih, M. Multiple adoption of climate-smart agriculture innovation for agricultural sustainability: Empirical evidence from the Upper Blue Nile Highlands of Ethiopia. *Clim. Risk Manag.39*, 100477 (2023). doi: 10.1016/J.CRM.2023.100477.
10. Djido, A. et al. To what extent do weather and climate information services drive the adoption of climate-smart agriculture practices in Ghana? *Clim. Risk Manag. 32*, 100309 (2021). doi: 10.1016/j.crm.2021.100309.
11. Dekens, J. et al. United Nations Development Programme CRISIS PREVENTION AND RECOVERY CLIMATE RISK MANAGEMENT FOR SUSTAINABLE CROP PRODUCTION IN UGANDA: RAKAI

A. AND KAPCHORWA DISTRICTS Prepared by the International Institute for Sustainable Development

B. (IISD) 2013. www.undp.org (accessed on 27 Oct. 2023).

12. Zougmoré, R. B., Partey, S. T., Ouédraogo, M., Torquebiau, E. and Campbell, B. M. Facing climate variability in sub-Saharan Africa: analysis of climate-smart agriculture opportunities to manage climate related risks. *Cah. Agric. 27*(3), 34001 (2018). doi: 10.1051/CAGRI/2018019.
13. Birir, A. Influence of Social Capital on Adoption of Climate Smart Agriculture: Evidence From Nyando Basin, Southwestern Kenya. University of Nairobi, 2021. http://erepository.uonbi.ac.ke/handle/11295/160232 (accessed on 27 Oct. 2023).
14. Negera, M., Alemu, T., Hagos, F. and Haileslassie, A. Determinants of adoption of climate smart agricultural practices among farmers in Bale-Eco region, Ethiopia. *Heliyon* 8(7): e09824, (2022). doi: 0.1016/j.heliyon.2022.e09824.
15. Owusu, V., Ma, W., Renwick, A. and Emuah, D. Does the use of climate information contribute to climate change adaptation? Evidence from Ghana. *Clim. Dev.13*(7), 616–629 (2020). doi: 10.1080/17565529.2020.1844612.
16. Oyawole, F. P., Dipeolu, A. O., Shittu, A. M., Obayelu, A. E. and Fabunmi, T. O. What Drives the Adoption of Climate Smart Agricultural Practices? Evidence from Maize Farmers in Northern Nigeria. *Niger. J. Agric. Econ. 9*(1), 14–28 (2019). doi: 10.22004/AG.ECON.304677.
17. Asrat, P. and Simane, B. Farmers' perception of climate change and adaptation strategies in the Dabus watershed, North-West Ethiopia. *Ecol. Process 7*: 7, (2018). doi: 10.1186/S13717-018-01188.
18. Stefanovic, J. O., Yang, H., Zhou, Y., Kamali, B. and Ogalleh, S. A. Adaption to climate change: a case study of two agricultural systems from Kenya. *Clim. Dev.11*(4), 319–337 (2017). doi:

A. 10.1080/17565529.2017.1411241.

19. Nyang'au, J. O., Mohamed, J. H., Mango, N., Makate, C. and Wangeci, A. N. Smallholder farmers' perception of climate change and adoption of climate smart agriculture practices in Masaba South Subcounty, Kisii, Kenya. *Heliyon 7*(4): e06789, (2021). doi: 10.1016/J.HELIYON.2021.E06789.
20. Adeagbo, O. A., Ojo, T. O. and Adetoro, A. A. Understanding the determinants of climate change adaptation strategies among smallholder maize farmers in South-west, Nigeria. *Heliyon* 7(2): e06231, (2021). doi: 10.1016/J.HELIYON.2021.E06231.

5th International Conference of Hyojeong Academy
International Joint Conference 2025

UNPACKING GOVERNANCE STRUCTURES IN KENYA'S RENEWABLE ENERGY SECTOR: THE NGONG HILLS WIND TURBINE PROJECT IN FOCUS

Jane Owino

Owino Bukachi & Company Advocates, Nairobi, Kenya
Technical University of Kenya, Nairobi, Kenya
Correspondence: bukachi@tukenya.ac.ke

Abstract: In light of the worldwide imperatives to tackle climate change and shift towards sustainable energy sources, this study examines the governance structures surrounding the Ngong Hills Wind Turbine Project within Kenya's renewable energy sector. The background underscores the urgency for renewable energy adoption globally and Kenya's pivotal role in the African context, with the Ngong Hills project serving as a microcosm of the nation's commitment to sustainable energy. The study's objectives are twofold: firstly, to find out the impact of stakeholder engagement on decision-making processes and project outcomes, and secondly, to examine how governance structures influence the distribution of benefits and potential challenges faced by local populations. These objectives frame an investigation into the institutional and stakeholder dynamics shaping the Ngong Hills project, guided by institutional and stakeholder theories. The statement of the problem addresses the existing knowledge gaps in understanding the governance intricacies of renewable energy initiatives, emphasizing the need for nuanced analyses that consider policy evolution, stakeholder collaborations, and socio-economic and environmental dimensions. The scope of the study is defined by a content analysis methodology, focusing on documents, policies, and interviews related to the Ngong Hills project. The significance lies in the potential to inform policy decisions, improve regulatory frameworks, and contribute to sustainable development practices in Kenya's renewable energy sector. Two theoretical frameworks guide the study: Institutional Theory for examining formal and informal influences on governance, and Stakeholder Theory for understanding collaboration dynamics and power relationships. Findings from the content analysis reveal a dynamic interplay of regulatory strengths and challenges, positive socio-economic impacts, and commendable environmental compliance. Conclusions drawn emphasize the need for ongoing policy evolution and inclusive stakeholder engagement. Recommendations highlight iterative policy adjustments, community-inclusive decision-making, and sustained environmental monitoring. This research offers valuable insights for policymakers, regulators, and stakeholders navigating the complex terrain of renewable energy governance, fostering informed decision-making and sustainable development in Kenya and beyond

Keywords: Liberals, conservatives, diversity, moral sphere, virtues, common values

1. Introduction

It Renewable energy has emerged as a critical focal point in global efforts to combat climate change and transition towards sustainable development. International agreements such as the Paris Agreement have underscored the urgency of shifting towards cleaner energy sources to mitigate greenhouse gas emissions [1]. This global momentum has led to increased attention on renewable energy projects worldwide, with wind power being a prominent component due to its scalability and relatively low environmental impact.

In the context of Sub-Saharan Africa, energy access remains a significant challenge, with millions of people lacking reliable electricity. This region also faces the adverse impacts of climate change, including extreme weather events and unpredictable rainfall patterns [2, 3]. As a response, many countries in Sub-Saharan Africa, including Kenya, have been exploring renewable energy sources to expand energy access while reducing reliance on fossil fuels. Kenya, in particular, has set ambitious targets for renewable energy deployment, aiming to achieve universal electricity access by 2022 through a mix of hydro, geothermal, solar, and wind power projects [4, 5].

The Ngong Hills Wind Turbine Project is a flagship initiative in Kenya's renewable energy sector. Situated near Nairobi, the capital city, the Ngong Hills project represents a significant investment in wind energy infrastructure

[6]. Kenya's government, in collaboration with private sector partners and international financiers, has spearheaded this project to harness the region's strong wind resources for electricity generation. The project not only contributes to Kenya's renewable energy targets but also aims to bolster local economic development through job creation, infrastructure improvement, and community engagement initiatives.

However, the implementation of such large-scale projects often involves complex governance structures, encompassing regulatory frameworks, stakeholder engagement mechanisms, and decision-making processes. Understanding these governance dynamics is crucial for evaluating the effectiveness, equity, and sustainability of renewable energy initiatives like the Ngong Hills Wind Turbine Project. Therefore, the study aims to unpack and analyze the governance structures underlying this project, shedding light on its implications for energy transition, environmental sustainability, and socio-economic development in Kenya's context.

1.1. Statement of the problem

The statement of the problem in this study addresses existing knowledge gaps in understanding the governance intricacies of renewable energy initiatives, emphasizing the need for nuanced analyses that consider various factors. Despite the increasing emphasis on renewable energy adoption globally, there remains a lack of comprehensive understanding regarding the governance structures governing such initiatives, particularly in the context of developing countries like Kenya [7]. This gap in knowledge inhibits informed decision-making and hinders the development of effective policies and regulatory frameworks.

Furthermore, the statement of the problem underscores the importance of considering policy evolution, stakeholder collaborations, and socio-economic and environmental dimensions in analyzing governance structures [8]. Existing literature often overlooks these crucial aspects, leading to a limited understanding of the complex dynamics at play in renewable energy projects. As a result, there is a need for research that delves deeper into these issues, providing insights that can inform policy decisions and contribute to more sustainable development practices.

By identifying and addressing these knowledge gaps, the study aims to contribute to the advancement of scholarly understanding in the field of renewable energy governance. It seeks to provide valuable insights that can guide policymakers, regulators, and stakeholders in navigating the complexities of renewable energy governance, ultimately fostering more informed decision-making processes and promoting sustainable development in Kenya and beyond.

1.2. Aim

The aim is unpacking governance structures in Kenya's renewable energy sector with reference to Ngong Hills wind turbine project in focus

1.3. Objectives

1. To find out the impact of stakeholder engagement on decision-making processes and project outcomes
2. To examine how governance structures influence the distribution of benefits and potential challenges faced by local populations

1.4. Research questions

1. What is the impact of stakeholder engagement on decision-making processes and project outcomes?
2. How does governance structures influence the distribution of benefits and potential challenges faced by local populations?

1.5. Scope and limitation

The scope of the study is defined by a content analysis methodology, focusing on documents, policies, and interviews related to the Ngong Hills project. However, the study's focus on a single project may limit the generalizability of findings to other renewable energy initiatives in Kenya or similar contexts. Additionally, the reliance on secondary data sources and interviews may present limitations in terms of data availability and potential biases. Despite these constraints, the study aims to provide valuable insights into governance structures and stakeholder dynamics within Kenya's renewable energy sector, contributing to the broader understanding of sustainable development practices.

1.6. Significance of the study

The significance of this study lies in its potential to inform policy decisions, improve regulatory frameworks, and contribute to sustainable development practices in Kenya's renewable energy sector. By examining the governance structures surrounding the Ngong Hills Wind Turbine Project, the study offers insights into the institutional and stakeholder dynamics shaping renewable energy initiatives. These insights can guide policymakers, regulators, and stakeholders in navigating the complexities of renewable energy governance, fostering more informed decision-making processes. Furthermore, the study's focus on stakeholder engagement and distribution of benefits addresses key concerns related to equity and inclusivity in sustainable development efforts. Ultimately, the findings have implications not only for Kenya but also for other developing countries striving to transition towards cleaner energy sources and achieve sustainable development goals.

2. Theoretical review

2.1. Institutional Theory

Institutional Theory, as applied in the context of governance structures surrounding renewable energy projects, examines the formal and informal influences shaping organizational behavior and decision-making processes [9]. Within the renewable energy sector, institutional factors such as government policies, regulations, and organizational norms play a significant role in shaping the governance mechanisms and outcomes of projects [10]. Institutions provide the rules, norms, and routines that guide actors' behavior and interactions within the sector [11].

In the case of the Ngong Hills Wind Turbine Project, Institutional Theory provides a framework for understanding how government policies and regulatory frameworks influence project development and implementation. For instance, the Kenyan government's renewable energy policies and regulations may shape the decision-making processes of project developers and influence the allocation of resources and benefits [12]. Additionally, organizational norms and practices within project stakeholders, such as Kenya Electricity Generating Company (KenGen), may be influenced by broader institutional pressures and expectations regarding environmental sustainability and community engagement [13].

In addition, Institutional Theory offers valuable insights into the formal and informal structures shaping governance dynamics within the renewable energy sector, allowing for a deeper understanding of how institutional factors influence project outcomes and stakeholder interactions.

2.2. Stakeholder Theory

Stakeholder Theory, within the context of governance structures in renewable energy projects, examines the roles, interests, and relationships of various stakeholders involved in project development and implementation [14]. In renewable energy initiatives like the Ngong Hills Wind Turbine Project, stakeholders typically include government agencies, local communities, private sector entities, non-governmental organizations, and other relevant actors [15].

Stakeholder Theory provides a framework for understanding how these diverse stakeholders interact, collaborate, and exert influence over decision-making processes and project outcomes [16]. For example, the theory helps in analyzing how community engagement practices influence the social acceptance and success of renewable energy projects [17]. Moreover, it allows for the assessment of power dynamics among stakeholders and the distribution of benefits and risks associated with the project [18].

In the case of the Ngong Hills Wind Turbine Project, Stakeholder Theory facilitates the examination of stakeholder engagement strategies employed by project developers and the impact of these strategies on project development and community relations [19]. By considering the interests and concerns of various stakeholders, including local communities and environmental groups, the theory supports the identification of win-win solutions that promote sustainable development and social equity in renewable energy projects [20].

2.3. Conceptual framework

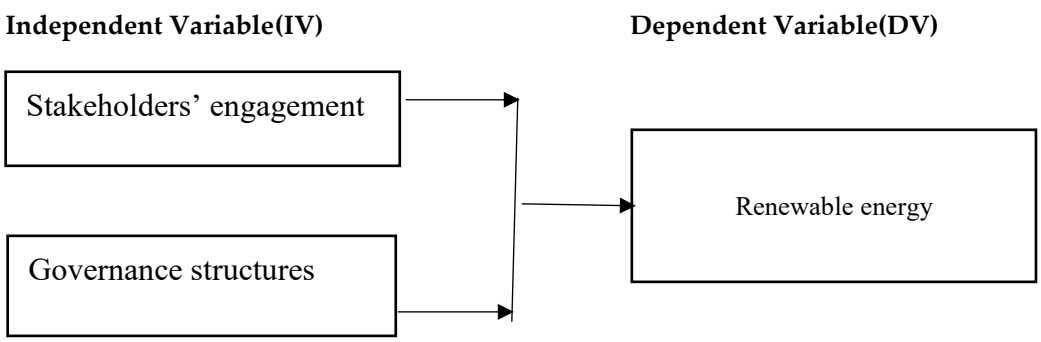

3. Methodology of the study

The methodology of the study employs content analysis, focusing on documents, policies, and interviews related to the Ngong Hills Wind Turbine Project. Content analysis involves systematically examining and interpreting textual data to identify patterns, themes, and relationships within the data [21]. This approach allows for a comprehensive examination of governance structures, stakeholder dynamics, and decision-making processes surrounding the project. By analyzing a diverse range of sources, including government reports, project documents, and stakeholder interviews, the study aims to uncover insights into the institutional and stakeholder factors shaping the Ngong Hills project and its implications for renewable energy governance in Kenya.

4. Results

4.1 Impact of stakeholder engagement on decision-making processes and project outcomes

Based on the first objective of evaluating the impact of stakeholder engagement on decision-making processes and project outcomes [22], findings reveal insights into the effectiveness of stakeholder involvement in shaping the Wind Turbine Project [23], suggesting stakeholder engagement practices, which aims at identifying patterns of collaboration, communication channels, and levels of influence exerted by different stakeholders [24]. Findings indicate the extent to which stakeholder input has been integrated into decision-making processes, potentially highlighting areas of alignment or divergence between stakeholder interests and project objectives [25]. Study uncovers the perceived benefits and challenges associated with stakeholder engagement, as reported by various stakeholders involved in the project. They continue giving the positive outcomes, such as increased project acceptance, enhanced community relations, and improved project design, may be identified alongside challenges such as conflicting interests, power imbalances, and communication barriers. Additionally, study assess the role of stakeholder engagement in addressing social, environmental, and economic concerns, providing insights into the broader impacts of stakeholder involvement on project sustainability and resilience [26].

In addition, proposed findings aimed at shedding light on the significance of stakeholder engagement in renewable energy governance, offering lessons and recommendations for improving decision-making processes and enhancing project outcomes in similar contexts [27].

4.2. How governance structures influence the distribution of benefits and potential challenges.

Study reveals important insights into the socio-economic and environmental impacts of the Wind Turbine Project [28]. In this their study, they were able to identify the mechanisms through which benefits are distributed among stakeholders, including local communities, government entities, and private sector partners [29]. Finding highlighted the extent to which governance structures promote equity, transparency, and accountability in resource allocation and decision-making processes [30].

Study uncovers the potential challenges faced by local populations as a result of the project, such as land use conflicts, changes in livelihood patterns, and environmental degradation. By examining the role of governance structures in addressing these challenges [31], study also assess the effectiveness of existing policies, regulations, and institutional frameworks in mitigating adverse impacts and promoting sustainable development outcomes.

Moreover, findings provided a comprehensive understanding of how governance structures shape the distribution of benefits and challenges associated with renewable energy projects [32]. By identifying areas for improvement and best practices, the study informed policy recommendations and strategies for enhancing the socio-economic and environmental sustainability of similar initiatives in Kenya and beyond.

5. Conclusion

In conclusion, this study has provided valuable insights into the governance structures surrounding the Ngong Hills Wind Turbine Project in Kenya's renewable energy sector. Through a content analysis methodology, the study has shed light on the institutional and stakeholder dynamics shaping the project and its outcomes.

The findings highlight the importance of stakeholder engagement in decision-making processes and project outcomes, demonstrating how collaboration among diverse stakeholders can lead to positive socio-economic and environmental impacts. Moreover, the study has identified governance structures that influence the distribution of benefits and challenges faced by local populations, emphasizing the need for equitable and transparent resource allocation mechanisms.

In assessing the study's findings in relation to the proposed theories, it is evident that both Institutional Theory and Stakeholder Theory have been supported. Institutional Theory has been corroborated by the identification of formal and informal influences on governance structures, including government policies and organizational norms. Similarly, Stakeholder Theory has been validated through the analysis of stakeholder engagement practices and their impact on project outcomes. Overall, the findings underscore the significance of these theoretical frameworks in understanding the complexities of renewable energy governance and informing sustainable development practices.

Recommendations

Enhance Stakeholder Engagement: Implement robust stakeholder engagement strategies that promote inclusivity, transparency, and meaningful participation throughout all stages of renewable energy projects. This can include establishing regular communication channels, conducting stakeholder consultations, and fostering partnerships with local communities and other relevant actors.

Strengthen Governance Structures: Improve governance mechanisms to ensure equitable distribution of benefits and effective management of potential challenges. This may involve enhancing regulatory frameworks, institutional capacities, and accountability mechanisms to promote fairness, transparency, and accountability in decision-making processes.

Foster Sustainable Development Practices: Integrate socio-economic and environmental considerations into project planning, implementation, and monitoring processes. This includes conducting comprehensive impact assessments, addressing community needs and concerns, and implementing measures to mitigate adverse environmental impacts.

Promote Capacity Building and Knowledge Sharing: Invest in capacity-building initiatives and knowledge-sharing platforms to empower local stakeholders, government agencies, and project developers with the necessary skills and information to effectively engage in renewable energy governance processes.

Encourage Iterative Policy Adjustments: Continuously review and adapt renewable energy policies and regulations to reflect evolving socio-economic, technological, and environmental dynamics. This can involve conducting regular policy evaluations, soliciting feedback from stakeholders, and incorporating lessons learned from project experiences.

References

1. Haidt, J. *African Economic Outlook 2020*: *Developing Africa's Workforce for the Future* (African Development Bank Group, 2020). https://www.afdb.org/en/knowledge/publications/african-economic-outlook
2. Sovacool, B. K. Energy policymaking in Kenya: examining the barriers to effective domestic renewable energy development. *Energy Policy 61*, 1031-1041 (2013).
3. Fofana, A. and Hughes, J. Exploring the Governance Structures of Renewable Energy Projects in Sub-Saharan Africa: A Case Study of Kenya's Ngong Hills Wind Turbine Project. *Journal of Sustainable Development*, *10*(1), 101-116 (2017).
4. *Global Renewable Energy Trends*: *Solar and Wind Move from Mainstream to Preferred* (International Renewable Energy Agency, 2020). https://www.irena.org/publications/2020/Jun/Global-Renewable-Energy-Trends-2020
5. Hughes, J. Renewable energy policy in Kenya: Policy-making in the face of implementation challenges. *Energy Policy 118*, 442-451 (2018).
6. Kenya Electricity Generating Company. Ngong Hills Wind Power Station. https://www.kengen.co.ke/index.php?page=ngong-hills-wind-power-station
7. Kariuki, P. and McDonald, A. Stakeholder engagement and policy-making in renewable energy development in Kenya. *Journal of Sustainable Development 13*(2), 151-165 (2020).

8. Nyangena, W., Kairu, J. K. and Wanyoike, D. M. Renewable energy governance in Kenya: a review of policy and regulatory frameworks. *Renewable and Sustainable Energy Reviews 82*, 2979-2992 (2018).
9. Scott, W. R. Institutions and Organizations: Ideas, Interests, and Identities (SAGE Publications, 2014)
10. Hughes, J. Renewable energy policy in Kenya: Policy-making in the face of implementation challenges. *Energy Policy 118*, 442-451 (2018).
11. DiMaggio, P. J. and Powell, W. W. The iron cage revisited: Institutional isomorphism and collective rationality in organizational fields. *American Sociological Review 48*(2), 147-160 (1983).
12. Kenya Ministry of Energy. Kenya National Electrification Strategy. https://www.energy.go.ke/index.php?option=com_phocadownload&view=category&id=1:national-strategies&Itemid=538
13. Nyangena, W., Kairu, J. K. and Wanyoike, D. M. Renewable energy governance in Kenya: a review of policy and regulatory frameworks. *Renewable and Sustainable Energy Reviews 82*, 2979-2992 (2018).
14. Freeman, R. E. *Strategic management: A stakeholder approach* (Pitman, 1984).
15. Mitchell, R. K., Agle, B. R. and Wood, D. J. Toward a theory of stakeholder identification and salience: Defining the principle of who and what really counts. *Academy of Management Review 22*(4), 853-886 (1997).
16. Clarkson, M. B. A stakeholder framework for analyzing and evaluating corporate social performance. *Academy of Management Review 20*(1), 92-117 (1995).
17. Kamau, W. and Hughes, J. Public participation in renewable energy project decision-making in Kenya: lessons from the Lake Turkana Wind Power Project. *Energy Policy 126*, 254-262 (2019).
18. Bryson, J. M., Crosby, B. C. and Stone, M. M. The design and implementation of cross-sector collaborations: Propositions from the literature. *Public Administration Review 66*(s1), 44-55 (2006).
19. Hughes, J. Renewable energy policy in Kenya: Policy-making in the face of implementation challenges. *Energy Policy 118*, 442-451 (2018).
20. Clarkson, M. B. A stakeholder framework for analyzing and evaluating corporate social performance. *Academy of Management Review 20*(1), 92-117 (1995).
21. Krippendorff, K. *Content analysis; An introduction to its methodology* (Sage publication, 2018).
22. Jones, M. L. and Jenkins, K. Stakeholder engagement and renewable energy development: Exploring the role of local communities in decision-making processes. *Renewable and Sustainable Energy Reviews 107*, 366-376 (2019).
23. Berman, E. P. and Goulart, S. Stakeholder engagement in renewable energy projects: An examination of key drivers and barriers. *Energy Policy 118*, 176-186 (2018).
24. Sarker, M. B. and Khan, N. Stakeholder engagement and renewable energy project success: A systematic review and future research directions. *Renewable and Sustainable Energy Reviews 134*: 110294, (2020).
25. Fuso Nerini, F. et al. Exploring the governance and politics of transitions towards sustainability: A cross-country comparison of renewable energy policymaking in Asia. *Environmental Policy and Governance 28*(2), 73-87 (2018).
26. Boons, F. and Wagner, M. Assessing the impact of stakeholder engagement on the sustainability of urban energy transition initiatives: A meta-analysis. *Sustainability 11*(14): 3815, (2019).
27. Boons, F. and Wagner, M. Assessing the impact of stakeholder engagement on the sustainability of urban energy transition initiatives: A meta-analysis. *Sustainability 11*(14): 3815, (2019).
28. Sovacool, B. K. and Linnér, B. O. The political economy of energy transitions: The case of South Africa. *Energy Research & Social Science 22*, 124-134 (2016).
29. Rai, V. Governing the transition to renewable energy: A review of impacts and policy issues in the small island developing states. *Renewable and Sustainable Energy Reviews 73*, 1100-1110 (2017).
30. Van der Horst, D. and Toke, D. Exploring the landscape of renewable energy citizenship: A case study of wind energy in the UK. *Energy Policy 38*(6), 2538-2547 (2010).
31. Aitken, M. Why we still don't understand the social aspects of wind power: A critique of key assumptions within the literature. *Energy Policy 38*(4), 1834-1841 (2010).
32. Middleton, C. and Parker, J. Renewable energy futures: Experts' views on the socio-economic drivers of change in the UK. *Energy Policy 87*, 523-533 (2015).

Proceedings of

THE 5th INTERNATIONAL CONFERENCE OF

HYOJEONG ACADEMY 2025

Session 2

Technologies for Co-Prosperity

www.ichja.org

5th International Conference of Hyojeong Academy
International Joint Conference 2025

A study on the improvement of corrosion fatigue strength of 7XXX series aluminum alloys by ultrasonic nanocrystal surface modification technology

Junhyong Kim[1], Auezhan Amanov[2,*], Inho Cho[1] and Youngsik Pyun[1]

[1]DesignMecha Co., Ltd, Asan 31414, Korea
[2]Tampere University, Tampere, Finland
*Correspondence: auezhan.amanov@tuni.fi

Abstract: The most commonly used material in civil aircraft is aluminum alloy. Aluminum is light and strong, making it suitable for aircraft structures. It is also easy to process and can be manufactured into various shapes. However, corrosion and corrosion fatigue occur depending on the environment in which it is used. When corrosion occurs, most parts are replaced with new ones to prevent corrosion fatigue. The aviation maintenance industry is trying to prevent corrosion and corrosion fatigue by developing excellent corrosion-resistant materials, reducing the corrosion environment, and reducing stress changes. Ultrasonic nanocrystal surface modification (UNSM) technology is a surface modification technology that applies compressive residual stress and can sufficiently delay the occurrence and growth of corrosion in aluminum alloys. In this study, we will verify the applicability of UNSM technology in a corrosive environment through corrosion fatigue tests of corroded 7XXX series aluminum alloy before and after UNSM treatment.

Keywords: Al7XXX, corrosion, corrosion fatigue, ultrasonic nanocrystal surface modification (UNSM)

1. Introduction

7XXX series aluminum alloys are widely used in aerospace and other high-performance applications, providing excellent strength-to-weight ratio and corrosion resistance. Most aircraft are composed of about 80% aluminum by weight, and 7XXX series aluminum alloys are used in parts that require strength [1, 2]. Among them, Al-Zn-Mg alloys such as Al7075 and Al7050 are mainly used, and are applied to the outer fuselage panels and structural members, wings and tail parts, landing gear struts, fuel tanks, and internal structures of aircraft. Meanwhile, Al7475 is an Al-Zn-Mg-Cu alloy with improved fatigue properties in salt environments, and is used in important parts that require excellent corrosion resistance and corrosion fatigue behavior [3]. Corrosion fatigue is an issue that aircraft manufacturers must address to increase safety and airworthiness. Technologies are being developed worldwide with the goal of developing excellent materials, reducing the corrosion environment, and minimizing stress changes to prevent corrosion fatigue, including aircraft corrosion. In this study, the possibility of applying surface modification technology to delay the occurrence and growth of corrosion fatigue was verified through corrosion fatigue tests on Al7075 aluminum alloy.

2. Ultrasonic nanocrystal surface modification technology

The main concept and mechanism of ultrasonic nanocrystal surface modification (UNSM) technology are shown in Figure 1. A tungsten carbide ball attached to an ultrasonic device that strikes the surface of a work-piece 20,000 or more times per second with 1,000 to 100,000 shots per square millimeter. These strikes, which can be described as micro cold-forging, bring severe plastic deformation (SPD) and elastic deformation to surface layers and thus generate nano-crystalline structure. This nano-structural modification of the surface layer can improve both the strength (hardness) and ductility (toughness) of the work-piece simultaneously according to the well-known Hall-Petch theory [4, 5]. This process also improves surface integrity, increases surface hardness, produces micro-dimples, and induces compressive residual stress in surface layers. The UNSM effects and their anticipated benefits are summarized in Table 1. The UNSM treatment conditions applied to the specimens for the corrosion fatigue test in this study are as shown in Table 2.

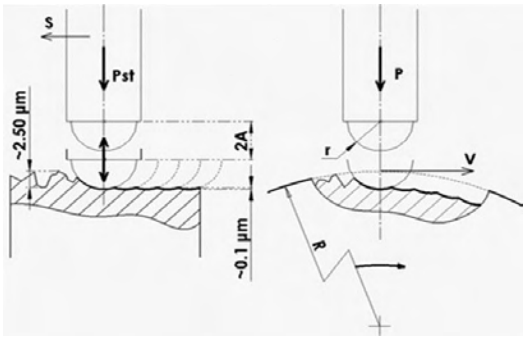

Figure 1. Mechanism of UNSM.

Table 1. The effects of UNSM treatment and their anticipated benefits

Effects of UNSM treatment	Anticipated benefits
Deep compressive residual stresses (Greater than 1,000MPa into depths of more than 2,000μm)	Improved LCF and HCF endurance limit Improved rolling contact fatigue strength Improved stress corrosion cracking resistance
Micro dimples surface (Area: 1-2μm², Depth: submicron, Pattern pitch: few μm)	Reduced surface roughness Decreased friction coefficient Reduced wear rate
Increased hardness (into depths of more than 1,500μm)	Reduced wear rate Improved LCF and HCF endurance limit
Nano-crystalline structure (Grain sizes of 50-200nm into depths of 100μm)	Increased tensile strength and hardness Increased fatigue strength Increased wear resistance

Table 2. UNSM treatment conditions for corrosion fatigue specimens

Frequency	Amplitude	Static load	Spindle speed	Feed rate	Tip diameter
20 kHz	30 μm	50 N	50 rpm	0.07 mm/rev	2.4 mm

3. Materials and methods

3.1. Material

The material used in this study is Al7075-T6 aluminum rod. The detailed chemical composition and mechanical properties are shown in Table 3 and Table 4.

Table 3. Chemical compositions of Al7075-T6 (in wt%)

Si	Fe	Cu	Mn	Mg	Cr	Zn	Ti	Al
0.091	0.112	1.68	0.009	2.598	0.208	5.364	0.02	Balance

Table 4. Mechanical properties of Al7075-T6

Ultimate tensile strength	Tensile yield strength	Elongation
579.8 N/mm²	485.9 N/mm²	14.6 %

3.2. Specimen

The specimen for the corrosion fatigue test is an hourglass-shaped specimen, and the diameter of the part where the stress is most concentrated is 3 mm. The surface roughness of the notch part after machining is approximately

Ra 0.1 um, and the runout tolerance is controlled to 0.005 mm or less. Detailed dimensions of the specimen are shown in Figure 2.

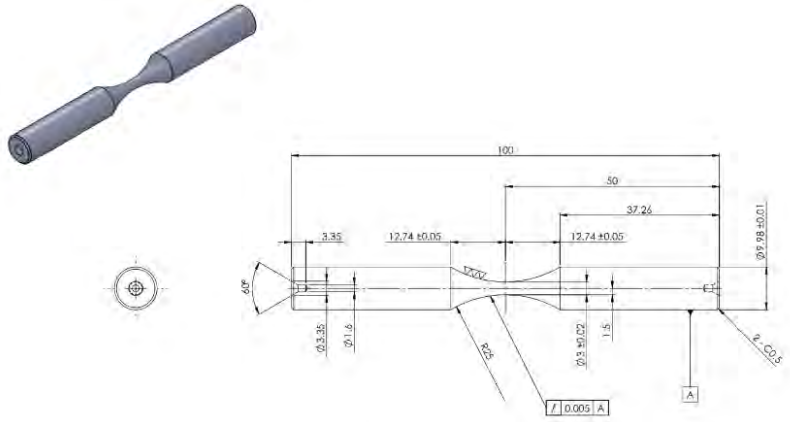

Figure 2. Configurations of corrosion fatigue specimen.

3.3. Corrosion condition

The corrosion conditions of the specimen refer to the following two standards, ASTM G69-97 [6] and ASTM G31-97 [7]. The test solution consists of 58.5 ± 0.1 g of NaCl and 9 ± 1 mL of 30 % hydrogen peroxide reagent per 1 L of aqueous solution. The specimen is immersed in the test solution for 12 hours to be corroded. Figure 3 shows the appearance of the specimen when it was first placed in the test solution and the corroded appearance after 12 hours.

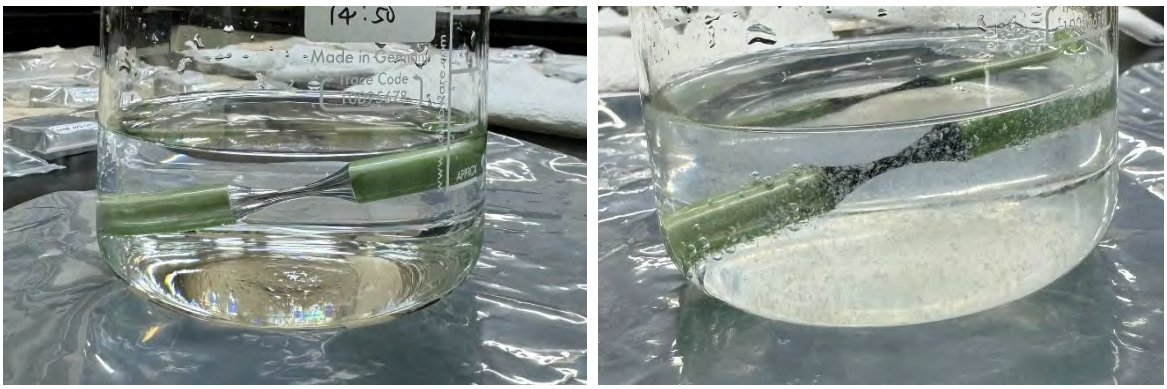

(a) (b)

Figure 3. Appearance of the specimen: (a) before; (b) after corrosion.

3.4. Fatigue test

Corrosion fatigue tests were conducted using a cantilever-type rotary bending fatigue tester (YRB200, Yamamoto, Japan) that uses four specimens simultaneously. The tests were performed under the conditions of a rotation speed of 3150 rpm, stress ratio R = -1, and bending stress of 120 to 300 MPa. Based on the test rotation speed, it takes approximately 2.2 days to reach 1 x 10^7 cycles. The composition of the specimens was classified into three types: Corrosion (C), Corrosion-UNSM (CU), and UNSM-Corrosion (UC).

4. Results and discussion

In previous papers R. Zhang et al. [8] and A. Sharma [9], the corrosion fatigue characteristics of Al7075-T6 material using UNSM technology were studied. The main results were that the fatigue life of the corroded specimens was significantly reduced, but the fatigue life of the specimens treated with UNSM increased by up to 20 times, and that UNSM treatment formed compressive residual stress and suppressed the propagation of fatigue cracks. In this study, UNSM treatment was performed after forced corrosion to confirm the corrosion fatigue delay after

UNSM application. In addition, the corrosion fatigue tendency when corrosion occurred after prior UNSM treatment was also confirmed. The test results are shown in Figure 4.

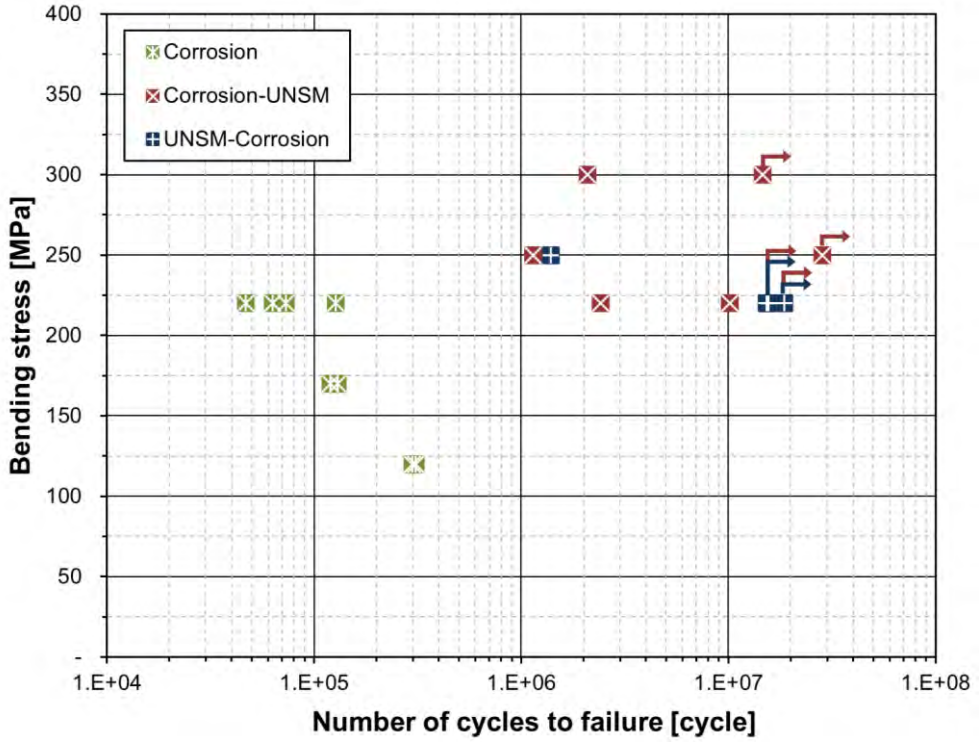

Figure 4. Corrosion fatigue test results of Al7075-T6.

Specimen C showed a fatigue life of 4.6 x 10^4 to 3.1 x 10^5 cycles at a bending stress range of 120 to 220 MPa. Since the fatigue life of normal untreated materials is about 1 x 10^5 cycles at a bending stress of 250 MPa [8], corrosion must be a factor that definitely affects the fatigue characteristics. The corrosion fatigue limit of the C specimen is expected to be formed in the bending stress range lower than 120 MPa. The two types of UNSM-treated groups showed significantly improved corrosion fatigue performance compared to the corrosion group. The CU specimen showed a fatigue life of 1.1 x 10^6 to 2.8 x 10^7 cycles in the bending stress range of 220 to 300 MPa, and the UC specimen showed a fatigue life of 1.3 x 10^6 to 1.8 x 10^7 cycles in the bending stress range of 220 to 250 MPa. The specimen indicated by the arrow in Figure 4 is not failure and is still in the test. In the same stress range, the fatigue life of the CU specimen was improved by about 145 times compared to the C specimen, and that of the UC specimen was improved by about 146 times. The biggest reason for the improvement of corrosion fatigue life is that compressive residual stress is formed on the surface, which delays corrosion cracking. It is generally accepted that the improvement of fatigue life in the non-corrosive state is most affected by compressive residual stress. However, since the fatigue characteristics in the corrosive state have a complex relationship, further research is needed.

5. Conclusions

UNSM treatment was applied to corroded Al7075-T6 aluminum alloy specimens to improve fatigue life. UNSM technology can be applied to surfaces before and after corrosion. The reason for the improved corrosion fatigue performance should be studied further in the future, but the formation of compressive residual stresses through UNSM treatment may be one of the reasons. In the future, fatigue fracture characteristics and trends will be confirmed through fatigue fracture surface analysis, and further research is needed on the relationship between corrosion fatigue delay and compressive residual stress.

References

1. Altenpohl, D. *Aluminum: Technology, Applications, and Environment: A Profile of a Modern Metal*, 6th ed. (TMS, 1998).
2. Verma, B., Atkinson, J. and Kumar. M. Study of fatigue behaviour of 7475 aluminium alloy. *Bull. Mater. Sci 24*(2), 231-236 (2001).
3. Jahn, M. T. and Jin, L. Tensile and fatigue properties of a thermomechanically treated 7475 aluminium alloy. *Journal of materials science 23*, 4115-4120 (1988).
4. Hall, E. The Deformation and ageing of mild steel: III discussion of results. *Proceedings of the Physical Society. Section B 64*, 747 (1951).
5. Petch, N. The cleavage strength of polycrystals. *The Journal of the Iron and Steel Institute 174*, 25-28 (1953).
6. ASTM G69-97. *Measurement of Corrosion Potentials of Aluminum Alloys* (ASTM International, 2017).
7. ASTM G31-21. *Standard Guide for Laboratory Immersion Corrosion Testing of Metals* (ASTM International, 2021).
8. Zhang, R. et al. Fatigue performance rejuvenation of corroded 7075-T651 aluminum alloy through ultrasonic nanocrystal surface modification. *International Journal of Fatigue 153*:106463, (2021).
9. Sharma, A. Effects of advanced surface treatments on microstructure, residual stress and corrosion-fatigue behavior of aluminum alloy 7075-T6. *Ph.D. thesis* 2021, University of Cincinnati, Cincinnati, Ohio, USA.

5th International Conference of Hyojeong Academy
International Joint Conference 2025

Optimized Isolation Balancing Circuit

Wanhae Jeon, Hikasa Akio, Paul Jeremia and Innyeal Oh*

Dept. of Mobility Semiconductor Engineering, Sun Moon University, Asan 31460, Korea
*Correspondence: innyealoh@sunmoon.ac.kr

Abstract: Battery balancing technology is essential to prevent thermal runaway in electric vehicles consisting of more than 7,000 battery cells. In this paper, an isolated balancing circuit is proposed to maintain stable balancing of each unit battery within a high-voltage battery pack structure. The control circuit signals are transmitted via a photo diode, and the balancing operation is controlled through a photo detector in an isolated structure. This design ensures that the low-voltage control circuit remains electrically isolated from the high-voltage system, allowing reliable balancing operation even at voltages of several thousand volts. Furthermore, the circuit is designed to function stably in PVT (Process, Voltage, Temperature) variation environments. Additionally, a cell-level register operation method is employed to ensure noise immunity and enable simultaneous balancing of multiple cells. The proposed balancing circuit operates at an ultra-low power of 180 μW, minimizing battery energy consumption during balancing operations.

Keywords: BMS, Balancing, PVT, Noise, High Voltage Isolation, Stability, Low Power Design, synchronization

1. Introduction

A recent study reports that batteries used in electric vehicles pose a risk of thermal runaway or fire [1, 2]. This risk arises due to voltage differences between cells in automotive battery packs consisting of more than 7,000 cells during continuous charging and discharging. These voltage imbalances can lead to cell overloading, thermal runaway, and ultimately vehicle fires. Therefore, reducing the voltage differences between battery cells is crucial for ensuring stable operation. Previous studies have managed up to 14 battery cells by connecting two semiconductor devices, each monitoring up to 7 cells, in parallel for multi-cell monitoring and balancing. Using passive balancing, which supplies a balancing current of 100mA, they maintained a switch-on resistance below 8Ω and suppressed heat generation to 80mW [3]. In another study, the system stacks two semiconductor devices and selects them via an extern [4]. Other study implemented balancing control by connecting two battery cells or two battery modules in series using a switch [5]. In different study, active balancing was implemented by connecting two cells with an inductor and a switch [6]. However, these all approach did not address potential issues arising from high-voltage and high-current environments. To address these issues, this study proposes a new isolated balancing circuit that mitigates heat generation caused by voltage differences and ensures stable balancing operation in high-voltage battery environments, including electric vehicles operating at voltages in the thousands of volts. Existing isolated structure studies [2, 7] suffer from operational constraints under PVT (Process, Voltage, Temperature) variations. Therefore, this paper presents a new circuit design to overcome these limitations.

2. Isolated Balancing Circuit Design

The proposed Isolated Balancing Circuit consists of an Isolation Interface Block and a Balancing Switch Block. The Isolation Interface Block receives control signals from the Electronic Control Unit (ECU) and controls the high-voltage Balancing Switch Block connected to the battery. To prevent electrical interference between the circuits, the high-voltage Balancing Switch Block is electrically isolated using a photo diode and a photo detector. This design ensures that the low-voltage control circuit in the ECU operates safely without being affected by high-voltage levels that can reach several thousand volts. Figure 1 illustrates the Isolated Balancing Circuit proposed in this paper.

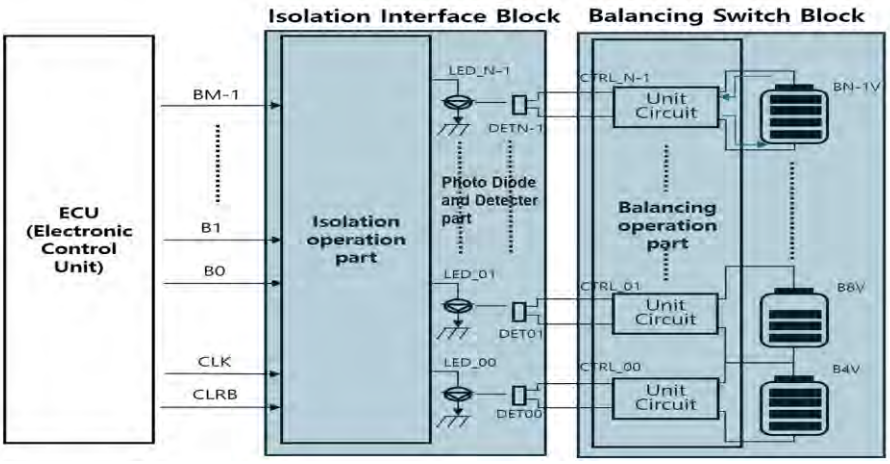

Figure 1. The proposed isolated balancing circuit.

Figure 1 shows the balancing operation in the isolated balancing circuit, and Figure 2 requires a stable operation design with the photo diode and the photo detector part, which are the core circuits controlled indirectly. For the stable operation of this circuit that is sensitive to the PVT environment, the Rd and Rb values were optimized through measurement.

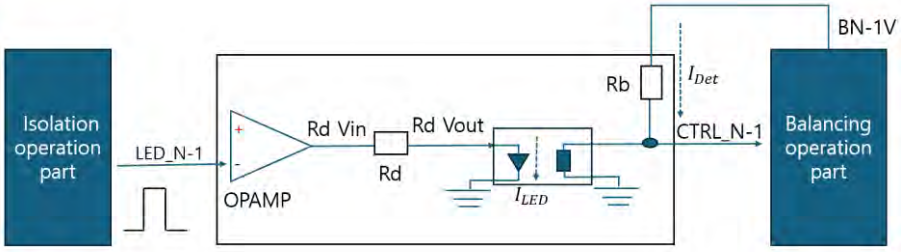

Figure 2. Test block diagram for defining resistance RD and RB values.

Figure 3 shows the experimental results defining the maximum input voltage (Rd Vout) of the photo diode (LED) according to the Rd value in the isolated balancing circuit. OPAMP limits the maximum output current to 6 mA and is designed to be less than 3 mA for stable operation.

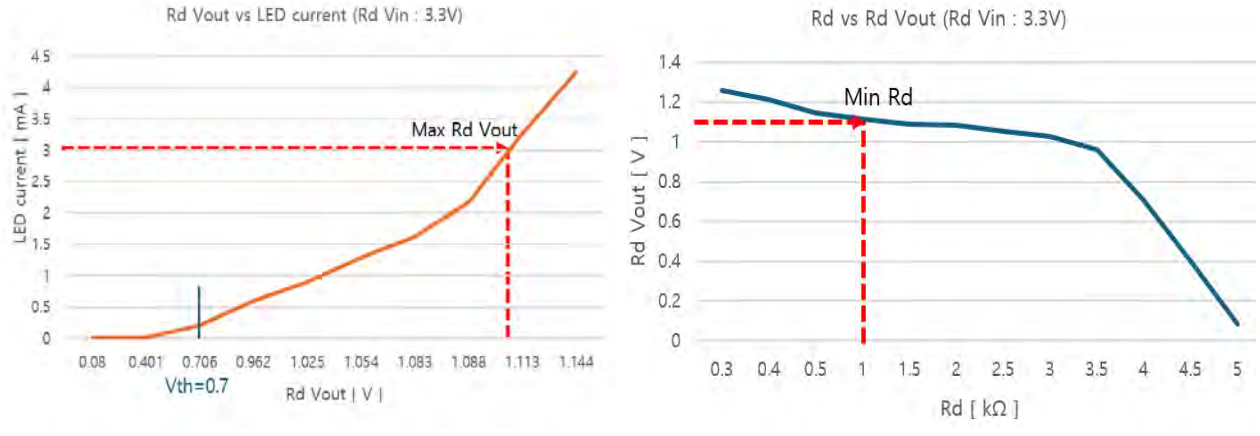

(**a**) (**b**)

Figure 3. Photo diode operating characteristics (a)Voltage for LED current (b)Rd value according to voltage.

As a result of the experiment in Figure 3, the maximum voltage is 1.113V, the minimum resistance value is 1kΩ, and the operation start voltage (Vth) of the photo diode is 0.7V.

In Figure 4, the balancing current was analyzed based on changes in Rb and Rd values. It was observed that a larger Rb value leads to an earlier initiation of balancing, and when Rb exceeds 5 kΩ, the circuit exhibits stable operational characteristics. Additionally, a higher Rd value reduces the OPAMP load, but if Rd is too large, the photo diode fails to operate. Therefore, it was confirmed that stable operation can be achieved by setting Rb to 5 kΩ or higher and optimizing the Rd value. In order for the balancing to operate stably, Rd should be less than 2kΩ and greater than 1kΩ, so the optimal Rd value was set to 1.5kΩ.

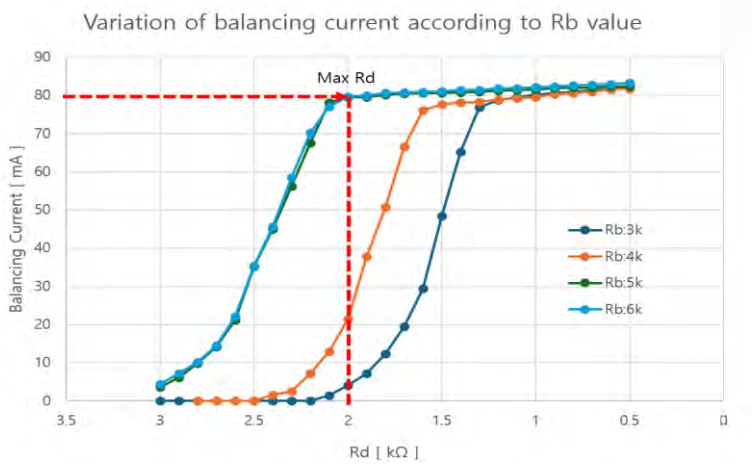

Figure 4. Variation of balancing current according to Rb value.

3. Results

Figure 5 shows the balancing circuit test results for the balancing current according to the battery input voltage (Vin) and compared with the PVT simulation results.

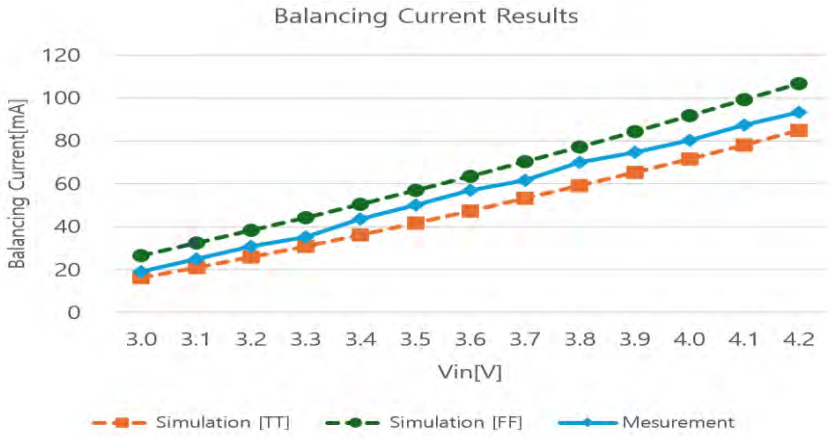

Figure 5. PVT Balancing Simulation and measurement result.

In the graph, it was confirmed that the actual measurement values are positioned between the TT (Typical-Typical) and FF (Fast-Fast) simulation values. TT represents the typical characteristics of both NMOS and PMOS, designed based on the average process performance. FF indicates a faster characteristic, where increased carrier mobility enhances current driving capability but also leads to higher power consumption. It was observed that a current of 20 mA or more flows at an input voltage of 3V, while a balancing current of 87 mA or more flows at 4.2V. The measured values were found to be between the TT and FF results. Additionally, the implemented circuit operates with ultra-low power consumption of 180 μW.

4. Conclusions

In this study, a new isolated balancing circuit utilizing LED-based optical signal transmission was proposed, and operation stability was verified through experimental and simulation results. Compared to conventional balancing circuits that use direct electrical connections, the proposed circuit enhances safety by completely isolating the high-voltage and low-voltage circuits. In particular, the balancing control signal operates stably by synchronizing with CLK, while the cell-level register operation method enables simultaneous balancing operation of multiple cells. The balancing current was measured at 87 mA. Additionally, the proposed balancing circuit demonstrated high energy efficiency, operating with low power consumption of 180 μW. This study makes an important contribution to enhancing the reliability of BMS (battery management systems) in high-voltage environments, and confirms its operational performance under various conditions.

References

1. Sun, P., Bisschop, R., Niu, H. and Huang, X. A Review of Battery Fires in Electric Vehicles. *Fire Technology 56*, 1361-1410 (2020).
2. Akio, H., Jeon, W., Hai, V. and Oh, I. High current operation high speed balancing switch design. In Proceedings of the 3rd Internation Conference of Hyojeong Academy, online, Korea (1-3 Feb. 2024).
3. Vulligaddala, V. et al. A 7-Cell, Stackable, Li-Ion Monitoring and Active/Passive Balancing IC With In-Built Cell Balancing Switches for Electric and Hybrid Vehicles. *IEEE Transactions on Industrial Informatics 16*(5), 3335-3344 (2019).
4. Manjunath, K. and Kalpana, R. A Modularized Two-Stage Active Cell Balancing Circuit for Series Connected Li-Ion Battery Packs. In Proceedings of IEEE International Conference on Power Electronics, Drives and Energy Systems, Jaipur, India (14-17 Dec. 2022).
5. Kulkarni, A. and Teodorescu, R. Closed-loop Control of MOSFET Gate Voltage for Charge Balance in a Smart Li-ion Battery Cell. In Proceedings of 11th International Conference on Power Electronics and ECCE Asia, Jeju, Korea (22-25 May 2023).
6. Valsan, V., Kini, S., Padmasali, A. and Nath, A. Study of the Effect of Temperature and C-Rate on Inductor Based Active Cell Balancing for a Li-Ion Based Battery. In Proceedings of 2024 IEEE International Conference on Distributed Computing, VLSI, Electrical Circuits and Robotics (DISCOVER), Mangaluru, India (18-19 Oct. 2024).
7. Akio, H. et al. Monitoring and balancing the battery's temperature compensation cells. In Proceedings of ASSK 2024, Kyungju, Korea (4-5 July 2024).

5th International Conference of Hyojeong Academy
International Joint Conference 2025

Transforming Clinical and Dermoscopic Images Using CycleGAN: Bridging Data Scarcity for AI-Driven Dermatology

Sarreha Tasmin Rikta and Wonsang You*

Dept. of Information and Communication Engineering, Sun Moon University, Asan 31460, Korea
*Correspondence: wyou@kaist.ac.kr

Abstract: Dermoscopy and clinical imaging are crucial for diagnosing skin conditions, as they offer complementary insights that deepen our understanding of the underlying issues. While clinical images can be relatively straightforward to obtain, capturing dermoscopic images often presents more difficulties due to practical constraints, budgetary issues, and the requirement for specialized equipment. This limited availability of dermoscopic data creates significant obstacles for developing effective deep learning models in dermatology. To tackle this challenge, we introduce an innovative approach utilizing CycleGAN (Cycle Generative Adversarial Network), a deep learning model tailored for bidirectional image-to-image translation, to create synthetic dermoscopic and clinical images from their respective counterparts. Our method converts clinical images into dermoscopic images and vice versa, creating a synthetic dataset that preserves the essential pathological features. The qualitative results show that CycleGAN successfully generates realistic synthetic images that are consistent with the underlying pathology, effectively bridging the gap between the two modalities. Our approach aims to enhance diagnostic accuracy and lessen the dependence on costly data collection methods. This study establishes a foundation for utilizing synthetic data in medical imaging, tackling the challenges posed by limited dermoscopic datasets, and promoting the integration of artificial intelligence into clinical practice.

Keywords: Dermoscopic, Clinical, Deep Learning, CycleGAN, Synthetic data

1. Introduction

Skin diseases are among the most prevalent health issues worldwide and a significant cause of mortality [1]. Diagnosing these conditions usually requires a thorough dermatological examination and sometimes a biopsy. Dermoscopes, which are handheld devices that can reveal skin structures not visible to the naked eye, are frequently employed in this process. Many of these devices now come equipped with cameras to capture images of lesions. These images can be valuable for obtaining second opinions, including through automated computer-aided diagnosis (CAD) systems. However, this diagnostic process can be both time-consuming and expensive. To address these challenges, researchers have been exploring the use of AI in the healthcare field for several years. The use of artificial intelligence (AI) in dermatology offers great potential for improving the accuracy and efficiency of diagnosing skin conditions [2, 3]. However, the effective implementation of AI algorithms heavily relies on having access to comprehensive and diverse training datasets. In dermatology, gathering large amounts of high-quality labeled images can be quite challenging, especially for rare skin diseases. This lack of sufficient data often results in imbalanced datasets, which can negatively impact the performance of AI (Artificial Intelligence) models, leading to lower generalization and accuracy when diagnosing conditions that are not well-represented in the training data. To overcome these challenges, new methods utilizing generative models, particularly CycleGAN (Cycle-Consistent Generative Adversarial Networks), have been developed as a promising solution for enhancing datasets in dermatology. CycleGAN is well-known for its capability to create new images by learning from existing unsupervised data, allowing for transformations between various image types without the need for paired images [4]. For example, CycleGAN can successfully produce synthetic clinical images from dermoscopic images, or the other way around, thus achieving a more balanced representation of skin conditions across different demographics.

In this study [5] CycleGANs is used to create realistic dermoscopic skin lesion images that are specific to different classes, serving as training data for supervised machine learning models. They proposed two innovative

methods for generating these synthetic images, which are subsequently assessed for their effectiveness in enhancing a convolutional neural network (CNN) tasked with a complex lesion classification challenge. In another study data augmentation techniques like CycleGAN are used to tackle the data scarcity issue to create detailed synthetic training samples [6]. The results show that integrating CycleGAN-augmented data with the EfficientNet B1 model not only lowers the costs of manual annotation but also significantly enhances classification accuracy. Irungu et al. currently presents a controllable image synthesis framework inspired by CycleGAN to tackle the challenges of breast lesion detection [7]. By utilizing semantic masks, the framework facilitates image-to-image translation, allowing for the introduction of realistic pathological features into healthy whole slide images at designated locations. The synthetic images are then combined with actual data from the BRACS dataset and traditional augmentation techniques to improve lesion detection. This enhanced dataset significantly boosts detection performance, achieving an area under the curve (AUC) nearing one, which reduces missed diagnoses and supports early cancer detection. This method highlights the potential of synthetic images in overcoming data limitations in biomedical imaging. In addition, CycleGAN-based image transformation method that utilizes convolutional autoencoders for domain translation improves privacy in deep learning models without sacrificing their utility [8]. In another paper, the author tackles the challenge of enough labeled data by utilizing Generative Adversarial Networks (GANs) to artificially expand the dataset, addressing the problem of limited training samples [9]. The CNN model is then used for automatic classification, which enhances the model's ability to distinguish between different categories. Experimental results indicate that this method improves classification performance, achieving an average accuracy of 94.5%, which is 1.9% higher than previous techniques.

However, all these papers have shown that Generative adversarial networks (GANs) is a powerful tool for synthetic data generation, offering the potential to address data scarcity in medical imaging. It has gained recognition for its ability to perform bidirectional image translation while preserving the structural integrity of the source images. As creating dermoscopic images is quite challenging due to the high cost of dermoscopic imaging devices, we are proposing the use of CycleGAN to transform clinical images into dermoscopic images and vice versa, enabling the generation of synthetic datasets that retain critical pathological features. By enhancing the availability of dermoscopic datasets, this research aims to bridge the data gap, facilitate AI-driven dermatology, and improve diagnostic accuracy. Our findings demonstrate that synthetic images generated by CycleGAN are both realistic and pathological-consistent, underscoring their potential utility in medical imaging. This work not only addresses a significant limitation in dermatology but also paves the way for further exploration of GAN-based data augmentation in medical and healthcare applications.

2. Materials and Methods

2.1. Dataset Preprocessing

In this project, we utilized the 7-point skin lesion malignancy dataset, which comprises over 2,000 clinical and dermoscopic color images. For our analysis, we specifically focused on 887 paired clinical and dermoscopic images, though these do not include ground truth annotations. The dataset preprocessing includes resizing all images to 256×256 pixels, converting them into PyTorch tensors, and normalizing the pixel values to a range centered around 0 with a standard deviation of 0.5 for each channel. These steps help maintain consistency and ensure the data is suitable for deep learning models.

2.2. Overview of CycleGAN architecture

CycleGAN is an innovative framework created for unpaired image-to-image translation. Its goal is to learn a mapping between two domains, X and Y, allowing an image from domain X to be transformed into domain Y and then back to domain X to reconstruct the original image. The fundamental idea is based on using two mappings: one from X to Y and another from Y to X. This method effectively tackles the issue of lacking paired examples in numerous real-world situations. The figure 1 represents the architecture of CycleGAN.

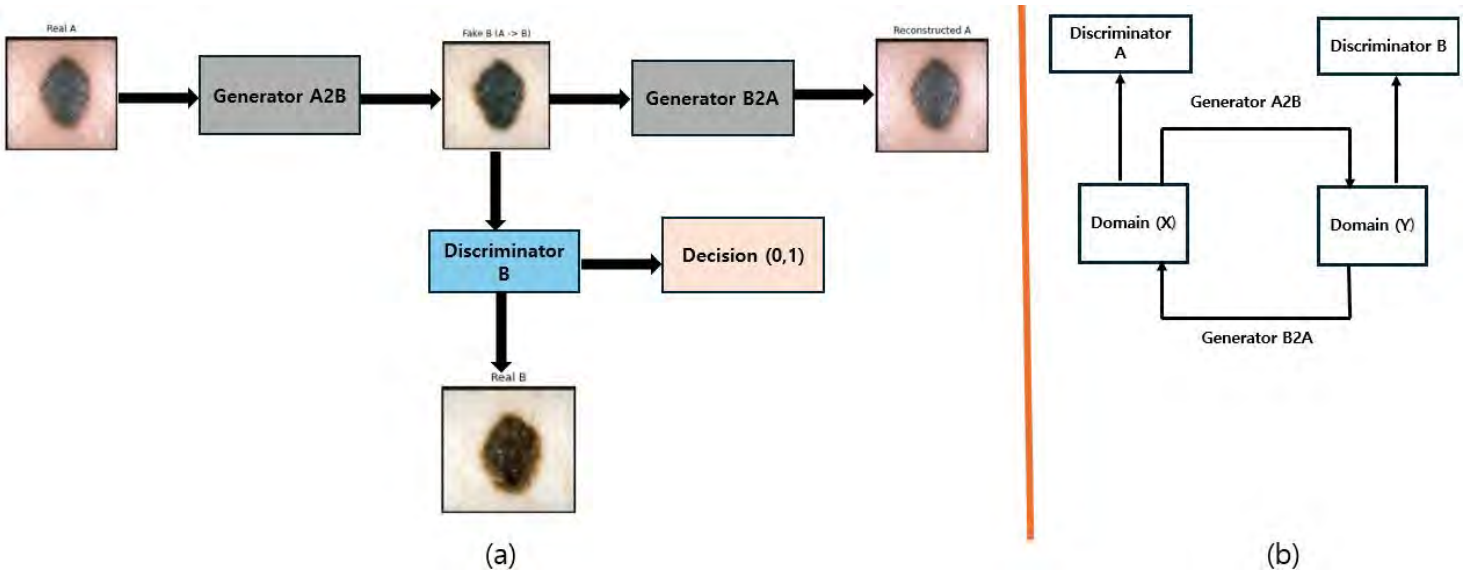

Figure 1. (a) Translation clinical (Domain X) to dermoscopic (Domain Y); (b) Full cyclic translation from domain X to domain Y and vice versa.

The architecture of CycleGAN features two generator networks and two discriminator networks [4]. The generators create images in the target domain based on input images from the source domain, while the discriminators assess the authenticity of these generated images. A key component of CycleGAN is the cycle consistency loss, which ensures that when an image is transformed from X to Y and then back to X, it should closely match the original image. This relationship is mathematically expressed as F(G(X)) ≈ X and G(F(Y)) ≈ Y. In this model, we have utilized multiple loss functions, including Adversarial Loss and Cycle Consistency Loss, to ensure effective training. Adversarial Loss helps ensure that the images generated from one domain appear realistic in the other domain. The mathematical equation for this is as follows [11]:

$$L_{GAN}(G, D_{y,}X, Y) = E_{y\sim p_{data(y)}}[log(D_Y(y))] + E_{x\sim p_{data(x)}}[log(1 - D_Y(G(x))] \quad (1)$$

The adversarial loss equation describes how domain X is mapped to domain Y using generator G, and domain Y follows the same process. In this context, G represents generator A, F denotes generator B, D(x) refers to discriminator A, and D(Y) indicates discriminator B. Another important aspect is Cycle Consistency Loss, which guarantees that the relationships between two domains, X and Y, remain consistent. This loss function promotes the idea that the transformation should maintain the original content when transitioning back and forth between the domains. Mathematically, it is represented as follows-

$$L_{cyc}(G, F) = \mathbb{E}_{x\sim P_{data}}(x)[\| F(G(x)) - x \|_1] + \mathbb{E}_{y\sim P_{data}(y)}[\| G(F(y)) - y \| 1] \quad (2)$$

So, the total loss will be [4]

$$L(G, F, D_x, D_y) = L_{GAN}(G, D_{y,}X, Y) + L_{GAN}(F, D_{x,}X, Y) + \lambda L_{cyc}(G, F) \quad (3)$$

where λcontrols the importance of cycle consistency.

3. Results and Discussion

In this study, we evaluated the qualitative performance of CycleGAN for bidirectional image translation between clinical and dermoscopic domains, with a focus on its ability to preserve important lesion characteristics. Qualitative analysis is used to assess the quality and effectiveness of the images generated. This section emphasizes the qualitative results, demonstrating how the model's output quality improved throughout the training process.

Figure 2 displays synthetic and reconstructed images produced at various training stages (epoch 100 and epoch 200). These visual comparisons offer valuable insights into the model's capability to capture domain-specific features and maintain image fidelity across different training iterations-

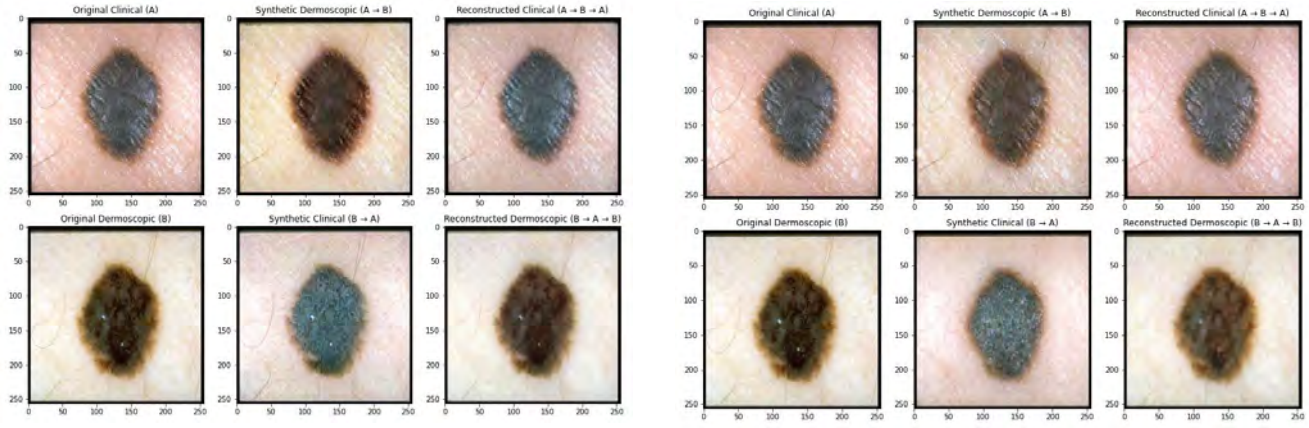

(a) **(b)**

Figure 2. Qualitative analysis of CycleGAN-generated images at various training epochs: (a) The outputs at epoch 100 indicate early advancements in domain translation, though they still exhibit some minor artifacts and inconsistencies; (b) The outputs at epoch 200 reflect enhanced quality, showcasing improved textures, greater color consistency, and maintained structural details, underscoring the benefits of prolonged training.

The synthetic images produced at epoch 100 show a good translation, effectively capturing key characteristics of lesions like shape, color, and texture. However, there are some minor artifacts and color tone inconsistencies, particularly in the synthetic dermoscopic images (A → B). By epoch 200, the model shows better consistency, with smoother and more polished textures in both synthetic and reconstructed images. The improved stability in the later epoch indicates that the CycleGAN model has converged well, minimizing artifacts while maintaining important clinical details. At epoch 200, the synthetic dermoscopic images (A → B) and synthetic clinical images (B → A) exhibit better color consistency and less artificial smoothing than those at epoch 100. The reconstructed clinical images (A → B → A) at epoch 200 closely match the original input, demonstrating improved cyclic consistency. Likewise, the reconstructed dermoscopic images (B → A → B) preserve the intricate structural details of lesions, showing enhanced contrast and fewer distortions. The findings at epoch 200 indicate that prolonged training allows the model to recognize subtle differences across domains, which is essential for analyzing medical images. The enhanced ability to reconstruct clinical and dermoscopic features by the final epoch guarantees the preservation of lesion characteristics, a vital aspect for diagnostic purposes.

The findings further highlight the model's ability to learn intricate relationships between clinical and dermoscopic images, effectively capturing specific features of each domain while preserving the key characteristics of the lesions. However, there is still potential for enhancement regarding image quality and computational efficiency. In our future work, we intend to investigate diffusion-based models for image translation. These models have recently shown impressive results in generating high-quality and varied images and applying them in this field could significantly improve the accuracy of synthetic images. Additionally, we plan to compare the outcomes of diffusion models with the existing CycleGAN-based method to provide a thorough assessment of their respective advantages and disadvantages. Furthermore, to tackle the challenges of computational demands often linked with cutting-edge generative models, we aim to explore innovative, lightweight techniques for image translation. These approaches would focus on minimizing resource usage while ensuring high-quality results, making them more applicable for real-time and resource-limited scenarios, such as mobile or edge computing in medical diagnostics. These initiatives mark a crucial advancement in the field of medical image translation, ensuring that the methods developed are both effective and practical for real-world applications.

5. Conclusions and future work

In this study, we explored the effectiveness of CycleGAN for translating between clinical and dermoscopic image types, tackling the challenges posed by the limited availability of dermoscopic datasets. The synthetic images produced by CycleGAN effectively maintained essential pathological features, demonstrating its ability to enhance dataset variety and aid in the creation of strong diagnostic models. Although our findings are encouraging, further investigation into diffusion models and more efficient generative techniques is needed to enhance image quality and reduce computational demands. These improvements will facilitate the wider use of synthetic data in medical imaging, promoting the integration of AI into clinical practices and ultimately leading to better diagnostic results in dermatology.

Author Contributions: Conceptualization, S.R. and W.Y.; methodology, S.R. and W.Y.; software, S.R.; validation, S.R; formal analysis, S.R.; writing—original draft preparation, S.R.; writing—review and editing, S.R. and W.Y.; visualization, S.R.; supervision, W.Y.; project administration, W.Y.; funding acquisition, W.Y. All authors have read and agreed to the published version of the manuscript.

Funding: This work was supported by the Basic Science Research Program (NRF-2022R1F1A1075204), the BK21 FOUR, and the Regional Innovation Strategy Project (2021RIS-004) through the National Research Foundation of Korea (NRF) funded by the Ministry of Education, South Korea.

Data Availability Statement: Not applicable

Conflicts of Interest: The funders had no role in the design of the study; in the collection, analyses, or interpretation of data; in the writing of the manuscript; or in the decision to publish the results.

References

1. Rikta, S.T. et al. Xml-gbm lung: An explainable machine learning-based application for the diagnosis of lung cancer. *Journal of Pathology Informatics 14*, 100307 (2023).
2. Lundervold, A.S. and Lundervold, A. An overview of deep learning in medical imaging focusing on MRI. *Zeitschrift für Medizinische Physik 29*(2), 102–127 (2019).
3. Litjens, G. et al. A survey on deep learning in medical image analysis. *Medical Image Analysis 42*, 60–88 (2017).
4. Zhu, J.-Y., Park, T., Isola, P. and Efros, A.A. Unpaired image-to-image translation using cycle-consistent adversarial networks. In Proceedings of the IEEE International Conference on Computer Vision, Venice, Italy (22-29 Oct. 2017).
5. Fossen-Romsaas, S., Storm-Johannessen, A. and Lundervold, A.S. Synthesizing skin lesion images using CycleGANs–a case study. *Norsk Informatikkonferanse 12* (2020).
6. Chen, Y., Zhu, Y. and Chang, Y. CycleGAN based data augmentation for melanoma images classification. In Proceedings of the 3rd International Conference on Artificial Intelligence and Pattern Recognition, Xiamen, China (26-28 June 2020).
7. Kawahara, J., Daneshvar, S., Argenziano, G. and Hamarneh, G. Seven-point checklist and skin lesion classification using multitask multimodal neural nets. *IEEE Journal of Biomedical and Health Informatics 23*(2), 538–546(2019).
8. An, T. and Joo, C. CycleGANAS: Differentiable neural architecture search for CycleGAN. In Proceedings of the IEEE/CVF Conference on Computer Vision and Pattern Recognition Workshops, Seattle, Canada (17-21 June 2024).
9. Rodriguez, D. and Krishnan, R. A Cycle-GAN based image encoding scheme for privacy enhanced deep neural networks. In *Information Systems Security* (Springer, 2023).
10. Tao, M. and Yan, Y. (2022) Identifying melanoma in lesion images using cycle-consistent adversarial networks-based data augmentation. In Proceedings of International Conference on Medical Imaging and Computer-Aided Diagnosis, Strasbourg, France (27 Sep. - 1 Oct. 2021).
11. Kawahara, J., Daneshvar, S., Argenziano, G. and Hamarneh, G. Seven-point checklist and skin lesion classification using multitask multimodal neural nets. *IEEE Journal of Biomedical and Health Informatics 23*(2), 538–546 (2019).

5th International Conference of Hyojeong Academy
International Joint Conference 2025

Analytical Approaches to Improving Power Efficiency in Reversed Doherty Power Amplifiers

Anidozie Lordsday Sunday, Khurshid Hussain, Paul Jeremaih, Wanhae Jeon and Innyeal Oh*

[1]Department Dept. of Mobility Semiconductor Eng. Sun Moon University, Asan 31460, Korea
*Correspondence: innyealoh@sunmoon.ac.kr

Abstract: This study investigates the performance in output power and efficiency enhancements of Reversed Doherty Power Amplifiers (RDPA) compared to Conventional Doherty Power Amplifiers (CDPA) under varying Quarter-Wave Transformer Losses (QWTL) from 1 dB to 5 dB. The RDPA achieves a comparable maximum output power (Psat) of 47.55 dBm, with a 6 dB back-off point showing consistent performance superiority, maintaining a lead of 0.7–2.9 dB across QWTL conditions. Despite a 1.25 dB decrease in saturation power due to QWTL, RDPA demonstrates a notable improvement in Power Added Efficiency (PAE), achieving 43% at 6 dB back-off, compared to CDPA's 35%. Efficiency at other load conditions (OBO) for RDPA also consistently outperforms CDPA, with PAE ranging from 3.79% to 25.83% depending on QWTL and Drain efficiencies (DE) of the carrier and peaking amplifiers. These results highlight the RDPA's resilience to QWT losses and its potential for energy-efficient wireless applications, positioning it as a strong candidate for next-generation high-efficiency amplifier designs.

Keywords: Quarter-wave line, Load modulations, Doherty power amplifier

1. Introduction

In recent advancements in power amplifier technology, the Reversed Doherty Power Amplifier (RDPA) has emerged as a groundbreaking architecture for improving energy efficiency and performance in modern wireless communication systems [1, 2]. While traditional Doherty Power Amplifiers (DPA) have proven effective, they rely on quarter-wave transformers (QWTs) that inherently introduce losses. These losses, particularly detrimental in the carrier amplifier, a linear amplifier, are exacerbated at lower frequencies where QWTs must be replaced with lumped elements [3]. This substitution significantly impacts efficiency and linearity, especially at back-off power levels, where most amplification occurs [2, 4]. The RDPA addresses these limitations through a reversed configuration that enhances power handling and efficiency at back-off levels, making it exceptionally well-suited for mobility-centric technologies [5]. In transmission technologies such as beamforming and carrier aggregation, which are integral to advanced vehicular communication systems, RDPAs will play a vital role in ensuring signal integrity and operational efficiency [5]. Their ability to adapt to varying QWT losses and drain efficiency conditions makes them well-suited for the stringent demands of Orthogonal Frequency Division Multiple Access (OFDMA) signals used in LTE, 5G, and WiMAX. These technologies, characterized by a high Peak-to-Average Power Ratio (PAPR) due to their multi-carrier nature, require amplifiers capable of achieving high efficiency during back-off operations [5, 6]. This PA can be used in future communication beamformers as discussed in Khurshid et al. [7].

This study presents a comprehensive analysis of RDPA performance under varying QWT losses, emphasizing its potential for enabling next-generation wireless communication systems and advancing mobility technologies.

2. Circuit Design

Our design introduces a Reversed Doherty Power Amplifier (RDPA) that achieves improved power efficiency and output performance by restructuring the placement of the quarter-wave transformer (QWT) within the peaking amplifier's path [3]. The design has been rigorously tested across QWT loss settings ranging from 1 to 5 dB, demonstrating optimized performance across both back-off and peak power levels for an efficient and reliable architecture. As illustrated in Figure 1, the RDPA positions the QWT after the peaking amplifier, enabling the carrier amplifier to directly drive the load during the output back-off (OBO) condition. This innovative configu-

ration significantly reduces efficiency and power losses in the carrier amplifier's path, enhancing back-off efficiency compared to conventional Doherty designs [4]. The RDPA incorporates precisely engineered output matching networks (OMNs) for both the carrier and peaking amplifiers. These OMNs provide accurate impedance transformation and effective power combination, ensuring minimal insertion losses and maintaining high linearity [8]. With its unique architecture, the RDPA delivers a high-efficiency solution for modern communication systems, offering superior power performance while maintaining a simple and adaptable design. This advancement represents a significant step forward in power amplifier technology, meeting the demands of next-generation wireless networks with precision and reliability [9].

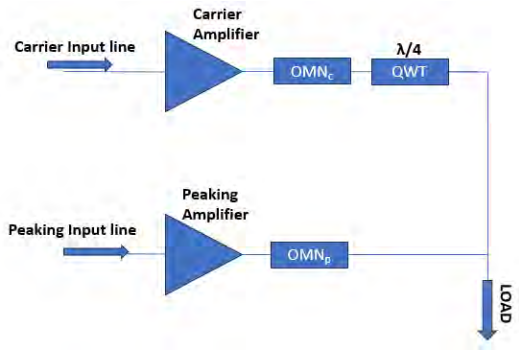

Figure 1. Conventional Doherty Power Amplifier.

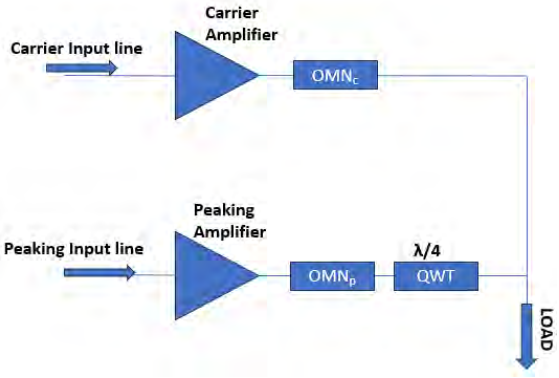

Figure 2. Reversed Doherty Power Amplifier.

3. Results

Figure 3 illustrates the power performance comparison between the RDPA and CDPA. At the saturation point, the output power of both systems is nearly identical. However, the RDPA demonstrates superior performance, maintaining a higher output power ranging from 0.7 dB to 2.9 dB for QWT losses of 1 dB to 5 dB, respectively.

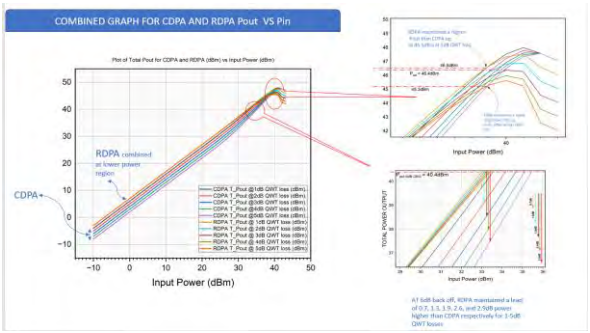

Figure 3. Combined Power for RDPA and CDPA.

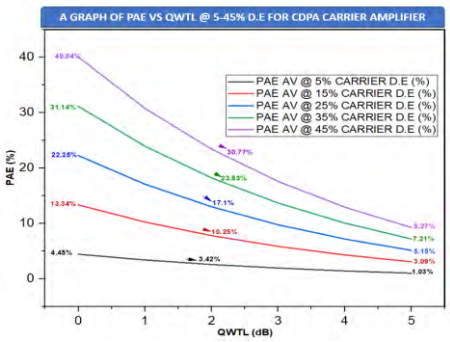

Figure 4. PAE Variations with QWTL

Figure 4 highlights the PAE loss of the carrier amplifier in the CDPA at the back-off region. With a QWT loss of 5 dB, the CDPA experiences a significant PAE reduction of up to 30%. This efficiency loss, predominantly in the back-off region—where most amplification occurs—is unique to the CDPA, giving the RDPA a clear performance advantage.

Table 1. Comparisons Table

S.NO	Our Work -RDPA	Our Work -CDPA	[5]	[6]
Topology	Reversed Doherty PA	Convectional Doherty PA	Load Insensitive Doherty PA	D-Band PA
Maximum Pout@6dBOBO	40.4, 40.3, 40.2, 40.1, 40dBm	39.7,39, 38.25,37.55, 36.9dBm	32.3dBm	15.4dBm
QWTL (1-5dB) effect on P6dBOBO	_	Lead CDPA with 0.7, 1.3, 1.9, 2.4 and 2.9dB	0.1dB	NA
OP_{1dB}	47dBm	47dBm	40dBm	NA
PAE @6dBOBO	35%	43%	_	Peaking 14.5%_
P_{sat}	***Approx 48dBm***	***Approx 48dBm***	NA	N

4. Conclusions

In conclusion, our developed Reversed Doherty Power Amplifier (RDPA) represents a groundbreaking advancement in RF amplifier technology. By leveraging innovative design principles, it outperforms conventional Doherty Power Amplifiers (CDPAs) in power efficiency and performance under back-off conditions. At saturation, the RDPA achieves comparable output power to the CDPA, while maintaining a superior output power advantage of 0.7 dB to 2.9 dB for QWT losses ranging from 1 dB to 5 dB. A significant efficiency enhancement is realized in the back-off region, where the RDPA eliminates the substantial PAE loss—up to 30%—experienced by the CDPA due to QWT losses. This critical improvement addresses the region where most amplification occurs, ensuring enhanced efficiency and reliability. Through these advancements, the RDPA establishes itself as a robust, energy-efficient solution for modern RF applications, setting a new standard in power amplifier design and paving the way for future innovations in RF systems [10].

References

1. Saraswat, P., Arrawatia, M. and Bhattacharjee, R. Doherty Power Amplifier Based TR front end Network for 5G Mm-Wave Applications. In Proceedings of 2024 22nd IEEE Interregional NEWCAS Conference (NEWCAS), Sherbrooke, QC, Canada (16-19 June 2024). doi: 10.1109/NewCAS58973.2024.10666333.
2. Kobi K. and Pindell, S. Design of High Efficiency Doherty Power Amplifier. https://digitalcommons.calpoly.edu/eesp/618.
3. Zhang, J. et al. A Compact 24-30GHz Doherty Power Amplifier with a Flexible T-Type L-C-L Series Combiner and New Power Sensing Method for 5G Communications. In Proceedings of 2023 IEEE MTT-S International Microwave Workshop Series on Advanced Materials and Processes for RF and THz Applications, Chengdu, China (13-15 Nov. 2023). doi: 10.1109/IMWS-AMP57814.2023.10381165.
4. Quaglia, R., Pang, J., Cripps, S. C. and Zhu, A. Load-Modulated Balanced Amplifier: From First Invention to Recent Development. *IEEE Microwave Magazine 23*(12), 60-70 (2022).
5. Deep, S. et al. A load insensitive Doherty power amplifier with better than− 39dBc ACLR on 2: 1 VSWR circle using a constant 50 Ω trained pre-distorted signal. In Proceedings of 2022 52nd European Microwave Conference, Milan, Italy (27-29 Sep. 2022).
6. Lei, Z. et al. A Compact 140-GHz Power Amplifier With 15.4-dBm Psat and 14.25% Peaking PAE in 28-nm Bulk CMOS Process. *IEEE Transactions on Microwave Theory and TechI want niques 72*, 3016-3030 (2024).
7. Khurshid, H. and Oh, I. Joint Radar, Communication, and Integration of Beamforming Technology. *Electronics 13*(8), 1531 (2024).

8. Peng, C. et al. Simplified Emulation of Active Load Modulation for a Millimeter-Wave GaN MMIC Doherty Power Amplifier Design. *IEEE Transactions on Microwave Theory and Techniques 72*, 149-159 (2024).
9. Shaofei, B. et al. Broadband GaAs HBT Doherty Power Amplifier for 5G NR Mobile Handset. *IEEE Transactions on Circuits and Systems II: Express Briefs 7*, 527-531 (2024).
10. Xiaoling, Z. et al. A 1.8-2.7 GHz High Efficiency Three-Stage GaAs HBT Doherty Power Amplifier. In Proceedings of 2024 International Conference on Microwave and Millimeter Wave Technology, Beijing, China (16-19 May 2024).

5th International Conference of Hyojeong Academy
International Joint Conference 2025

Influence of Fear on Adoption of Telecommuting Platforms in the Post-Coronavirus Era: an Artificial Neural Networks Approach

Chi-Hoon Song[1] and Jun-Young Song[2,*]

[1]Department of IT Management, Sun Moon University, Asan 31460, Korea
[2]Department of Aquatic Life Medical Sciences, Sun Moon University
*Correspondence: jysong80@sunmoon.ac.kr

Abstract: Telecommuting systems are spreading rapidly, but little research has been done to understand determinants that affect its adoption at the individual level. Moreover, research methodologies have tended to be constrained to conventional approaches. This study seeks to identify factors that influence telecommuting platform adoption, with a focus on the effect of perceived fear against a new health crisis during the post-coronavirus era. This study endeavored to combine perceived fear with technology acceptance model, and applied an artificial neural network (ANN) to analyze the data collected by an online survey in South Korea. The results show that our ANN model achieved acceptable prediction accuracy. Perceived fear influences behavioral intention to adopt telecommuting platforms in the face of a new pandemic in the future. Perceived usefulness and perceived ease of use are crucial considerations to adopt the technology. These findings can provide researchers and industrial practitioners with a differentiated view into individual-level adoption of telecommuting systems.

Keywords: Technology acceptance, telecommuting, post-Coronavirus, machine learning, ANN

1. Introduction

The global post-coronavirus crisis two years ago changed the way people work [1, 2]: the shift from working at office to working remotely based on information technology and information systems (IT/IS). The trigger for such a dramatic change was the fear that stemmed from the coronavirus [3, 4]. However, the fear is staying around us even during the post-coronavirus era [5], and a fear of a new pandemic is still a challenge because of the continuous emergence of new variants (e.g., Delta) [6]. Fear (perceived fear: PF) is defined as "an adaptative response to a perceived risk" [7]. Even in the post-coronavirus era, the growing uncertainty about new pandemic infections develops into an endless risk of being infected [8], making it even more likely that individuals will take preemptive measures [9] such as using telecommuting platforms (e.g., Zoom, Teams).

Telecommuting is referred as "working at home or at a location close to home instead of commuting to a conventional work location" [9, 10]; work-from-home platform is a set of technologies that support working from a remote location. Compared to the past [8], current telecommuting platforms are much more technology intensive [11]: the core technologies include cloud platforms based on distributed parallel computing systems, communication and collaboration applications, project management tools and security. Prior studies have shown that telecommuting platform is one of the most effective adaptive defenses against new threatening situations [2, 3], and its use is expected to continue to increase even after the post coronavirus era [10, 11]. However, our literature review found a lack of research examining the drivers of accepting telecommuting platforms at the individual level, particularly with a focus on perceived fear of a new pandemic during the post-coronavirus era.

Technology acceptance research (e.g., accepting telecommuting platforms) has used various theoretical frameworks and approach methodologies to understand users' acceptance of a certain technology [12–14]. Regarding the theoretical frameworks used, technology acceptance model (TAM) has been one of the most widely-known models because of its simplicity [13, 15, 16]. TAM proposes that perceived usefulness (PU) and perceived ease of use (PE) determine individuals' behavioral intention (BI) to adopt a certain technology; the easiness affects the usefulness of a technology [17]. Regarding the analysis methods used, probability-based statistical analysis techniques such as structural equation modeling (SEM) are the most employed approaches [18, 19]. Interestingly, our literature review found that work-from-home acceptance studies using nonlinear approaches (e.g., artificial neural networks: ANN) are still rare. SEM oversimplifies the relationship between latent constructs that make up research model, which limits modeling the complexity of the decision-making process [19, 20] such as telecommuting platform acceptance, whereas ANN, one of the machine learning techniques, captures both linearity and

nonlinearity between variables based on uncompensated relationships [14, 21].

To bridge the research gaps identified in the above, our study seeks to identify factors that influence telecommuting platform adoption, with a focus on the effect of perceived fear against a new health crisis, by using the ANN approach.

2. Materials and Methods

2.1. Research model design

This study proposes a conceptual research model that integrates perceived fear with TAM (Figure 1): TAM serves as a baseline model, and perceived fear is introduced as an external variable. Actual usage is excluded from the original TAM model because we accept that actual usage is the strongest predictor of behavioral intention to accept a certain technology [12, 13].

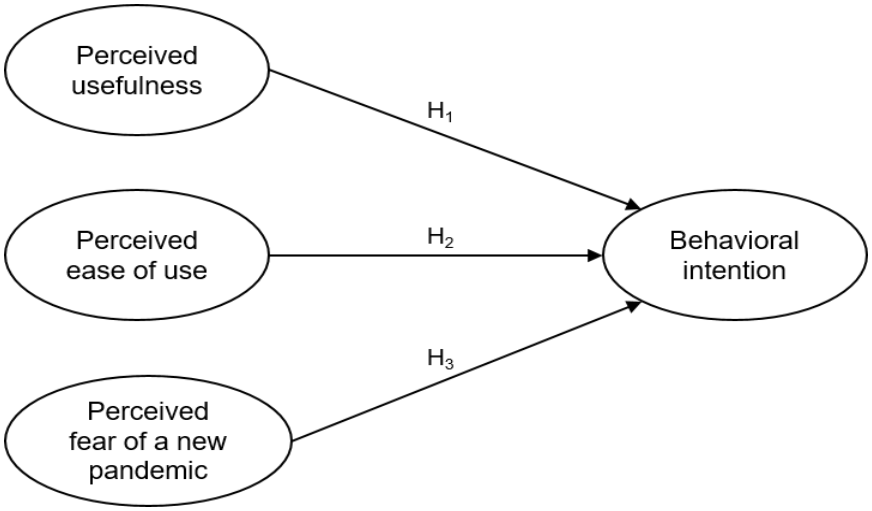

Figure 1. Conceptual research model.

Based on the conceptual research model, our study designed an ANN research model that has three neurons (PU, PE, PF) and one neuron (BI) (Figure 2). Our study conducted a preliminary test to find the optimal network structure of our ANN model, so the result showed that our optimal network configuration has one hidden layer.

2.2. Hypothesis development

PU (perceived usefulness) is defined as the degree to which an individual perceives that using a certain technology would increase the effectiveness and efficiency of his or her task, while PE (perceived ease of use) refers to the degree to which an individual perceives that using a certain technology would be used without much effort [13, 17]. PF (perceived fear), an adaptative response [7], measures an emotional response caused by being aware of risk [3, 4, 15]. In the face of a new health crisis, if individuals believe that telecommuting platforms are more efficient and ease to use for their works than other adaptive measures and can lower the risk of new pandemic infections, they are more likely to use telecommuting platforms. Previous research have demonstrated the positive relationships between them and behavioral intention to adopt certain technologies: for the relationship with the usefulness and the easiness in the context of health application [15] and e-government service [16]; for the relationship with the fear in the context of google meeting solution [3] and mobile shopping [4]. Thus, our study proposes the following hypotheses.

H1. Perceived usefulness increases behavioral intent to adopt telecommuting platform.

H2. Perceived ease of use increases behavioral intent to adopt telecommuting platform.

H3. Perceived fear of a new pandemic increases behavioral intent to adopt telecommuting platform.

2.3. Data collection and analysis steps

Our study surveyed 380 individuals who have experienced remote work in South Korea: 50.3% were male and 49.7% were female; respondents aged 30-40 years made up the largest age group (67.4%), followed by 50s (16.8%) and 20s (12.1%); 28.9% of them were employed in manufacturing, followed by services (20.5%) and information communication technology (11.6%). The survey measurement items were drawn from the previously validated research [3, 4, 15, 16] using a 5-point Likert scale. After the frequency analysis on the demographic profiles of respondents, this study applied the ANN analysis using SPSS 3.3 to verify the proposed research model.

3. Results

This study applied a multilayer perceptron, an ANN algorithm, to train and test the ANN model built on our conceptual research model (Figure 2). A ten-fold cross validation was conducted in which 90% of the data was allocated for training while 10% was used for testing to mitigate the problem of data overfitting. Hyperbolic tangent and scaled conjugate gradient were used as activation function for hidden and output layers and optimization algorithm, respectively.

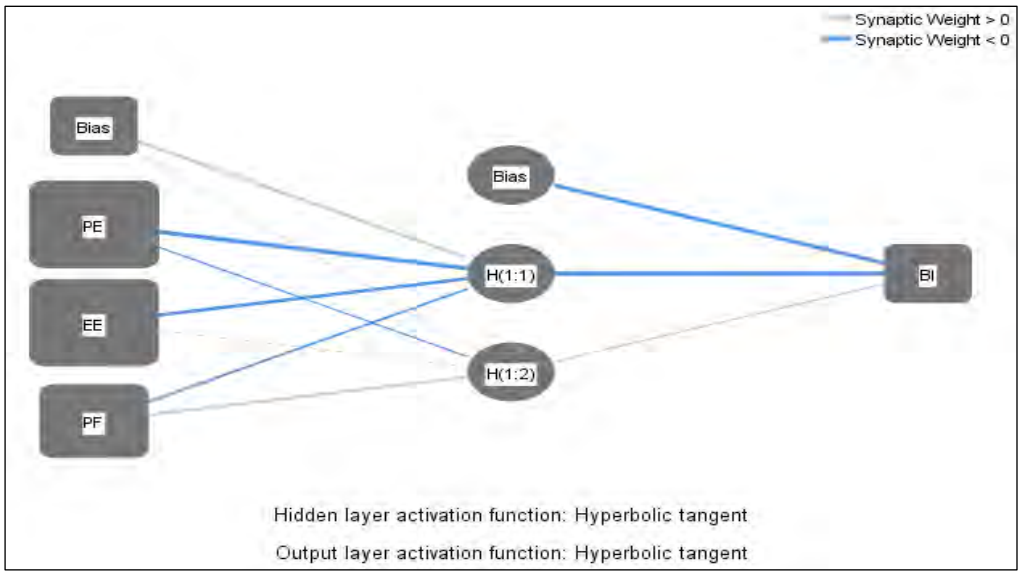

Figure 2. ANN research model.
Notes: PU: perceived usefulness; PE: perceived ease of use, PF: perceived fear of a new pandemic; BI: behavioral intention

Our study used root mean square error (RMSE) and coefficient of determinants (R^2) to evaluate the prediction accuracy of our research model; they are commonly used criteria [18, 20]. Our study used the following formula to calculate R^2: [21] $R^2 = 1 - (RMSE/S^2)$ where S^2 means the variance of the preferred output. R^2 values of 0.75, 0.50 and 0.25 indicate substantial, moderate and weak explanatory power, respectively [19]; low RMSE depicts high predictive power [20].

Our results showed an acceptable prediction accuracy of our research model (Table 1). The RMSE ranged from 0.2154 to 0.2447 (mean = 0.2296) for training data and from 0.1753 to 0.2749 (mean = 0.2097) for testing data; 98.7% and 88.8% of the variance in BI were predicted by the input nodes for training and testing, respectively. These results indicated that our ANN model was reliable to some degree [14, 21].

Table 1. RMSE values

Neural network	Training			Testing		
	SSE	RMSE	N	SSE	RMSE	N
1	17.5682	0.2266	342	1.2206	0.1792	38
2	17.1834	0.2245	341	2.1970	0.2373	39
3	19.0295	0.2380	336	1.5417	0.1872	44
4	16.8128	0.2254	331	2.2606	0.2148	49
5	19.9979	0.2447	334	2.4134	0.2291	46
6	18.1267	0.2316	338	1.2914	0.1753	42
7	15.9073	0.2154	343	2.7952	0.2749	37
8	17.6106	0.2296	334	1.8670	0.2015	46
9	17.4051	0.2256	342	1.5508	0.2020	38
10	18.6229	0.2344	339	1.5772	0.1961	41
Mean	17.8264	0.2296		1.8715	0.2097	
Standard deviation		0.0244			0.0913	

Notes: Self-calculated values; SSE: sum of square error; RMSE: root mean square error; N: number of samples

Our study conducted sensitivity analysis to verify input variables that affect BI to adopt telecommuting platform [14, 20]. The normalized importance ranged from 48.8% to 100%. These results indicated that PU was the key concern in predicting BI, followed by PE of use 93.1%) and PF (48.8%).

Table 2. Sensitivity analysis

Neural network	Model (output: BI)		
	PU	EE	PF
1	.382	.355	.263
2	.250	.541	.209
3	.569	.331	.099
4	.282	.414	.304
5	.382	.355	.263
6	.469	.382	.149
7	.361	.396	.242
8	.418	.411	.171
9	.364	.361	.275
10	.655	.302	.043
Mean relative importance	.413	.385	.202
Normalized relative importance (%)	100.0	93.1	48.8

Notes: Self-calculated values; PU: perceived usefulness; PE: perceived ease of use, PF: perceived fear of a new pandemic

4. Findings and discussion

Our study confirmed that perceived fear influences behavioral intention to adopt telecommuting platform in the face of a new pandemic in the future. These findings are interesting. This finding indicates the level of fear that caused by a new pandemic outbreak directly affects the evaluation of using telecommuting platform. Thus, we infer that once an individual perceives the fear of a new pandemic outbreak as real and serious, he or she is likely to regard telecommuting platform as an efficient preventive measure even in the face of a new health crisis.

Our study confirmed that perceived usefulness and perceived ease of use are crucial considerations to adopt telecommuting platform. These findings are informative. These findings suggest that increase in an individual' perception of perceived usefulness and perceived ease of use of using telecommuting platform can increase in beliefs with regard to the behavioral intention to use the technology. Thus, we infer that an individual will decide to adopt telecommuting platform by assessing whether it can improve the efficiency of his or her tasks and reduce the degree of efforts he or she have to spend.

5. Contribution and implication

Our study has some theoretical contribution and industrial implications. Regarding theoretical contribution, our study successfully combined perceived fear with the TAM. Our argument is guaranteed by the prediction accuracy of our ANN model. Secondly, our study advances the extant literature of methodology with regard to evaluating of technology acceptance. Our study is among the few that have employed the ANN approach to identify the determinants of using telecommuting platform. Regarding industrial implication, telecommuting platform providers must enhance their efforts to maximize the level of the usefulness and the easiness of their platforms, considering the level of fear that people perceive in the context of a new pandemic situation.

6. Limitations and directions for future research

However, our study has some limitations. The first limitation comes from the simplicity of our research model. Our study excluded some moderating variables (e.g. age) and the relationship between perceived usefulness and perceived ease of use. The second limitation is about the methodological suitability. ANN is suitable for model prediction; ANN may not be optimized for hypothesis testing. In addition, this study did not test other activation functions and optimization algorithms; this means that our findings may differ under different neural network architecture conditions. Thus, this study recommend that researcher consider these limitations when they conduct a similar research approach.

7. Conclusion

Our study focused on examining the drivers of telecommuting platforms adoption using the ANN technique. This study addressed two research gaps: the lack of examining determinants of telecommuting platforms adoption, and the lack of various methodological approaches (e.g., nonlinear techniques). Our study provides several interesting and empirical evidences; these findings can provide researchers and industrial practitioners with a differentiated view into individual-level adoption of telecommuting systems.

Funding: This research received no external funding.

Data Availability: Data will be available on request from the researchers.

Conflicts of Interest: The authors declare no conflict of interest. /

References

1. Battisti, E., Alfiero, S. and Leonidou, E. Remote working and digital transformation during the COVID-19 pandemic: Economic–financial impacts and psychological drivers for employees. *Journal of Business Research 150*, 38–50 (2022). doi:10.1016/j.jbusres.2022.06.010.
2. Hedayati, S., Damghanian, H., Farhadinejad, M. and Rastgar, A. Meta-analysis on application of Protection Motivation Theory in preventive behaviors against COVID-19. *International Journal of Disaster Risk Reduction 94*, 1–13 (2023). doi 10.1016/j.ijdrr.2023.103758.
3. Al-Maroof, R. S., Salloum, S. A., Hassanien, A. E. and Shaalan, K. Fear from COVID-19 and technology adoption: the impact of Google Meet during Coronavirus pandemic. *Interactive Learning Environments 31*(3) 1–17 (2020). doi:10.1080/10494820.2020.1830121.
4. Amin, M. A. et al. Evaluating the Determinants of Customers' Mobile Grocery Shopping Application (MGSA) Adoption during COVID-19 Pandemic. *Journal of Global Marketing 35*(3) 1–22 (2022). doi:10.1080/08911762.2021.1980640.
5. Norman, A. A. Technology Dependency and Impact During COVID-19: A Systematic Literature Review and Open Challenges. *IEEE Access 11*(11), 40741–40760 (2023). doi: 10.1109/ACCESS.2023.3250770.
6. Wadhar, S. B., Shahani, R., Zhou, R., Siddiquei, A. N. and Ye, Q. What Factors Will Influence Chinese International Traveling for Leisure in the Post-COVID-19 Era: Role of Health Priorities and Health-Related Information Literacy. *healthcare 11*(3), 1–23 (2023). doi: 10.3390/healthcare11030315.

7. Witte, K. Putting the fear back into fear appeals: The extended parallel process model. *Communication Monographs 59*(4), 329–349 (1992). doi:10.1080/03637759209376276.
8. Arunprasad, P., Dey, C., Jebli, F., Manimuthu, A. and Hathat, Z. E. Exploring the remote work challenges in the era of COVID-19 pandemic: review and application model. *Benchmarking: An International Journal 29*(10), 3333–3355 (2022). doi:10.1108/BIJ-07-2021-0421.
9. Athanasiadou, C. and Theriou, G. Telework: systematic literature review and future research agenda. *Heliyon 7*(10), 1–19 (2021). doi: 10.1016/j.heliyon.2021.e08165.
10. Obada-Obieh, B., Huang, Y. and Beznosov, K. Challenges and Threats of Mass Telecommuting: A Qualitative Study of Workers. In Proceedings of the Seventeenth Symposium on Usable Privacy and Security, Virtual conference (9-10 August 2021).
11. Mark, G., Kun, A. L., Rintel, S. and Sellen, A. Introduction to this special issue: the future of remote work: responses to the pandemic. *Human–Computer Interaction 37*(5), 397–403 (2022). doi 10.1080/07370024.2022.2038.
12. Venkatesh, V., Morris, M. G., Davis, G. B. and Davis, F. D. User Acceptance of Information Technology: Toward a Unified View. *MIS Quarterly 27*(3), 425–478 (2003). doi: 10.2307/30036540.
13. Momani, A. M., Jamous, M. M. and Hilles, S. M. S. Technology Acceptance Theories: Review and Classification. *International Journal of Cyber Behavior, Psychology and Learning 7*(2), 1–14 (2017). doi:10.4018/IJCBPL.2017040101.
14. Leong, L. Y., Hew, T. S., Ooi, K. B., Lee, V. H. and Hew, J. J. A hybrid SEM-neural network analysis of social media addiction. *Expert Systems With Applications 133*, 296–316 (2019). doi:10.1016/j.eswa.2019.05.024.
15. Alsyouf, A. et al. Risk of Fear and Anxiety in Utilising Health App Surveillance Due to COVID-19: Gender Differences Analysis. *risks 9*(179), 1–19 (2021). doi:10.3390/risks9100179.
16. Nguyen, T. Citizens' intentions to use e-government during the COVI D-19 pandemic: integrating the technology acceptance model and perceived risk theory. *Kybernetes 52*(7), 2329–2346 (2022). doi:10.1108/K-07-2022- 1023.
17. Venkatesh, V. and Davis, F. D. A model of the antecedents of perceived ease of use: Development and test. *Decision Sciences 27*(3), 451–481 (2009). doi:j.1540-5915.1996.tb00860.x.
18. Hair, J., Ringle, C. M., Hult, G. T. M. and Sarstedt, M. *A Primer on Partial Least Squares Structural Equation Modeling*, 2nd ed. (SAGE, 2016).
19. Risher, J., Ringle, C. M. and Sarstedt, M. When to use and how to report the results of PLS-SEM. *European Business Review 31*(1), 2–24 (2018). doi:10.1108/EBR-11-2018-0203.
20. Hair, J. F., Black, W. C., Babin, B. J. and Anderson, R. E. *Multivariate Data Analysis*, 8th ed. (Cengage, 2018).
21. Phillips, P., Zigan, K., Silva, M. M. S. and Schegg, R. The interactive effects of online reviews on the determinants of Swiss hotel performance: A neural network analysis. *Tourism Management 50*, 130–141 (2015). doi:10.1016/j.tourman.2015.01.028.

5th International Conference of Hyojeong Academy
International Joint Conference 2025

A Study on the Enhancement of Wear Resistance of Al7075-T6 Alloy by UNSM Technology

Auezhan Amanov [1,*], Junhyong Kim[2], Inho Cho[2] and Youngsik Pyun[2]

[1]Tampere University ; auezhan.amanov@tuni.fi
[2]DesignMecha Co., Ltd.
*Correspondence: auezhan.amanov@tuni.fi

Abstract: Al7075-T6 alloy, widely used in aerospace applications, is prized for its high strength-to-weight ratio but often requires enhanced surface properties to meet the demands of high-wear environments. This study investigates the enhancement of wear resistance in Al7075-T6 alloy through ultrasonic nanocrystal surface modification (UNSM), a surface engineering technique that refines the microstructure, increases hardness and induces compressive residual stresses. The treatment generates a nanocrystalline layer on the alloy surface, significantly improving hardness, reducing friction, and mitigating wear under dynamic loading conditions. Microstructural analysis revealed a substantial grain refinement, with average grain sizes reduced to the nanometer scale near the treated surface. Tribological testing demonstrated a notable reduction in wear rates and friction coefficients compared to untreated samples, underscoring the effectiveness of UNSM in improving wear performance. Additionally, the influence of key parameters, such as ultrasonic energy intensity, tool geometry, and process duration, was systematically evaluated to optimize the surface modification. This research highlights UNSM as a viable post-processing technique for enhancing the durability and performance of Al7075-T6 alloy in wear-intensive applications, bridging the gap between material properties and the stringent requirements of advanced engineering systems.

Keywords: Al7075-T6 alloy, hardness, roughness, grain size, friction, wear resistance, surface modification

1. Introduction

Aluminum 7075-T6 alloy is widely used in structural applications requiring high strength and low weight, such as aerospace and automotive industries. However, its susceptibility to wear limits its service life in high-friction applications. Over the past few decades, various surface treatments have been explored to enhance the wear resistance of metallic alloys, including laser shock peening (LSP), shot peening (SP), cavitation peening (CP), low plastic burnishing (LPB), and ultrasonic nanocrystal surface modification (UNSM) [1-4]. These treatments introduce compressive residual stresses and alter the near-surface microstructure through surface severe plastic deformation. SP has been widely used due to its cost-effectiveness and adaptability to different component sizes. However, it presents limitations such as shallow depth of compression and increased surface roughness, particularly in lightweight metals, making it less suitable for aluminum alloys. Given the growing need for materials with enhanced wear resistance, advanced surface engineering techniques like LSP and UNSM have gained significant attention. These treatments have demonstrated their ability to enhance wear resistance by increasing the hardness. Meanwhile, UNSM is an advanced mechanical surface treatment that results in grain refinement, work hardening, and compressive residual stress, all of which contribute to improved wear resistance. This study focuses on evaluating the tribological performance of Al7075-T6 alloy treated with UNSM technology and its implications for practical applications. This study focusses on understanding the effects of the surface roughness, hardness, compressive residual stress and nanostructured surface layer induced by UNSM treatment on the wear resistance of Al7075-T6 alloy.

2. Materials and Methods

The plate samples made of Al7075-T6 alloy were machined into 20 mm × 15 mm × 4 mm coupons. Samples were polished using SiC papers up to 1200 grit and cleaned with acetone before UNSM treatment. UNSM treatment was performed using a tungsten carbide tool oscillating at 20 kHz, applying static and dynamic loads to the sample surface. Parameters such as tool feed rate, impact force, and spacing interval were optimized to maximize wear resistance as listed in Table 1. The wear track generated on the surface of the untreated and UNSM-treated

samples were analyzed using scanning electron microscopy (SEM) to understand the occurrence of wear mechanisms. Micro-hardness tests were conducted to measure hardness variations through the depth of treated and untreated samples. Tribological performance was assessed using a pin-on-disk wear test under dry conditions at an applied normal load of 10 N, sliding speed of 5 m/s for 1 hour. SAE 52100 bearing steel ball with a diameter of 6.35 mm was used as a counterbody. The coefficient of friction (COF) and wear rate (WR) were recorded and compared between UNSM-treated and untreated samples.

Table 1. UNSM treatment parameters used in this study.

Frequency, kHz	Amplitude, μm	Static load, N	Linear speed, mm/min	Interval, μm	Ball size, mm	Ball material
20	50	60 (UNSM-1) 80 (UNSM-2)	1000	25	2.38	WC

3. Results

Fig. 1 shows 2D images of untreated and UNSM-treated samples. Measured surface roughness values of the untreated and UNSM-treated samples are also shown in Fig. 1. It can be seen from Fig. 1(a) that the surface of the untreated specimen appears rough with noticeable peaks and valleys, indicated by the color variations in the height scale. The rough texture suggests high surface roughness values. As shown in Fig. 1(b) that the surface texture is visibly smoother compared to the untreated sample with a reduction in height variations. This indicates that the UNSM treatment reduced the roughness. Fig. 1(c) shows that the surface appears even more refined and uniform by increasing the static load of the UNSM treatment with minimal peaks and valleys, suggesting a further decrease in roughness. Fig. 1(d) presents surface roughness parameters (Ra and Rz) for the untreated and UNSM-treated samples. It can be concluded that surface roughness showed a significant reduction from the untreated sample to UNSM-1 and further decreases in UNSM-2, while the maximum height of surface irregularities followed a similar decreasing trend, confirming that the surface becomes smoother with increasing UNSM treatment intensity. The reduction in roughness is likely due to the plastic deformation and grain refinement caused by UNSM treatment, which eliminates surface asperity. It is well-known that smoother surfaces lead to improved tribological performance, reducing friction and wear, which is beneficial for applications requiring high durability. The difference between UNSM-1 and UNSM-2 treated samples suggests that further processing enhances surface smoothness, but diminishing returns may occur at higher treatment levels.

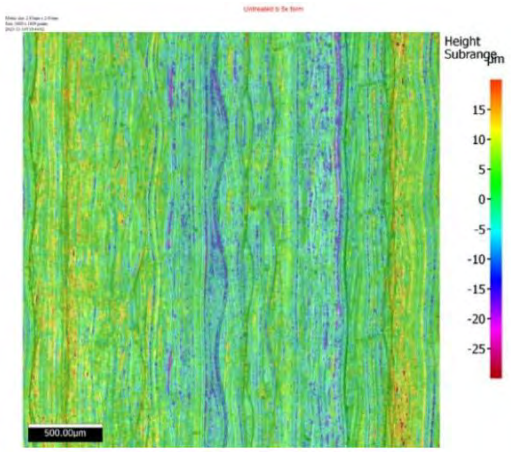

(a)

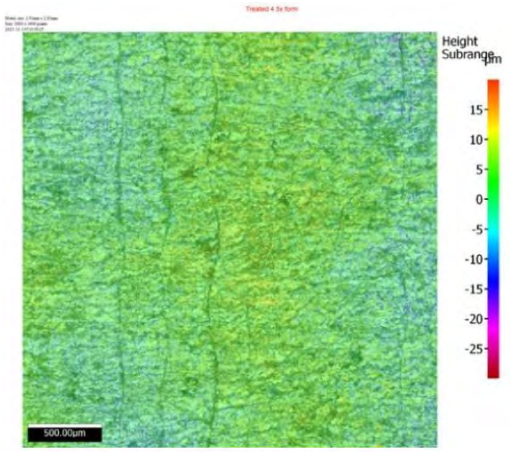

(b)

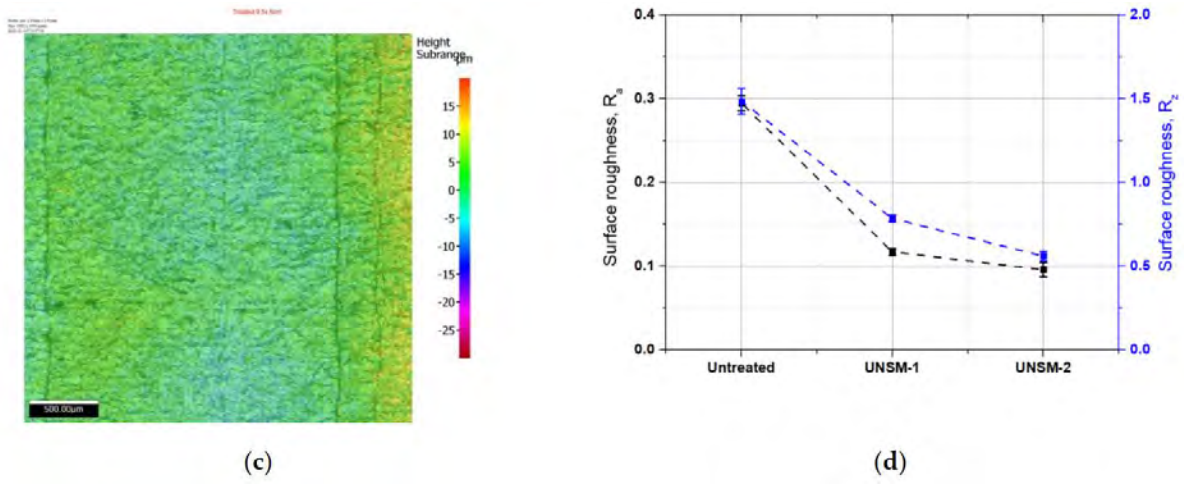

Figure 1. 2D image of the untreated (a) and UNSM-treated at 60 N (b) and 80 N (c) samples. Surface roughness of the untreated and UNSM-treated (d) samples.

Fig. 2(a) shows the surface hardness results of the untreated and UNSM-treated samples. It is observed that there is a significant increase in surface hardness after UNSM treatment, with UNSM-2 showing the highest hardness, where an initial hardness of 165 HV was increased up to 198 HV. The increase in surface hardness may be attributed to the surface severe plastic deformation from ultrasonic impacts, leading to grain refinement. It is also known that introduction of compressive residual stresses, which hinder plastic deformation and work hardening effects from repeated high-frequency impacts. Increased hardness directly correlates with better wear resistance, as seen in the wear rate shown in Fig. 2(b). The UNSM-2 sample had the lowest wear rate, demonstrating the cumulative benefits of higher UNSM intensity. It is also reported that the UNSM treatment also reduced COF from 0.35 to 0.15, which is a significant reduction due to smoothing phenomenon. It is worth noting that the increased hardness results in a reduction in surface asperity deformation under load in relative motion. Fig. 3 shows the SEM images of the wear track generated on the surface of the untreated and UNSM-2 samples. The wear track generated on the surface of the untreated sample was found to be wider and rougher wear track with visible plowing, grooves, and severe material loss compared to the wear track generated on the surface of the UNSM-2 sample. It means that UNSM-2 sample had less material removal, indicating improved wear resistance. Smoother surface due to the reduction of surface asperities from UNSM treatment. It was reported that adhesive and abrasive wear mechanisms are found to be dominant. UNSM significantly improves the wear resistance of Al7075-T6 alloy by inducing grain refinement, increasing hardness, and reducing friction.

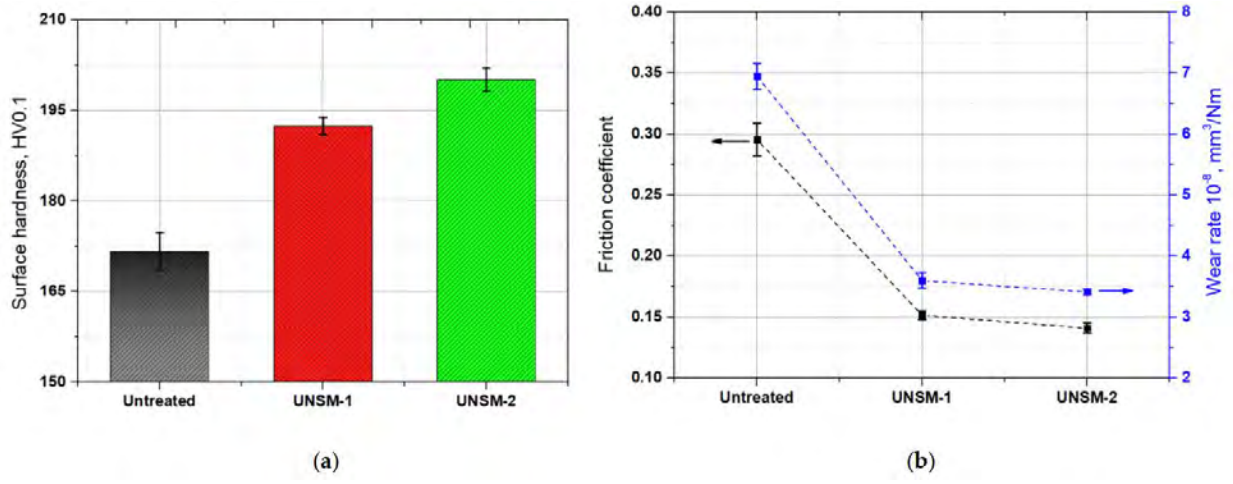

Figure 2. Surface hardness (a) and COF and WR (b) of the untreated and UNSM-treated samples.

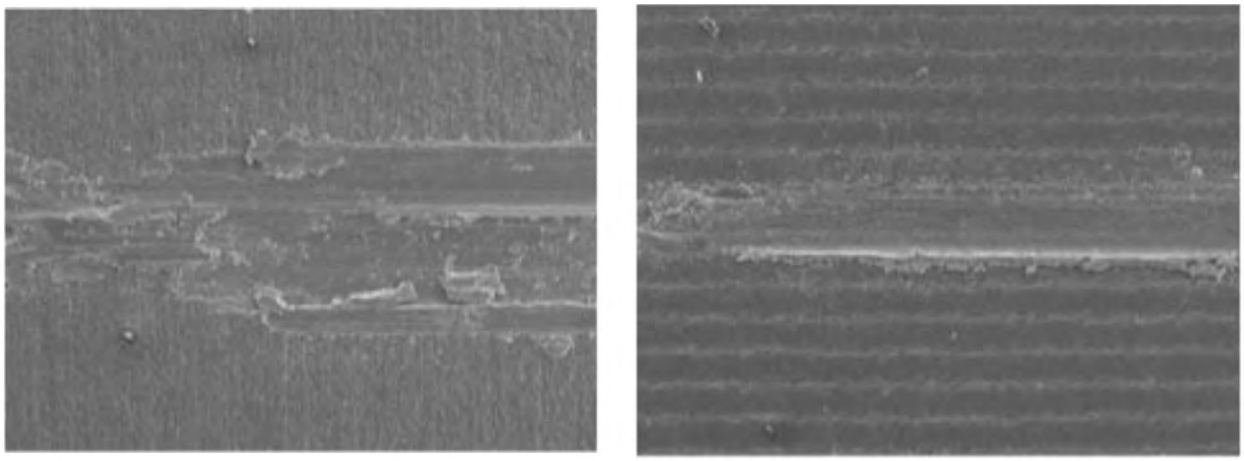

Figure 3. Comparison in SEM images of the wear track generated on the surface of the untreated(a) and UNSM-2(b) samples.

4. Conclusions

The study highlights the potential of UNSM treatment as an effective surface treatment for enhancing the wear resistance of components used in aerospace applications. The UNSM treatment reduced surface roughness, where smoother surfaces lead to improved tribological performance, reducing friction and wear, which is beneficial for applications requiring high durability. Hardness increases significantly after UNSM treatment, contributing to improved wear resistance. Friction coefficient and wear rate decrease, making the treated surfaces more durable under dynamic loading conditions. SEM images confirmed reduced wear damage, with UNSM-treated samples exhibiting a smoother, less damaged surface, while the UNSM-2 sample provided the best overall improvement, indicating that higher UNSM intensity further enhances tribological properties.

Author Contributions: "Conceptualization, A.A. and Y.S.P.; methodology, A.A. and K.J.H.; formal analysis, A.A., I.H.C.; investigation, A.A. and K.J.H.; data curation, A.A.; writing—original draft preparation, A.A.; writing—review and editing, A.A.; Y.S.P; supervision, A.A., Y.S.P.; project administration, A.A.; funding acquisition, A.A., I.H.C. All authors have read and agreed to the published version of the manuscript."

Funding: This research was financially supported by the Ministry of Trade, Industry and Energy (MOTIE) and the Korea Institute for Advancement of Technology (KIAT) through the International Cooperative R&D Program (P0022403).

Data Availability Statement: "Not applicable".

Conflicts of Interest: "The authors declare no conflict of interest." "The funders had no role in the design of the study; in the collection, analyses, or interpretation of data; in the writing of the manuscript; or in the decision to publish the results".

References

1. Mostafa, A.M., Hameed, M. and Obayya, S.S. Effect of laser shock peening on the hardness of AL-7075 alloy. *J. King Saud Univ.* 31(4), 472-478 (2019) https://doi.org/10.1016/j.jksus.2017.07.012
2. Khun, N.W., Trung, P.Q. and Butler, D.L. Study on hardness and wear resistance of shot peened AA7075-T6 aluminum alloy. *Eng. Res. Express* 3(1) 015031 (2021) https://doi.org/10.1088/2631-8695/abea0a
3. Prevey, P.S., Cammett, J.T. The influence of surface enhancement by low plasticity burnishing on the corrosion fatigue performance of AA7075-T6, *Int. J. Fatigue* 26(9) 975-982 (2004). https://doi.org/10.1016/j.ijfatigue.2004.01.010
4. Efe, Y., Karademir, I., Husem, F., Maleki, E., Karinbaev, R., Amanov, A. and Unal. O. Enhancement in microstructural and mechanical performance of AA7075 aluminum alloy via severe shot peening and ultrasonic nanocrystal surface modification. *Appl. Surf. Sci.* 528, 146922 (2020). https://doi.org/10.1016/j.apsusc.2020.146922

Proceedings of
THE 5th INTERNATIONAL CONFERENCE OF
HYOJEONG ACADEMY 2025

Session 3

Physical Science for Co-Prosperity

www.ichja.org

5th International Conference of Hyojeong Academy
International Joint Conference 2025

Model for regular X-ray flares in low mass X-ray binary systems – a case of IGR J17498-2921

Ivan Chelovekov

Space Research Institute, Profsoyuznaya 84/32, Moscow, Russian Federation
Correspondence: chelovekov@cosmos.ru

Abstract: Low mass X-ray binaries are binary star systems, consisting of a late type main sequence star and a compact object. This class of objects is known to emit regular X-ray flares on the time scales of years to decades. In our work we present an energy balance stage model for such a behavior and apply it to the case of IGR J17498-2921 2023 Apr. flare. We present the results of our analysis of NUSTAR and Spektr-RG/ART-XC observations of the source. Each of the satellites detected 2 type I X-ray bursts from the source, which let us determine burst recurrence period during flare activity, estimate its possible value during the quiescence period and gave a hint on accreted material composition. Comparatively low burst duration witnesses of a H poor accreted material and so a highly evolved optical companion star. Burst spectra were well fitted with absorbed thermal radiation model, while persistent radiation spectra also required a hot corona, accretion disk and reflection of coronal radiation from the disk components to be added to the model.

Keywords: X-ray pulsar, X-ray burster, transient X-ray binary system

1. Introduction

Accreting millisecond pulsars are fast spinning neutron stars in close binary systems that accrete matter from the companion star and gradually spin up to several kHz frequencies due to angular momentum inflow. The first source of the class - SAX J1808.4-3658 was discovered in 1998 [1] and now we know of over 2 dozens of them. X-ray transient source IGR J17498-2921 being one of the class was discovered by IBIS/ISGRI telescope onboard the INTEGRAL orbital observatory on Aug. 11, 2011 [2]. On the next day RXTE TOO observation revealed a 401 Hz coherent signal from the source making it an accreting millisecond pulsar candidate [3-4]. Swift/XRT observations of the source allowed to refine its position and provided its persistent spectrum, which was well fitted with power law using photon index 1.9±0.2 (consistent with INTEGRAL results) implying absorption column density of N_H=3.0±0.3x10^{22} cm^{-2} [5-6]. Based on the Chandra observatory data even more accurate position of the source was provided: RA=267.48073(6) DEC=-29.32214(6) (J2000) [7-8], while spectrum fitting yielded N_H=2.87±0.04x10^{22} cm^{-2} and Γ=1.75±0.02. Chandra archival data allowed to estimate 0.5-10 keV luminosity of the source in quiescence to be ~10^{32} erg s^{-1} (Oct. 29-30, 2006).

Analysis of JEM-X/INTEGRAL telescope data revealed a type I X-ray burst from the source that lasted for 15 s and corresponded to radiation of black body with temperature 1.4±0.4 keV and radius $\mathbf{19^{+15}_{-8}}$ km, defining it as an X-ray burster [9]. RXTE observations of the source revealed a Photospheric Radius Expansion (PRE) burst with 401 Hz QPO in its tail [10]. Assuming that the maximum luminosity during the burst was equal to the value, found for PRE-bursts 3.8x10^{38} erg s^{-1} [11], distance to the source was estimated to be 7.6 kpc. RXTE data also allowed to put weak constrains on the magnetic field strength 2x10^7 G<B<1.6x10^9 G [12]. It should also be mentioned that this burster might emit not only PRE-bursts, as several an order weaker bursts possibly from this source were reported based on the RXTE data [13-14]. Two more type I X-ray bursts were detected with Swift/XRT [15]. Several attempts were made to find orbital solution for the binary system based on the RXTE observatory data, resulting in prediction of the orbital period T_{orb}=13835.615(1) s [4, 16-18]). Measured mass function f(M_2,M_1,i)=0.00203807(8) $M_\odot$ allowed to set a lower limit of 0.17 $M_\odot$ on the mass of the companion star, while an upper limit of 0.48 $M_\odot$ was set by imposing that the companion star does not overfill its Roche lobe.

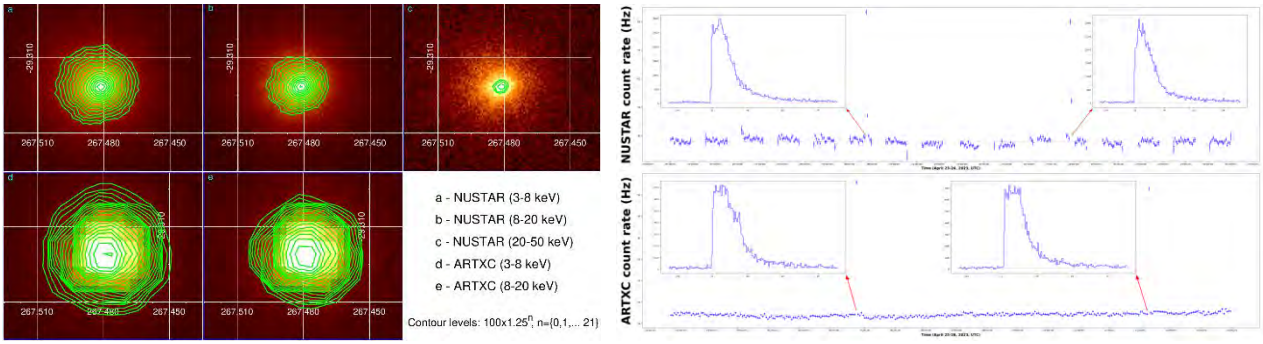

(a) **(b)**

Figure 1. (a) Images of the sky inside the field of view of NUSTAR(FPMA) and ART-XC (all 7 detectors), containing IGR J17498-2921, constructed based on all the data collected during its 2023 flare; (b) IGR J17498-2921 3-20 keV light curves, constructed based on summed FPMA+FPMB NUSTAR telescope data, collected during Apr. 23-24, 2023 (UTC) observations (top panel), and on summed data of 7 modules of ART-XC telescope, collected during Apr. 25-26 2023 (UTC) observations (bottom panel). Inserts show detailed profiles of 4 type I X-ray bursts, detected from the source.

An up to ~35% flux variability on the 1000 s timescale was detected in Swift/XRT data, while corresponding spectral variability was not observed - it was well modeled by absorbed power law with Γ=1.7-2.0 [4]. A broadband 0.6-300.0 keV joint INTEGRAL/ISGRI, RXTE/PCA and Swift/XRT spectrum was well fit with thermal Comptonization model with T_e~50 keV, T_b~1 keV and τ~1 during the raise, peak and decay of the flare [19]. Timing analysis of this data revealed a soft lag in pulse profiles for energies over 4 keV, that saturated at ~60 μs for E > ~10 keV. The pulsed flux fraction was 6-7%, it was seen up to 65 keV and was energy independent. An infrared counterpart candidate (possibly a late type K or early type M dwarf) was found at 0.6" from the source coordinates [20], but further investigation pushes one to be skeptical towards this result [21]. A likely faint optical counterpart (magnitude i'=22.5±0.7) was found within 0.6" from the Chandra position of the source and within 0.1" of the mentioned infrared counterpart [22], although it as well might be a case of chance alignment [23]. According to the Swift observations, IGR J17498-2921 Aug. 2011 outburst lasted for about 40 days till the source went down to a quiescent state with luminosity upper limit of 3.36×10^{33} erg cm^{-2} s^{-1} [24], while during the outburst the source luminosity reached $5.1 \pm 0.2 \times 10^{36}$ $d_{7.6}^2$ erg cm^{-2} s^{-1} [24]. Spectrum of the source at the decay of the outburst became softer and could be described by black body radiation with T=0.6±0.1 keV or a power law with photon index 3.2±0.3. Bolometric fluence of the outburst was estimated to be $4.1 \pm 0.6 \times 10^{-3}$ $d_{7.6}^2$ erg cm^{-2} [4].

Twelve years later in April 2023 a new outburst from the source was again detected by INTEGRAL observatory [25] and confirmed by NICER observatory [26]. NICER observations confirm presence of 401 Hz pulsations and did not reveal any significant spin evolution. Persistent spectrum is well described by a sum of black body (0.30(3) keV) and Comptonization (power-law index 1.76(2)) components with absorption column density of $2.0(1) \times 10^{22}$ cm^{-2}.

Here we present a short overview of the results of our analysis of Spektr-RG/ART-XC and NUSTAR observations of the source during the 2023 flare and offer a model to explain a possible 12- year period of such flares using the case as an example.

1.1. Observations and data analysis

In this paper we use data from M.N. Pavlinskiy ART-XC telescope onboard the Spektr-RG orbital observatory and both FPMA and FPMB detectors of the NUSTAR orbital observatory (publically available through the NASA HEASARC archive). NUSTAR observations lasted for 91.8 ks and were performed during 2023-04-23T10:21:09 (UTC) - 2023-04-24T11:51:09 (UTC). ART-XC observations started on 2023-04-25T21:38:43 (UTC) and lasted for 66 ks until 2023-04-26T16:00:00 (UTC). To process NUSTAR data we used HEASOFT 6.32

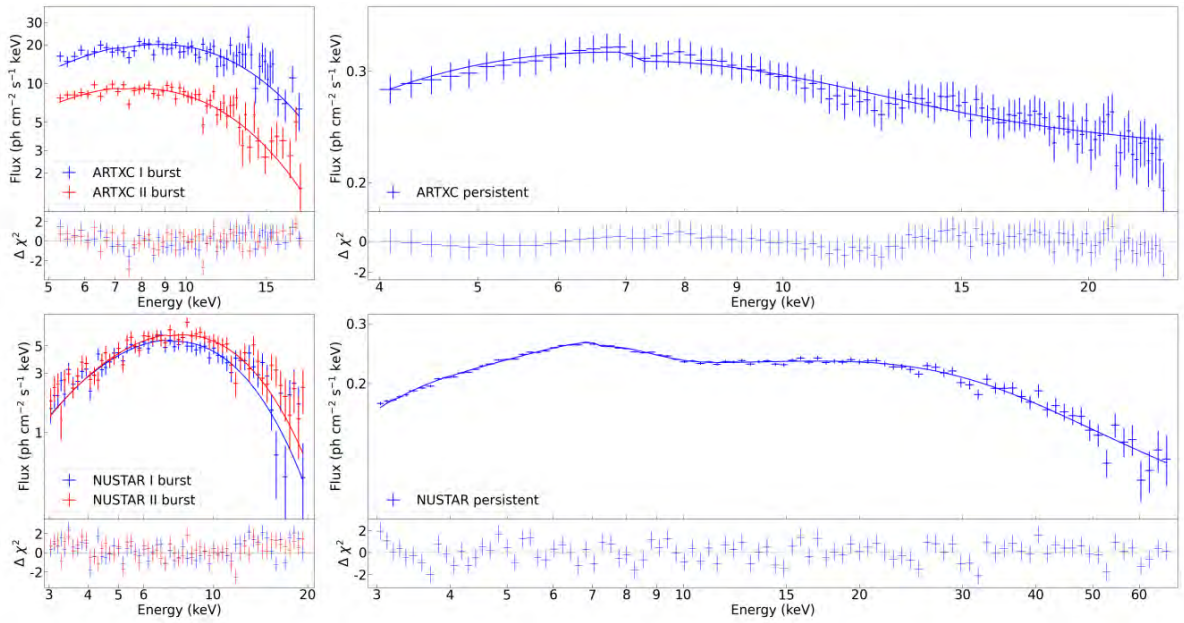

(a) **(b)**

Figure 2. Burst (a) and persistent (b) νF_ν spectra of IGR J17498-2921 radiation, constructed based on ART-XC/Spektr-RG (top) and NUSTAR (bottom) data, collected during the 2023 flare.

and the most fresh CALDB available to the date. ART-XC data was processed by dedicated software package Artpipeline 1.0 and CALDB version 1.0. Figure 1.a shows sky images inside the fields of view of the NUSTAR and ART-XC telescopes, constructed based on all the data of NUSTAR/FPMA and all the 7 ART-XC telescopes, accumulated in 3 energy bands during 2023 Apr. 23-24 and 25-26 observations correspondingly. It shows flat and homogeneous source suburbs in ART-XC data that were comfortably used to evaluate the background radiation in our research. For this purpose we chose 4 regions of the same size as the source outside it's skirts in different directions from it. Spectra from these regions were added, re-normalized and used as background for the source spectrum. Contour levels are described on the plot.

2. Results

Figure 1(b) shows IGR J17498-2921 light curves. All curves here are constructed in 3-20 keV energy range. Top panel contains 200 s binned NUSTAR FPMA+FPMB curve. Bottom panel similarly contains 200 s binned ART-XC curve, constructed based on all 7 modules data. We detected 2 type I X-ray bursts during each of these observations. Inserts in each of the panels show 0.3 s binned light curves, providing detailed profiles of the 4 bursts. Figure 2 shows burst and persistent spectra of the source during 2023 flare constructed based on ART-XC and NUSTAR observations. Burst spectra are well fit by the black body radiation model, while persistent spectra required an addition of Comptonization model for up scattering soft photons by hot electron cloud and accretion disk reflection part. Interstellar absorption with N_H=3x10^{22} cm^{-2} was taken into account while fitting all the spectra. More images, light curves, bursts and spectra parameters and more details on the results may be found in our paper, which will be out within a few months.

2.1. The model

So far we know of just 2 flares from IGR J17498-2921, separated by ~12 years. This does not allow one to determine the period of such events but we can at least try to put a lower limit to the value. Our research based on data from the INTEGRAL - one of the main wide field of view X-ray telescopes observatory that has been in orbit for last 22 years, shows that the source was monitored regularly, but over 40 times the gaps in the observations exceeded 3 months, so in principle the source could have had more flares during this period, though none were detected by any of our observatories. Yet, if we assume, that 12 years may be close the period of such events it will inevitably remind us of the 11±3 years half period in solar activity, which is as we believe now connected to the redirection

of the star's magnetic field. We know, that connected to such events solar activity goes high at the peaks of the cycle and we see much more solar flares (number of them is reaching ~200 per month), emitting H into our system, than usual causing a stronger stellar wind which we feel for example through the Forbush effect. As we know optical star in a studied binary system is of some late type, most likely M, which means it is smaller, than the Sun, it has stronger magnetic field and most important - there may be an order more flares than our star has (we know it from observations of closer stars of a kind). What if these coronal mass ejections from the optic star emit enough matter to be responsible for observed X-flares from the system?

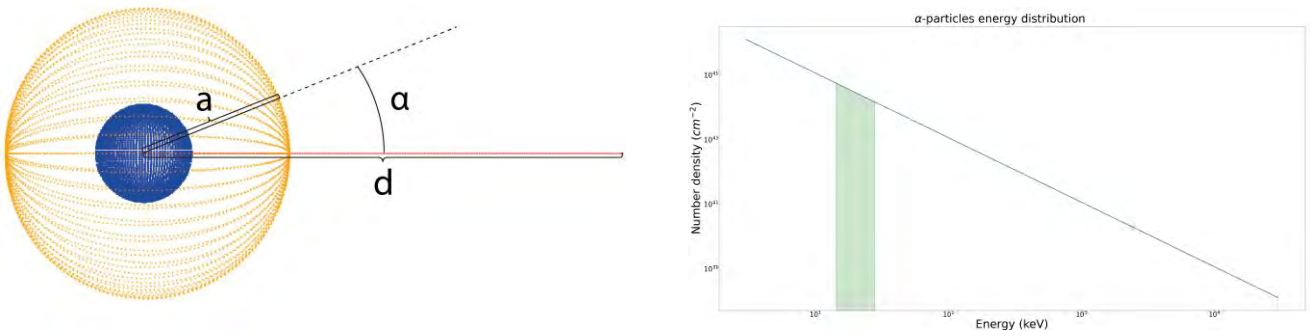

(a) **(b)**

Figure 3. (a) Binary star system with true scales. Blue sphere on the left is a late type (M) optical star, while a tiny dot on the right is a neutron star. Orange sphere is a Hill surfce corresponding to the border of the Roche lobe of the optical star; **(b)** Particular case of possible α-particles energy distribution according to a power law with Γ=2 renormalized through the number of 30 MeV protons detected from the Sun flares at the Earth vicinity (red line). Green bar shows an approximate energy band, corresponding to α-particles leaving the Roche lobe of the optical star but remaining in the systems gravity well.

Let us estimate an amount of accreted matter mass $\boldsymbol{M_{tot}}$ that is necessary for a τ = ~1 month long X-ray flare. If L_X~5 10^{36} erg s^{-1} (based on the persistent source spectrum, see Figure 2 and our upcoming paper) is an average X-ray luminosity of the system during this period, M_X~1.4 $M_\odot$ and R_X~10 km are mass and radius of the neutron star, then under assumption that all the gravitational energy of the accreted material is reprocessed into X-ray radiation we get:

$$\boldsymbol{M_{tot}} \sim \frac{\boldsymbol{\lambda R_X L_X \tau}}{\boldsymbol{G M_X}} = 1.5 \times 10^{23} \left(\frac{\boldsymbol{M_\odot}}{\boldsymbol{M_X}}\right)\left(\frac{\boldsymbol{R_X}}{\boldsymbol{10\ km}}\right) \text{ g} \qquad (1)$$

which is ~10^{23} g for an ordinary neutron star. Here λ is the bolometric coefficient which we assume to be unity for the sake of an order of magnitude estimates.

Let us now estimate the mass emitted by the optic star through coronal mass ejections during the peak month of the cycle. In the paper by Struminskii and Sadovskii [27] we find an estimate of the number of 30 MeV protons ejected in one flare by the M-class star based on the observations of the solar flare protons density at the Earth suburbs, which, scaled to our case, gives one $\mathbf{N}_\alpha$~1.3 10^{38} α-particles. We are only interested in those particles that reach boundary of the Roche lobe but are not energetic enough for the runaway. It is easy to estimate such $\mathbf{E}_{min}$ and $\mathbf{E}_{max}$ values for a particle in gravitation potentials of two stars and centrifugal quasi potential if we assume that particles are radiated solely in the radial direction. It is an axi-symmetric task, so if we introduce an angle $\boldsymbol{\alpha}$ between the direction under consideration and direction to the neutron star (Figure 3.a) we get:

$$\boldsymbol{E_{min}}(\alpha)=\boldsymbol{E_0}\left(1-\frac{1}{\varepsilon}+\frac{\beta}{\sqrt{1+\Upsilon^2-2\Upsilon\cos\alpha}}-\frac{\beta}{\sqrt{\varepsilon^2+\Upsilon^2-2\varepsilon\Upsilon\cos\alpha}}+\frac{1+\beta}{2\Upsilon^3}(\varepsilon\text{-}1)\cos\alpha\left(\frac{2\Upsilon\beta}{1+\beta}-(1+\varepsilon)\cos\alpha\right)\right) \qquad (2)$$

$$\boldsymbol{E_{max}}(\alpha)=\boldsymbol{E_0}\left(1+\frac{\beta}{\sqrt{1+\Upsilon^2-2\Upsilon\cos\alpha}}-\frac{1+\beta}{2\Upsilon^2}\left(\frac{\Upsilon\beta}{1+\beta}-\cos\alpha\right)^2\right) \qquad (3)$$

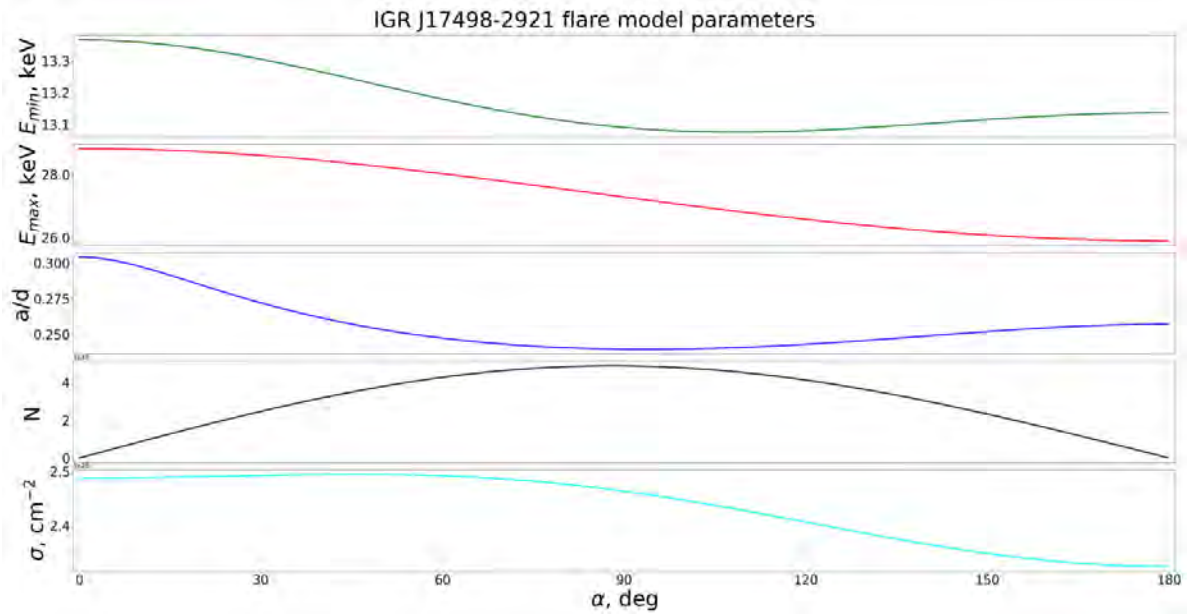

Figure 4. Dependence on the angle α of (top to bottom): E_{min} – minimum energy α-particle must have to leave the Roche lobe of the optical companion star, E_{max} – system runaway energy of an α-particle, a/d – ratio of the distance to the Hill surface, corresponding to the Roche lobe boundary, to the interstellar distance, N – number of α-particle emitted in all the flares during the stellar cycle peak month, σ – surface density of emitted particles.

where $E_O=\frac{GM_O}{R_O}$, **M**o~0.4 $M_\odot$ and **R**o~0.1 $R_\odot$ are the mass and the radius of the optical star, $\beta=\frac{M_X}{M_O}$, $\Upsilon=\frac{d}{R_O}$, $\varepsilon=\frac{a}{R_O}$, and **a** is the distance to the Hill surface, corresponding to the Roche lobe boundary at the given $\boldsymbol{\alpha}$ direction. In such a parameterization we can calculate the total number of emitted particles, that will leave the Roche lobe of the optic star during the peak month of the cycle, but remain in the gravity well of the system as:

$$N = 2\pi \boldsymbol{R_O^2} \int_0^{\pi} \boldsymbol{\sigma}\, \boldsymbol{\sin\alpha}\, \boldsymbol{d\alpha} \qquad (4) \qquad \sigma(\alpha)=\frac{N_F}{4\pi R_O^2} \int_{E_{min}}^{E_{max}} \boldsymbol{n(E)dE} \qquad (5)$$

where $\boldsymbol{\sigma}$ is the one Month total surface density of the "good" ($E_{min} < E < E_{max}$) α particles with E_{min} and E_{max} given by equations (2) and (3). N_F here is the number of coronal mass ejection episodes during the peak month of the stellar cycle and) we assume it to be ~2000. If we then assume the energy spectrum of such particles to be a simple power law $n(E)=k\boldsymbol{E^{-\Gamma}}$ with Γ=2, the number of emitted particles based on equations (4) and (5) turns out to be:

$$N=\frac{kN_F}{2(1-\Gamma)} \int_0^{\pi} \left(\boldsymbol{E_{max}^{1-\Gamma}} - \boldsymbol{E_{min}^{1-\Gamma}}\right) \boldsymbol{\sin\alpha}\, \boldsymbol{d\alpha} \qquad (6)$$

Distribution constant **k** may be estimated based on the N_α (see Figure 3(b)) which gives k~6 10^{38}. Figure 4 shows the results of our calculations of E_{min}, E_{max}, $\frac{a}{d}$, N and σ dependence on the angle $\boldsymbol{\alpha}$.

In the regarded case the accretion flow does not pass through the inner Lagrange point (L1) but matter is rather emitted through the whole Hill surface, so in order for some particles to enter the neutron star Roche lobe and be accreted they need to get rid of extra energy and angular momentum, so far not all the α particles, emitted from the optical star will follow this destiny – some will have to carry away energy and angular momentum of the others. Let's assume these particle groups are equal, then equation (6) gives us ~10^{23} g which is exactly how much we need to explain an X-ray flare in equation (1). Of course this is just a rough mass balance level model which needs further tuning based on more accurate assumptions, but one thing is clear – accreted matter amount wise our model seems to be quite a possible explanation of the phenomenon.

References

1. Wijnands, R. and van der Klis, M. A millisecond pulsar in an X-ray binary system. *Nature 394*, 344-346 (1998). DOI: 10.1038/28557
2. Gibaud, L. et al. A new hard X-ray transient discovered by INTEGRAL: IGRJ17498-2921. *ATEL 3551* (2011).
3. Papitto, A. et al. RXTE detects a coherent signal at ~ 401 Hz from IGR J17498-2921. *ATEL 3556* (2011).
4. Papitto, A. et al. the discovery of the 401 Hz accreting millisecond pulsar IGR J17498-2921 in a 3.8 h orbit. *A&A 535* id. L4 (2011). DOI: 10.1051/0004-6361/201117995
5. Bozzo, E., Ferrigno, C., Papitto, A. and Gibaud, L. Swift localization of the new hard X-ray transient IGR J17498-2921. *ATEL 3555* (2011).
6. Bozzo, E., Beardmore, A., Papitto, A., Ferrigno, C. and Gibaud, L. IGR J17498-2921: improved Swift/XRT position. *ATEL 3558* (2011).
7. Jonker, P. et al. Chandra detection of IGR J17498-2921 in quiescence. *ATEL 3559* (2011).
8. Chakrabarty, D., Markwardt, C., Linares, M. and Jonker, P. Chandra Localization of the Accretion-Powered Millisecond Pulsar IGR J17498-2921. *ATEL 3606* (2011).
9. Ferrigno, C., Bozzo, E., Belloni, L., Gibaud, A. and Papitto, A. INTEGRAL detects a Type I X-ray burst from IGR J17498-2921. *ATEL 3560* (2011).
10. Linares, M. et al. RXTE detection of a thermonuclear burst from IGR J17498-2921: distance estimate and burst oscillations. *ATEL 3568* (2011).
11. Kuulkers, E. et al. Photospheric radius expansion X-ray bursts as standard candles. *A&A 399*, 663-680 (2003). DOI: 10.1051/0004-6361:20021781.
12. Mukherjee, D., Bult, P., van der Klis, M. and Bhattacharya, D. The magnetic-field strength of accreting millisecond pulsars. *MNRAS 452*, 3994-4012 (2015). DOI: 10.1093/mnras/stv1542.
13. Chakraborty, M. and Bhattacharyya, S. Thermonuclear burst oscillations from the 401 Hz pulsar IGR J17498-2921. *ATEL 3643* (2011).
14. Chakraborty, M. and Bhattacharyya, S. Thermonuclear bursts frm the 401-Hz accreting pusar IGR J17498-2921: indication of burning in confined regions. *MNRAS 422*, 2351-2356 (2012). DOI: 10.1111/j.1365-2966.2012.20786.x.
15. In't Zand, J., Kreis, M., Palmer, D. and Degenaar,N. Searching for the most powerful thermonuclear X-ray bursts with the Neil Gehrels Swift Observatory. *A&A 621*, id. A53 (2019). DOI: 10.1051/0004-6361/201834270.
16. Markwardt, C., Strohmayer, T. and Smith, E. Preliminary Candidate Binary Orbit Solutions for IGR J17498-2921. *ATEL 3561* (2011).
17. Markwardt, C. and Strohmayer, T. Refined Orbit Timing Solution for IGR J17498-2921. *ATEL 3601* (2011).
18. Papitto, A. et al. A preliminary orbital solution for the newly discovered AMSP, IGR J17498-2921. *ATEL 3563* (2011).
19. Falanga, M. et al. Spectral and timing properties of the accreting X-ray millisecond pulsar IGR J17498-2921. *A&A 545*, id. A26 (2012). DOI: 10.1051/0004-6361/201219582.
20. Greiss, S. et al. Search for NIR counterpart to IGR J17498-2921 in quiescence. *ATEL 3562* (2011).
21. Torres, M. et al. Outburst near-infrared and Chandra observations of the ms-pulsar IGR J17498-2921. *ATEL 2628* (2011).
22. Russell, D., Lewis, F., Altamirano, D. and Roche, P. The optical counterpart of the accreting millisecond X-ray pulsar IGR J17498-2921. *ATEL 3622* (2011).
23. Van den Berg, M., Grindlay, J., Zhao, P., Hong, J. and Servillat, M. Pre-outburst optical/NIR observations of the field around the accreting milliseconf X-ray pulsar IGR J17498-2921. *ATEL 3634* (2011).
24. Linares, M. et al. Swift observations of the accreting millisecond pulsar IGR J17498-2921: from outburst to quiescence. *ATEL 3661* (2011).
25. Grebenev, S., Bryksin, S. and Sunyaev, R. X-ray activity of the transient burster IGR J17498-2921 detected with INTEGRAL. *ATEL 15996* (2023).
26. Sanna, A. et al. NICER confirms a new outburst from IGR J17498-2921. *ATEL 15998* (2023).
27. Struminsky, A. and Sadovski, A. Stellar Cosmic Rays in Habitable Zone. Sars: from Collapse to Collapse, *ASP Conference Series 510* (2017).

5th International Conference of Hyojeong Academy
International Joint Conference 2025

Effective parameter evaluation of cylindrically propagating elastic waves

Chung Il Park

Dept. of Mechanical and Biomedical, Mechatronics Engineering, Kangwon Nat'l Univ., Chuncheon, Korea
Correspondence: cipark@kangwon.ac.kr

Abstract: This study proposes a methodology to interpret cylindrically propagating elastic waves as analogous to waves propagating in Cartesian coordinates. By employing coordinate transformations and leveraging the symmetry of wave propagation, the approach simplifies the complexities inherent in cylindrical coordinate systems. This framework enables the application of existing Cartesian-based analytical techniques to cylindrical wave problems, providing enhanced computational efficiency. The proposed method holds potential for various engineering applications, including elastic wave-based nondestructive testing and structural optimization, particularly in complex media and structures.

Keywords: Elastic metamaterial, Wave propagation, Transfer matrix

1. Introduction

Understanding the elastic effective properties of materials is crucial in a wide range of engineering applications, from aerospace structures to biomedical devices [1, 2]. These properties provide insights into the material's ability to withstand mechanical forces, propagate stress waves, and perform under dynamic conditions. In recent years, the study of wave propagation in complex materials has garnered significant attention, as it offers a deeper understanding of the interplay between material structure and mechanical behavior.

Among the various methodologies available for studying wave propagation, the transfer matrix method (TMM) has emerged as a powerful analytical and numerical tool [3, 4]. Its ability to efficiently model wave behavior in layered media and periodic structures makes it particularly well-suited for exploring cylindrically propagating waves. Cylindrical wave propagation, which is characterized by its radial symmetry and dependence on azimuthal and radial coordinates, is highly relevant in scenarios involving cylindrical geometries, such as pipelines, acoustic sensors, and composite cylindrical shells.

Despite the extensive research on TMM and its applications to planar wave propagation, relatively few studies have focused on its application to cylindrical wave propagation, especially in the context of determining elastic effective properties. This gap in the literature presents a significant opportunity to extend the utility of TMM to cylindrical geometries, enabling accurate and efficient modeling of wave mechanics in these systems.

This study aims to develop a comprehensive framework for determining the elastic effective properties of materials subjected to cylindrically propagating waves using the transfer matrix method. By leveraging the inherent advantages of TMM, such as its modularity and ability to handle multi-layered systems, this approach provides a robust means of analyzing wave behavior in complex cylindrical configurations. Additionally, the findings of this study will have implications for the design and optimization of materials and structures with tailored wave propagation characteristics.

In the following sections, one first presents a detailed overview of the theoretical foundation of the transfer matrix method as applied to cylindrical wave propagation. One then describes the derivation of the elastic effective properties and validates the proposed methodology. Finally, one discusses the broader implications of this research and suggests potential directions for future studies in this domain.

2. Materials and Methods

The wave propagation of a longitudinal wave on isotropic elastic medium in the cylindrical coordinate can be described by using scalar potential function φ :

$$\varphi(\omega; r,t) = AH_\nu^{(1)}(k_r r)e^{-i\omega t} + BH_\nu^{(2)}(k_r r)e^{-i\omega t} \tag{1}$$

where ω denotes angular frequency and r and t respectively represent radial coordinate and time. A and B are wave amplitude for positive *r*-going and negative *r*-going wave respectively. $H_\nu^{(1)}$ and $H_\nu^{(2)}$ are Hankel function of the first and second kind respectively with order number ν. k_r represents wavenumber along the *r*-direction. Here, for simplicity, one only considers the *r*-going wave only. The wave number along the θ and z directions, k_θ and k_z, are set to be zero which otherwise can be written as $\nu = k_\theta = 0$ i is the imaginary unit. This scalar longitudinal wave potential provides displacement and strain field as

$$u_r = \frac{\partial\varphi}{\partial r} = Ak_r\left(\frac{H_{\nu-1}^{(1)}(k_r r) - H_{\nu+1}^{(1)}(k_r r)}{2}\right) + Bk_r\left(\frac{H_{\nu-1}^{(2)}(k_r r) - H_{\nu+1}^{(2)}(k_r r)}{2}\right) \tag{2a}$$

$$u_\theta = u_z = 0 \tag{2b}$$

$$\varepsilon_{rr} = \frac{\partial^2\varphi}{\partial r^2} = Ak_r^2\left(\frac{H_{\nu-2}^{(1)}(k_r r) - 2H_\nu^{(1)}(k_r r) + H_{\nu+2}^{(1)}(k_r r)}{4}\right) + Bk^2\left(\frac{H_{\nu-2}^{(2)}(k_r r) - 2H_\nu^{(2)}(k_r r) + H_{\nu+2}^{(2)}(k_r r)}{4}\right) \tag{3a}$$

$$\varepsilon_{\theta\theta} = \frac{1}{r}\frac{\partial u_\theta}{\partial\theta} + \frac{u_r}{r} = A\frac{k_r}{r}\left(\frac{H_{\nu-1}^{(1)}(k_r r) - H_{\nu+1}^{(1)}(k_r r)}{2}\right) + B\frac{k_r}{r}\left(\frac{H_{\nu-1}^{(2)}(k_r r) - H_{\nu+1}^{(2)}(k_r r)}{2}\right) \tag{3b}$$

$$\varepsilon_{zz} = \varepsilon_{r\theta} = \varepsilon_{\theta z} = \varepsilon_{zr} = 0 \tag{3c}$$

Here one omits time harmonic term $e^{-i\omega t}$ for simplicity without loss of generality. One assumes that the propagating medium is isotropic satisfying $\sigma_{ij} = \lambda e\delta_{ij} + 2\mu\varepsilon_{ij}\,(i, j = r,\theta,z)$, which in turn provides velocity and stress field as

$$v_r = \frac{\partial u_r}{\partial t r} = -i\omega Ak_r\left(\frac{H_{\nu-1}^{(1)}(k_r r) - H_{\nu+1}^{(1)}(k_r r)}{2}\right) - i\omega Bk_r\left(\frac{H_{\nu-1}^{(2)}(k_r r) - H_{\nu+1}^{(2)}(k_r r)}{2}\right) \tag{4}$$

$$\begin{aligned}\sigma_{rr} = (\lambda+2\mu)\varepsilon_{rr} + \lambda\varepsilon_{\theta\theta} &= \left\{(\lambda+2\mu)k_r^2\left(\frac{H_{\nu-2}^{(1)}(k_r r) - 2H_\nu^{(1)}(k_r r) + H_{\nu+2}^{(1)}(k_r r)}{4}\right) + \frac{k_r}{r}\left(\frac{H_{\nu-1}^{(1)}(k_r r) - H_{\nu+1}^{(1)}(k_r r)}{2}\right)\right\}A \\ &+ \left\{(\lambda+2\mu)k_r^2\left(\frac{H_{\nu-2}^{(2)}(k_r r) - 2H_\nu^{(2)}(k_r r) + H_{\nu+2}^{(2)}(k_r r)}{4}\right) + \frac{k_r}{r}\left(\frac{H_{\nu-1}^{(2)}(k_r r) - H_{\nu+1}^{(2)}(k_r r)}{2}\right)\right\}B\end{aligned} \tag{5}$$

λ and μ are the Lame's constant. $e = \varepsilon_{rr} + \varepsilon_{\theta\theta} + \varepsilon_{zz}$ is dilation and δ_{ij} is Kronecker delta. These displacement and stress fields provide major physical information of the wave propagation phenomena. The propagation of the fields variables otherwise can be written as

$$\begin{bmatrix} u_r \\ \sigma_{rr} \end{bmatrix} = \mathbf{M}_{Cyl}(k_r, r)\,\mathbf{N}_{Cyl}(k_r, r)\begin{bmatrix} A \\ B \end{bmatrix} \tag{6a}$$

where

$$\mathbf{M}_{Cyl}(k_r, r) = \begin{bmatrix} -i\omega k_r\Pi_\nu^{(1)} & -i\omega k_r\Pi_\nu^{(2)} \\ (\lambda+2\mu)k_r^2\Theta_\nu^{(1)} + \lambda\dfrac{k_r}{r}\Pi_\nu^{(1)} & (\lambda+2\mu)k_r^2\Theta_\nu^{(2)} + \lambda\dfrac{k_r}{r}\Pi_\nu^{(2)} \end{bmatrix},\quad \mathbf{N}_{Cyl}(k_r, r) = \begin{bmatrix} H_\nu^{(1)}(k_r r) & 0 \\ 0 & H_\nu^{(2)}(k_r r) \end{bmatrix} \tag{6b}$$

with

$$\Pi_{\nu}^{(n)}=\frac{H_{\nu-1}^{(n)}\left(k_r r\right)-H_{\nu+1}^{(n)}\left(k_r r\right)}{2H_{\nu}^{(n)}\left(k_r r\right)} \text{ and } \Theta_{\nu}^{(n)}=\frac{H_{\nu-2}^{(n)}\left(k_r r\right)-2H_{\nu}^{(n)}\left(k_r r\right)+H_{\nu+2}^{(n)}\left(k_r r\right)}{4H_{\nu}^{(n)}\left(k_r r\right)} \quad \left(n=1,2\right). \tag{6c}$$

One introduces so-called transfer matrix method for a cylindrically propagating elastic longitudinal wave. The field variable matrix at point r_1 and r_2 has linear matrix relation as

$$\left\lfloor \begin{matrix} u_r \\ \sigma_{rr} \end{matrix} \right\rfloor_{r_2} = \mathbf{T}_{Cyl}\left(k_r, r_1, r_2\right) \left\lfloor \begin{matrix} u_r \\ \sigma_{rr} \end{matrix} \right\rfloor_{r_1} \tag{7a}$$

where

$$\mathbf{T}_{Cyl}\left(k_r, r_1, r_2\right)=\mathbf{M}_{Cyl}\left(k_r, r_2\right)\mathbf{N}_{Cyl}\left(k_r, r_2\right)\mathbf{N}_{Cyl}^{-1}\left(k_r, r_1\right)\mathbf{M}_{Cyl}^{-1}\left(k_r, r_1\right) \tag{7b}$$

Here matrix $\mathbf{T}_{Cyl}$ is referred to as the transfer matrix in the cylindrical coordinate. This transfer matrix has a strong analogy to that of the Cartesian one, which can be written as

$$\mathbf{T}_{Car}\left(k_x, x_1, x_2\right)=\mathbf{M}_{Car}\left(k_x, x_2\right)\mathbf{N}_{Car}\left(k_x, x_2\right)\mathbf{N}_{Car}^{-1}\left(k_x, x_1\right)\mathbf{M}_{Car}^{-1}\left(k_x, x_1\right) \tag{8a}$$

$$\mathbf{M}_{Car}\left(k_x, x\right)=\begin{bmatrix} -\omega k_x & \omega k_x \\ -\left(\lambda+2\mu\right)k_x^2 & -\left(\lambda+2\mu\right)k_x^2 \end{bmatrix},\ \mathbf{N}_{Car}\left(k_x, x\right)=\begin{bmatrix} e^{+ik_x x} & 0 \\ 0 & e^{-ik_x x} \end{bmatrix} \tag{8b}$$

where k_x denotes wavenumber along *x*-direction and x represents a coordinate. The diagonalization of the transfer matrix $\mathbf{T}_{Car}\left(k_x, x_1, x_2\right)$ provides the Eigenvalue matrix which is equal to $\mathbf{N}_{Car}\left(k_x, r_2\right)\mathbf{N}_{Car}^{-1}\left(k_x, r_1\right)$, while one of the Eigenvector matrix is given as $\mathbf{M}_{Car}$. The Eigenvalue matrix otherwise can be calculated as

$$\mathbf{M}_{Car}\left(k_x, x\right)=-\omega k_x\begin{bmatrix} 1 & -1 \\ Z & Z \end{bmatrix} \tag{9}$$

where $Z=\rho c_p$ represents characteristic impedance of medium with density ρ and phase velocity $c_p=\sqrt{\left(\lambda+2\mu\right)/\rho}$.

Here one assumes that matrix $\mathbf{M}_{Cyl}\left(k_r, r_2\right)$ is equal to one of the Eigenvector matrix of $\mathbf{T}_{Cyl}\left(k_r, r_1, r_2\right)$ while $\mathbf{N}_{Car}\left(k_x, x_2\right)\mathbf{N}_{Car}^{-1}\left(k_x, x_1\right)$ is equal to Eigenvalue matrix. This assume is approximately exact at a far-field ($r_2, r_1 \gg 1$). Similarly, the eigenvector matrix $\mathbf{M}_{Cyl}\left(k_r, r\right)$ can be simplified as

$$\mathbf{M}_{Cyl}\left(k_r, r\right)=\omega k_r\begin{bmatrix} -i\Pi_{\nu}^{(1)} & -i\Pi_{\nu}^{(2)} \\ \left(\lambda+2\mu\right)\dfrac{k_r}{\omega}\Theta_{\nu}^{(1)}+\lambda\dfrac{1}{r\omega}\Pi_{\nu}^{(1)} & \left(\lambda+2\mu\right)\dfrac{k_r}{\omega}\Theta_{\nu}^{(2)}+\lambda\dfrac{1}{r\omega}\Pi_{\nu}^{(2)} \end{bmatrix} \tag{10}$$

Since Eigenvector matrices otherwise can be calculated as

$$\bar{\mathbf{M}}_{Cyl}\left(k_r, r\right)=\omega k_r\begin{bmatrix} 1 & 1 \\ i\left(\lambda+2\mu\right)\dfrac{k_r}{\omega}\dfrac{\Theta_{\nu}^{(1)}}{\Pi_{\nu}^{(1)}}+i\dfrac{\lambda}{r\omega} & i\left(\lambda+2\mu\right)\dfrac{k_r}{\omega}\dfrac{\Theta_{\nu}^{(2)}}{\Pi_{\nu}^{(2)}}+i\dfrac{\lambda}{r\omega} \end{bmatrix} \tag{11}$$

Thus the component of $\bar{\mathbf{M}}_{Cyl}$ can be seen as an effective impedance $Z_{eff}^{(n)}$ of the cylindrical coordinate as

$$Z_{eff}^{(1)}=i\left(\lambda+2\mu\right)\frac{k_r}{\omega}\frac{\Theta_{\nu}^{(1)}}{\Pi_{\nu}^{(1)}}+i\frac{\lambda}{r\omega},\quad Z_{eff}^{(2)}=-i\left(\lambda+2\mu\right)\frac{k_r}{\omega}\frac{\Theta_{\nu}^{(2)}}{\Pi_{\nu}^{(2)}}-i\frac{\lambda}{r\omega} \tag{12}$$

Similarly, one now uses analog of the Eigen value matrices and calculates the effective phase shift $\beta_{eff}^{(n)}$ as

$$\beta_{eff}^{(n)}=\angle H_{\nu}^{(n)}\left(k_r r_2\right)/H_{\nu}^{(n)}\left(k_r r_1\right)=\tan^{-1}\left(\frac{\mathrm{Im}\left(H_{\nu}^{(n)}\left(k_r r_2\right)/H_{\nu}^{(n)}\left(k_r r_1\right)\right)}{\mathrm{Re}\left(H_{\nu}^{(n)}\left(k_r r_2\right)/H_{\nu}^{(n)}\left(k_r r_1\right)\right)}\right),\ \left(n=1,2\right) \tag{13}$$

Then the effective phase velocity $c_{eff}^{(n)}$, density $\rho_{eff}^{(n)}$, and stiffness $C_{11eff}^{(n)}$ are calculated as

$$c_{eff}^{(n)} = \tan^{-1}\left(\frac{\mathrm{Im}\left(H_\nu^{(1)}(k_r r_2)/H_\nu^{(1)}(k_r r_1)\right)}{\mathrm{Re}\left(H_\nu^{(1)}(k_r r_2)/H_\nu^{(1)}(k_r r_1)\right)}\right)/\omega d,\ (n=1,2) \tag{14}$$

$$\rho_{eff}^{(n)} = 1/c_{eff}^{(n)} Z_{eff}^{(n)},\ (n=1,2) \tag{15}$$

$$C_{11eff}^{(n)} = c_{eff}^{(n)} Z_{eff}^{(n)},\ (n=1,2) \tag{16}$$

Using these effective properties describe the wave propagation in a Cartesian coordinate can be seen as that in a cylindrical coordinate.

3. Results

This section is devoted to describing the effective properties of the cylindrical wave propagation and the effectiveness of the approach. Figure 1 shows the schematic drawing of the wave propagation. Axisymmetric geometry is considered to present cylindrical wave propagation. The background medium is set to be aluminum (density ρ = 2700 kg·m^{-3}, Young's modulus E =70 GPa, Poisson's ratio ν =0.33), while the medium of interest is set to be steel (ρ = 8000 kg·m^{-3}, E =200 GPa, Poisson's ratio ν =0.29). r_0 and d are the inner radius and thickness of the medium of interest, respectively. The upper and lower boundaries are subjected to a periodic condition as follows:

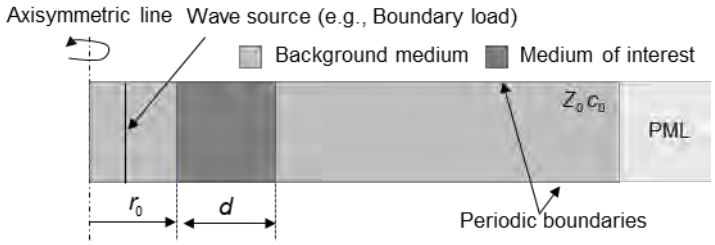

Figure 1. Schematic drawing of a medium of interest to calculate effective parameters.

Equations (12) to (16) provide the effective parameters of the target cylindrical wave. Unlike the Cartesian counterpart, the effective properties of the cylindrical wave vary regarding not only the inner radius but also the thickness of the medium and frequency. For simplicity one only focuses on the effect of the inner radius r_0. Figure 2 presents the effective parameters with respect to r_0. The frequency is set to be 100 kHz and d = 5mm. The effective impedance in Figure 2(a) presents sharply varying section roughly ranging from 1×10^{0} to 2×10^{1}. Presented by a blue shade box. One refers to this section as cylindrical-dominant range. Impedance in this section has complex impedance meaning that decaying of the wave amplitude as the wave travels. As r_0 increases, the effective impedance converges to 3.96×10 kg·m^{-2}·s^{-1} and impedance imaginary converges to zero. Note that this value is the impedance in a Cartesian coordinate. This stems from the fact that wave propagation for considerably large inner radius may be regarded as the propagation in the Cartesian coordinate. This tendency can be also found in effective phase, density, and stiffness plot in Figure 2(b) to 2(d). Their values also converge to the Cartesian one. The complex values in the cylindrical dominant section are observed.

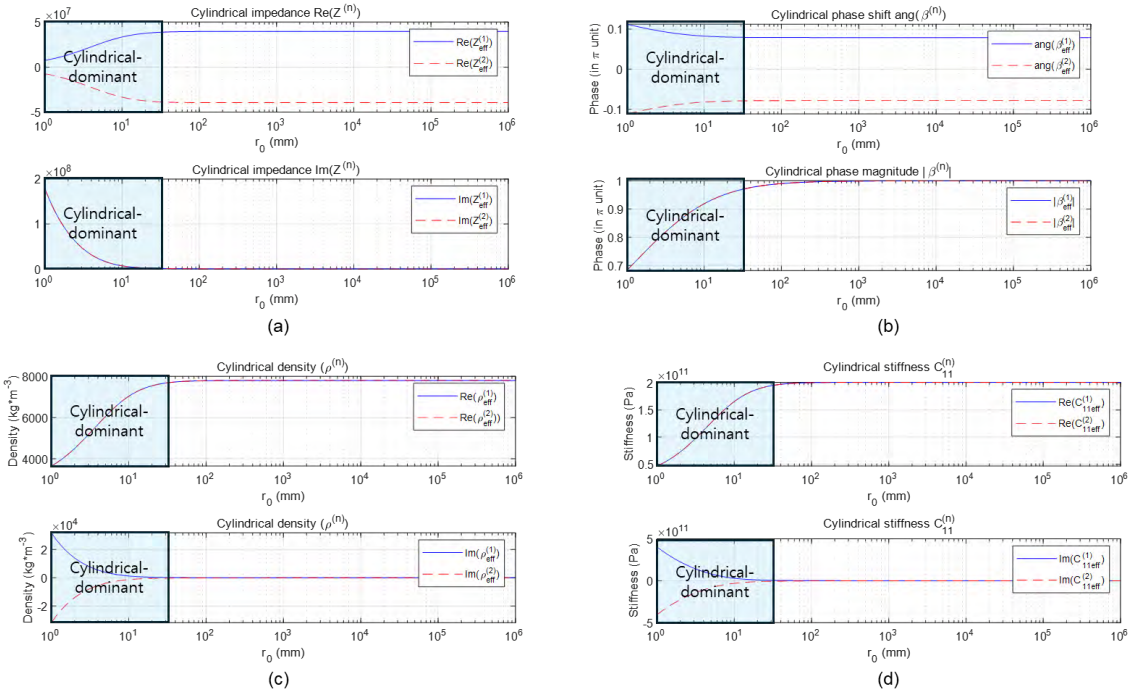

Figure 2. Effective properties that represent the wave propagation in a cylindrical coordinate: (a) Effective impedance; (b) effective phase shift; (c) effective density; (d) effective stiffness.

4. Discussion

The cylindrical effective parameters converge to Cartesian's. This convergence indicates the validity of suggested approach, since the wave propagation in considerably large size of radius can approximately be considered as Cartesian wave propagation. Much meaningful region is cylindrical-dominant range at a relatively small r_0. This varying material property indicates that translating the wave physics of a cylindrical coordinate requires complicated material properties even complex. However, considering that understanding of a near field (or small r_0) physics remains conundrum, these artificially calculated effective properties may provide clues for deeper understanding. For the future study, verification of this estimated parameters will be performed. One considers comparison of the transmission and reflection coefficient over frequencies between original cylindrical wave and Cartesian estimation using effective parameters for a given r_0.

5. Conclusions

Unlike wave propagation in a Cartesian coordinate, those in a cylindrical coordinate are relatively less revealed. If one can utilize the profound understanding of Cartesian wave propagation, it provides great possibility to understand the wave physics in a cylindrical coordinate. To this end, one introduces cylindrical effective parameters—impedance, phase shift, density, and stiffness—that translate complicate wave phenomena of the cylindrical coordinate to Cartesian one based on the transfer matrix method-based approach. One utilizes the similarity of the transfer matrices in both coordinates and assumes that composition matrix of the cylindrical may be treated as equivalent one to the Cartesian one. This assumption subsequently provides cylindrical effective parameters. The obtained parameters vary considerably for the relatively small values of inner radius r_0 but converge to the Cartesian parameters for the large r_0.

Funding: This research received no external funding.

Supplementary Materials: No Supplementary Materials are presented.

Author Contributions: For research articles with several authors, a short paragraph specifying their individual contributions must be provided. The following statements should be used "Conceptualization, C.I.P.; methodology, C.I.P.; software, C.I.P.; validation, C.I.P.; formal analysis, C.I.P.; investigation, C.I.P.; resources, C.I.P.; data curation, C.I.P.; writing—original draft preparation, C.I.P.; writing—review and editing, C.I.P.; visualization, C.I.P.; supervision, C.I.P.; project administration, C.I.P. All authors have read and agreed to the published version of the manuscript.

Data Availability Statement: Not applicable.

Acknowledgments: One thanks to Y.Y. Kim and J.H. Oh for providing profound perspective on the elastic wave propagation.

Conflicts of Interest: The authors declare no conflict of interest.

References

1. Huan, H. et al. Mechanical strength evaluation of elastic materials by multiphysical nondestructive methods: a review. *Appl. Sci. 10*: 1588, (2020). https://doi.org/10.3390/app10051588
2. Marazzani, J., Cavalagli, N. and Gusella, V. Elastic properties estimation of masonry walls through the propagation of elastic waves: an experimental investigation. *Appl. Sci. 11*: 9091, (2021).
3. Song, B.H. and Bolton, J.S. A transfer-matrix approach for estimating the characteristic impedance and wave numbers of limp and rigid porous materials. *J. Acoust. Soc. Am. 107(*3), 1131-1152 (2000).
4. Yeh, J.-Y. and Chen, L.-W. Wave propagations of a periodic sandwich beam by FEM and the transfer matrix method. *Composite Struct. 73*(1), 53-60 (2006).

Proceedings of
THE 5th INTERNATIONAL CONFERENCE OF
HYOJEONG ACADEMY 2025

Session 4

Bio Science for Co-Prosperity

www.ichja.org

5th International Conference of Hyojeong Academy
International Joint Conference 2025

Glycosylation of Anthraquinone by UGT-1: Biosynthesis of compound with potential biological activity

Min-Su Kim and Tae-Jin Oh*

Department of Life Science and Biochemical Engineering, Sun Moon University, Asan 31460, Korea
*Correspondence: tjoh3782@sunmoon.ac.kr

Abstract: Anthraquinones are secondary metabolites of plants and are widely distributed in various species. They are known to exhibit a wide range of biological activities, including anticancer, anti-inflammation, antioxidant, antibacterial, anti-damage, and anti-osteoporosis. Anthraquinones are generally lipophilic, which results in relatively low solubility and bioavailability. These limitations can be addressed through enzymatic reactions such as glycosylation and hydroxylation. In this study, we attempted the glycosylation of two anthraquinone compounds, anthraflavic acid and xanthopurpurin, using microbial UDP-glycosyltransferase UGT-1. UGT-1 could catalyze the O-glucosylation of anthraquinones to form glucoside-type products, which were confirmed by HPLC and high-resolution LC-MS analyses. This study demonstrated that glycosyltransferase UGT-1 could be a good candidate for producing modified steroids with potential biological activities.

Keywords: Glycosyltransferase, Anthraquinone, Biosynthesis

1. Introduction

Natural compounds have been of significant interest in the fields of pharmacology, food science, and the cosmetics industry due to their diverse biological properties [1, 2]. In particular, anthraquinone compounds are excellent research subjects due to their various biological properties such as antibacterial, antioxidant, antitumor, and antihypertensive effects. Anthraquinone is a multifunctional polyphenol compound widely distributed in the plant kingdom. It is a compound derived from anthracene with two ketone groups attached at positions 9 and 10 [3, 4]. These compounds are structurally complex and have limited physicochemical properties such as hydrophilicity and lipophilicity, often resulting in reduced efficiency in absorption, distribution, metabolism, and excretion processes within the body. Various biosynthetic processes are being studied to improve bioavailability and stability [5, 6]. In particular, glycosylation, which involves adding sugars to compounds, is known to be an effective method for increasing the solubility of compounds and ensuring stability against enzymatic or chemical degradation within the body [7].

Glycosyltransferases (GTs) catalyze glycosylation reactions on a wide range of substrates, such as secondary metabolites, nucleic acids, polysaccharides, and protein lipids [8]. Glycosylation is the most common modification in plant secondary metabolites, enhancing the biological activity, stability, and solubility of receptor molecules. It also has significant physiological effects, such as regulating the balance of plant hormones and contributing to plant detoxification and defense responses. These reactions generally occur through UDP-glucosyltransferases, which catalyze glycosylation reactions using UDP-glucose as a donor [9].

In particular, UGT-1 is well known for its efficiency and substrate specificity through studies on the glycosylation reactions of steroid compounds. The glycosylation of steroid compounds plays an important role in increasing the solubility of the compounds and regulating their biological activity, and such research utilizing the characteristics of UGT-1 has made significant contributions to drug development and biological research [10, 11]. However, research on the glycosylation of anthraquinone compounds using UGT-1 is relatively lacking, and further studies are required.

This study focuses on exploring the glycosylation potential of anthraquinone derivatives using UGT-1. Through this, we aim to present the applicability of enzymatic modification using UGT-1.

2. Materials and Methods

2.1. Materials

Xanthopurpurin used in this study was purchased from ChemFaces (Wuhan ChemFaces Biochemical Co., Ltd., Wuhan, China), and anthraflavic acid was obtained from TCI (Tokyo Chemical Industry Co., Ltd., Tokyo, Japan). UDP-glucose was purchased from GeneChem, Korea. All other high-grade reagents were obtained from commercial sources.

2.2. Enzymatic in-vitro assay of anthrquinones

The heterologous expression and purification of glucosyltransferase UGT-1 were carried out according to previously published papers. In the case of in vitro analysis, the reaction mixture consisted of a final concentration of 10 μg/ml UGT-1, 100 mM Tris-HCl buffer (pH 8.5), 10 mM $MgCl_2 \cdot 6H_2O$, 2 mM UDP-glucose, and 0.4 mM substrate. The reaction was carried out at 35℃ for 2 hours with shaking. We added twice the amount of methanol relative to the reaction volume to stop the reaction and then centrifuged it. Later, the supernatant was collected and analyzed using high-performance liquid chromatography (HPLC) and liquid chromatography-mass spectrometry (LC-MS).

2.3. Analysis of glycosylated anthraquinones

Products were analyzed with a Nexera UHPLC system (Shimadzu, Japan) using a GIS C18 column (Shim-pack, 4.6 × 250 mm, particle size 5 μm HSS). The mobile phase consisted of solvent A (HPLC grade water + 0.05% trifluoroacetic acid (TFA)) and solvent B (HPLC grade 100% acetonitrile). The flow rate was set at 1ml/min for a 35 min program. The oven temperature was maintained at 30°C. Acetonitrile(ACN) concentrations were 10% (0 – 10 min), 10 to 20% (25 min), 100 % (28 min), 70% (30 min), and then 10% (30 - 35 min). The injection volume was 20μL. Detection of both substrate and product was performed by UV absorbance at 280nm.

After completing the in-vitro experiment, the supernatant collected by adding HPLC-grade methanol was used for mass spectrometry analysis. High-resolution quadrupole time-of-flight electrospray ionization mass spectrometry (HQ-QTOF ESI/MS) was performed in positive ion mode, and the analysis was conducted using Waters Crop. (Milford, MA, USA) ACQUITY UPLC and SYNAPT GS-2 equipment.

2.4. In-silico analysis

The *in-silico* protein structure of UGT-1 was performed through the AlphaFold server(https://alphafold-server.com/) [12]. The homology model was validated for structural accuracy using ERRAT [13], Verify3D [14], and PROCHECK [15]. AutoDock Vina [16] was used to conduct molecular docking studies and predict the binding affinity between anthraflavic acid and xanthofulvin, and ProteinPlus (https://proteins.plus/)[17] was utilized to thoroughly examine the interactions between the enzyme residues and the substrate. We selected the predominant ligand conformation and analyzed the binding mode with UGT. The visualization of the results was performed using PyMoL [18].

3. Results and Discussion

3.1. In-vitro biotransformation of anthraquinones

We performed the in vitro biotransformation of anthraquinone. The HPLC results showed two peaks in the biotransformation analysis of anthrapurpurin and xanthopurpurin, respectively. The peaks of the products were observed at shorter retention times compared to the substrate peaks, indicating the presence of glucosylated products (Figure 1).

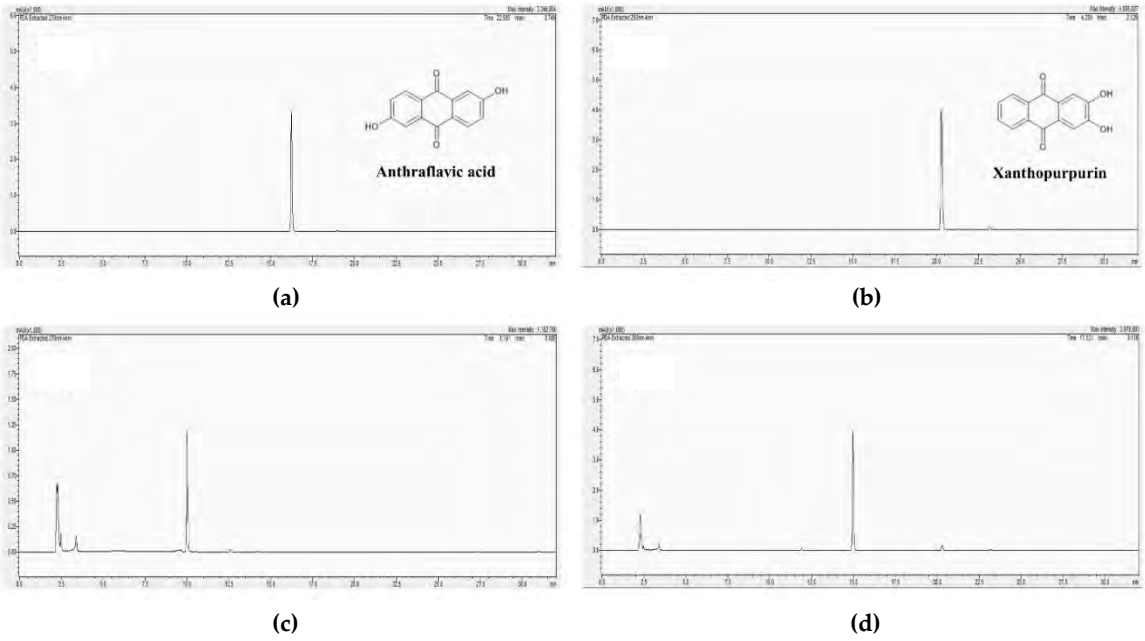

Figure 1. HPLC chromatogram of glycosylated anthraquinones: (a) Anthraflavic acid standard; (b) Reaction product of anthraflavic acid and UGT-1; (c) Xanthopurpurin standard; (d) Reaction product of xanthopurpurin and UGT-1.

The conversion rates of anthraflavic acid and xanthopurpurin were both over 95%. These detected products were further analyzed in positive ion mode LC-QTOF-ESI/MS for more accurate confirmation. The mass spectrum showed the exact mass of anthraflavic acid $[M + H]^+$ m/z^+ ~ 241.049. The reaction products of anthraflavic acid showed a mass spectrum of $[M + H]^+$ m/z^+ ~ 403.102 and 565.156, which were similar to the mono- and di-glucoside derivatives of anthraflavic acid. Similarly, the mass spectrum of xanthopurpurin showed a mass of $[M + H]^+$ m/z^+ ~ 241.049. The product peaks of xanthopurpurin showed masses of $[M + H]^+$ m/z^+ ~ 403.102 and 565.154. This was similar to the mono- and di-glucose conjugates of xanthopurpurin (Figure 2).

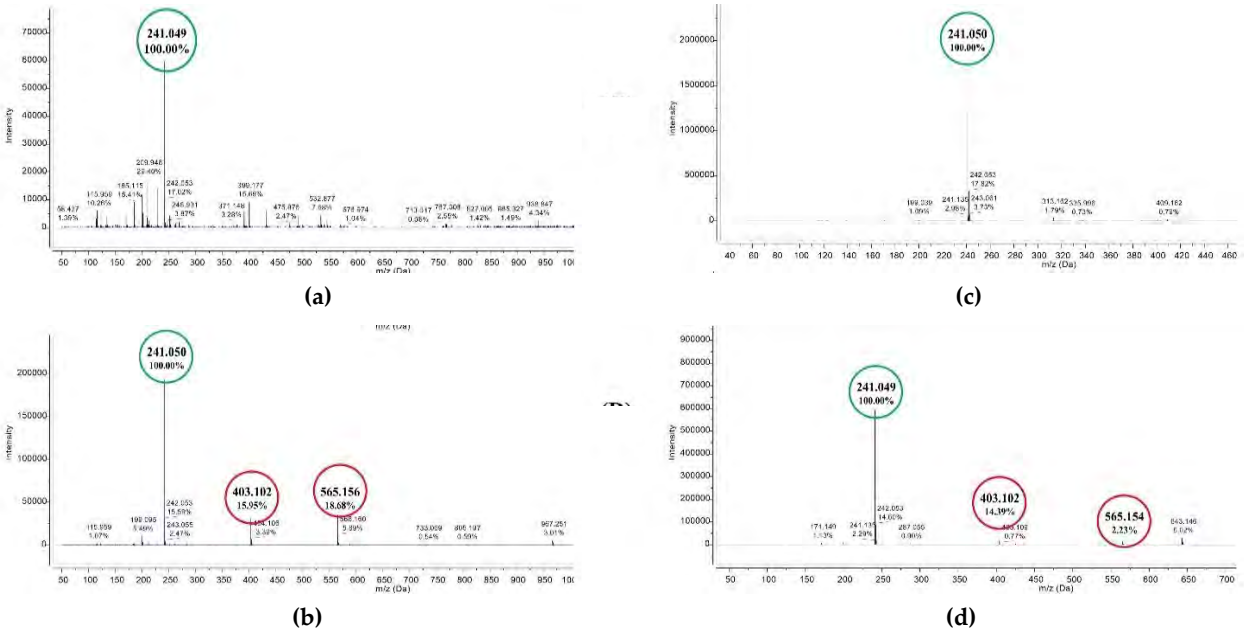

Figure 2. LC-MS spectrum of glycosylated anthraquinones: (a) Anthraflavic acid standard; (b) Xanthopurpurin standard; (c) Reaction product of anthraflavic acid and UGT-1; (d) Reaction product of xanthopurpurin and UGT-1. The mass of the substrate was indicated using a green circle, and the mass of the reactant was indicated using a red circle.

3.2. Homology Modeling of UGT-1

The homology model of UGT-1 was obtained using the AlphaFold Server. If the predicted template modeling (pTM) of a homology model is above 0.5, it means that the predicted structure is similar to the actual structure, and the higher the value, the more similar it is to the actual structure [19, 20]. Since the pTM of the UGT-1 homolgy model is 0.93, it means that the structure predicted by the AlphaFold Server is similar to the actual structure. To verify the quality of the homology model of UGT-1, we used the online programs ERRAT, VERIFY3D, and ERRAT. The ERRAT analysis results showed an overall quality index of 98.11, indicating that the homology model of UGT-1 is a highly reliable structure. In the VERIFY3D analysis, 87.02% of the residues in the model recorded values above 0.1 in the 3D/1D profile score, indicating that most of the residues are in environmentally suitable positions within the structure. As a result of evaluating the stereochemical quality of the protein structure using PROCHECK, the Ramachandran plot analysis showed that 95.4% of the residues were located in the core region, and the remaining 4.6% were found in the additionally allowed region. When comprehensively reviewing these results, the homology model of UGT-1 obtained using the AlphaFold Server is considered to be of reliable structural quality.

The modeled 3D structure of UGT-1 showed a structure composed of two separate Rossmann-fold domains (β/α/β) connected by a linker region, which is a form typically seen in GT-B folds. The active site was located between the two Rossmann-fold domains [21]. The active site was located in the inter-domain cleft formed by two flexibly linked Rossmann fold domains. The substrate binding site was present in the N-terminal domain, which had a flexible and structurally plastic loop region. In contrast, the donor substrate binding site was located in the more conserved and structurally rigid C-terminal domain [22].

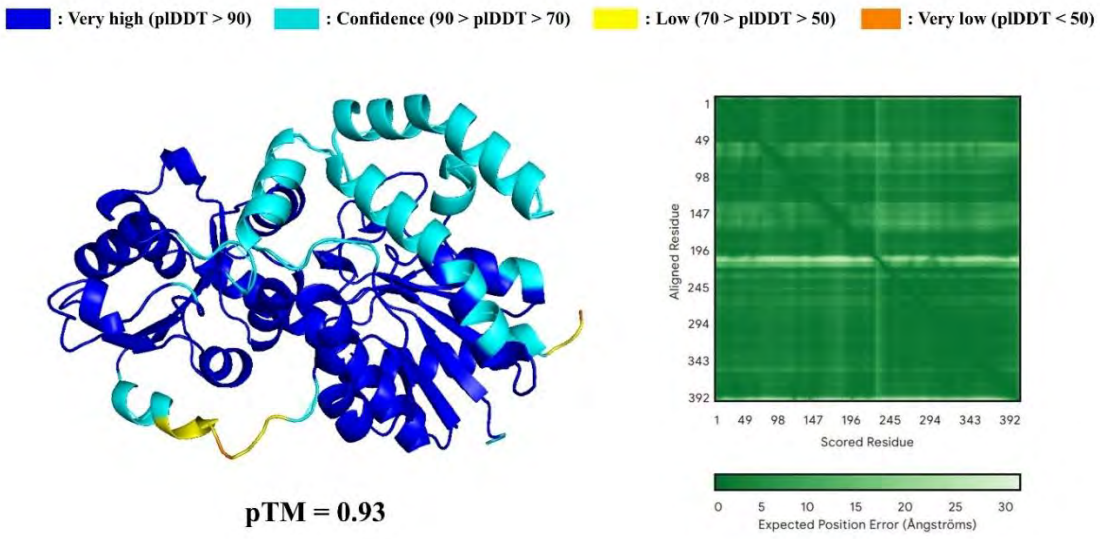

Figure 3. The homology model of UGT-1 obtained from the AlphaFold Server. plDDT indicates that the closer it is to 100, the higher the confidence per atom. plDDT: predicted local Distance Difference Test, pTM: predicted template modeling.

3.3. Molecular docking

Molecular docking analyses were performed to anticipate the potential binding configurations of sugar donors and receptor molecules at the active site. The analysis of the docked complex of UGT-1 with the ligand revealed a predilection for a comparable orientation within the active site. The docking locations of the sugar source UDP-glucose, anthraflavic acid, and xanthopurpurin were identified in a conformation conducive to the glucosyl transfer process, signifying a thermodynamically advantageous orientation. The projected lowest binding energies for anthraflavic acid and xanthopurpurin are -7.6 kcal/mol and -7.8 kcal/mol, respectively. The docked complex of UGT-1 and UDP-glucose revealed the presence of UGT-glucose in the C-domain. The docking analysis of anthraflavic acid and UGT-1 revealed interactions with His294, Asn298, and Glu318 residues of UGT-

1. The docking results of xanthopurpurin and UGT-1 indicated interactions with His294, Asn298, and His16. Given these observations, Asn298 and His294 are anticipated to be pivotal in the reaction with UGT-1 (Figure 4). Furthermore, numerous investigations have demonstrated that histidine and aspartic acid function as catalytic bases, and this has been identified as a highly conserved residue. UGT-1 possesses histidine and aspartic acid at analogous locations relative to other UGTs, serving as catalytic bases [11]. The results are also evident in our UGT-1 and xanthopurpurin complex. Nonetheless, the architecture of UGT-1 remains incompletely characterized, and our docking findings indicate that the residues of UGT-1 are not situated within 3 Å of UDP-glucose and the substrate, suggesting that our results require validation with a more precise structure in the future. We intend to clarify the structure of UGT-1 in the future to resolve these difficulties.

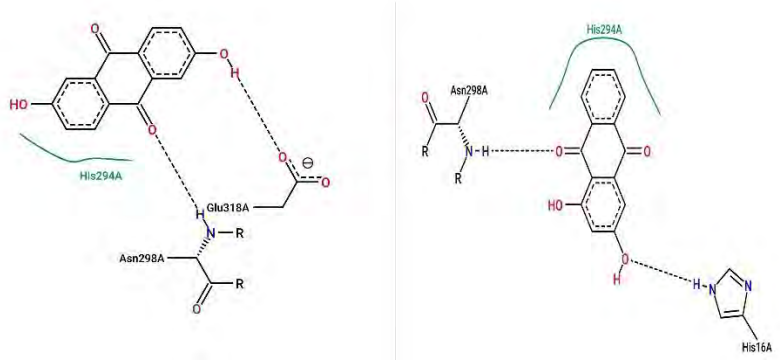

(a) (b)

Figure 4. Analysis of the interaction between UGT-1 and substrates by ProteinPlus: (a) UGT-1 and anthraflavic acid complex; (b) UGT-1 and xanthopurpurin complex.

4. Conclusions

In this study, we successfully performed the enzymatic glycosylation of anthraquinone compounds using UDP-glycosyltransferase UGT-1. Through in vitro experiments, anthraflavic acid and xanthopurpurin were efficiently converted into mono- and di-glucoside derivatives, achieving a high conversion rate of over 95%. These results were confirmed through HPLC and LC-MS analysis, demonstrating that glycosylation is an effective method for enhancing the solubility and bioavailability of anthraquinone derivatives.

Additionally, through homology modeling of UGT-1, we identified important structural features, including the conserved Rossmann-fold domain and the active site structure. Molecular docking analysis predicted that the His294 and Asp298 residues play crucial roles in substrate binding and catalytic activity. These results not only expand the functional understanding of UGT-1 but also highlight the potential application of UGT-1 in the enzymatic modification of bioactive compounds.

However, although the docking results indicated thermodynamically favorable interactions, additional validation through experimental methods is necessary due to the structural limitations of the predicted UGT-1 model. Future research should focus on precisely improving the UGT-1 structure of glycosylated anthraquinone to enhance docking accuracy.

This study suggests the potential of UGT-1 as a versatile biocatalyst for the development of new bioactive compounds and demonstrates its applicability in the pharmaceutical and biotechnology fields.

Funding: This work was carried out with the support of "Cooperative Research Program for Agriculture Science and Technology Development (Project No. RS-2023-00231177)" Rural Development Administration, Republic of Korea.

Data Availability Statement: Not applicable.

Conflicts of Interest: The authors declare no conflict of interest.

References

1. Rybczyńska-Tkaczyk, K., Grenda, A., Jakubczyk, A., Kiersnowska, K. and Bik-Małodzińska, M. Natural Compounds with Antimicrobial Properties in Cosmetics. *Pathogens 12(2)*, 320(2023). https://doi.org/10.3390/pathogens12020320
2. Narayanankutty, A., Famurewa, A. C. and Oprea, E. Natural bioactive compounds and human health. *Molecules 29(14)*, 3372(2024). https://doi.org/10.3390/molecules29143372
3. Koblitz, H. Anthraquinones. *Phytochemicals in Plant Cell Cultures*. 113–139(1988). https://doi.org/10.1016/b978-0-12-715005-5.50014-5
4. Yi, S. et al. Discovery and characterization of four glycosyltransferases involved in anthraquinone glycoside biosynthesis in Rubia yunnanensis. *Organic Chemistry Frontiers 7(17)*, 2442–2448(2020). https://doi.org/10.1039/d0qo00579g
5. Rajput, A. et al. A biocatalytic approach towards the preparation of natural deoxyanthraquinones and their impact on cellular viability. *New Journal of Chemistry 46(7)*, 3087–3090(2022). https://doi.org/10.1039/d1nj05513e
6. Amantino, C. F. et al. Anthraquinone encapsulation into polymeric nanocapsules as a new drug from biotechnological origin designed for photodynamic therapy. *Photodiagnosis and Photodynamic Therapy 31*, 101815(2020). https://doi.org/10.1016/j.pdpdt.2020.101815
7. Hu, S. et al. Advances and challenges in biomanufacturing of glycosylation of natural products. *Fermentation 10(7)*, 349(2024). https://doi.org/10.3390/fermentation10070349
8. Gantt, R. W. and Thorson, J. S. High-throughput colorimetric assays for nucleotide sugar formation and glycosyl transfer. *Methods Enzymol 516*, 345-360(2012). https://doi.org/10.1016/B978-0-12-394291-3.00009-5.
9. Lairson, L. L., Henrissat, B., Davies, G. J. and Withers, S. G. Glycosyltransferases: structures, functions, and mechanisms. *Annu Rev Biochem 77*, 521-555(2008). https://doi.org/10.1146/annurev.biochem.76.061005.092322
10. Yu, E. et al. Enzymatic Synthesis of Anabolic Steroid Glycosides by Glucosyltransferase from Terribacillus sp. PAMC 23288. *Journal of Microbiology and Biotechnology 30(4)*, 604–614(2020). https://doi.org/10.4014/jmb.1911.11057
11. Subedi, P., Kim, M., Lee, J., Park, J. K. and Oh, T. Insight into glucocorticoids glucosylation by glucosyltransferase: A combined experimental and in-silico approach. *Biophysical Chemistry 289*, 106875(2022). https://doi.org/10.1016/j.bpc.2022.106875
12. Abramson, J. et al. Accurate structure prediction of biomolecular interactions with AlphaFold 3. *Nature 630*(8016), 493–500 (2024). https://doi.org/10.1038/s41586-024-07487-w
13. Colovos C. and Yeates, T. O. Verification of protein structures: patterns of nonbonded atomic interactions. *Protein Sci 2(9)*, 1511-1519(1993). https://doi.org/10.1002/pro.5560020916
14. Eisenberg, D., Lüthy, R. and Bowie, J. U. VERIFY3D: assessment of protein models with three-dimensional profiles. *Methods Enzymol 277*, 396-404(1997). https://doi.org/10.1016/S0076-6879(97)77022-8
15. Laskowski, R. A., MacArthur, M. W., Moss, D. S. and Thornton, J. M. PROCHECK: a program to check the stereochemical quality of protein structures. *Journal of Applied Crystallography 26(2)*, 283–291(1993). https://doi.org/10.1107/s0021889892009944
16. Macari, G., Toti, D., Pasquadibisceglie, A. and Polticelli, F. DockingApp RF: a State-of-the-Art novel scoring function for molecular docking in a User-Friendly interface to AutoDock VINA. *International Journal of Molecular Sciences, 21*(24), 9548(2020). https://doi.org/10.3390/ijms21249548
17. Fährrolfes, R. et al. ProteinsPlus: a web portal for structure analysis of macromolecules. *Nucleic Acids Res 45(W1)*, W337-W343(2017). https://doi.org/10.1093/nar/gkx333
18. DeLano, W. L. Pymol: an Open-Source Molecular Graphics Tool. *CCP4 Newsletter On Protein Crystallography*, 88-92(2002).
19. Zhang, Y. and Skolnick, J. Scoring function for automated assessment of protein structure template quality. *Proteins Structure Function and Bioinformatics 57(4)*, 702–710(2004). https://doi.org/10.1002/prot.20264
20. Xu, J. and Zhang, Y. How significant is a protein structure similarity with TM-score = 0.5?. *Bioinformatics 26(7)*, 889–895(2010). https://doi.org/10.1093/bioinformatics/btq066
21. Lairson, L., Henrissat, B., Davies, G. and Withers, S. Glycosyltransferases: structures, functions, and mechanisms. *Annual Review of Biochemistry 77(1)*, 521–555(2007). https://doi.org/10.1146/annurev.biochem.76.061005.092322
22. Dai, L. et al. Structural dissection of unnatural ginsenoside-biosynthetic UDP-glycosyltransferase Bs-YjiC from Bacillus subtilis for substrate promiscuity. *Biochemical and Biophysical Research Communications 534*, 73–78(2020). https://doi.org/10.1016/j.bbrc.2020.11.104

5th International Conference of Hyojeong Academy
International Joint Conference 2025

Structural analysis of Chalcone synthase-like gene from *Senna occidentalis*

Woo-Haeng Lee and Tae-Jin Oh*

Department of Life Science and Biochemical Engineering, Sun Moon University, Asan 31460, Korea
*Correspondence: tjoh3782@sunmoon.ac.kr

Abstract: Bacterial/fungal biosynthetic pathways of anthraquinones have been well-known, but plant anthraquinone biosynthetic pathways remain unexplored. In this paper, we identified several chalcone synthase genes predicted to associate with anthraquinone biosynthesis, through transcriptomic, metabolomic and genomic analyses of *Senna occidentalis*. In *in-vitro* assay, chalcone synthase-like (SocCHS-L2) of *Senna occidentalis* was identified to produce atrochrysone carboxylic acid and endocrocin anthrone through LC-MS/MS analysis. Additionally, through X-ray crystallography, we successfully got the crystal structure of free-form (2.1 Å) and substrate-bound-form (2.2 Å) of SocCHS-L2. Structural pairwise analysis revealed that SocCHS-L2 shares high similarity with *Tr*ADS (*Tetradium ruticarpum*, PDB ID: 5WX3) and *Fh*CHS1 (*Freesia hybrid cultivar*, PDB ID: 4WUM), with approximately 56% sequence identity. SocCHS-L2 was conserved with active-site traid, Cys-His-Asn, but it shows different residual compositions. Compared with *Tr*ADS structure, SocCHS-L2 was replaced with Ile136 and Gln262, and the direction of Tyr264 side chain seems to be un-rotatable through formation of hydrogen bond with His211, only found in SocCHS-L2. The volume analysis indicates that the condensation of SocCHS-L2 has 274.1 $Å^3$, whereas *Tr*ADS has un undetectable pocket size. Additionally, SocCHS-L2 seems to be different shape of condensation pocket with octaketide synthase (AaOKS, PDB ID: 7DTQ) from *Aloe arborescens*. AaOKS catalyze the condensation of eight malonyl-CoA units to produce octaketo-beta-acyl chain, same as SocCHS-L2, but it produced different product, SEK4 and SEK4b. Although the internal cavity shapes of SocCHS-L2 and AaOKS provide sufficient space to polymerize the same intermediates, the variations in the internal residues and spatial configuration explain the production of different final products.

Keywords: Anthraquinone, Type III polyketide synthase, Octaketide synthase

1. Introduction

Anthraquinones are a type of polycyclic compound that feature a quinonoid structure and are found in a diverse array of organisms, including bacteria, fungi, algae, insects, and plants [1]. Chemically, anthraquinone are derived from a 9,10-antracene structure that consists of three benzene rings labeled as A, B, and C [Duval et al., 2016; Lu et al., 2013]. The chemical and structural diversity of anthraquinones is determined by the substitution of the hydrogen atoms in their core structure with various functional groups such as -OH, $-CH_3$, $-OCH_3$, $-CH_2OH$, -CHO, and -COOH. This substitution pattern forms one of the most significant groups of anthraquinone compounds [2]. For example, numerous derivatives are formed depending on the presence of hydroxyl, methoxy, methyl radicals, hydroxymethyl, and glycoside groups on the A and C rings.

Anthraquinones are abundant in plants from families such as Polygonaceae, Rubiaceae, Rhamnaceae, and Leguminosae. But, in plant anthraquinone biosynthetic process, there is no definitive clue as to how to biosynthesis the anthraquinone. Previous research suggests that anthraquinones can be synthesized through these pathways: the o-succinylbenzoate pathway and polyketide pathway. However, studies identifying the key enzyme genes involved are still insufficient, and there is a lack of direct and compelling evidence to fully elucidate these biosynthetic mechanisms. This gap highlights the need for further investigative efforts to understand the genetic and enzymatic underpinnings of anthraquinone biosynthesis, which could significantly enhance our knowledge of plant secondary metabolism and its applications in various industries.

In previous research [3], we confirmed through *in-vitro* reactions that a chalcone synthase-like enzyme, a class of Type III Polyketide Synthase (PKS), produces atrochrysone carboxylic acid and endocrocin anthrone, which are precursors of emodin. In this study, we aim to identify chalcone synthase-like enzymes involved in the anthraquinone biosynthetic pathway in *Senna occidentalis*, a plant of the same genus as *Senna tora*. By analyzing the

activity and structure of this enzyme, we seek to provide a deep understanding and insight into the biosynthesis of anthraquinone compounds by plant.

2. Materials and Methods

2.1. Bacterial over-expression and protein purification

For over-expression, the recombinant strains of Senna genus CHS-like genes were cultured in 3 ml of LB containing 100 ㎍/ml of ampicillin at 37 ℃ for 6 hours, and well-grown cells were transferred to 100 ml in 250 ml flask. When the optical density of the cultures at 600 nm reached 0.3-0.7, 0.5 mM IPTG was added into the cultures to induce the recombinant protein expression. After an incubation at 20 ℃ for 36-48 hours, the cells were harvested by centrifugation at 3,500 rpm for 15 min at 4 ℃. Harvested cells was washed twice times using 50 mM potassium phosphate buffer (pH 7.4) and resuspended with 10 ml of 50 mM potassium phosphate buffer (pH 7.4). The samples were disrupted by sonication. The homogenate was centrifuged at 13,500 rpm for 15 min at 4 ℃ to be isolated from insoluble fraction. The expression of proteins was analyzed by 12 % sodium dodecyl sulfate polyacrylamide gel electrophoresis (SDS-PAGE).

The supernatant was mixed and keep on a shaker with Talon resin (Takara, Japan) for about 1 hour following protocol of Immobilized Metal Affinity Chromatography (IMAC) method. After the sample was applied to the column, non-specifically bound proteins were removed with four- and six-times volumes of equilibrium buffer by 50 mM potassium phosphate buffer (pH 7.4) with/without 10 mM imidazole, respectively. And then, the bound protein was eluted with two times volumes of potassium phosphate buffer (pH 7.4) containing 200 mM imidazole. All samples were washed and concentrated by Amicon Ultra Centirfugal Filter (50 kDa MWCO) and were measured by the Broadford method. All the purified proteins were also analyzed by 15% SDS-PAGE.

2.2. Enzymatic assay

The purified proteins of CHS-like gene were prepared to verify the function of polyketide synthesis. The standard reaction mixture consisted of 0.5mM starter -CoA, 1mM malonyl-CoA, 200 ㎍ of the purified recombinant *Senna* genus CHS-like proteins and 50 mM phosphate buffer (pH 7.4) in a total volume of 250 ㎕. The control reaction was conducted in a similar manner including *Senna* CHS-L and boiled protein. The reactions were incubated at 30 ℃ for 4 hours. Afterward, the reaction products were extracted by adding twice the total volume of ethyl acetate and shaking at 200 rpm for about 1 min. To separate the extract layer, centrifugation is performed at 13,000 rpm, and only the top layer is transferred to another tube. After evaporating all the upper solution using decompression concentration, dissolve the extract by adding methanol, filter it using a 0.22 μm filter, and use it for UPLC and MS analysis.

The reaction products were analyzed and quantified by Thermo UltiMate 3000 with Xselect HSS T3 (2.1 x 150 mm, 2.5 ㎛) connected to a PDA detector and electrospray ionization (ESI) mass source combined with Thermo U300-LTQ XL ion trap mass spectrometer (Thermo Scientific, USA). The flow rate is 0.3 mL/min and mobile phases A and B contained 0.1 % formic acid, water, and acetonitrile, respectively. Gradient elution was performed as follows: 5-100% B for 0-15 min with a linear gradient, followed by 5 min of 100% of B. The MS/MS system was operated in ESI mode. Mass spectra were acquired in the m/z range of 10-2,000 by applying three micro scans and a maximum ion injection time of 100ms. Data-dependent mass spectrometry experiments were controlled using mass control plug-in provided in MestReNova software.

2.3. Crystallization and structure determination

Recombinant proteins with approximately 95% purity were employed to generate protein crystals under various crystallization conditions using the sitting-drop vapor diffusion method at 22°C. Initial crystallization conditions were further optimized to enhance crystal size and quality by adjusting specific parameters such as temperature, pH, and salt concentration. The optimal crystals were achieved by incorporating 0.08 M Tris-HCl (pH 8.5), 0.16 M $MgCl_2$, 24% (w/v) PEG 4000, and 20% (v/v) glycerol into the reservoir solution, with crystal formation observed after 2 days using the sitting-drop vapor diffusion technique. These protein crystals were then mounted in a stream of cold nitrogen gas to prevent thermal damage during data collection on the BL-5C beamline at the Po-

hang Accelerator Laboratory (Pohang, Korea). Data processing was performed using XDS software [4]. For complex formation with CoA, a soaking method was employed, where the crystals were incubated with CoA dissolved in the crystallization buffer for 20 min at 22°C.

The phases of CHS-like protein coordinates were determined using the molecular replacement method with the MOLREP program from the CCP4i suite. The initial search model was based on the structure predicted by Alphafold [5]. Following the initial round of refinement, difference density maps enabled the correct orientation of side chains to be incorporated into each structural model. The quality of the initial coordinates was further enhanced through iterative rebuilding and refinement using Coot [Emsley et al., 2010], REFMAC5 [6], and phenix.refine [7]. Final coordinates were validated for quality using MolProbity [8]. Structural representations were generated using PyMOL [9].

3. Results

3.1. Over-expression and protein purification of Chalcone synthase in Senna occidentalis

The full-length cDNA sequences of the CHS-L gene from *Senna occidentalis* were obtained through the genome information of *S. occidentalis*. Experiments were conducted according to PCR applications to obtain novel designed cDNA encoding CHS-L, and the cDNAs were expressed using an *E. coli* heterologous expression system following general experimental methods. A total of three genes were used in these experiments. Except for SocCHS-L1, the other two genes were easily expressed to obtain soluble protein, and the proteins, approximately 60kDa in size (Figure 1A and 1B), were purified using IMAC (Immobilized Metal Chelate Affinity Chromatography) application (Figure 1(c)).

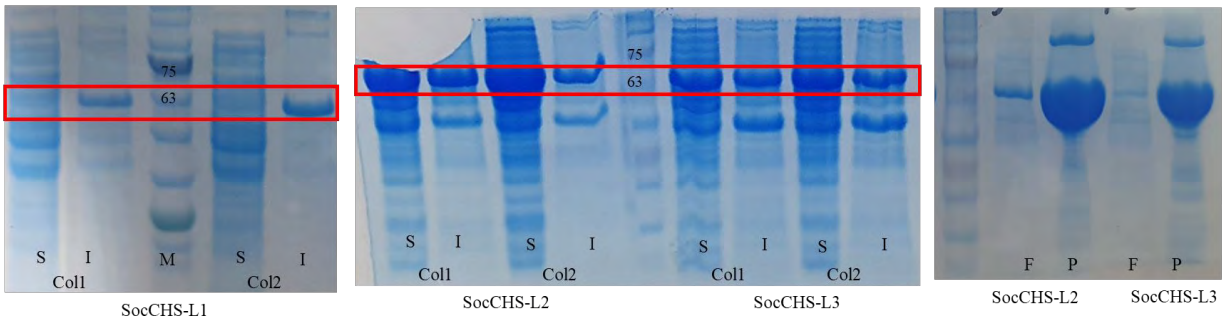

Figure 1. SDS-PAGE of *Senna occidentalis* CHS-L proteins: (a) Expression results of SocCHS-L1; (b) Expression results of SocCHS-L2 and SocCHS-L3; (c) Purification results of SocCHS-L2 and SocCHS-L3 (S: Soluble fraction, I: Insoluble fraction, M: Marker, F: soluble fraction, P: purified fraction).

3.2. Enzymatic assay and LC-ESI-MS/MS analysis

Type III polyketide synthase (PKS) usually uses aliphatic type CoA and aromatic type CoA as starter substrates and repeatedly polymerizes short-chain extender units such as malonyl-CoA to form intermediates. The start substrates and the number of polymerized units vary depending on the function and structure of type III PKS, which is why type III PKS produces a variety of products.

Acetyl-CoA and *p*-coumaroyl-CoA were used as starter units, and malonyl-CoA was used as the extender unit to react with SocCHS-L2. The reaction products were analyzed using the LC-ESI-MS/MS technique. The analysis revealed a product with an m/z value of 272, presumed to be p-coumaroyltriacetate lactone (CTAL), at approximately 8.91 minutes in liquid chromatograph of the sample using p-coumaroyl-CoA. And products with m/z value of 317 at 7.89 minutes and 299 at 9.22 minutes were observed in liquid chromatograph of the sample using acetyl-CoA (Figure 2). To confirm the exact structure of products, emodin and aloe-emodin, sharing the same anthraquinone scaffold, were analyzed under the same LC-ESI-MS/MS conditions. The MS/MS fragmentation pattern comparison confirmed that the products were atrochrysone carboxylic acid and endocorcin anthrone at 7.88 and 9.22 minutes, respectively.

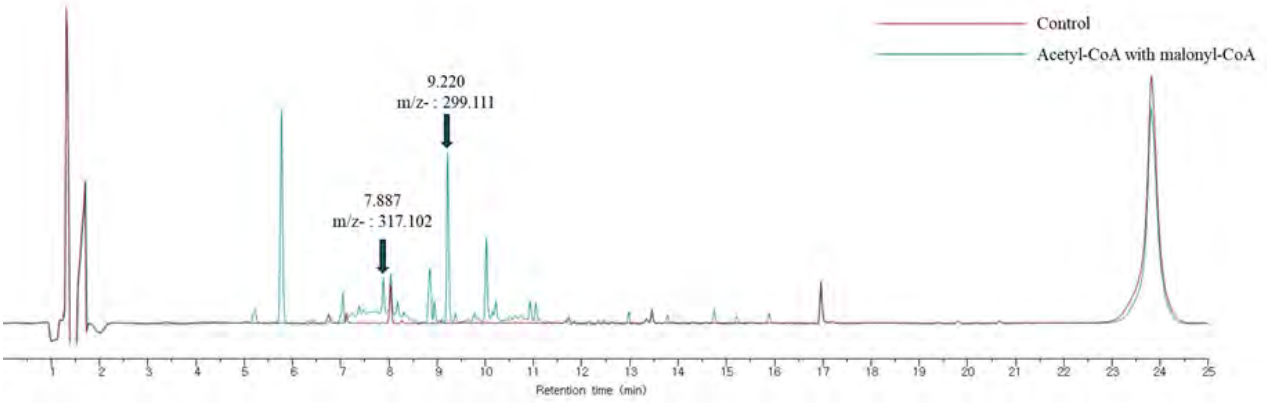

Figure 2. Liquid chromatogram of control (red) and reaction mixture of SocCHS-L2 (cyan).

3.3. Structure determination and comparison of SocCHS-L2 structure to other type III PKS

The crystal structure of SocCHS-L2 was determined by molecular replacement (MR) using homology modeling of AlphaFold [5]. From refinement, the crystal structure of SocCHS-L2 was determined at 2.1 Å. The structure of SocCHS-L2 is like that of homologous structures found in other species in terms of structural folds (Figure 3), with a unique structural topology that includes a specific upper domain '$\alpha\beta\alpha\beta\alpha$' (ketosynthase domain) [10], that is conserved in all structural homologs. The active site domain is composed of two twisted β-sheets surrounded by helices and separated by two long helices, H8 and H15. The CoA binding domain is composed of six helices (H1-H4, H9, and H10) and two strands (S9 and S10). The SocCHS-L2 protein is found in a homodimer state in solution, as indicated by SEC analysis. The dimerization interaction is primarily mediated by loops between S4 and H7, S5, H8, and S9, with a large interface area of 2169.2 Å^2.

The BlastP search using the SocCHS-L2 sequence against the Protein Data Bank (PDB) identified the top 5 analogues displaying high sequence similarity with both SocCHS-L2, each exhibiting over 50% similarity (Table 1). The results highlight that these homologues share similarities, particularly in the residues that constitute the active site and are highly identical to one another. However, specific distinctions in SocCHS-L2 merit particular attention. For instance, TrADS, the closest orthologue identified in the PDB, features a critical Tyr259 located adjacent to the active site triad, which plays a pivotal role in determining the size of the condensation pocket (Figure 4). Comparable confirmations of aromatic residues are observed in other homologues. Notably, in SocCHS-L2, the corresponding residue, Tyr264, is angled differently, interacting with water molecules and His211. This orientation of the Tyr264 side chain appears to be fixed, given that the hydroxyl group of Tyr264 forms a stable hydrogen bond with His211 – a unique interaction found only in SocCHS-Ls. Additionally, the residues Met130 and Met257 in TrADS are substituted with Ile136 and Gln262 in SocCHS-L2, respectively. These substitutions contribute to a larger condensation pocket in SocCHS-L2, measured at 274.1 Å^3, compared to the undetectable pocket size in TrADS. Consequently, SocCHS-L2 is likely capable of facilitating reactions with multiple molecules of malonyl-CoA, leading to larger product sizes than those observed with TrADS.

Furthermore, a comparison of the pocket structure among SocCHS-L2, FhCHS1, and OsPKS revealed distinct conformations of the condensation pocket. While FhCHS1 and OsPKS share a similar pocket shape, positioned between the central two helices and the twisted β-sheets, SocCHS-L2 features a lengthy tunnel-like pocket directed towards the dimerization interface. A key distinguishing residue, Trp341, alters the shape and orientation of the pocket in these proteins. In SocCHS-L2, this bulky residue is stabilized by a T-shaped π-stacking interaction with Phe214 and is uniquely present only in SocCHS-L2 and TrADS. This suggests a unique mechanism in SocCHS-L2 for substrate condensation, distinguishing it from other homologues.

Octaketide synthase (ArOKS) derived from *Aloe arborescens* is a type III PKS known to produce octaketide as intermediates. We noted that SocCHS-L2 produces octaketides as intermediates similar to ArOKS and conducted a structural comparison analysis (Figure 5). We found that SocCHS-L2 has a total internal cavity volume of 411.25 Å^3 and a total surface area of 389.33 Å^2, whereas ArOKS has an internal cavity volume and total surface area of 485.78 Å^3 and 467.99 Å^2, respectively. Additionally, a comparison of the condensation pocket structures of SocCHS-L2 and ArOKS revealed that the two enzymes have different structural forms. ArOKS has a pocket formed

between two α-helices on the side of a twisted β-sheet, while SocCHS-L2 features a long tunnel-shaped pocket directed towards the dimerization interface.

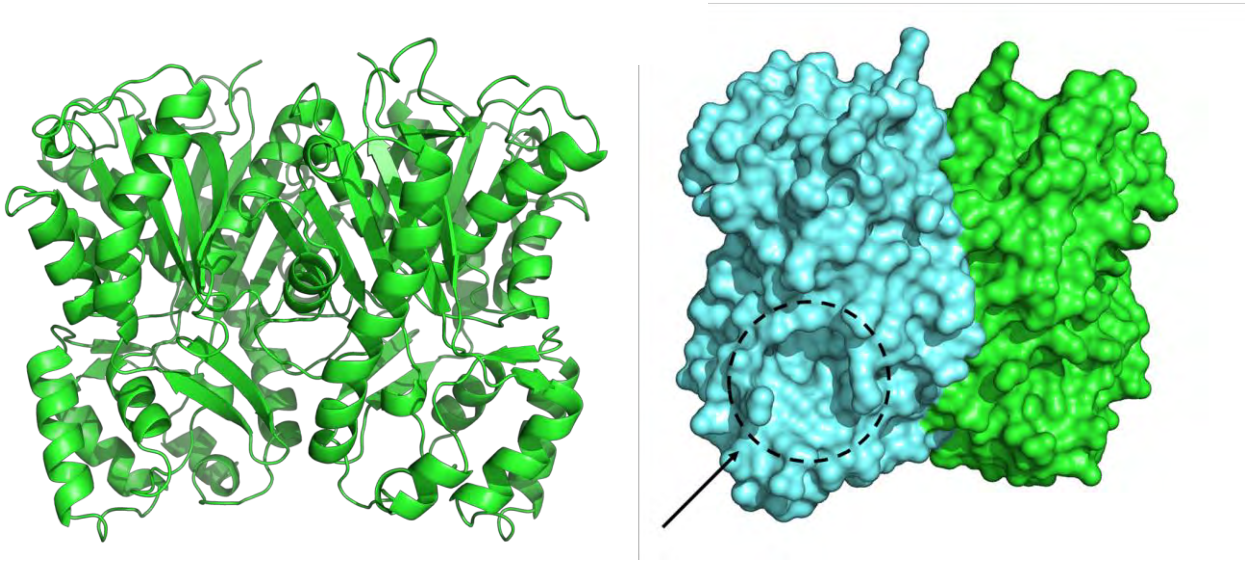

(a) (b)

Figure 3. Overall structure of SocCHS-L2: (a) Overall views of dimeric structure of SocCHS-L2 represented with carbon; (b) Overall surface views of dimeric structure of SocCHS-L2.

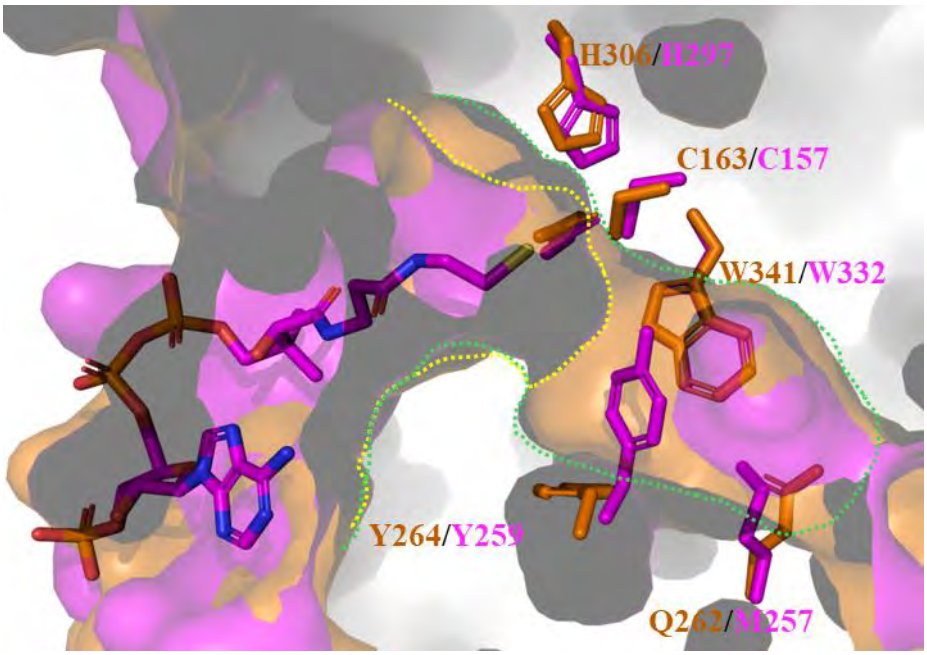

Figure 4. Comparison of the active site with other homologues: The structure of SocCHS-L2 (orange) is superimposed with TrADS from *Tetradium ruticarpum* (magenta, PDB ID: 5WX3).

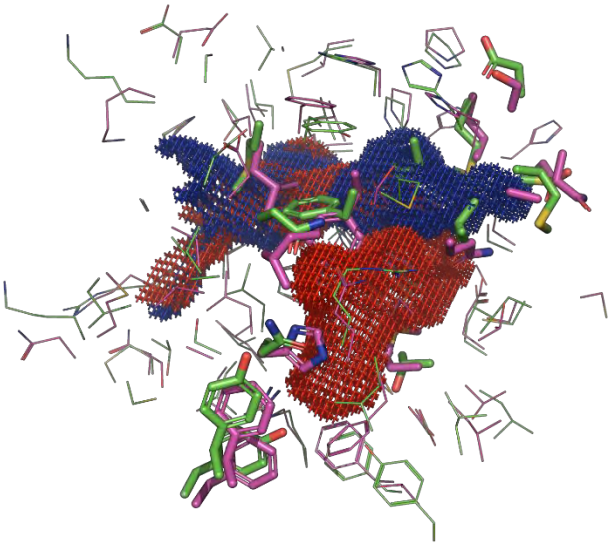

Figure 5. Comparison of internal cavity with SocCHS-L2 (Blue) and ArOKS (red): The OKS structure (purple) is super posed with SocCHS-L2 (green).

Table 1. The BlastP search result using the SocCHS-L2 sequence against the Protein Data Bank (PDB)

Rank	Description	Species	Query coverage	Per. Ident	Acc Len	PDB ID	Accession (uniprot)
1	Tr*ADS*	*Tetradiumruticarpum*	*95%*	*55.94*	*396*	*5WX3*	*A0A1W7GKH6*
2	Fh*CHS1*	*Freesia hybrid cultivar*	*95%*	*55.79*	*389*	*4WUM*	*G3FJ87*
3	Os*PKS*	*Oryza sativa Indica Group*	*96%*	*54.83*	*398*	*4YJY*	*A2ZEX7*
4	At*CHS*	*Arabidopsis thaliana*	*95%*	*55.91*	*395*	*6DXB*	*P13114*
5	Md*CHS2*	*Malus domestica*	*95%*	*54.07*	*390*	*5UC5*	*K9MUA0*

4. Discussion

Octaketide synthase (OKS) derived from *Hypericum perforatum* and *Aloe arborescens* is known as a type III PKS that produces octaketides in plants. Some researchers have speculated that these enzymes are involved in the anthraquinone biosynthetic pathway. However, both enzymes have only been shown to produce octaketides like SEK4 and SEK4b *in-vitro*, with no direct evidence of their involvement in anthraquinone biosynthesis.

A structural comparison between ArOKS and SocCHS-L2 revealed that, unlike other type III PKSs, both enzymes possess large internal pockets. Studies on ArOKS mutants have shown that these large pockets can accommodate more acyl units, facilitating the formation of larger condensation products. Despite this similarity, there are notable differences in the shapes of their internal pockets. ArOKS features a bent, large condensation pocket, whereas SocCHS-L2 has a long, tunnel-shaped pocket. This difference suggests that, while both enzymes can condense octaketide intermediates, the shape of their pockets may influence the intramolecular cyclization stage.

Through *in-vitro* reactions, we confirmed that SocCHS-L2 forms atrochrysone carboxylic acid and endocrocin anthrone, which are precursors to emodin. Analysis of the crystal structure of SocCHS-L2 revealed not only a sufficiently large internal pocket to form octaketides, but also a tunnel-shaped pocket conductive to forming emodin precursors. This study provides deep insights into type III PKSs and enhances our understanding of the critical enzymes involved in the biosynthesis of anthraquinone compounds in plants.

References

1. Malik, E. M. and Müller, C. E. Anthraquinones as Pharmacological Tools and Drugs. *Medicinal research reviews 36*(4), 705–748 (2016). https://doi.org/10.1002/med.21391
2. Fouillaud, M., Venkatachalam, M., Girard-Valenciennes, E., Caro, Y. and Dufossé, L. Anthraquinones and Derivatives from Marine-Derived Fungi: Structural Diversity and Selected Biological Activities. *Marine drugs 14*(4), 64 (2016). https://doi.org/10.3390/md14040064
3. Kang, S. H. et al. Genome-enabled discovery of anthraquinone biosynthesis in Senna tora. *Nature communications 11*(1), 5875 (2020).
4. Kabsch, W. eds. *Acta Crystallographica Section D: Biological Crystallography 66*(2), 125-132 (2010).
5. Jumper, J. et al. Highly accurate protein structure prediction with AlphaFold. *Nature 596*(7873), 583-589 (2021).
6. Murshudov, G. N. et al. REFMAC5 for the refinement of macromolecular crystal structures. *Acta Crystallographica Section D: Biological Crystallography 67*(4), 355-367 (2011).
7. Liebschner, D. et al. Macromolecular structure determination using X-rays, neutrons and electrons: recent developments in Phenix. *Acta Crystallographica Section D: Structural Biology 75*(10), 861-877 (2019).
8. Williams, C. J. et al. MolProbity: More and better reference data for improved all-atom structure validation. *Protein Sci 27*, 293-315 (2018).
9. DeLano, W. L. Pymol: An open-source molecular graphics tool. *CCP4 Newsl. Protein Crystallogr 40*(1), 82-92 (2002).
10. Bräuer, A. et al. Structural snapshots of the minimal PKS system responsible for octaketide biosynthesis. *Nature chemistry 12*(8), 755–763 (2020). https://doi.org/10.1038/s41557-020-0491-7

5th International Conference of Hyojeong Academy
International Joint Conference 2025

Exploring Potential of Antarctic Moss: Unveiling Its Scientific and Biotechnological Applications

Hirotake Yamaguchi, Ryoichi Yamada, Kristina Lama and Tae-Jin Oh*

Department of Life Science and Biochemical Engineering, Sun Moon University, Asan 31460, Korea
*Correspondence: tjoh3782@sunmoon.ac.kr

Abstract: Antarctic mosses represent an untapped treasure trove of bioactive compounds with potential applications in a variety of fields. The aim of this study was to evaluate the bioactivity of extracts from Antarctic mosses using a combination of metabolomic and *in silico* analyses to identify active compounds. In the first bioactivity assay, significant antioxidant and enzyme inhibitory activities were observed in selected moss extracts. The extract that exhibited the highest biological activity was subjected to comprehensive metabolomic profiling using LC-MS/MS to identify the major secondary metabolites. Molecular docking studies were performed on these metabolites to predict their binding affinities and interactions with target proteins to elucidate potential mechanisms underlying the observed biological activities. These findings suggest that Antarctic mosses contain unique metabolites with promising biological activities and provide insight into adaptive mechanisms in extreme environments. This study highlights the potential pharmaceutical and biotechnological applications of compounds derived from the moss and paves the way for further *in vitro* and in vivo investigations to validate their efficacy.

Keywords: Antarctic moss, Metabolomics profiling, molecular docking.

1. Introduction

Antarctic mosses are one of the major plant groups that grow in extreme polar environments and have evolved sophisticated biochemical mechanisms to adapt to the harsh environment of sub-zero temperatures, high levels of UV radiation, strong winds, and limited nutrients [1]. However, despite the ecological importance and biochemical adaptations of Antarctic mosses, the study of their secondary metabolites is largely unexplored [2].

Unlocking the potential of these metabolites will provide insights into their ecological roles and opportunities for health and medical applications, particularly in the areas of antioxidant activity, enzyme inhibition, and anti-inflammatory effects.

Advances in metabolomics, coupled with computational techniques such as molecular docking, have revolutionized the discovery and characterization of bioactive compounds. Metabolomics provides a comprehensive platform for analyzing the chemical profiles of complex biological samples, enabling the identification of metabolites with potential biological activity [3]. Molecular docking, on the other hand, enables the prediction of interactions between bioactive compounds and specific target proteins and the elucidation of potential mechanisms of action [4].

In this study, we focus on Antarctic mosses as a source of bioactive compounds and aim to fill the gap in our knowledge of their chemical composition and bioactivity. By integrating bioactivity assessment, metabolomics analysis, and molecular docking, we will identify active compounds and predict their roles. This research will not only highlight the pharmaceutical potential of mosses but will also contribute to our understanding of how plants biochemically adapt to extreme environments.

2. Materials and Methods

2.1. Sample Collection and Extraction

Warnstorfia fontinaliopsis was acquired from the Polar Natural Products Chemistry Laboratory at the Korean Polar Research Institute. The samples were dried and pulverized prior to use. One gram of the powdered *Warnstorfia fontinaliopsis* was added to a flask containing 100 mL of methanol, stirred at ambient temperature in the dark for three hours, and subsequently extracted.

2.2. Metabolite Profiling

Metabolite profiling of An-MS1 was conducted using untargeted LC-MS/MS analysis. The resulting MS/MS data were processed via the GNPS platform [5] to generate a molecular network, enabling metabolite identification through fragmentation pattern analysis.

2.3. In silico Pharmacological Analysis

2.3.1. Molecular docking

Molecular docking was carried out using AutoDock Vina [6] to assess interactions between identified metabolites and key enzymes associated with obesity (Human pancreatic lipase). Enzyme crystal structures (1LPB) were retrieved from the Protein Data Bank (PDB). Docking protocols included preparing protein and ligand structures, defining docking grids, and conducting docking simulations. Binding affinities and interaction patterns of metabolites were analyzed to determine potential enzyme inhibitors.

2.3.2. Swiss ADME analysis

The pharmacokinetic properties of identified metabolites were assessed with the SwissADME tool [7]. Factors like absorption, distribution, metabolism, and excretion (ADME) were examined to predict drug-likeness and compound bioavailability.

3. Results

3.1. In vitro results

Bioactive compounds from *W. fontinaliopsis* were extracted using four solvents of varying polarity: methanol (M), acetone (A), ethyl acetate (EA), and water (W). Limited moss samples (1 g each) were used per extraction. Extracts were dried, quantified, and evaluated for antioxidant activities (ABTS, DPPH, and FRAP assays) and lipase inhibition (Fig. 1). ABTS assay: At 1 mg/mL, activity was observed in M (9.1%), A (10.5%), and W (10.5%), but not in EA. Ascorbic acid (positive control) showed 49% activity at 125 mM. DPPH assay: A (2% at 1 mg/mL) and B (5% at 0.25 mg/mL) exhibited activity; no activity was observed in EA or W. Ascorbic acid showed 71% activity at 250 mM. FRAP assay: Results were compared to ascorbic acid concentrations (M, 94 mM; A, 241 mM; EA, 370 mM; and W, 39 mM at 1 mg/mL). Lipase inhibition: At 2 mg/mL, activity was observed in M (11%) and W (6.6%), but not in A or EA. Orlistat (positive control) showed 75% inhibition at 10 μM.

3.2. LC-MS/MS Profiling of Methanol Extract from Warnstorfia fontinaliopsis

We conducted an untargeted metabolomics investigation on the methanol extract of *Warnstorfia fontinaliopsis*. This approach is efficient for analyzing intricate mixtures, offering valuable information about the molecular profile of the sample. LC-MS/MS's high sensitivity detects compounds in trace amounts, addressing sample volume limitations. The methanol extract, showing lipase inhibition, was examined. A molecular network was constructed from the MS/MS data, consisting of 881 precursor ions. The study revealed 30 clusters and 169 individual nodes, indicating diverse compound families. Twelve metabolites, including DGTS 16:0, sucrose, hyocholic acid, and pheophorbide A, were confidently identified (Table 1). These metabolites are associated with cellular protection, such as resistance to dehydration and UV-induced oxidative damage. Functional groups like hydroxyl, carboxyl, and carbonyl improve solubility and facilitate enzyme interactions, emphasizing their pharmaceutical application potential.

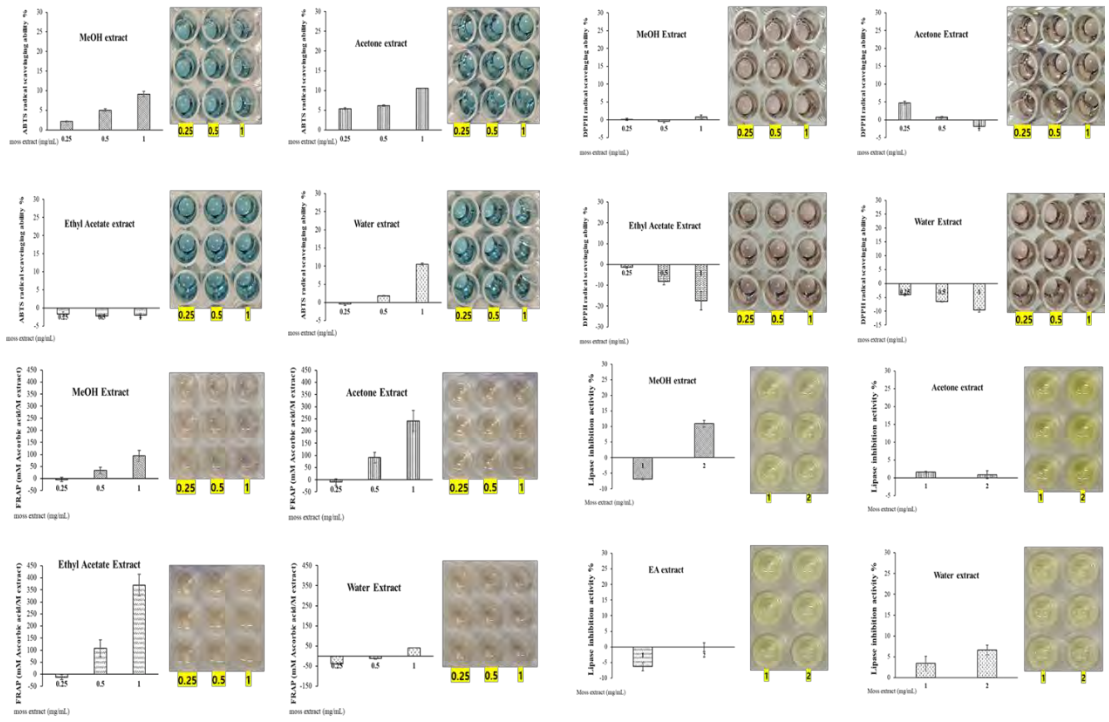

Figure 1. *In vitro* assay results.

Table 1. Compounds identified in *W. fontinaliopsis* extracts

Compounds	MassDiff (Da)	LibMZ	Cosine	Chemical formula	Retention time (min)
DGTS 16:0	0.001	474.38	0.8	C44H79NO7	14.59
1-Linoleoyl-sn-glycero-3-phosphocholine	0.001	520.34	0.88	C26H50NO7P	8.37
Sucrose	0	325.11	0.98	C12H22O11	0.59
SCHEMBL26641914	0.001	518.33	0.88	$C26H49NO7P^+$	7.98
lysophosphatidylcholine(16:0)	0	496.34	0.96	C24H50NO7P	8.68
hyocholic acid	0	158.15	0.96	C24H40O5	6.95
lysoPC(18:3(6Z,9Z,12Z))	0.003	518.33	0.88	C26H48NO7P	7.86
melezitose	0.001	522.2	0.96	C18H32O16	0.59
Ncgc00385962-01_C16H24O3_	0.003	247.17	0.91	C16H24O3	14.71
1-(9Z,12Z-octadecadienoyl)-sn-glycero-3-phosphocholine	0.002	520.34	0.87	C26H50NO7P	8.25
lactulose	0.001	360.15	0.87	C12H22O11	0.59
pheophorbide A	0.006	593.27	0.85	C35H36N4O5	9.9

3.3. Molecular docking with lipase

Molecular docking was conducted to examine protein-ligand interactions and identify metabolites responsible for lipase inhibition from 12 compounds detected by LC-MS/MS in *W. fontinaliopsis*. Orlistat, a well-known lipase inhibitor, was used as a reference. Binding affinities, hydrogen bonding interactions, and involved amino acids were evaluated. Six metabolites (sucrose, hyocholic acid, melezitose, Ncgc00385962-01_C16H24O3_, lactulose, and pheophorbide A) showed stronger binding than orlistat (-6.5 kcal/mol, His263) (Table 2). Hyocholic acid and pheophorbide A had the highest binding energies (-8.4 and -9.3 kcal/mol, respectively).

Table 2. Molecular docking results for detected compounds

Compounds	1LPB(kcal/mol)	Amino acids involved in hydrogen bonding	Distance/Å	Number of hydrogen bond
DGTS 16:0	-5.4	-	-	-
1-Linoleoyl-sn-glycero-3-phosphocholine	-5.9	Arg256	2.6	1
sucrose	-6.9	Asn212, Glu233, Asp205, Gly214, Asn262, Asp257, Cys237, Phe258	2.3, 3.61, 1.82, 3.7, 2.98, 2.15, 2.86, 2.18	8
SCHEMBL26641914	-6.5	Phe77, Arg256	2.36, 2.59	2
lysophosphatidylcholine(16:0)	-5.4	Arg256	3.02	1
hyocholic acid	-8.4	Phe77, His151, Ser152	3.03, 2.39, 3.6	3
lysoPC(18:3(6Z,9Z,12Z))	-6.1	Cys181, Pro180	2.29, 3.52	2
melezitose	-6.6	Glu233, Ala259, Phe258, Leu213, Asp205, Gln244, Cys261, Phe215	2.38, 2.4, 2.58, 2.85, 2.34, 2.41, 2.34, 2.91	7
Ncgc00385962-01 C16H24O3	-8.3	-	-	-
1-(9Z,12Z-octadecadienoyl)-sn-glycero-3-phosphocholine	-5.9	Arg256	2.86	1
lactulose	-7.4	Phe258, Asp257, Gln244, Glu233, Leu213, Asp205	2.28, 2.56, 2.78, 3.03, 2.39, 2.55	6
pheophorbide A	-9.3	Arg256	2.59	1
orlistat	-6.5	His263	2.78	1

3.4. Computational pharmacokinetics analysis

Characterizing the ADME (absorption, distribution, metabolism, and excretion) profile is crucial for assessing potential drug candidates. Swiss ADME is a computational tool that predicts ADME properties based on a compound's structure, solubility, bioavailability, and other physicochemical factors. ESOL evaluates solubility in intestinal fluids, with lower values being less favorable. GIA represents intestinal absorption, and BBB permeability examines the compound's ability to pass through the blood-brain barrier, though it's not vital for lipase inhibitors targeting the pancreas or intestine. P-glycoprotein (P-gp) controls efflux, which may limit central nervous system penetration. CYP enzymes are central to drug metabolism, and their inhibition can cause toxic accumulation. The bioavailability score predicts the likelihood of oral absorption.

For most compounds, bioavailability scores ranged from 0.55–0.56, indicating moderate absorption potential in vivo. However, sucrose, melezitose, and lactulose had lower values (0.17), indicating difficulty in passive diffusion due to their hydrophilic properties (Table 3). Compounds like pheophorbide A and hyocholic acid showed minimal inhibition of critical CYP enzymes, reducing the risk of drug-drug interactions. Some compounds, such as DGTS 16:0 and lysophosphatidylcholine, were P-gp substrates, limiting absorption. SCHEMBL26641914 and hyocholic acid exhibited BBB permeability, suggesting potential for central nervous system applications. Hydrophobic compounds, such as DGTS 16:0 and pheophorbide A, may face solubility issues, but these can be addressed with optimized formulations.

Table 3. Swiss ADME profiling of detected compounds

Compound name	Bioavailability score	CYP1A2 inhibitor	CYP3A4 inhibitor	P-gp substrate	BBB permeant	GIA	ESOL(LogS)
DGTS 16:0	0.55	No	No	Yes	No	Low	-10.26
1-Linoleoyl-sn-glycero-3-phosphocholine	0.55	No	No	Yes	No	Low	-4.7
sucrose	0.17	No	No	Yes	No	Low	0.7
SCHEMBL26641914	0.55	No	Yes	Yes	NO	High	-3.29
lysophosphatidylcholine(16:0)	0.55	No	Yes	Yes	No	Low	-4.88
hyocholic acid	0.56	No	No	Yes	No	High	-3.87
lysoPC(18:3(6Z,9Z,12Z))	0.55	No	No	Yes	No	Low	-4.31
melezitose	0.17	No	No	Yes	No	Low	1.25
Ncgc00385962-01 C16H24O3	0.55	No	Yes	No	Yes	High	-3.95
1-(9Z,12Z-octadecadienoyl)-sn-glycero-3-phosphocholine	0.55	No	Yes	Yes	No	Low	-4.69
lactulose	0.17	No	No	Yes	No	Low	1.05
pheophorbide A	0.56	No	No	Yes	No	Low	-4.79
orlistat	0.55	No	No	Yes	No	Low	-7.6

4. Discussion

The methanol extract of *Warnstorfia fontinaliopsis* exhibited significant lipase inhibition and antioxidant activity, suggesting its potential utility in combating obesity and oxidative stress-related conditions. Through LC-MS/MS analysis, 12 compounds were identified, including sucrose, pheophorbide A, and hyocholic acid, many of which have been associated with protective roles under extreme environmental conditions. For example, sugars like sucrose and lactulose are known to function as cryoprotectants, while lipids such as hyocholic acid contribute to membrane fluidity and repair at low temperatures.

Molecular docking studies revealed that several compounds, notably pheophorbide A and hyocholic acid, exhibited stronger binding affinities to lipase than the standard inhibitor orlistat. The strong interactions, characterized by binding energies of -8.4 to -9.3 kcal/mol, suggest that these compounds may act as effective inhibitors.

Pharmacokinetic analysis using SwissADME provided further insights into the potential therapeutic applications of the identified compounds. Importantly, compounds like pheophorbide A and hyocholic acid showed minimal inhibition of cytochrome P450 enzymes, reducing the likelihood of adverse drug-drug interactions. The presence of compounds with cryoprotective and antioxidative properties underscores the role of secondary metabolites in *Warnstorfia fontinaliopsis*'s adaptation to Antarctica's harsh conditions.

Additionally, the discovery of lipase inhibition activity in moss extracts represents a novel finding, expanding the known functional diversity of Antarctic mosses. These findings highlight the untapped potential of Antarctic mosses as sources of bioactive compounds for pharmaceutical and nutraceutical applications. Future studies could focus on scaling up extraction, improving compound bioavailability, and exploring the molecular mechanisms underlying the observed bioactivities. Moreover, advanced techniques like genome-scale metabolic modeling and machine learning could provide deeper insights into the metabolic networks driving these adaptations.

5. Conclusions

This study explores the biological and chemical potential of *Warnstorfia fontinaliopsis*, an Antarctic moss adapted to extreme environments. Methanol extracts showed significant lipase inhibitory and antioxidant activity, indicating their potential for the management of obesity and oxidative stress LC-MS/MS analysis identified 12 bioactive compounds, including pheoforbide A and hyocholic acid, which showed stronger than orlistat in molecular docking studies They showed stronger lipase binding affinity than orlistat in molecular docking studies. Pharmacokinetic analysis suggested moderate bioavailability, but formulation modifications were needed for several metabolites. The findings highlight the unique adaptations of moss, such as cryoprotection

and antioxidants, and their potential for pharmaceutical applications, which require further investigation and optimization.

Author Contributions: Conceptualization, H.Y., R.Y., K.L. and T.-J.O.; methodology, H.Y., R.Y., K.L. ; formal analysis, H.Y., R.Y. and K.L.; investigation, H.Y., R.Y. and K.L. ; resources, T.-J.O.; writing-original draft preparation, H.Y., R.Y., K.L. and T.-J.O.; writ-ing-review and editing, H.Y., R.Y., K.L. and T.-J.O.; supervision, T.-J.O.; project administration, T.-J.O.; funding acquisition, T.-J.O. All authors have read and agreed to the published version of the manuscript.

Fundings: This research was supported by the project titled "Development of potential antibiotic compounds using polar organism resources (20200610)", funded by the Ministry of Oceans and Fisheries, Korea.

Data Availability Statement: Not applicable.

Conflicts of Interest: The authors declare no conflict of interest.

References

1. Zhang L et al. Extreme environmental adaptation mechanisms of Antarctic bryophytes are mainly the activation of antioxidants, secondary metabolites and photosynthetic pathways. *BMC Plant Biol. 23*(1), 399 (2023).
2. Amsler, C. D., McClintock, J. B. and Baker, B. J. Secondary metabolites as mediators of trophic interactions among Antarctic marine organisms. *American Zool. 41*(1), 17-26 (2001).
3. Zhang, A., Sun, H., Wang, P., Han, Y. and Wang, X. Modern analytical techniques in metabolomics analysis. *Analyst. 137*(2), 293-300 (2012).
4. Morris, G. M. and Lim-Wilby, M. Molecular docking. *Methods Mol. Biol. 443*(1), 365-382 (2008).
5. Wang M. et al. Sharing and community curation of mass spectrometry data with Global Natural Products Social Molecular Networking. *Nature Biotechnol. 34*(8), 828-837 (2016).
6. Trott, O. and Olson, A. J. AutoDock Vina: improving the speed and accuracy of docking with a new scoring function, efficient optimization, and multithreading. *J. Comput. Chem. 31*(2), 455-461 (2010).
7. Daina, A., Michielin, O. and Zoete, V. SwissADME: a free web tool to evaluate pharmacokinetics, drug-likeness and medicinal chemistry friendliness of small molecules. *Sci. Rep. 7*(1), 42717 (2017).

Proceedings of
THE 5th INTERNATIONAL CONFERENCE OF
HYOJEONG ACADEMY 2025

Session 5

Medical & Health Studies for Co-Prosperity

www.ichja.org

5th International Conference of Hyojeong Academy
International Joint Conference 2025

Therapeutic Potential of V. amygdalina leaf-derived Biomaterial (AMX) on Chronic Ulcerative Skin Lesions in Diabetic Patients: Case Reports

Nlandu R. Ngatu[1, 2,*], Miezi Marie-Nsimba[1, 3], Luzitu S. Nangana[1, 4], Christian-Mapong Wansu[1, 5] and Nzunzu Jose-Lami[1, 3]

[1]Congo-Japan Research Group, D.R. Congo
[2]Kagawa University Faculty of Medicine, Kagawa, Japan
[3]Faculty of Pharmaceutical Sciences, University of Kinshasa, Kinshasa, D.R. Congo
[4]Hopital Kimbanguiste de Kinshasa, Kinshasa, D.R. Congo
[5]Division of Health Sciences, Institut Superieur Song-Hwa (ISTS), Kinshasa, D.R. Congo
*Correspondence: ngatunlandu@gmail.com

Abstract: Foot ulcer is a common skin disorder in diabetic patients worldwide. A number of factors are associated with wound healing impairment in diabetic foot ulcer (DFU), including peripheral neuropathy (PN), peripheral arterial disease (PAD), and infection. Here, we present two cases of chronic and recalcitrant DFU in African diabetic patients with a history of treatment failure in both patients, and right foot toe amputation in one of them, prior to wound management with a topical ointment containing *Vernonia amygdalina* leaf-derived biomaterial (AMX). Case 1 was a 53-year old male diabetic patient who developed type 2 diabetes mellitus 3 years before, had uncontrolled fasting blood glucose (FBG) level, and underwent toe amputation due to a complicated DFU on his left foot (Type IV, Kobe foot ulcer classification). He received wound care with the use of a topical antiseptic and disinfectant solution (Betadine iodine) once every two days and daily antibiotics, in addition to antidiabetic medication. Given that a second amputation was envisaged, his doctor who knew about our product (AMX) requested a sample in 2019. Case 2 was a 34-year old female diabetic patient who had a long-lasting ulcerative skin wound on her left lower limb for almost 10 years (Type IV class ulcer). She has been using topical Dakin's solution for wound care. With topical application of AMX, rapid soft tissue regeneration and wound closure was observed after 2 months of treatment in Patient1. On the other hand, a wound closure was observed at day10 of AMX treatment in Patient 2. Blood glucose was controlled thanks to the use of an alga-based phytomedicine (NBF) from our research group as adjuvant antidiabetic therapy. Observations from this case report suggest that AMX, known as skin filaggrin (FLG) and TNF-alpha modulator with anti-bacterial activity, has a potential to serve as alternative treatment for ulcerative skin disorders.

Keywords: Diabetic foot ulcer, Filaggrin modulator, Ngatu bio-formula (NBF), Skin ulcer, *Vernonia amygdalina*.

1. Introduction

Chronic or non-healing wounds are those that are slow to progress through the healing phases, or wounds with delayed healing due to intrinsic and extrinsic factors. Managing the underlying diseases, such as diabetes and vascular disorders (venous, arterial ulcer, pressure ulcer) or cancers is essential. Furthermore, peripheral neuropathy (PN), peripheral arterial disease (PAD) and infection in lower extremities are known as factors that contribute to wound healing impairment; and they are the leading causes of disability and amputations in some countries [1-3].

Diabetes mellitus (DM) has an increasing prevalence worldwide, and individuals with this metabolic disorder have a 25% probability of developing diabetic foot ulcer (DFU) in their lifetime. The annual incidence of DFU ranges from 1.9 to 26.1 million, with a mortality rate of approximately 5% within the first 12 months and 42% within five years. DFU has severe complications, including high rate of disability, recurrence, mortality, and high treatment cost and prolonged hospitalization as well [4, 5].

The poor prognosis of DFU imposes a high financial burden the patient, his family, as well the medical system; thus, prevention and early diagnosis in high-risk patients and effective treatment are indispensable [5, 6].

Vernonia amygdalina is an African plant used as food as well as in phototherapy for a number of ailments. We previously reported on the anti-inflammatory property of V. amygdalina leaf extracts (AMX) and AMX-contained Vernodalin, bioactive terpenoid compound, on atopic and contact dermatitis [7, 8].

Here, we two we present two cases of chronic and recalcitrant DFU in African diabetic patients with a history of medication failure in both subjects and right foot toe amputation in one of them, prior to treatment with a topical ointment containing *Vernonia amygdalina* leaf-derived biomaterial (AMX).

2. Materials and Methods

2.1. Design, subjects and treatment

This report includes two clinical cases of DFU in African patients. They were taken care in Kinshasa, D.R. Congo, using an ointment containing AMX. Originally, AMX-RN (or AMX in short) derived from the names of the source plant (**AM**ygdalina e**X**tracts) and its inventor and patent holder (Roger Ngatu). The extracts have filaggrin (FLG) production up-regulating property, whereas they down regulates tumor necrosis factor alpha (TNF-α) production in the skin.

2.2. Treatment

In both patients, ulcerative lesions were treated with an ointment made of *V. amygdalina* leaf extracts, namely AMX, in addition to daily wound care using antiseptic solution (betadine iodine or Dakin's solution). During the course of treatment, in order to control blood glucose level, edible alga-based phytomedicine (NBF) also from our research team was used as adjuvant therapy. NBF stands for 'Ngatu bio-formula'.

Previously, we have reported that alcoholic extracts of *V. amygadalina* leaf main compounds were terpenoids, including *Vernodalin* and *Vernodalinol* (Figures 1(a) and 1(b)), and lipids; the aqueous extracts' main chemical compounds were polyphenols, saponins and lipids by high performance liquid chromatography (HPLC) and gas chromatography mass spectrometry (GC-MS) analyses [7, 8]. During the treatment course, in order to control blood sugar level and eventually allow wound healing, daily intake of NBF, an alga-based phytomedicine discovered by our research team, was recommended [9].

2.3. DFU classification

In common practice, treatment depends on the severity or type of skin ulcer. Wagner classification system and the "University of Texas wound classification" are among most employed. The first one, which is basically anatomical (superficial ulcer, deep ulcer, abscess osteitis and foot gangrene), is reported to be not always suitable for assessing wound therapy. On the other hand, the second grading system assesses not only ulcer depth but also wound infection and the presence of clinical signs of lower extremity ischemia, making up 16 categories. That makes it quite difficult to understand and deal with [10].

The Kobe DFU classification has been established in the second decade of 21st century by a Japanese research team, and it comprises four ulcer types: type I, type II, type III and type IV. Type I wounds result mainly from peripheral neuropathy (PN), including motor neuropathy, sensory neuropathy and autonomic neuropathy. Type II wounds result from peripheral arterial disease (PAD), for which adequate blood flow to the wound is needed with revascularization therapy. Type III wounds are mainly characterized by infection. Various types of severe infection occur in patients with diabetes mellitus, often requiring surgical attention. Type IV wounds are those that combine all three factors: PN, PAD and infection [10].

2.4. Ethical consideration

Both patients were adult subjects and provided informed consent to their care providers for the use of AMX and NBF, after receiving a thorough explanation about the nature and composition of both phototherapeutic products.

3. Results

3.1. Case 1

It was a 53-year old male diabetic patient who developed type 2 diabetes mellitus 3 years before, had uncontrolled fasting blood glucose (FBG: 308 mg/dL at baseline) mainly due complications such as infection. Later on, he developed a DFU on left foot, due to complications (infection), he underwent toe amputation in 2018 at a specialized surgical clinic. Local wound care with Betadine iodine solution combined with oral antibiotics did not improve the prognosis. A second amputation was envisaged; however, his doctor who heard about AMX on local media

requested a sample in November 2019. Thus, in December 2019, he started the topical application of AMX once daily.

On day1 of topical AMX, it was a deep wound of approximately 6 cm long and 3.5 cm large, with important loss of soft tissue (Type IV, Kobe DFU ulcer classification scale). Rapid soft tissue regeneration was observed from the second week of treatment. Progressively, re-epithelization of the wound surface followed by wound closure was observed by week 8 of treatment (Figures 1(c) and 1(d)). Blood glucose was controlled at 33 mg/dL at week8 of antidiabetic therapy with NBF.

3.2. Case 2

It was a 34-year-old female diabetic patient who had a long-lasting ulcerative wound on her left lower limb for almost 10 years. The patient has been taken care at a local referral hospital for almost 4 years. However, due to lack of clinical improvement, she decided to undergo treatment at home, with wound dressing using topical Dakin's solution. The presence of infection, observed skin lesions and clinical signs were suggestive of type IV DFU, according to the Kobe classification system. The wound was unclean with a purulent surface. She was introduced to one of our local research team members, who is a medical doctor. She had an uncontrolled FBG (147 mg/dL at baseline).

Upon a request from a member of the medical team who witnessed the beneficial effects of AMX in another DFU patient, we provided a sample which was used in addition to daily topical Dakin's solution. Within the first week of AMX treatment, a rapid improvement was observed daily, and a complete wound closure was observed by day10 (**Figure 1e-i**). Wound management with AMX was continued until completing 3 weeks treatment. Her metabolic health improved considerably with a FBG of 117 mg/dL at week8 of NBF therapy.

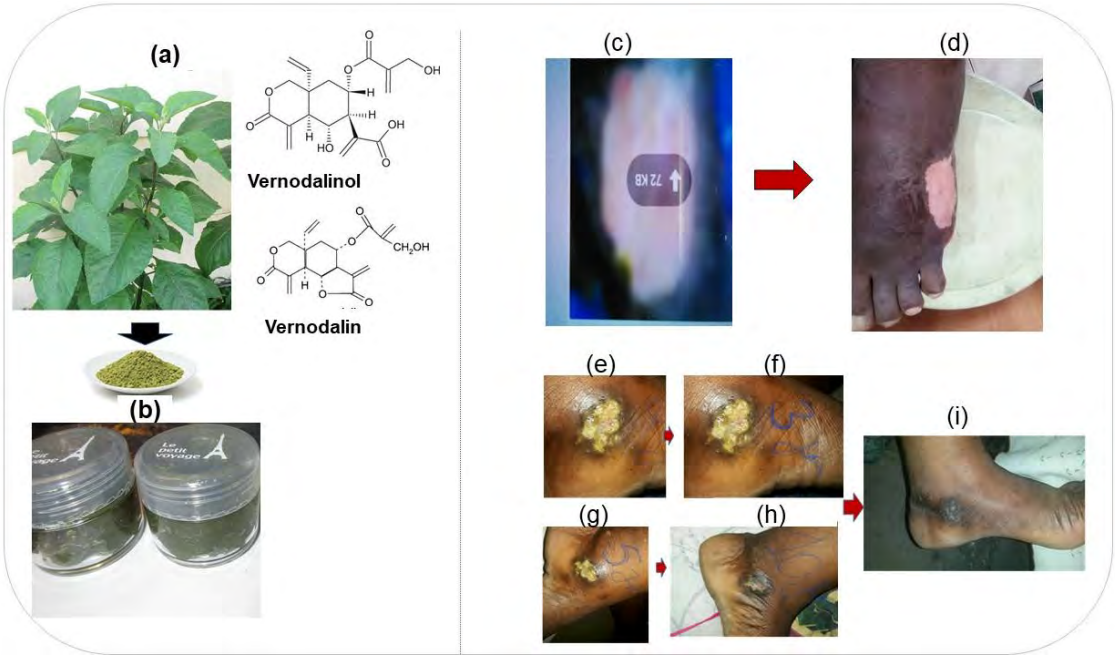

Figure 1. Images of Vernonia amygdalia plant: (a) main bioactive terpenoids Vernodalin and Vernodalinol; (b) V. amygdalina leaf extracts-based ointment; (c) DFU in patient 1 on day1 of AMX treatment; (d) 8 weeks later; (e) DFU in patient 2 on day1; (f) day3; (g) day5; (h) day10; (i) day14.

4. Discussion

This report describes two chronic and recalcitrant DFU in African type 2 diabetic patients with a history of unsuccessful treatment consisting mainly of dressing with antiseptic solutions. Case 1 underwent toe amputation, in addition to topical treatment, due to complications.

Treatment with topical AMX improved the wound remarkably in both patients with soft tissue regeneration and wound closure after a relatively short period of time. In fact, *V. amygdalina* leaf extracts have not only anti-inflammatory activity; they also possess antibacterial property particularly against gram positive bacteria species [11, 12]. This beneficial health effect may explain why AMX provided better outcome in the management of infected wound.

5. Conclusion

The outcomes observed in both DFU cases presented in this report suggest that topical AMX has a potential to serve as alternative treatment for ulcerative skin disorders. Further clinical investigations are needed to confirm its effectiveness.

Author Contributions: Conceptualization, N.R.N. and L.S.N.; Methodology, M.M.N., L.S.N. and N.J.L.; Writing the manuscript, N.R.N., C.W.M. and M.M.N., Supervision, N.R.N.

Funding: This research received no external funding.

Data Availability Statement: Not applicable.

Acknowledgments: The authors would like to thank Professor Michel Kabamba Nzaji, dean of the Faculty of Medicine, University of Kamina, in the Democratic Republic of the Congo, for his support to this "AMX and Skin Diseases" project.

Conflicts of Interest: The authors declare no conflict of interest.

References

1. Sibbald, R., Elliott, J. and Somayaji, R. Optimizing the moisture management tightrope with wound bed preparation. *Adv. Skin Wound Care 28*(10), 466-476 (2015).
2. Naude, L. et al. An observational pilot study to collect safety and efficacy data on wound care using whole blood clot technology on hard-to-treat wounds. *Wounds International 12*(2), 42-51 (2021).
3. Ylitalo, K., Sowers, M. and Heeringa, S. Peripheral vascular disease and peripheral neuropathy in individuals with cardiometabolic clustering and obesity. *Diabetes Care 34*(7), 1642-1647 (2011).
4. Chen, L., Sun, S., Gao, Y. and Ran, X. Global mortality of diabetic foot ulcer: a systematic review and meta-analysis of observational studies. *Diabetes Obes. Metab. 25*(1), 36-45 (2023).
5. Piran, N., Farhadian, M., Soltanian, A. and Borzouei, S. Diabetic foot ulcer risk prediction in patients with type 2 diabetes using classifier based on associations rule mining. *Sci. Rep. 24*, 635 (2024).
6. Tomita, M. et al. Development and assessment of a simple scoring system for the risk of developing diabetic foot ulcer. *Diabetol. Int. 6*, 212-218 (2015).
7. Ngatu, R. et al. *Allergol. Int. 61*(4), 597-607 (2012).
8. Ngatu, R. Clinical anti-allergic effects of African vernonia amygdalina leaf extracts. In *Environmental and occupational skin disorders*, 1st ed. (Springer, 2018).
9. Ngatu, R., Ikeda, M., Tonduangu, D., Nangana, S. and Hirao, T. Modulatory effects of NBF1, an algal fiber-rich bioformula, on adiponectin and C-reactive protein levels, and its therapeutic prospects for metabolic syndrome and type 2 diabetes patients. *Biomedicines 10*(10): 2572, (2022).
10. Terashi, H., Kitano, I. and Tsuji, Y. Total management of diabetic foot ulcerations – Kobe classification as a new classification of diabetic foot wounds. *Keio J Med. 60*(1), 17-21 (2011).
11. Evbuomwan, L., Chukwuka, E., Obazenu, E. and Ilevbare, L. *Appl. Sci. Environ. Manage. 22(*1), 17-21 (2018).
12. Tura, A., Anbessa, M., Tulu, E. and Tilinti, B. Exploring Vernonia amygdalina's leaf extracts for phytochemical screening and its anti-bacterial activities. *Int J Food Properties 27*(1), 960-974 (2024).

5th International Conference of Hyojeong Academy
International Joint Conference 2025

The Review of Oriental Medicine for Restless Legs Syndrome

Mikyoung Lee, Joseph Rothstein, Adrianus Wong, Eunhee Yu and Sanghyun Lee*

Wongu University of Oriental Medicine, Las Vegas, NV 89123, USA
*Correspondence: sanglee@wongu.edu

Abstract: Restless legs syndrome (RLS) is a sleep-related neurological disorder that causes an uncomfortable feeling in the legs and an irresistible urge to move them. It is also known as Willis-Ekbom disease. The exact cause is unknown, but it may be related to dopamine, a brain chemical that helps with muscle movement. Some cases may be inherited. Mild RLS can be treated with exercise, leg massages, and warm baths. For severe symptoms, some medications such as dopaminergic agents (levodopa), antiseizure agents (gabapentin), BZDs (clonazepam), and opioids are prescribed. However, many of the pharmaceuticals have unwanted side effects, and the potential for tolerance and dependence. In contrast to Western medicine, Oriental medicine such as acupuncture and herbal formula has a treatment modality with potential efficacy and few side effects. In Traditional Chinese Medicine (TCM), the theory for the cause of RLS is disclosed as reduction in the legs blood Yin and Xue (blood) which is responsible for body and brain relaxation. Shaoyao Gancao Tang is a classic formulation of TCM and was first recorded in the Treatise of Cold Damage written by Zhang Zhongjing (150-219 AD) for halting spasms and cramps of legs. In recent years, an increasing number of clinical trials has been conducted and published to demonstrate the effectiveness of Shaoyao Gancao Tang for the treatment of RLS. The major goal of RLS treatment is to provide symptom relief. The purpose of this study is to examine the additive effect of medical acupuncture and herbal formula on controlling the symptoms of RLS.

Keywords: Restless legs syndrome, neurological disorder, oriental medicine, Shaoyao Gancao Tang

1. Introduction

Restless legs syndrome (RLS) is a neurological disorder characterized by an uncomfortable and unpleasant sensation in the legs that appears at rest, which induces an irresistible urge to move the legs [1]. RLS symptoms are more prominent in the evening and at bedtime and usually disrupt patient sleep [1]. The incidence of this disease worsens with age and the incidence is twice as high in females [1]. The etiology of primary RLS remains unknown [2]. It seems that both age and genes play an important role for the susceptibility and clinical expression of RLS [2]. A possible mechanism for the production of symptoms involves disinhibition of normal central nervous system pacemakers [2]. Underlying pathophysiology of RLS is still not fully understood [1]. The most accredited hypothesis recognizes an involvement of the diencephalic A11 dopaminergic neurons [1]. Three main causative reasons of the secondary type of this disease are pregnancy, iron deficiency anemia, and renal failure [1]. The most effective drug treatment for RLS is dopamine agonists, which possess some side effects [1]. Many nonpharmaceutical methods such as exercise, massage therapy, near-infrared light, or pneumatic compressed have been applied to cure RLS [1]. Decrease use of caffeine, alcohol, and tobacco, and maintaining a regular sleep pattern might provide some relief for patients with RLS [1]. In Chinese medical acupuncture, the theory for the cause of RLS is disclosed as reduction in the legs blood Yin and Xue (blood) which is responsible for body and brain relaxation [1]. Particularly, the lack of liver Xue and Yin which controls activity of legs at night is the main cause of RLS [1]. Acupoints such as Shenshu (BL23), Xuehai (SP10), Chenshan (BL57), Zusanli (ST36), Sanyinjiao (SP6), and Taixi (KD3) are commonly involved in the treatment of RLS [3]. Shaoyao Gancao Tang is a classic formulation of TCM and was first recorded in the Treatise of Cold Damage written by Zhang Zhongjing (150-219 AD) for halting spasms and cramps of legs [4]. In recent years, an increasing number of clinical trials has been conducted and published to demonstrate the effectiveness of Shaoyao Cancao Tang for the treatment of RLS [4]. The purpose of this study is to examine the additive effect of medical acupuncture and herbal formula on controlling the symptoms of RLS.

2. Discussion

2.1. Sleep Mechanism

RLS is sleep-related movement disorder. Sleep is part of what is called the sleep-wake cycle [5]. Sleep is a period of inactivity and restoration of mental and physical function [5]. Sleep provides time for entering information that has been acquired during periods of wakefulness into memory and for reestablishing communication between various parts of the brain [5]. Sleep also is a time when other body systems restore energy and repair tissues [5]. Muscle activity and digestion decrease, and sympathetic nervous system activity is diminished [5]. Many hormones, such as growth hormone, are produced in a cyclic manner correlating with the sleep-wake cycle, suggesting that growth and tissue repair may occur during sleep [5].

2.1.1. Neural Structures and Pathway

Anatomically, the sleep-wake cycle involves structures in the thalamus, associated areas of the cerebral cortex, and interneurons in the reticular formation of the midbrain, pons, and brain stem (Fig. 1(A)) [5]. The reticular formation of the midbrain, pons, and brain stem monitors and modulates the activity of various circuits controlling wakefulness [5]. The thalamus and the cerebral cortex function in tandem, with all sensory information being relayed to the thalamus and from there to the cerebral cortex [5]. For example, visual impulses from the retina go to the thalamus and are then relayed to the visual cortex (Fig. 1(B)) [5]. The pathways between each sensory area of the thalamus and the cortex form two-way communication loops called the thalamocortical system (Figs. 2(A) and 2(B)) [5-7]. Communication between each sensory area of the thalamus and its companion area in the cortex is kept orderly by several neuronal control systems, including the midbrain reticular formation, which controls the level of background activity so that external stimuli can be processed [5].

2.1.2. Sleep-Wake Cycle

The sleep-wake cycle normally consists of a synchronous pattern of wakefulness and sleep [5]. During wakefulness, both the thalamocortical system and brain stem centers are active [5]. A full repertoire of motor movements is made possible by corticospinal circuits that travel through the brain stem [5]. Sleep represents a period of diminished consciousness from which a person can be aroused by sensory or other stimuli [5]. It occurs in stages during which the brain remains active but does not effectively process sensory information [5]. However, during sleep, a person does have inward conscious experiences such as dreams [5].

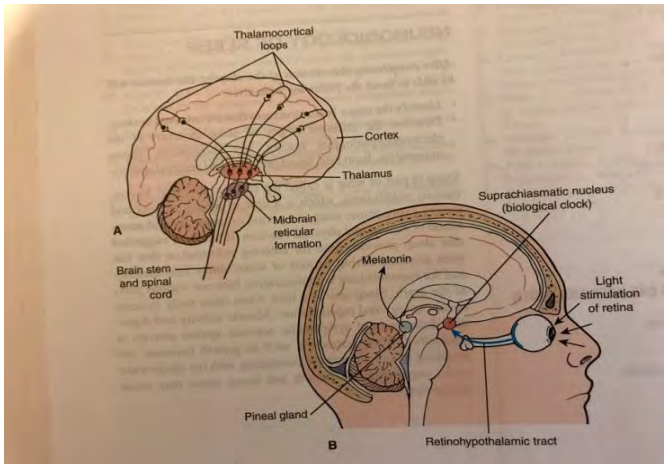

Figure 1. (A) Brain structures involved in sleep; (B) Location of the SCN (biologic clock) with input from the retina and its association with the pineal gland and melatonin production.

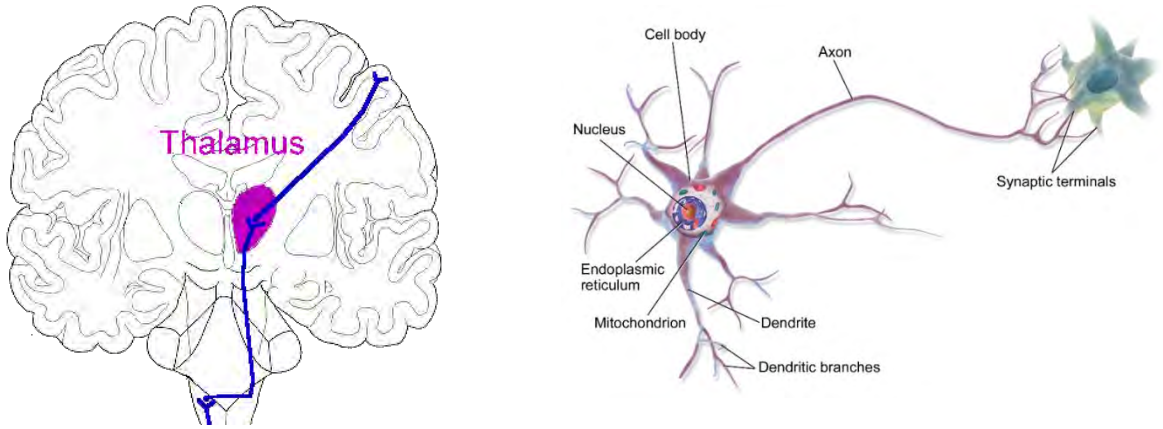

(a) (b)

Figure 2. (a) Thalamo-cortical system; (b) The Thalamocortical Plasma Globe.

2.1.3. Sleep Stages

There are two types of sleep: rapid eye movement (REM) and non-rapid eye movement (NREM) sleep [5]. These two types of sleep alternate with each other and are characterized by differences in eye movements, muscle tone and body movements, heart rate and blood pressure (BP), breathing patterns, brain wave activity, and dreaming [5]. A complete sleep cycle takes about 90 to 110 minutes [5]. NREM sleep is a quiet type of sleep characterized by a relatively inactive, yet fully regulating brain and a fully movable body [5]. It accounts for about 80% of sleep [5]. The brain stem coordinates activity between the spinal cord and various reflexes such as swallowing and chewing [5]. NREM sleep normally is encountered when the person first becomes drowsy [5]. Falling asleep does not occur all at once [5]. It is divided into four stages that reflect an increasing depth of sleep (Fig 3) [5].

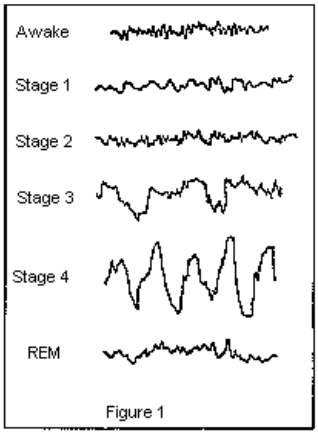

Figure 3. Brain waves during wakefulness: NREM sleep stages 1, 2, 3, and 4 and REM sleep.

Stage 1 is a brief transitional stage that occurs at the onset of sleep, during which a person is easily aroused [5]. Stage 2 is a deeper sleep, lasting approximately 10 to 25 minutes, during which EEG activity is interrupted by sleep spindles consisting of bursts of high-frequency waves [5]. Stages 3 and 4 represent deep sleep, during which the muscles of the body relax, the heart rate and BP decrease, and gastrointestinal activity is slowed [5]. Sleep a variety of spontaneous limb movements occur during normal sleep [5]. Many of these movements demonstrate characteristic rates and patterns during certain stages of sleep [5]. Many movement disorders occur during stage 2 NREM sleep [5].

2.2. Restless Legs Syndrome

RLS is a sleep disorder characterized by an urge to move the limbs with or without sensations, worsening at rest or inactivity, improving with activity or movement, and worsening in the evening or night [5]. The disorder, which is thought to have its origin in the central nervous system (CNS), can occur as a primary or secondary disorder [5]. There is a high familial incidence of primary RLS, suggesting a genetic disorder [5]. Secondary causes of RLS include iron deficiency, neurologic disorders such as spinal cord and peripheral nerve lesions, pregnancy, uremia, and medications [5]. Although the neurologic basis of RLS has not been determined, recent research suggests that it may involve homeostatic mechanisms that regulate the influx and efflux of iron from cells of the CNS that regulate motor movements [5]. Cerebrospinal fluid ferritin (the main iron storage molecules in the CNS) levels are lower in people with RLS [5]. Of interest is the role of iron in dopaminergic transmission in the CNS [5]. Iron is an important cofactor for tyrosine hydroxylase, the rate-limiting enzyme in dopamine synthesis, and also plays a major role in the functioning of postsynaptic dopamine receptors [5]. Diagnosis of RLS is based on a history of

1. A compelling urge to move the legs, usually associated with unpleasant sensations
2. Motor restlessness, as seen by activities such as pacing, tossing and turning in bed, or rubbing the legs
3. Symptoms that become worse at rest and are relieved by activity
4. Symptoms that are worse in the evening or at night [5]

Laboratory tests to determine secondary causes of RLS usually are done [5]. Because RLS may be a symptom of iron deficiency, serum ferritin and iron saturation should be assessed [5]. This is important because iron deficiency is frequently present in the absence of anemia [5]. Sleep studies usually are not required because the condition can be diagnosed on the basis of history and clinical findings [5].

Treatment of RLS varies depending on the severity of symptoms [5]. Dopaminergic agents are the first-line drugs for most people with RLS [5]. These include ropinirole (Requip), pramipexole (Mirapex), levodopa, and carbidopa (Sinemet). Antiseizure agents (gabapentin), BZDs (e.g., clonazepam, temazepam), and opioids (e.g., codeine, propoxyphene, or oxycodone) are second-line agents [5]. The analogues of gamma-aminobutyric acid such as gabapentin have been shown to be safe and efficacious in treating RLS of hemodialysis patients [3]. Although pharmacologic treatment is helpful for many people with RLS, those with mild symptoms may not require medications [5]. Repetitive transcranial magnetic stimulation, pneumatic compression devices, counter-strain manipulation, infrared therapy, vibration pads, yoga, cryotherapy, and acupuncture are among the notable non-pharmacological treatments of RLS [3]. For many people, deliberate manipulation of the muscles through ambulation, kicking movements, stretching, or massage may provide relief [5]. Good sleep habits are important [5]. Because a high prevalence of iron deficiency has been found among people with RLS, treatment of the deficiency may improve or resolve symptoms [5].

While RLS is a disease in Western medicine, traditional Chinese medicine (TCM) sees it as a symptom [2]. Although RLS has no definite name in TCM, the description of RLS symptoms can be found in some ancient Chinese literature [2]. The oldest preserved written Chinese possible scientific description of RLS symptoms dates back to Lingshu (Spiritual Pivot) in Huangdi Neijing (The Inner Canon of Huangdi, Yellow Emperor's Inner Canon) [2]. Chinese medical therapy for RLS would primarily involve tonifying the deficiencies and promoting blood circulation [2]. The deficiency syndrome appears to mainly involve the liver and kidney (possibly also the heart), and the stasis mainly involves the legs [2]. The TCM prescription is tailored for each patient and even for a specific situation or stage [2]. Thus, there are different clinical trials using different prescriptions even under the same TCM diagnosis [2].

2.3. Acupuncture

Acupuncture is an integral part of TCM, which dates back more than 2000 years [8]. According to a TCM theory, acupuncture restores the balance between Yin and Yang and regulates Qi (essence) and blood [1]. Acupuncture is especially known for its effectiveness in reducing pain due to triggering a release of analgesic neuropeptides [1]. Previous studies have shown that the neuroprotective effect of acupuncture is mediated through the same common mechanisms as other neuroprotective agents, including antioxidative stress, anti-inflammatory, and antiapoptotic pathways at molecular and cellular levels [1]. In recent years, acupuncture has been studied in the treatment of serious neurological diseases such as neurodegeneration diseases [8]. RLS has been proposed to be one of the initial stages of neurodegenerative disease [8]. In the theory of TCM, RLS is considered a deficiency of "Yin" and "Xue (blood) of the legs, because Yin and Xue are in effect at night and function to relax the mind and

body [8]. According to TCM, the activity and function of legs are controlled by liver function, and thus the deficiency of "Yin" and "Xue" of the liver at night is the main cause of RLS [8]. When Yin and Xue become deficient, which may also be associated with Qi imbalances, the conditions like RLS develop [3]. Shenshu (BL23, bilateral), Mingmen (DU4), and Chenshan (BL57, unilateral) have effects on uncomfortable waist and leg symptoms, Shenshu (BL23, bilateral), and Mingmen (DU4) can also improve "Shen Qi" (energy and immunity) and increase the "Yin" of the waist and legs, and Xuehai (SP10, unilateral) increases "Xue" (blood) of the body, which means it can tranquilize the legs [8]. Taichun (LV3, bilateral), Zusanli (ST36, unilateral), Sanyinjiao (SP6, bilateral), and Taixi (KD3, bilateral) increases both "Yin" and "Xue" of the body [8]. Yanglingquan (GB34), Xuanzhong (GB39), Zusanli (ST36), and Shanyijiao (SP6) provide neuroprotection of dopaminergic neurons of the substantia nigra [1]. The mechanism of acupuncture treatment for RLS is still unclear [1]. As far as the mechanism of action is concerned, it is suggested that acupuncture may target the autonomic nervous system (ANS) to manifest its effects [3].

2.4. Herbal medicine

Herbal medicine can treat restless legs syndrome. According to a recent study, 'Shao Yao (Paeoniae Radix)', one of herbal medicines, can be effective in the treatment of RLS. According to an analysis by a research team at Kyung Hee University Korean Medicine Hospital, patients who took herbal medicine containing Shao Yao showed higher symptom improvement than those who took only Western medicine. Particularly noteworthy is that paeoniflorin (Fig. 4) [9], a major component of Shao Yao, can activate the adenosine A1 receptor (Fig. 5) [10] and alleviate symptoms of RLS.

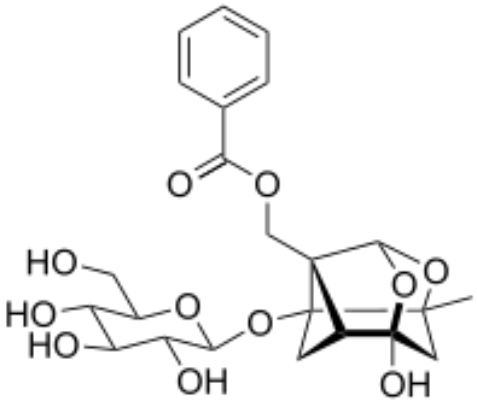

Figure 4. Paeoniflorin Chemical formula C23H28O11.

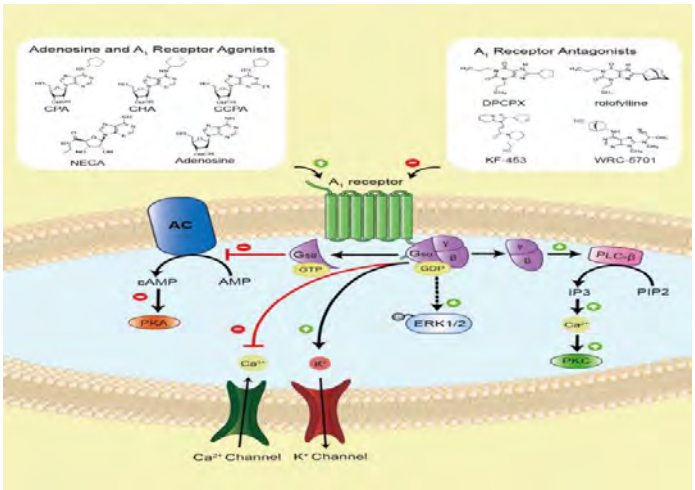

Figure 5. Adenesin A1 receptor on immune cell.

2.4.1. Shao Yao Gan Cao Tang (Peony and Licorice Decoction)

It is a prescription based on Shao Yao (Paeoniae Radix) and Gan Cao (Glycyrrhizae Radix). It nourishes the blood, augments the yin, moderates painful spasms, and alleviates pain. The chief herb is Bai Shao (Paeoniae Radix alba), which nourishes the blood and preserves the yin. Bai Shao is one form of Shao Yao and relaxes spasms. It enters the Spleen, softens the Liver, and alleviates pain. This herb is effective in moderating the wayward inclinations of the Liver qi, especially when it overacts on earth, and preserving the Liver yin. Zhi Gan Cao augments the qi of the middle burner, especially that of the Spleen, and moderates urgency. Together, these herbs regulate the relationship between the Liver and Spleen and nourish the sinews and blood, which in turn stops the spasms and pain.

2.4.2. Huang Qi Gui Zhi Wu Wu Tang (Astragalus and Cinnamon Twig Five-Substance Decoction)

It consists of Huang Qi (Astragali Radix), Shao Yao (Paeoniae Radix), Gui Zhi (Cinnamomi Ramulus), Sheng Jiang (Zingiberis Rhizoma recens), and Da Zao (Jujubae Fructus). It augments the qi, warms and harmonizes the channels, and unblocks painful obstruction. This formula utilizes a strategy of warming the channels and tonifying deficiency in order to overcome peripheral obstructions to the movement of blood. Huang Qi strongly tonifies the original qi, helping the normal qi to expel pathogenic qi while simultaneously firming up the skin and exterior. Gui Zhi warms the nutritive qi in the channels and unblocks the yang. In combination, the two chief herbs, Huang Qi and Gui Zhi synergistically augment the qi, warm the yang, harmonize the blood, and unblock the channels. Shao Yao nourishes the blood, harmonizes the nutritive qi, and unblocks painful obstruction, functions as the deputy. Shao Yao nourishes the yin in combination with Huang Qi.

2.4.3. Chai Hu Gui Zhi Tang (Bupleurum and Cinnamon Twig Decoction)

It consists of Gui Zhi (Cinnamomi Ramulus), Huang Qin (Scutellariae Radix), Ren Shen (Ginseng Radix), Gan Cao (Glycyrrhizae Radix), Zhi Ban Xia (Pinelliae Rhizoma praeparatum), Shao Yao (Paeoniae Radix), Chai Hu (Bupleuri Radix), Sheng Jiang (Zingiberis Rhizoma recens), and Da Zao (Jujubae Fructus). It releases the exterior and muscle layer, harmonizes and releases the Shao Yang, harmonizes the Liver, Spleen, and Intestines, and dispels water accumulation. The prescription containing Shao Yao can help to the restless legs syndrome improvement. Bai Shao (Paeoniae Radix alba) nourishes the blood, regulates the menses, calms and curbs Liver Yang, alleviates pain, preserves Yin, and adjusts the Ying and Wei.

2.4.4. Gui Zhi Fu Ling Wan (Cinnamon and Poria Pills)

It consists of Gui Zhi (Cinnamomi), Fu Ling (Poria), Shao Yao (Paeoniae Radix), Mu Dan Pi (Moutan Cortex), and Tao Ren (Persicae Semen). It invigorates the blood, transforms blood stasis, and reduces fixed abdominal masses. This formula was designed by Zhang Zhongjing for treating blood stasis during pregnancy. Gui Zhi unblock the blood vessels and reduce the stasis of blood by promoting circulation. The ability of Fu Ling to leach downward can help promote the downward circulation of blood in cases of blood stasis. It also nourishes the qi of the heart and Spleen, quiets the heart, and calms the spirit. Shao Yao has the two kinds by the nature of the condition. Chi Shao (Paeoniae Radix rubra) promotes the circulation of blood to alleviate stasis, while Bai Shao (Paeoniae Radix alba) relaxes spasms and alleviates abdominal pain; if necessary, both forms of the herb may be used. Mu Dan Pi and Tao Ren cool and invigorate the blood, break up and dispel blood stasis, reduce fixed abdominal masses, and disperse accumulation [11].

3. Conclusion

RLS is a chronic neurological disorder that causes an uncomfortable feeling in the legs and a very strong urge to move them. It typically happens in the evening or at night when sitting or lying down and interferes with sleep. The exact cause of RLS is unknown, but there are several possible factors that may contribute to it. RLS may be inherited, as about half of people with RLS have a close relative with the condition. RLS may be caused by an imbalance of dopamine, a brain chemical that controls muscle movement. Low levels of iron in the brain may be a factor in RLS. Certain medications can aggravate RLS symptoms, including rhinitis drugs (antihistamines), antidepressants (increased serotonin), and antipsychotic drugs (blocking dopamine). RLS may be linked to other conditions, such as diabetes, kidney disease, liver disease, pregnancy, nerve damage, and Parkinson's disease. Caffeine, alcohol, smoking, being overweight or obese, and inconsistent sleep habits can aggravate RLS symptoms. Chocolate, sugary sodas, fried foods, and other foods or beverages that contain caffeine can make RLS symptoms worse. RLS can develop at any age, but it most often begins in middle age. It is more common in

women and people assigned female at birth (AFAB) than in men. Restless legs syndrome is characterized by itching, crawling, pulling, throbbing, or pricking sensations that typically are more intense at rest. Temporary relief is obtained by moving the legs. There is not cure for RLS, but treatment is available. In Oriental medicine, even if the symptoms are the same, the treatment may vary from person to person depending on the patient's constitution, condition, pulse, and other accompanying symptoms. For effective treatment of RLS, it is important to take an integrated approach such as acupuncture treatment, regular sleeping habits, proper exercise, and stress management along with herbal medicine treatment. It is also a good way to relax the overall tension through aroma therapy, meditation, and breathing methods. According to one study, the combination of acupuncture with gabapentin had additive therapeutic effects over gabapentin alone [1]. RLS is a disease that greatly reduces the quality of life, but the effects of various medicinal herbs including Shao Yao (Paeoniae Radix) have been scientifically proven, and more effective treatment is possible though customized prescriptions tailored to individual constitution and symptoms. Of course, Oriental medicine treatment alone does not solve everything. For effective treatment of RLS, it is important to consult with a specialist to find the best treatment for the patient.

References

1. Raissi, G.R.et al. Evaluation of Acupuncture in the Treatment of Restless Legs Syndrome: A Randomized Controlled Trial. *J. Acupuncture and Meridian Studies 10*(5), 346-350 (2017). https://doi.org/10.1016/j.jams.2017.08.004
2. Yan, X. et al. Traditional Chinese medicine herbal preparations in restless legs syndrome (RLS) treatment: A review and probable first description of RLS in 1529. *Sleep Medicine Reviews 16*(6), 509-518 (2012). https://doi.org/10.1016/j.smrv.2012.01.003
3. Huang, C., Tang, J., Sun, W., Wang, L. and Jin, Y. Effectiveness of acupuncture in the management of restless leg syndrome: a systematic review and meta-analysis. *Annals of Palliative Medicine 10*(10), 10495-10505 (2021). https://apm.amegroups.org/article/view/82101/html
4. Chen, Y. et al. Effectiveness and safety of traditional Chinese medicine Shaoyao Gancao Tang for the treatment of restless leg syndrome: A protocol for systematic review and meta-analysis. *Medicine 99*(40): e22401, (2020). https://journals.lww.com/md-journal/toc/2020/10020
5. Norris, T. L. *PORTH'S Pathophysiology: Concepts of Altered Health States*, 10th ed. (Wolters Kluwer, 2019).
6. Kandel, E., Schwarts, J., Jessell, T., Einfuhrung, E. and Heidelberg, S. The brain in sleep: Thalamocortical system. https://www.pharma.uzh.ch/static/sleepcd/demo/brain/chap3/ab0084a.htm
7. Binz, K. The Thalamocortical Plasma Glove. https://kevinbinz.com/2015/10/07/the-thalamocortical-plasma-globe
8. Pan, W. Actigraph Evaluation of Acupuncture for Treating Restless Legs Syndrome. *Evidence-Based Complementary and Alternative Medicine 2015*(1), 1-7 (2015). https://doi.org/10.1155/2015/343201
9. Wikipedia: Paeoniflorin. https://en.wikipedia.org/wiki/Paeoniflorin
10. Zhong, L., Peng, Q. and Zeng, X. The role of adenosine A_1 receptor on immune cells. *Inflammation Research 71*, 1203-1212 (2022). https://link.springer.com/article/10.1007/s00011-022-01607-w
11. Scheid, V., Bensky, D., Ellis, A. and Barolet, R. *CHINESS HERBAL MEDICINE Formulas & Strategies*, 2nd ed. (Eastland Press, 2015).

5th International Conference of Hyojeong Academy
International Joint Conference 2025

Acupuncture and the Spirit World

Shu Miyahara

Gengido Acupuncture Center, Nerima city, Japan
Correspondence: miyahara@dr-shu.com

Abstract: The acupuncture I do uses spirituality. I use spirituality in both diagnosis and treatment. And in the process of guiding from diagnosis to treatment, we receive the cooperation of the spirit world. However, there are still few people who recognize acupuncture in this way. Some acupuncturists do not use spirituality. Many acupuncturists use spirituality but do not recognize it as spirituality. Therefore, I decided to discuss acupuncture as a spiritual treatment from three perspectives. I tried to explain specifically how I use spirituality when I do acupuncture.

Keywords: spirituality, acupuncture

1. Introduction

Acupuncture improves the patient's physical condition. However, it cannot be explained by the action of the flesh alone. There is a big difference between inserting a needle into a blood vessel in the arm when collecting blood at a hospital and inserting an acupuncture needle in the same place during acupuncture treatment.

Despite the fact that the acupuncture needles are thinner than injection needles, the impact of the needle is large and can reach a long distance. This is because acupuncture works not only on the physical body, but also on the spiritual body. For example, the point of taihaku (SP-3) at the base of the big toe is effective for neurasthenia, insomnia, and hysteria [1]. I think it is difficult for modern medicine to explain this phenomenon.

For more than 1,000 years, acupuncturists have used the concepts of qi and meridians to explain this. In other words, there is a circuit called the meridians from the feet to the head, and it is said that qi flows through them. Meridians are like spiritual blood vessels. The word qi is used in many ways, but here it refers to the spiritual energy flowing through the meridians. However, since the dissection of the human body has been performed, no meridians have been found in the human body. Invisible meridians have come to be ignored as if they were non-existent.

The invisible God is ignored in science. In the same way, it is often ignored by scientists because it does not see qi or meridians, but acupuncture saves many patients every day. Qi and meridians are spiritual beings, just like God. Spiritual things are not unified in terms and concepts. Even within Oriental medicine, there is a difference between Chinese medicine and acupuncture. In this paper, we will discuss using the words and concepts written in the Divine Principle [2]. According to the Divine Principle, a living person has not only a physical body but also a spiritual body. In other words, human beings have a dual structure of spiritual and physical bodies. And they influence each other.

2. Spirituality in Acupuncture

2.1. The relationship between the form of healing and the spirit world

First, let's classify the ways in which the flesh heals from the perspective of the Divine Principle. The spirit world is involved in treatment in (2), (3), (5) and (6). Acupuncture falls under (4), (5) and (6).

(1) Cure not by a healer, but by a substance or environment. Treatment with food, water, light, air, etc.

(2) Your spiritual body heals your body. Healing through prayer, etc.

(3) The spirit world acts on the spirit body, and the physical body is healed under its influence. Healing by the mercy of God, etc.

(4) The therapist applies physical stimulation to the patient's body to heal it; massage, occupational therapy, etc.

(5) Acupuncture in which the healer treats the patient's spiritual body and physical body

(6) The healer receives the assistance of the spirit world to treat the patient's spiritual body and physical body.

In my case, it was (4) in the early days, but eventually it became (5), and in recent years, the proportion of (6) has increased. In the early days, I focused only on the physical body of the patient. Eventually, I began to treat with an awareness of qi and meridians. Meridians exist across both the spiritual body and the physical body. That's why I treat both the spiritual body and the physical body.

In recent years, I have frequently received spiritual assistance as in (6). Spirits began to help with the treatment. In this way, the acupuncture I do has changed. My spirituality is also changing. This will be described in detail below.

2.2. Acupuncture Change and Spirituality

2.2.1. Changes in diagnosis

Use the five senses when diagnosing.

In the early stages, diagnosis was made using only the five physical senses, that is, the sensory organs of the flesh. Eventually, in addition to this, I began to use my five spiritual senses. The five spiritual senses are often indistinguishable from the senses obtained by the five physical senses, and are recognized as they are. Intelligent analysis is needed to make the distinction.

In addition to the five senses, there are also spiritual senses that we are directly aware of. I use it to locate the affected area of the patient. It may be sensing abnormalities in the minute electromagnetic waves emitted by the human body. I look forward to future research on this point.

The spiritual sensibility seeks out the affected area faster and more accurately than the five physical senses.

2.2.2. Changes in treatment

As spiritual sensitivity increases, spiritual objects are often treated.

In the early days, the effect of the treatment was very close to the place where the acupuncture needle was inserted.

In the middle period, the effect began to extend along the meridians to distant distances.

Recently, the effects of my mind have begun to extend beyond the meridians. The action of the mind can also send qi to the brain and heart. There are times when energy is sent to places that cannot be expressed in three dimensions.

2.2.3. Change in the process from diagnosis to treatment decision

In the early days, I decided to treat based on textbook knowledge and clinical experience.

Recently, I have been using my knowledge of clinical experience through spiritual sensitivity to inform treatment decisions. In addition, there are cases where diagnosis and treatment decisions are made only based on spiritual sensitivity without such preconceived notions. When the affected area is clarified by the spiritual diagnosis, the corresponding treatment points are also clarified. I know a couple of formulas that derive treatment points from the affected area. However, since the diagnosis and treatment decision are made in a different way than those formulas, it can be said that the answer was obtained by spiritual methods.

There are two kinds of this spiritual method. One is based on my own spiritual sensitivity. The other method is through the cooperation of the spirit world. Cooperation in the spirit world is the acquisition of knowledge, emotions, and power through the cooperation of spiritual beings such as spirit people. This method has become very popular recently.

2.3. Actual treatment decision process by spirit world cooperation

Recognize the patient's condition by diagnosis and identify the affected area.

On the other hand, the spirit person will tell you the treatment point.

The teachings of spiritual people are mostly non-verbal and difficult to explain. The treatment point cannot be expressed in three dimensions. But in my brain, it's clearly identified. When the point is stimulated, a further stimulus vector is indicated. While changing the vector several times, the treatment point may move.

By the way, the information from the spirit world cooperation enters your spirit body. Therefore, it is difficult to distinguish whether the treatment decision is made by oneself or taught by another spiritual person.

Here are two examples of information that can be identified as information from a spiritual person. The first is when I deny it when I make a treatment decision. It must be a spiritual person who denies the treatment I am trying to do and makes me stop my hand.

The second is the spiritual world cooperation by Dr. Kazuo Miyahara [3]. He was recognizable because he had a characteristic treatment.

2.4. The spiritual world cooperation by Dr. Kazuo Miyahara

Dr. Kazuo Miyahara is a doctor of medicine who wrote the New Japan Life Extension Studies in Showa 15. The point of contact between him and me was a copy of the book. About 20 years ago, I read this and was impressed. Then, in order to incorporate it into my treatment, I repeated the practice based on the knowledge I had read in the book. I couldn't understand it well because it was written in a simple book, and even if I tried to imitate it, I couldn't get the same result. And 10 years ago, I felt the limit and gave up and forgot about him.

Recently, however, I began to experience spiritual aid, and when I looked at the contents, I found that I was doing something similar to the treatment described in his book. Treatments that could not be mastered in books became possible with the help of the spirit world.

2.5. Case Report

The information used for diagnosis and treatment is classified as follows.

A. Knowledge stored in the brain, information from school and clinical experience
B. Information based on the five physiological senses
C. Information from the five spiritual senses reflected in the five physiological senses
D. Information from other spirits

2.5.1. Case Report Patient with Uterine Fibroids, 44-year-old female

The patient has had multiple fibroids for more than 10 years, and there are five fibroids that can be seen externally. It is difficult to produce urine and stool, and it is severely swollen from the lower abdomen to the thighs. She has pain in her hips and heels.

I treat it with the goal of improving back pain, heel pain, and reducing swelling in the abdomen to make it easier to urinate. After the diagnosis and treatment that I do on a daily basis, the swelling in my stomach has decreased a little. However, the pain in the heel did not improve. I remembered that when I gave her acupuncture on Hyakue (GV-20) with the help of the spirit world, it made her whole leg easier, so I decided to try acupuncture in the direction of Hyakue. I identified the point where I actually did acupuncture with my spiritual sensitivity, and tried acupuncture. Then I received a spiritual instruction to "a little more to the right." The acupuncture needle was removed and reinserted about 5mm to the right. The treatment was terminated because the pain disappeared.

2.5.2. Symptom Report Patient with Restlessness Disorder Female in 50 years old

The patient has become anxious due to excessive stress at work and has been taking stabilizers for less than a year.

I did the usual diagnostic treatment, but she felt something was not clear. When I pointed out the stiffness in her left ribs, she felt something stuck there. I stimulated the area with acupuncture and low-frequency electrotherapy, but it did not get rid of the delay. One point on the inner thigh was shown by the help of the spirit world. When I pressed my thumb on it, she was very painful, and eventually the swelling in her abdomen improved and she felt refreshed.

3. Discussion

I described my subjective feelings about spiritual sensibilities. There is also a theory that explains this in terms of the unconscious and the collective unconscious.

Leo Sakaguchi argued as follows. "The sense of presence belongs to the unconscious realm of detection of minute changes beyond the conventional five senses, as well as deep sensations and somatosensory sensations. These perceptions occur in the process of the individual's sensory system capturing minute physical fluctuations emanating from the surrounding environment, such as air flow and minute sound vibrations, and cognitively reconstructing them through the complex information processing mechanisms of the nervous system [4]."

Since the spiritual senses are ultimately perceived through the five physical senses, it is difficult to distinguish between the two. Therefore, the above interpretation is also quite true. Also, if spiritual sensitivity can be measured and recorded, its existence can be objectively proven.

There is a high possibility that the information about the help of the spirit world is from others. The possibility that the information is from the collective unconscious cannot be ruled out. Again, it is difficult to measure and record, and it has not been objectively proven.

This time, we have published such a subjective record. Originally, I was going to interview and compare the records of several of my colleagues' acupuncturists, and make an objective presentation. However, my fellow acupuncturists did not treat with a sense of spirituality like I did. So it was a very subjective record release.

I described my subjective feelings about spiritual sensibilities. There is also a theory that explains this in terms of the unconscious and the collective unconscious.

Leo Sakaguchi argued in "Considering the Leading Edge of Mind-Body Correlation Research" as follows [3]:

"The sense of presence belongs to the unconscious realm of deep sensation and somatosensory sensation, as well as the detection of minute changes beyond the conventional five senses." Spiritual sensibility is ultimately recognized through physical sensibility, so I think there are cases where you feel the above way. However, spiritual sensibilities are not only weak sensations, but also those that leave a clear and vivid impression. Even so, it is difficult to measure or record spiritual sensitivity, so its existence cannot be objectively proven.

There is a high possibility that the information about the spirit world cooperation is from others, but it cannot be ruled out that it is information from memories or the collective unconscious. Again, it is difficult to measure and record, and it has not been objectively proven.

This time, we have published such a subjective record. Originally, I was going to interview and compare the records of several of my colleagues' acupuncturists, and make an objective presentation. However, my fellow acupuncturists did not treat me with a sense of spirituality like I did. So it was a very subjective record release.

4. conclusion

I mentioned that the acupuncture I practice on a daily basis has something to do with spirituality and described the use of spirituality in the process of diagnosis, treatment, and treatment decision-making. In particular, regarding the cooperation of the spirit world, we receive information clearly and directly from spiritual people.

References

1. Honma, S. *Shinkyu jituyou keiketugaku* (Ido no nihon sha, 1955).
2. Unification Church *Divine Principle* (Kogensha, 1994).
3. Miyahara, K. *Shin nihon enmeigaku* (Shin nihon enmeigaku institute, 1970).
4. Sakaguchi, L. *Considering the Leading Edge of Mind-Body Correlation Research* (Tumugishobo, 2024).

Proceedings of
THE 5th INTERNATIONAL CONFERENCE OF
HYOJEONG ACADEMY 2025

Session 6

Social & Religious Studies for Co-Righteousness

www.ichja.org

5th International Conference of Hyojeong Academy
International Joint Conference 2025

A Study on the Relationship between Heavenly Parent's Love and Mathematics

Ikumatsu Fujimoto[1*], MinSang Kim[2] and YoungSik Pyun[3]

[1]Okuwa Technical Research center, Japan
[2] Cheon Won Co., Ltd, Korea
[3]Institute for Manufacturing Systems Technology, Sun Moon University, Asan 31460, Korea
*Correspondence: fujimoto.ikumatsu@gmail.com

Abstract: This study examines the profound connection between Heavenly Parent's love and mathematics, presenting a novel perspective to bridge the realms of religion and science. By highlighting the mathematical precision and beauty evident in the universe, it reveals how the inherent order in mathematical laws reflects the love and harmony of Heavenly Parent. Specific examples, such as the Dirac equation, Euler's formula, the Fibonacci sequence, Cauchy's integral theorem, and the Hahn-Banach theorem, illustrate how mathematical principles embody universal beauty and order as expressions of Heavenly Parent's intention in creation. This research illustrates how one can experience the love of the Heavenly Parent through mathematics, the foundation of modern science and technology, thereby contributing to the realization of an ideal world.

Keywords: Heavenly Parent's Love, Mathematical Harmony, Simplicity, Universality, Religion and Science, Dirac Equation, Euler's Formula, Einstein's Equation, Cauchy's Integral Theorem, Han-Banach Theorem

1. Introduction

Recently, an increasing number of young people, especially second-generation members of the Family Federation, have begun to truly feel the love and sorrowful heart of the Heavenly Parent. This trend is not only evidence of the progression of Heavenly Parent's providence but also marks a deepening bond between Heavenly Parent and humanity. It is a profound blessing to feel close to Heavenly Parent and to walk with them.

Experiencing Heavenly Parent's love is not confined to prayer and religious activities. Nature itself abundantly reflects Heavenly Parent's love. For instance, the sight of autumn leaves dancing in the wind seems to symbolize Heavenly Parent's intention to soothe human hearts. The sky, earth, sea, mountains, trees, and the activities of animals—all of creation—embodies Heavenly Parent's profound love for humanity. Developing sensitivity to Heavenly Parent's presence and love is vital for creating the harmonious world envisioned by Heavenly Parent and humanity.

According to the Unification Principle's "Principle of Creation," Heavenly Parent and humans share a parent-child relationship. Heavenly Parent's purpose in creation is to experience joy through the reciprocal give-and-receive of love and beauty with humans. As a result, all of creation is imbued with Heavenly Parent's infinite love [1]. Unification Thought further teaches that Heavenly Parent possesses an "Inner Hyungsang," which includes mathematical characteristics such as numbers, formulas, and principles [2]. This perspective presents Heavenly Parent as a mathematical being, with mathematics serving as the foundational structure for the creation of the universe.

Mathematics' universality, simplicity, and harmony have enduring value across cultures and eras. The mathematical laws and theorems describing natural and societal phenomena encapsulate beauty and harmony, revealing Heavenly Parent's love.

The ancient Greek philosopher Pythagoras once stated, "All things are numbers," emphasizing the mathematical order governing nature. Similarly, Galileo Galilei's assertion that "The book of nature is written in the language of mathematics" and Newton's discovery of calculus—which provided a framework for explaining celestial motion and physical phenomena—further illustrate mathematics' profound significance. In modern times, string theory's mathematical frameworks continue to unveil keys to understanding the universe's structure and operation.

This paper explores the connection between mathematics and Heavenly Parent's love from the following perspectives:

(1) The Mathematical Precision and Beauty Observed in the Universe: Examples such as the symmetry of electron behavior described by Paul Dirac's equation demonstrate how mathematical order in creation reflects Heavenly Parent's love.
(2) Heavenly Parent's Love Found in Mathematical Concepts and Theorems: By examining Euler's formula, the Fibonacci sequence, the golden ratio, Cauchy's integral theorem, and the Hahn-Banach theorem, this paper highlights how these concepts embody beauty and order as expressions of Heavenly Parent's love.

Through these explorations, this paper presents a novel perspective: viewing mathematics as tangible evidence of the Heavenly Parent's deep affection for humanity. Cultivating sensitivity to Heavenly Parent's love through mathematics can deepen the relationship between religion and science, promoting their unification.

As the president of the Family Federation for World Peace and Unification, Dr. Hak Ja Han Moon, who leads Heavenly Parent's providence for humanity's salvation, has declared that God is the Heavenly Parent and that Heavenly Parent's providence has progressed to a more intrinsic and essential level. The understanding of God as both Father and Mother emphasizes this shift toward a deeper, internal phase of Heavenly Parent's providence. This approach to mathematics—from discovering new insights to uncovering of the Heavenly Parent embedded within the concept—is aligned with developing a deeper, more profound worldview, marking a significant step in this academic journey.

2. What Is Mathematics?

Mathematics has been a symbol of human intelligence and divine essence since ancient times and continues to play a crucial role in modern technological advancements. This section explores the essence and universality of mathematics and its connection to Heavenly Parent's love, supported by historical perspectives.

2.1. The Essence and Universality of Mathematics

The universality of mathematics arises from its logical consistency and rigor. Mathematical results transcend specific cultures and eras, standing as universal truths. For example, theorems derived from the axioms of Euclidean geometry remain true across time and place. This universality stems from mathematics being built upon logical foundations like axioms and theorems.

Studying mathematics is an endeavor to pursue eternal and universal truths, bringing profound peace and respect. It is deeply felt that Mathematics is not merely a tool but a bridge connecting humanity to the eternal realm.

2.2. Perspectives of Historical Mathematicians on Mathematics

Prominent mathematicians have highlighted the harmony, universality and beauty of mathematics:
(1) Carl Friedrich Gauss: "Mathematics is the queen of the sciences," emphasizing its elegance and foundational role of science [3]. Key points from Gauss's perspective: (a) Universal Language: Mathematics serves as an essential language across all scientific fields. (b) Rigor and Beauty: The logical rigor and beauty of mathematics surpass other sciences. (c) Foundation of Science: Other sciences cannot exist without mathematics, which unveils the fundamental laws of nature.
(2) Leonhard Euler: "Mathematics is the language of God," linking mathematics to cosmic order [4].
(3) Henri Poincaré: "Mathematics is the science of harmony," underscoring its role in unifying phenomena [5].

Other notable views include Newton's association of numbers with creation, Einstein's focus on the eternal nature of equations, and Cantor's connection of infinity to divinity [6].

2.3. The Relationship Between Mathematics and Science

While mathematics and science are deeply interconnected, they maintain distinct characteristics [7]:
(1) Differences: Mathematics is abstract and deductive, focusing on principles derived from logical reasoning, whereas science is empirical and inductive, based on observation and experimentation.
(2) Commonalities: Both disciplines strive for universal truths and rely on each other for advancements. Mathematics provides essential tools for scientific inquiry, while discoveries in science continually inspire new mathematical theories.

2.4. The Relationship Between Mathematics and Religion

Despite their different methodologies, mathematics and religion both pursue order, harmony, and infinity [8]:

(1) Differences: Mathematics focuses on abstract universal truths through logical reasoning and formal proofs. Religion is based on faith and revelation, interpreting the divine through personal spiritual experiences
(2) Commonalities: Both strive to uncover deep truths that transcend individual, cultural, and temporal boundaries. Each inspires awe, with mathematics through its elegant proofs and religion through its spiritual insights.

2.5. The Simplicity, Universality, Infinity, and Beauty of Mathematics in Relation to Heavenly Parent's Love

Mathematics reflects Heavenly Parent's love through its key characteristics:

(1) Simplicity: Compact expressions like Euler's formula symbolize Heavenly Parent's dedication.
(2) Universality: Concepts like π and the Pythagorean theorem mirror love transcending all boundaries.
(3) Infinity: Infinite series and fractals evoke the boundless grace of Heavenly Parent.
(4) Beauty: Symmetry and harmony in mathematics reflect divine artistry.

These characteristics position mathematics as a medium through which humans can experience the profound love of the Heavenly Parent, connecting us more deeply to the divine.

3. The Precision and Beauty Found in the Universe [9, 10]

3.1. The Quest for the Theory of Everything

The universe displays remarkable precision and harmony, evident in its physical laws and mathematical structures. Constants such as the speed of light c, the gravitational constant G, and Planck's constant $\hbar$ enable the evolution of the cosmos, reflecting a deep underlying order. Symmetries in nature, from snowflakes to particle physics (e.g., *SU(3), SU(2), U(1)*), and patterns like the golden ratio and Fibonacci sequence, further underscore this inherent design. These mathematical phenomena suggest intentional creation and align with the love and harmony of the Heavenly Parent.

Physicists strive to uncover a unifying "Theory of Everything" (TOE), an equation that harmonizes all fundamental forces. This quest began with Newton's law of universal gravitation: $F = G\frac{m_1 m_2}{r^2}$,

where F is the gravitational force, G is the gravitational constant, m_1 and m_2 are masses, and r is the distance between them. While successful on a macroscopic scale, this law fails at relativistic speeds or quantum scales.

Maxwell's equations of electromagnetism unified electric and magnetic fields, laying the groundwork for the Standard Model and illustrating light as an electromagnetic wave. However, the unification of gravity with quantum mechanics remains unresolved, with string theory and loop quantum gravity proposing frameworks to address this challenge.

3.2. The Standard Model

The Standard Model describes fundamental particles (e.g., electrons, quarks) and unifies electromagnetic, weak, and strong nuclear forces. It successfully incorporates the Higgs boson, which provides mass to particles, and explains particle interactions with remarkable precision. However, gravity remains excluded, highlighting the challenge of developing a truly unified theory.

3.3. The Dirac Equation [11]

Paul Dirac's proposal of the Dirac equation in 1928 marked a significant advancement in theoretical physics, building on the groundwork laid by Erwin Schrödinger's wave equation. While Schrödinger's formulation was instrumental in developing quantum mechanics by describing particles probabilistically as wave functions, it fell short in accounting for relativistic effects and particle spin. Dirac's equation resolved these limitations by integrating Einstein's special theory of relativity with quantum mechanics, leading to a more comprehensive description of spin-1/2 fermions such as electrons, neutrinos, and quarks.

The Dirac equation is celebrated for its mathematical beauty and deep physical insights, revealing the intrinsic connections between various fundamental aspects of the universe. It describes not only the motion and energy of particles but also their spin and the possible existence of corresponding antiparticles, thus playing a crucial

role in the formulation of the Standard Model of particle physics. Dirac emphasized the importance of aesthetic considerations and physical symmetries in his theoretical constructs, which include rotational, translational, and Lorentz symmetries—ensuring that physical laws remain consistent across different frames of reference and positions.

Dirac's belief that "beautiful equations are more likely to be true" reflects in his equation's ability to unify various fundamental elements of physics, illustrating the profound interconnectedness of time, space, energy, momentum, and matter-antimatter relationships. This unification and the equation's predictive power underscore its pivotal role in modern physics, illustrating the harmony across all dimensions of time and space.

The Dirac equation, often considered one of the most elegant in physics, describes spin-1/2 particles (e.g., electrons, neutrinos, quarks) by integrating quantum mechanics and relativity in natural units (physical constants $\hbar$=c=1):

$$\left(i\boldsymbol{\gamma}^0 \frac{\partial}{\partial t} + i \sum_{j=1}^{3} \boldsymbol{\gamma}^j \frac{\partial}{\partial x_j} \right) \boldsymbol{\varphi} = m\boldsymbol{\varphi}$$

Here, $\boldsymbol{\varphi} = \boldsymbol{\varphi}(t, \boldsymbol{x})$ is the wave function, and $\gamma 0$, γ^j are Dirac matrices that capture energy, momentum, spin, and mass. The equation predicts particles and their corresponding antiparticles, as well as relativistic properties like spin and magnetic moments. It also unifies concepts such as spacetime, energy, and momentum, illustrating a harmony that reflects Heavenly Parent's love. When expressed as: $\varphi(t, \boldsymbol{x}) = u(\boldsymbol{p})\exp\{-i(Et - \boldsymbol{p} \cdot \boldsymbol{x})\}$, it leads to the relativistic energy-momentum relation: $\boldsymbol{E}^2 = (\boldsymbol{p}, \boldsymbol{p}) + m^2$ revealing the unity between kinetic and rest energy. The Dirac equation's prediction of positrons, experimentally confirmed later, underscores its profound accuracy and beauty.

3.4. The Dirac Equation and Heavenly Parent's Love

At its core, the Dirac equation embodies harmony and unity, uniting disparate concepts like particles and antiparticles, space and time. This harmonious structure mirrors the Heavenly Parent's love, which binds and sustains all creation. Dirac's remark that the equation he developed was smarter than himself suggests that this equation might indeed reflect the intention of God. The conservation of spin and energy, the symmetry of particle behavior, and the existence of antiparticles can all be seen as mathematical expressions of the harmony instilled by the Heavenly Parent.

4. Heavenly Parent's Love Found in Mathematical Concepts and Theorems

Mathematics serves as a profound reflection of Heavenly Parent's love, with its principles and theorems embodying beauty, harmony, and universality. This chapter highlights some mathematical concepts that illustrate this connection.

4.1. Euler's Formula

Euler's formula: $\exp(i\pi) + 1 = 0$ is often celebrated as the "jewel of mathematics" for its simplicity and elegance. By uniting fundamental mathematical constants—e, i, π, 1, and 0—it exemplifies harmony and unity. This formula reflects Heavenly Parent's love by showcasing the profound connections between seemingly disparate elements of mathematics.

4.2 Einstein's Equation: The Equation of Relativity

Einstein's famous equation: $E = mc^2$ demonstrates the equivalence of energy (E) and mass (m), with c representing the speed of light. This equation reveals the deep unity underlying physical reality and aligns with the Divine Principle's view of creation as an interconnected whole. The simplicity and universality of this equation symbolize the divine harmony and order imbued by Heavenly Parent in the cosmos.

4.3 Fibonacci Sequence and the Golden Ratio

The Fibonacci sequence is defined by the following recurrence relation:

$$F(0) = 0, F(1) = 1, F(n+2) = F(n+1) + F(n)\ (n \geq 0)$$

The ratio of adjacent terms in the Fibonacci sequence converges to the golden ratio:

$$\varphi = \frac{1+\sqrt{5}}{2} \approx 1.618 \ , \lim_{n\to\infty} \frac{F_{n+1}}{F_n} = \frac{1+\sqrt{5}}{2} \approx 1.618$$

This mathematical harmony appears in numerous natural phenomena, such as the arrangement of leaves, the spirals of seashells, and the structure of galaxies. These instances demonstrate the harmony and beauty of the natural world created by Heavenly Parent, expressed through the universal language of mathematics.

4.4. Cauchy's Integral Theorem

Cauchy's integral theorem in complex analysis states:

$$\oint_\gamma f(z)\,dz = 0$$

for any holomorphic function *f(z)* over a closed contour γ. Here, a holomorphic function is one that is differentiable everywhere in its domain. This theorem reflects the harmony and balance of mathematical systems, where the integral value remains zero regardless of the contour's shape or position, as long as it lies within the domain [12]. This harmony and balance resonate with the idea that Heavenly Parent's love is unchanging and present in all times and places.

4.5 Hahn-Banach Theorem

The Hahn-Banach Theorem, a cornerstone of functional analysis, allows the extension of a linear functional $f:S \to R$ defined on a subspace $S \subset X$ of a normed vector space X to the entire space while preserving linearity and boundedness:

(1) $\tilde{f}(x) = f(x)\ \forall x \in S$ (preservation of the original functional), and

(2) $\left|\tilde{f}(x)\right| \leq \|x\|\ \forall x \in X$ (boundedness is maintained).

This theorem implies that a linear functional defined on a subspace can be extended to the entire space without contradiction, preserving its linearity and boundedness.

Connection to Heavenly Parent's Love is as follows.

(a) Universal Extendability: The theorem illustrates that properties defined in a subset can extend universally, mirroring Heavenly Parent's love, which embraces all humanity without restriction.

(b) Harmony and Consistency: The preservation of linearity and boundedness in the extension reflects the consistent and harmonious nature of Heavenly Parent's love.

5. Conclusion

This paper explored the relationship between Heavenly Parent's love and mathematics. To realize the ideal of one human family centered on Heavenly Parent and to build a society of coexistence, co-prosperity, and common righteousness, it is essential to experience the presence and love of Heavenly Parent, the Creator. Through a life of faith, including prayer, it is crucial to encounter Heavenly Parent and deeply feel Their presence. Additionally, perceiving the breath and heart of Heavenly Parent through the natural world They created is an equally important means of understanding.

Heavenly Parent is a mathematical being, encompassing innumerable numerical principles and formulas. Mathematics represents the fundamental structure of creation. As Galileo Galilei famously stated, "The book of nature is written in the language of mathematics," signifying that mathematics is the blueprint of the universe's creation.

From this perspective, mastering mathematics also becomes a pathway to a deeper understanding of Heavenly Parent. Furthermore, mathematics not only provides clues about how the world was created but also serves as one of the keys to building a better society. Mathematics is the foundation of science and technology, and mathematical advancements deeply impact human life across various fields, reflecting the love of Heavenly Parent through tangible blessings. These innovations demonstrate how Heavenly Parent's love brings specific benefits to humanity.

Reverend Sun Myung Moon once said, "Mathematics, which deals with the invisible world, shares an intrinsic connection with religion. To accomplish great tasks, one must excel in the power of mathematics [13]. " These words underscore the critical importance of mathematics in understanding Heavenly Parent's heart and fulfilling our mission.

Moreover, within the essence of mathematics lies the infinite love that Heavenly Parent bestows upon Their children. Developing the sensitivity to perceive Heavenly Parent's love through the study of mathematics is undoubtedly one of the vital roles we must play in realizing an ideal world.

Kiyoshi Oka (1901–1978), a renowned Japanese mathematician who made significant contributions to the theory of functions of several complex variables, profoundly influencing the development of analysis and geometry in modern mathematics, emphasized the deep connection between mathematics and emotion:

"Mathematics is rooted in emotion."

"The creation and discovery of mathematics are driven by emotion, guided by intuition, and refined by logic."

"Mathematics seeks to reveal the harmony of nature and the universe, with emotion at its core [14]."

From these statements, it is evident that mathematics resonates with Heavenly Parent's loving heart.

References

1. World Peace Family Federation. *Exposition of the Divine Principle* (Seiwa Publishing, 1989).
2. Institute of Unification Thought (Ed.). *Outline of Unification Thought* (Kogensha, 1994).
3. Sautoy, M. *The Queen of Mathematics: A World of Numbers* (HarperCollins Publishers, 2008).
4. Calinger, R. *Leonhard Euler: Mathematical Genius in the Enlightenment* (Princeton University Press, 2016).
5. Poincaré, H. *Science and Hypothesis* (Chikuma Shobo, 2022).
6. Science for All Americans. https://www.project2061.org/publications/sfaa/online/sfaatoc.htm.
7. Penrose, R. *The Road to Reality: A Complete Guide to the Laws of the Universe* (Vintage Books, 2004).
8. Livio, M. (translated by Toshio Chiba) *Is God a Mathematician?* (Hayakawa Publishing, 2011).
9. NHK *The Equation of God I* (NHK Enterprises, 2014).
10. Kaku, M. *The God Equation* (NHK Publishing, 2023).
11. Dirac, P. A. M. The Quantum Theory of the Electron. *Proceedings of the Royal Society A*, (1928).
12. Cochrane, R. *The Secret Life of EQUATIONS: the 50 greatest equations* (Newton Press, 2021).
13. Moon, S. M. *As a Peace-Loving Global Citizen: Autobiography of Sun Myung Moon* (Sogei Publishing, 2010).
14. Oka, K. *To Those Aspiring to Mathematics* (Heibonsha, 2015).

5th International Conference of Hyojeong Academy
International Joint Conference 2025

The Diversity Deficit in the Moral Sphere

Colin Turfus and Don Trubshaw*

Independent researcher
*Correspondence: c.turfus.8o@cantab.net

Abstract: The difference in perspective between liberals and conservatives is not so much in the values they espouse as in the weights they assign to them, with liberals in particular citing the embodiment of care (kindness) as the overriding moral imperative at the expense of essentially all other virtues. This moral priority is increasingly expressed through advocacy for the avoidance of harm and the promotion of equality. To advance their cause in the public space, conservatives are increasingly led to justify their moral choices in those terms. The result we see is a hollowing out of the public moral discourse, with considerations of mainstream traditional concepts of virtue still influencing the members of communities who have a shared source of authority, but increasingly found to be absent from the wider public discussion. What is to be done? If we are right in our diagnosis that the intractability of political discourse in the present age is due to a dearth of common values, and more specifically a lack of diversity in the values perspective of the progressive left, then it is better to acknowledge this and look to deal with it, rather than ignoring it. If greater common ground is to be found between liberals and conservatives, it is the latter group who must establish it and look to defend it, challenging the former's monopoly on the idea of what constitutes "kindness" and enriching it by offering a more diverse palette of values and virtues allowing a more inclusive moral debate.

Keywords: Liberals, conservatives, diversity, moral sphere, virtues, common values

1. Introduction

It was observed by Haidt [1] based on his moral foundations theory that the difference in perspective between liberals and conservatives is not so much in the values they espouse as in the weights they assign to them, with liberals in particular citing the embodiment of care (kindness) and the pursuit of equality as the overriding moral imperatives at the expense of essentially all other virtues, such as loyalty/patriotism, sanctity, respect for authority and upholding liberty. This bias in liberal thinking has been picked up and elaborated on more recently by Kaufmann [2], who sets out his view of how this has led over time to two important consequences.

First there is a decline in the scope of people's inherent sense of personal virtue. "Private morality narrowed in wider elite society: beliefs about how to be a good person and what to feel guilty about rotated away from religion, patriotism, and sexual propriety to center solely on care/harm and equality [2]."

Secondly, what Kaufmann calls the sacralization of race has further narrowed the focus of leftist moral deliberations to the extent that a claim that disadvantage (physical or psychological) has arisen based on a purported victim's (non-white) race precludes virtually any moral counterargument. Similar considerations apply in relation to those purported to be victimized based on their sexuality or gender identity. "With collective sources of morality such as religious and national particularism stripped away, it only remained to fetishize the remaining moral "taste buds" of care/harm and equality of outcome, especially as directed toward racial (and later, sexual) minorities. This created an unbalanced public morality, the consequences of which we are currently living through [2]."

As noted by Turfus [3], while Haidt's care/harm moral foundation can be equated with the virtue of kindness, the moral foundation Kaufmann refers to as equality of outcome cannot be equated with a corresponding personal virtue since it is rather a view about how society should be constituted. This means that kindness is the only significant virtue fully recognized by left liberals. The importance of the other virtues typically upheld as important by conservatives are downplayed or even dismissed as "problematic", for example religious, particularly Christian, values.

But although there may be agreement on the importance of kindness, that is no guarantee of agreement about the degree and scope of kindness which should be expressed. This is normally most evident in disputes about parenting: between grandparents and parents, for example, or between mother and father.

2. Discussion

2.1. Bias in Liberal Thinking

The problem in relation to public morality is that human psychology is hardwired to express (and withhold) kindness selectively and this predisposition can be reinforced and amplified through social conditioning. In relation to wrongs, present or historical, perpetrated against sacralized identity groups, Kaufmann [4] observes elsewhere: "We are taught to feel warm and protective emotions toward the descendants of those wronged by these episodes (or those who look like people who were wronged) and anger and hostility toward the descendants of those who did wrong (or those who look like those who did wrong). This is reinforced both in institutions like schools and workplaces and in everyday life. If we show insufficient respect to a person from a sacralized identity group, they - or members of the majority who set themselves up as the moral enforcers and protectors of minorities - reinforce the message that we have transgressed a sacred value by expressing their anger and shock. If we praise white people, masculine culture or otherwise laud historically advantaged groups we get a disgust response [4]."

Thus, if you belong to one of the sacralized groups (black race, Muslim, LGB, transgender, etc.) strenuous effort will be expended by those of left-liberal persuasion to avoid harm or offence being caused to you, but if you are someone who has shown themselves to be less than sympathetic to any aspect of the left-liberal moral agenda, you should not be surprised if you are denigrated, bullied, denied opportunities for employment or promotion, or cancelled (viz. you, your associates and/or your business boycotted). Those who seek to enforce the left-liberal value agenda in this intrusive way are referred to by Kaufmann [2] as cultural socialists.

From the perspective of cultural socialism, then, the only recognized way in which a person can really embody virtue within themselves is by expressing a partisan kindness skewed towards those deemed by its proponents to be historically marginalized and/or oppressed. Other than that, virtue is assessed solely in terms of one's commitment (if not in practice, then through professed belief/aspiration) towards more equitable societal outcomes.

It is worth noting here that concern for the environment and a commitment to sustainable development and biodiversity have in recent times become important virtues the practice of which falls outside the purview of what Kaufmann has termed cultural socialism. Here the concern is not for equitable societal outcomes but rather for a form of ecological (or environmental) justice. Since the care/concern moral foundation is the most obviously relevant, this area is one where liberals and conservatives might expect to find greater agreement, and such indeed seems to be the case. However, there remain significant differences of nuance.

For example, liberals' concern for the environment tends to be demonstrated through a commitment to a shared project. To that end, campaigning for legislation and regulation binding others into going along with their green agenda tends to be viewed as more important than lifestyle choices. For conservatives, virtues such as duty and integrity are likely to be of greater weight in moral deliberations, which would incline them less towards activism. So, from a liberal perspective the use of a private jet can be justified in relation to Net Zero goals provided donations are made to facilitate the planting of enough trees to offset the carbon emissions (much as indulgences were sold in the Middle Ages). Those of a more conservative bent, for example Christians who see their commitment to sustainable development as a requirement of the stewardship granted them by God over the created world, would tend to assess environmental credentials through the lens of sanctity and the demonstration of integrity through limiting one's appetite for consumption rather than justifying it in a utilitarian manner through a calculus of carbon credits.

So, it is perhaps not surprising that the only usage you are likely to hear of the word "virtue" in public moral discourse these days is in the odd reiteration of old sayings such as "patience is a virtue" or else in the denigratory term "virtue signaling," used mainly by conservative critics of left liberals who seek to have their commitment to more just societal outcomes recognized by their peers, this being the preferred way to embody "virtue" within the compass of their belief system.

2.2. Wider Societal Impact

An interesting question here is why it appears that almost all public discourse is affected by this, not only the viewpoints expressed by those of a left-liberal persuasion. Kaufmann [2] describes this phenomenon as a "cultural socialist hegemony within the wider elite culture and its institutions, typically cloaked in the velvet glove of 'equity, diversity, and inclusion.'" While the ideology is adhered to and enforced most obviously by committed

cultural socialists, its impact through cultural hegemony is on potentially everyone in society. One may not be excited by the idea of social transformation through the pursuit of equity, diversity and inclusion, but does one feel strongly enough against them that one would risk expressing dissent or even disinterest, with all the concomitant denigration and stigmatization to which one might then be subjected?

A natural further question is, if the spread of cultural socialist morality is through a form of cultural hegemony, do those on whom this is imposed and who feel obliged to conform to its dictates really believe in the morality or are they merely behaving as if they do? Interestingly, the survey data of Kaufmann [2] in relation to cancel culture suggests that it frequently results in people conforming not only in their behavior but also apparently in their acceptance of the imposed ideology.

Although an alternative explanation might be offered in terms of "preference falsification" of employees' true beliefs when operating under an enforced corporate morality. "The counterargument is that employees truly believe in the hegemonic ideology. For many graduate professions, especially in the cultural sphere, I'm afraid this comes closer to the truth [2]."

Why should this be? We would go along with Kaufmann [2] in suggesting that an explanation lies in understanding in terms of human psychology/cognition how identity and morality work: "Once a person comes to be strongly attached to an ideological package, this set of beliefs crystallizes into an important aspect of a person's identity, a key source of meaning in their lives [2]." We consider next in a little more detail how this works in practice.

2.3. The New Puritanism

We take the view here that our morality is in essence what we consider to be the legitimate demands and constraints imposed on us by society and the world we inhabit. Core to this is the idea of authority. While we often believe we are being rational in our determination of what is right and wrong, it is not really a feasible goal to establish and maintain a moral framework from first principles. Rather we infer a framework from observing how things work in society and by considering the moral arguments expressed by others. To the extent we apply rationality, it is in deciding who or what we consider authoritative and worthy of taking into account in our deliberations. For some that will be the tenets of a scriptural text, mediated through a faith community, while for others it may be a political party or ruler, a peer group of colleagues or fellow students, or the newspapers or internet influencers they subscribe to.

We may consider such things as whether those whose opinion we care about will be favorable in relation to our behavior, whether our interests (or those of others we care about) will be damaged or promoted by our actions, or whether a certain course of action is consistent with other moral concerns. Having committed to a moral framework on that basis, we tend to operate within that, rather than revisiting it each time we face a moral choice. Our moral framework then tends to evolve in line with that of the moral community with which we have aligned ourselves. In other words, we tend to be rational and reasonable about whom or what we trust, but less so about the beliefs we consequently take on board.

For example, in their influential article on The Coddling of the American Mind, Lukianoff and Haidt [5] relate how students succumbing to peer pressure on US campuses has led to a censorious atmosphere, characterized by an excessive sensitivity to what are termed "microaggressions" and to language deemed "offensive". The authors conclude that this has resulted in a self-perpetuating punitive microculture amongst students of "vindictive protectiveness", in which "everyone must think twice before speaking up, lest they face charges of insensitivity, aggression, or worse."

As we have seen, there are different sensitivities to different moral pressures on the left and on the right. In particular, while those of a conservative persuasion will typically have a wider range of virtues they would look to uphold, many of these are connected to sources of authority not acknowledged by those on the left, who will be reluctant to accept such conclusions unless arguments can be made based on considerations of kindness, the avoidance of harm and/or the establishment of social justice. So, to advance their cause in the public space, those of a conservative disposition are increasingly led to advocate for their moral preferences in such terms. The result we see playing out in society is a hollowing out of the public moral discourse, with considerations of traditional concepts of virtue still influencing the members of communities who have a shared source of authority but increasingly found to be absent from the wider public discussion.

Note here that, although members of non-native religions are often able to demand that their moral sensitivities be respected by virtue of their being considered historically marginalized minorities, this is based on an appeal

to principles of fairness and social justice, not an acknowledgement of the validity of their moral perspective: their entitlement is only to special pleading such as might reduce the inequity experienced by members of their group.

Indeed, the admission that one's moral perspective has been shaped by a source of authority not acknowledged within the cultural socialist milieu can result in one being personally delegitimized, to the point where one's moral judgement is construed or portrayed as untrustworthy. For example, the admission by Kate Forbes, when questioned, that she would not have voted for gay marriage on account of her Christian faith is widely seen as having been fatal to her bid for the leadership of the Scottish National Party in 2023. Numerous other examples could be adduced. Indeed, many if not most instances of cancel culture are of this kind where, rather than someone being punished for actual wrongdoing, they are censured for their apparent sympathy for a belief founded on an authority or perspective viewed by the cultural socialists as 'problematic' or as 'giving rise to a hostile environment', as it were committing an act of heresy by expressing allegiance to a false god.

As Kaufmann [2] indicates, this naturally has a chilling effect on free speech as conservatives increasingly self-censor to avoid censure: "each time a person loses their job or has their reputation monstered online, the effect is like a pebble falling into a placid pond. The ripple effects reach a wider audience who feel the shock, learning not to stick their heads above the parapet, not to challenge the cultural socialist perspective. Political prejudice is arguably even more insidious. While it may seem a softer form of authoritarianism than firing, boycotting, or deplatforming, political peer pressure shapes a far wider experience: whether you are hired, promoted, published, or socially included [2]."

Such puritanical attitudes are of course not new in anglophone society (as the etymology of this term indicates). Indeed, culture warriors enacting cancel culture have been described by Applebaum [6] and Doyle [7] as "The New Puritans". What is new is that the modern-day Puritans are acting against traditional sources of authority rather than in support. History teaches us that puritanical hegemony can be effective for a time as a strategy for influencing people's moral perspectives and behavior. But there is invariably a backlash as people tire of it and the innate desire of the human spirit for autonomy and freedom of expression reassert themselves (as with the original Puritan movements in 17th century England and New England). There is also the problem of the inefficiencies engendered by the resultant absence of viewpoint diversity, aka "groupthink", causing a cumulative harm to society (as with Soviet communism). As Mounk [8] opines: "if those who hold power are able to censor what they consider noxious views, then the ideas of the powerful are going to be systematically favored over those of the powerless, perpetuating the kind of injustice that progressive opponents of free speech rightly abhor; the stakes of who gets to hold power vastly increase, incentivizing political partisans to refuse to accept the outcome of elections or even engage in violence; and society will lose a crucial safety valve that allows the victims of bad public policies to protest the status quo, making it harder to achieve much-needed social change."

3. Conclusion

While some would suggest that such a backlash is already happening and see the recent re-election of Donald Trump in the US as a watershed, we would tend to agree with the conclusion of Mounk [8] and Kaufmann [2] that there remains a long way to go to address the current imbalance. But an important first step in the pushback against cultural socialist hegemony is in recognizing and publicizing the ways in which it is being exercised and in understanding the contours of the contemporary moral landscape which facilitate the hegemony. There needs to be a reclaiming of corporations, national institutions and regulatory bodies which have been ideologically captured and become vehicles for the pursuit and promotion of cultural socialist agendas. And, if greater common ground is to be found between liberals and conservatives, it is the latter group who must establish it and look to defend it, challenging the former's monopoly on the idea of what constitutes "kindness" and enriching it by offering a more diverse palette of values and virtues allowing a more inclusive moral debate.

References

1. Haidt, J. *The righteous mind: Why good people are divided by politics and religion*, 1st ed. (Vintage Books, 2012).
2. Kaufmann, E. (2024a). *The Third Awokening: A 12-Point Plan for Rolling Back Progressive Extremism* (Bombardier Books, 2024). (Published in the UK by Forum as Taboo: *How Making Race Sacred Produced a Cultural Revolution*).
3. Turfus, C. The Illusory Quest for Shared Values. https://www.societalvalues.co.uk/the-illusory-quest-for-shared-values/.
4. Kaufmann, E. The Woke Emotional Regime: Why our Moral Topography, not just our Moral Cartography, Matters. https://erickaufmann.substack.com/p/the-woke-emotional-regime.

5. Lukianoff, G. and Haidt, J. *The Coddling of the American Mind* (Penguin Press, 2018).
6. Applebaum, A. *Twilight of Democracy: The Seductive Lure of Authoritarianism* (Vintage, 2021).
7. Doyle, A. *The New Puritans: How the Religion of Social Justice Captured the Western World* (Constable, 2023).
8. Mounk, Y. (2023). *The Identity Trap: A Story of Ideas and Power in Our Time* (Penguin, 2023).

Organized by

Hyojeong Academic Foundation

Hosted by

Sun Moon University
Sunhak Educational Foundation
Hyojeog Magnolia Global Medical Foundation

ISBN 979-11-981561-6-7 (93060)